

Offshore structures under extreme loads:

A methodology
to determine
design loads

Andreas Florian Haselsteiner

Offshore structures under extreme loads: A methodology to determine design loads

Vom Fachbereich Produktionstechnik

der

UNIVERSITÄT BREMEN

zur Erlangung des Grades
Doktor der Ingenieurwissenschaften (Dr.-Ing.)
genehmigte

Dissertation

von

Andreas Florian Haselsteiner

Gutachter: Prof. Dr.-Ing. habil. Klaus-Dieter Thoben (Universität Bremen)
Prof. Dr. Joachim Peinke (Universität Oldenburg)

Tag der mündlichen Prüfung: 20. April 2022

May 2022

ABSTRACT

The majority of the Earth's surface is covered by oceans. Waves, currents, and winds are phenomena that act as load requirements in the design process of any offshore structure. While there are many types of offshore structures such as bridges, oil platforms, or wave energy converters, one type of structure currently gets the most attention: offshore wind turbines, which are expected to become one of the main sources of future energy supply. They are typically designed for a design life of 20 or 25 years and therefore must withstand all environmental conditions that can reasonably be expected during this time. To evaluate a design, one estimates its structural response under given environmental loading. This requires a description of the expected environmental conditions and a method to decide which environmental conditions should be considered as design requirements.

This thesis addresses the design process of offshore structures. Engineering standards and guidelines describe the state of the art of this process and recommend models that shall be used to describe the environment and to estimate the extreme structural response. In particular, three design process steps where current methods can lead to problems are addressed: (1) Modeling the probability distribution of significant wave height; (2) modeling the joint distribution of wind speed and wave height; and (3) determining 50-year joint environmental extremes. New methods to deal with these three steps are proposed and evaluated. Finally, a case study on a 5 MW wind turbine is conducted.

Addressing the first step, this thesis shows that the long-term distribution of significant wave height can be modeled with an exponentiated Weibull distribution. The exponentiated Weibull distribution is a generalization of the common two-parameter Weibull distribution. It has two shape parameters, which provide the model with the required flexibility to describe the shape of the empirical distribution. In a study based on six wave height datasets, using the exponentiated Weibull distribution was evaluated. The distribution parameters were estimated with a weighted least squares method. The exponentiated Weibull distribution predicted the height of the highest 0.1% waves with a mean absolute error of 0.4 ± 0.1 m (mean \pm standard deviation over the six datasets) while the state-of-the-art method led to an error of 1.8 ± 0.5 m.

For the second step, to improve current joint distribution models for wind and wave, this thesis explores the idea of modeling the dependence structure of the environmental variables with physically interpretable relationships. In the proposed model, the dependence structure of wind speed and significant wave height is modeled such that the median significant wave height \tilde{h}_s conditional on wind speed v increases with $\tilde{h}_s = c_6 + c_7 v^{c_8}$ where c_6 , c_7 , and c_8 are parameters that are estimated based on empirical data. The advantage of this model structure is that one can interpret c_6 as the part of significant wave height that is not generated by wind at the same place and the same time and the second term that contains c_7 and c_8 as the part that is generated by local wind. Then c_8 is a parameter that describes the type of wind sea. Oceanographers have developed various theories for wind seas that imply different values of c_8 . Based on the same datasets as in the study on the first step, it was found that the novel model structure can describe the dependence between wind speed and wave height better than the model structure that is currently recommended in engineering guidelines.

The third step that is addressed in this thesis concerns the question of how N -year environmental extremes can be defined that lead to an N -year structural response. As the method that is currently used mostly to define such joint extremes, the inverse first-order reliability method (IFORM), can underestimate the structural response; an alternative definition for joint environmental extremes was proposed: N -year environmental extremes can be defined as the boundary of a highest density region that is exceeded on average once every N years anywhere. When the response of an offshore structure is evaluated at the environmental conditions along such an N -year highest density contour, the highest structural response will always have a return period of at least N years (assuming the response is

deterministic). Thus, this definition of joint environmental extremes will lead to conservative design loads, irrespective of the topological characteristics of the response function. Conservative design loads ensure that an offshore structure fulfills its target reliability.

These three contributions – two new models for the long-term distribution of the environment and a new method to define joint environmental extremes – were integrated into a formal description of the overall design process of an offshore structure. This methodology to derive design loads and to evaluate the structural response is based on the process described in the international design standard for offshore wind turbines by the International Electrotechnical Commission, the IEC 61400-3-1 standard. It was generalized to be applicable to any offshore structure and its description of how extreme load cases should be handled was adapted.

The three contributions of this thesis were also implemented in an open-source software intended to support researchers and practitioners who design or analyze offshore structures. In addition, this software contains state-of-the-art methods that can be used as an alternative to the models and methods proposed in this thesis. The software already has external users, for example, engineers who design wind turbines.

To analyze the current design practice, a case study on the long-term extreme response of an offshore wind turbine was conducted. The case study focused on the question of how accurate environmental contour methods can estimate the extreme loads that lead to a 50-year extreme response. It was found that estimates that are based on environmental contour methods can lead to a strong underestimation of the extreme response. Different sources contribute to the overall error. In this case study, bias due to ignoring the response's short-term variability was particularly high. Ignoring short-term variability led to an underestimation of up to 28% of the true 50-year response. This suggests that in the future, the international standard that regulates wind turbine design should include methods to compensate for ignoring short-term variability.

Finally, topics for future research are proposed. It would be interesting to investigate which physics explains why significant wave height observations roughly follow an exponentiated Weibull distribution. Another interesting question is how current knowledge about climate change could be incorporated into the methods that are used to define extreme loads. Lastly, the idea of using design contours in fields other than structural engineering is discussed. Generally, contours describe joint extremes that serve as requirements in the design process. Such contours could also be useful in the field of ergonomics to define requirements for joint distributions of variables such as total height and hip height. A general methodology for deriving extreme design requirements could potentially be developed by connecting the fields of engineering design and statistics of extremes.

ZUSAMMENFASSUNG

Der größte Teil der Erdoberfläche ist vom Meer bedeckt. Wellen, Strömungen und Winde sind Phänomene, die als Lastanforderungen im Entwurfsprozess jeder Offshore-Struktur wirken. Während es viele Arten von Offshore-Strukturen gibt, wie zum Beispiel Brücken, Bohrinseln oder Wellenkraftwerke, erhält eine Art von Struktur derzeit die meiste Aufmerksamkeit: Offshore-Windkraftanlagen, welche wahrscheinlich eine der Hauptquellen der zukünftigen Energieversorgung werden. Sie werden typischerweise für eine Lebensdauer von 20 oder 25 Jahren ausgelegt und müssen daher allen Umweltbedingungen standhalten, die während dieses Zeitraums vernünftigerweise zu erwarten sind. Um einen Entwurf zu bewerten, schätzt man sein Strukturverhalten unter gegebenen Lasten ab. Dies erfordert eine Beschreibung der zu erwartenden Umweltbedingungen und eine Methode, um zu entscheiden, welche Umweltbedingungen als Auslegungsanforderungen berücksichtigt werden sollten.

Diese Arbeit befasst sich mit dem Entwurfsprozess von Offshore-Strukturen. Technische Normen und Richtlinien beschreiben den Stand der Technik dieses Prozesses und empfehlen Modelle, die zur Beschreibung der Umweltbedingungen und zur Abschätzung der extremen Strukturantwort verwendet werden sollen. Im Besonderen werden drei Teilschritte des Entwurfsprozesses adressiert, bei denen die derzeitigen Methoden zu Problemen führen können: (1) Die Modellierung der Wahrscheinlichkeitsverteilung der signifikanten Wellenhöhe, (2) die Modellierung der gemeinsamen Verteilung von Windgeschwindigkeit und Wellenhöhe und (3) das Bestimmen der 50-jährigen gemeinsamen Umweltextreme. Neue Methoden zum Umgang mit diesen drei Schritten werden vorgeschlagen und bewertet. Schließlich wird eine Fallstudie an einer 5-MW-Windkraftanlage durchgeführt.

Den ersten Schritt betreffend, zeigt diese Arbeit, dass die langfristige Verteilung der signifikanten Wellenhöhe mit einer potenzierten Weibull-Verteilung modelliert werden kann. Die potenzierte Weibull-Verteilung ist eine Verallgemeinerung der gemeinen Zwei-Parameter-Weibullverteilung. Sie hat einen zweiten Formparameter, der dem Modell die notwendige Flexibilität bietet, um die Form der empirischen Verteilung zu beschreiben. In einer Studie, die auf sechs Wellenhöhe-Datensätzen basiert, wurde die Verwendung der potenzierten Weibull-Verteilung evaluiert. Die Verteilungsparameter wurden mit einer gewichteten Methode der kleinsten Quadrate geschätzt. Mit der potenzierten Weibullverteilung konnte die Höhe der höchsten 0,1 % Wellen mit einem mittleren absoluten Fehler von $0,4 \pm 0,1$ m (Mittelwert \pm Standardabweichung über die sechs Datensätze) vorhergesagt werden, während die Methode nach dem Stand der Technik zu einem Fehler von $1,8 \pm 0,5$ m führte.

Für den zweiten Schritt, die Verbesserung der derzeitigen gemeinsamen Verteilungsmodelle für Wind und Welle, wird in dieser Arbeit die Idee untersucht, die Abhängigkeitsstruktur der Umweltvariablen mit physikalisch interpretierbaren Beziehungen zu modellieren. In dem vorgeschlagenen Modell wird die Abhängigkeitsstruktur von Windgeschwindigkeit und signifikanter Wellenhöhe so modelliert, dass der Median der signifikante Wellenhöhe \tilde{h}_s in Abhängigkeit von der Windgeschwindigkeit v mit $\tilde{h}_s = c_6 + c_7 v^{c_8}$ ansteigt, wobei c_6 , c_7 und c_8 Parameter sind, die auf der Grundlage empirischer Daten geschätzt werden. Der Vorteil dieser Modellstruktur ist, dass man c_6 als den Teil der signifikanten Wellenhöhe interpretieren kann, der nicht am gleichen Ort und zur gleichen Zeit vom Wind erzeugt wird, und der zweite Term, der c_7 und c_8 enthält, als den Teil, der vom lokalen Wind erzeugt wird. Dann ist c_8 ein Parameter, der die Art der Windsee beschreibt. Ozeanographen haben verschiedene Theorien für Windseen entwickelt, die unterschiedliche Werte für c_8 implizieren. Mithilfe der selben Datensätze wie in der Studie zum ersten Schritt, zeigt diese Arbeit, dass die neuartige Modellstruktur die Abhängigkeit zwischen Windgeschwindigkeit und Wellenhöhe besser beschreiben kann als die derzeit in technischen Richtlinien empfohlene Modellstruktur.

Der dritte Schritt, den diese Arbeit behandelt, betrifft die Frage, wie N -jährige Umweltextreme definiert werden können, die zu einer N -jährigen Strukturantwort führen. Da die derzeit meistver-

wendete Methode zur Definition solcher gemeinsamer Extreme, die inverse Zuverlässigkeitsmethode erster Ordnung (IFORM), die Strukturantwort unterschätzen kann, wurde eine alternative Definition für gemeinsame Umweltextreme vorgeschlagen: N -Jahres-Umweltextreme können als die Grenze einer Region höchster Wahrscheinlichkeitsdichte definiert werden, die im Durchschnitt einmal alle N Jahre irgendwo überschritten wird. Wenn man die Antwort einer Offshore-Struktur bei den Umweltbedingungen entlang einer solchen N -Jahres-Höchstdichtekontur bewertet, hat die höchste Strukturantwort immer eine Wiederkehrperiode von mindestens N Jahren (unter der Annahme, dass die Antwort deterministisch ist). Somit führt diese Definition für gemeinsame Umweltextreme zu konservativen Entwurfslasten, unabhängig von den topologischen Eigenschaften der Antwortfunktion. Konservative Entwurfslasten stellen sicher, dass eine Offshore-Struktur die angestrebte Zuverlässigkeit erfüllt.

Diese drei Beiträge – zwei neue Modelle für die Langzeitverteilung der Umweltbedingungen und eine neue Methode zur Definition gemeinsamer Umweltextreme – wurden in eine formale Beschreibung des gesamten Entwurfsprozesses einer Offshore-Struktur integriert. Diese Methodik, um Entwurfslasten zu bestimmen und die Strukturantworten zu evaluieren, basiert auf dem Prozess, der in der internationalen Norm für das Auslegen von Offshore-Windkraftanlagen der Internationalen Elektrotechnischen Kommission, der IEC 61400-3-1 Norm, beschrieben ist. Die Methodik wurde generalisiert, um auf jegliche Offshore-Strukturen anwendbar zu sein. Außerdem wurde die Beschreibung, wie Extremlastfälle gehandhabt werden sollen, verändert.

Die drei Beiträge dieser Thesis wurden auch in einer Open-Source-Software implementiert, welche Forschern und Praktikern, die Offshore-Strukturen entwerfen oder analysieren, unterstützen soll. Die Software enthält außerdem Stand-der-Technik-Methoden, die als Alternativen zu den Modellen und Methoden, welche in dieser Arbeit vorgeschlagen wurden, genutzt werden können. Sie hat bereits externe Nutzer, zum Beispiel Ingenieure die Windkraftanlagen entwerfen.

Um die derzeitige Entwurfspraxis zu analysieren, wurde eine Fallstudie über die langfristige maximale Strukturantwort einer Offshore-Windkraftanlage durchgeführt. Die Fallstudie konzentrierte sich auf die Frage, wie genau Umweltkonturmethoden extreme Lasten schätzen können, die zur 50-Jahres-Strukturantwort führen. Es wurde festgestellt, dass Schätzungen, die auf Umweltkonturmethoden basieren, zu einer starken Unterschätzung der extremen Strukturantwort führen können. Dabei tragen verschiedene Quellen zum Gesamtfehler bei. In der Fallstudie war der Fehler aufgrund der Vernachlässigung der kurzfristigen Variabilität der Strukturantwort besonders groß. Das Ignorieren der kurzfristigen Variabilität führt zu einer Unterschätzung von bis zu 28 % der wahren 50-Jahres-Strukturantwort. Das deutet darauf hin, dass in der Zukunft die internationale Norm, die die Auslegung von Windkraftanlagen regelt, Methoden zur Kompensation der Vernachlässigung der kurzfristigen Variabilität aufnehmen sollte.

Abschließend werden Themen für zukünftige Forschungen vorgeschlagen. Es wäre interessant zu untersuchen, welche Physik erklärt, warum Beobachtungen der signifikanten Wellenhöhe in etwa einer potenzierten Weibull-Verteilung folgen. Eine weitere interessante Frage ist, wie das aktuelle Wissen über den Klimawandel in die Methoden zur Definition extremer Belastungen einfließen könnte. Schließlich wird die Idee diskutiert, die Konturmethode auch in anderen Feldern als der Strukturauslegung einzusetzen. Im Allgemeinen beschreiben Konturen gemeinsame Extreme, die als Anforderungen im Entwurfsprozess dienen. Solche Konturen könnten auch im Feld der Ergonomie nützlich sein, um Anforderungen für Variablen wie Körpergröße und Hüfthöhe zu definieren. Potenziell könnte eine allgemeine Methodik für die Ableitung von extremen Produktentwicklungsanforderungen entwickelt werden, indem die Felder der Produktentwicklung und der Extremewertstatistik miteinander verbunden werden.

ACKNOWLEDGEMENTS

November 17, 2021

A doctoral project does not happen in isolation. While it helps one to become an independent researcher, it is also a team project. My co-authors, colleagues, students, friends, and family supported me to finish this multi-year project. The next two pages are devoted to thanking these people.

First, I would like to thank my doctoral supervisor, my *Doktorvater* Klaus-Dieter Thoben. Thank you for offering me the chance to join your group at University of Bremen, for giving me the freedom to let me pick a thesis topic independently, for introducing me to the research community on product development, for your skillful mentoring, and generally for being open to all kinds of unconventional ideas: a research stay in Singapore, a thesis topic that connects your group's expertise in the field of engineering design with some fields which were more distant to our group such as extreme value statistics and ocean engineering and even ideas that luckily did not materialize such as writing this thesis as a textbook.

I am also very grateful to some senior academics. Thank you, Joachim Peinke, for inviting me to give a talk at the ForWind seminar and for agreeing to review this thesis. Your questions after the seminar helped me see my work from new angles and I am looking forward to the discussion during the *Kolloquium* with you. Lucienne Blessing, thank you very much for the wonderful summer school you organized and for welcoming me warmly at SUTD. Your way of thinking about design research is clear, your knowledge of the literature extensive, and your cheerful sentiment infectious. Jan-Hendrik Ohlendorf, many thanks for providing me the chance to work in your group, for offering me interesting research projects to work on, for your advice on research and engineering, and for always being open for new ideas and making much possible: your support of my stay in Singapore, of new research projects that I proposed, and of the idea of Aljoscha and myself to start a company is highly appreciated.

When I was planning my thesis project, I was offered the chance to discuss my ideas with distinguished professors from the field of product development: Beate Bender and Dieter Krause, thank you very much for offering me your time and for the productive discussions that helped me plan my doctoral project. Raimund Rolfes, Jan Häfele, and Clemens Hübler, thank you for inviting me for a fruitful discussion to Hanover in the beginning of my doctoral project. Erik Vanem, thank you for helping me with questions about modeling the offshore environment when I started getting into the topic and for good discussions on the environmental contour method. Sverre Haver, thank you for sharing your knowledge on the history of the contour method.

Ryan Coe, meeting you at OMAE 2018 and our discussions there went a long way: We organized the benchmarking exercise on environmental contours, and we collaborated on developing software that supports engineers who design offshore structures. Thank you for making this happen. Your can-do attitude and your positivity are great. Lance Manuel thank you for joining in on the benchmarking effort, for our discussions on contours, for your advice on various topics of academic publishing, and for your hands-on editing in our joint publications. Thanks also for treating me like an equal in our discussions and our collaborations: you are a distinguished professor and accomplished expert on reliability and offshore wind turbines and I was a doctoral researcher who just joined the field. Vincent Neary many thanks for inviting me to join you on the project to develop the “Design Load Case Generator” and for the fruitful discussions we had during the project

on sea states, extreme values, and structural design. Aubrey Eckert, Nevin Martin, Phong Nguyen – thank you very much for our collaboration on the benchmarking exercise. Ed Mackay, we met at OMAE 2019 where I tried to convince you to join this exercise. I would have never expected that we would collaborate on multiple papers in the next years. I learned much from your deep knowledge about statistics and your exquisite writing style. Thank you very much for our collaborations and for the good and fun discussions we had – so far mainly on video calls. Werner Wosniok, many thanks for your skillful introduction to advanced statistics in the beginning of my doctoral project.

André, Aljoscha, Dennis, Fabian, Hendrik, Jan, Likith, Marvin, Marit, Micha, Michael, Maite, Stephan, Thimo, thank you very much for the companionship we had and have as colleagues. Micha, thanks for being such a great office mate. Starting from our 6 (?) square meters office, moving into the IW 1/2 building, and then escaping to work from home when Covid stroke, having you on the other side of the table was pleasant, helpful, and fun. The evening at Hamburg's Wind Energy Conference was unforgettable. Aljoscha, the ride since we became colleagues has been amazing. Our joint work on research projects, your fresh and bold views on research and work culture were enriching. Then we even founded a company. Thanks for the amazing ride and for your contributions to this thesis. Vladimir Vutov, thank you very much for the fruitful discussions in the GW2 cafeteria we had on how to evaluate a distribution's goodness-of-fit. Lena, dear sister, thanks a lot for your constructive feedback on the wave height study and on parts of my dissertation. Andrew, Aljoscha, Hendrik, and Kai, many thanks for reading and commenting on drafts of my thesis!

Part of the joy and of the learning experience of a typical German engineering doctoral training is advising, supervising, and mentoring Bachelor's and Master's students. I was lucky that some fantastic students joined the work on my research projects. Malte Frieling, Lena Ströer, and Kai Windmeier, I got to know you early in your Bachelor's studies and we are still working together. Thank you for your contributions to this thesis. Malte, you fully mastered wind turbine simulation with OpenFast over the years and your ability to work independently and conscientiously is highly appreciated. Lena and Kai, I enjoyed our teamwork on the DLC Generator and on virocon. Lena, your willingness to enthusiastically move into various topics of wind energy and Kai, your programming skills, and your ability to communicate well, are remarkable and they contributed to this thesis. Thanks! The software virocon that you two worked on and which is described in this thesis was and is a true team effort. I would also like to thank Filip Barl, Adrian Drewinski, Jannis Lehmkühl, and Tobias Pape for their contributions to the software.

Finally, there are people who did not directly contribute to this thesis, but who I am very grateful nevertheless and who might have enabled me to start or finish this doctoral project. Albert Baars, you are a great professor and teacher of physics. Your teaching encouraged me to move further towards science and engineering. Thanks! Jane Wang, many thanks for warmly welcoming me in your lab at Cornell University while I was a curious but inexperienced undergraduate student. The time in your lab made me want to become a researcher. Your mentoring, your enthusiasm, your high standards for analytical thinking and publications, your friendliness and respect, impressed me and shaped my view of how science should be conducted. Mama, Papa, you always supported my education, also my wish to leave Austria for it. Thanks! Steffi, you supported me over the complete duration of this doctoral project, even when I had regular late-night sessions in my home office in our bedroom during the Covid pandemic. Thank you!

CONTENTS

1	INTRODUCTION	1
1.1	Motivation	1
1.2	Problem description and research goal	3
1.3	Research approach and structure of this thesis	3
2	THEORETICAL BACKGROUND AND LITERATURE REVIEW	7
2.1	Engineering design theories and methodologies	7
2.2	Extreme values in engineering design	15
2.3	Designing offshore structures	18
3	LONG-TERM DISTRIBUTION OF THE SIGNIFICANT WAVE HEIGHT	39
3.1	Introduction	39
3.2	The exponentiated Weibull distribution	41
3.3	Research methodology	41
3.4	Results	44
3.5	Discussion	50
3.6	Conclusions	53
4	JOINT DISTRIBUTION OF WIND SPEED, WAVE HEIGHT, AND WAVE PERIOD	55
4.1	Introduction	55
4.2	Research methodology	56
4.3	Results	59
4.4	Conclusions	71
5	ENVIRONMENTAL CONTOURS FROM HIGHEST DENSITY REGIONS	73
5.1	Introduction	73
5.2	Highest density contour	79
5.3	Examples	82
5.4	Conclusions	96
6	SUPPORT FOR THE DESIGN PROCESS	99
6.1	Methodology to determine design loads	99
6.2	Software implementation	102
7	CASE STUDY: STRUCTURAL DESIGN OF AN OFFSHORE WIND TURBINE	113
7.1	Introduction	113
7.2	Estimating the long-term extreme response	114
7.3	Research methodology	122
7.4	Results and discussion	135
7.5	Conclusions	144

Contents

8 CONCLUSIONS AND OUTLOOK	147
8.1 Main findings	147
8.2 Open questions and future research	148
A APPENDIX	153
A.1 Definitions for bivariate exceedance	153
A.2 Long-term distribution of the significant wave height	156
A.3 Case study	159
BIBLIOGRAPHY	165
DECLARATIONS	185
Published papers	185
Authorship statements and collaborations	187
Würdigung studentischer Arbeiten	189
Cover page's artwork	190

1 INTRODUCTION

1.1 MOTIVATION

The majority of the Earth's surface is covered by water. Humans use the seas and oceans to ship goods, fish, and extract energy. While fossil energy is being extracted offshore since at least the 1940s [144], in recent decades humans started to extract renewable energy at sea, mainly by converting wind energy into electric energy. The first offshore wind turbine was deployed in Sweden in 1990 and had a rated power of only 220 kW [56]. Today, offshore wind turbines have power ratings of up to 14 MW and rotor diameters of up to 220 m [71, 149]. These giant machines are seen as one of the most important technologies to supply the world with renewable energy. While now offshore wind only provides 0.3% of the global electricity supply [40, p. 16], the annually added wind capacity steadily increases. In 2018 a total of 4.6 GW of new wind capacity was added [40, p. 15] and the annual added wind capacity grew by a yearly rate of nearly 30% from 2010 to 2018 [40, p. 15]. If technology's costs keep falling, offshore wind will keep growing and will play a big part in the world's future energy mix. Its energy potential exceeds the world's total electric energy demand [43] (Figure 1.1) and experts believe that costs will keep falling [266].

An important way to improve offshore wind turbines to enable them to produce electricity at lower costs is increasing their size. Designing large, reliable, and cost-effective offshore wind turbines, however, is challenging. Larger turbines become more flexible such that the interaction with the environment becomes more important. The turbine is subject to the harsh offshore environment where unsteady winds and waves are the main sources of environmental loads. These loads drive the turbine's design in the sense that the turbine's structure must be strong enough to withstand the loads but should be as light as possible because lighter structures are easier to transport, easier to install and – as they require less material – often cheaper to produce. However, wind and wave loads are difficult to predict because the weather itself is difficult to predict. Both, underestimating and overestimating wind speeds and wave heights have undesired consequences: If environmental loads are underestimated a design based on them will be unreliable and if the loads are overestimated the resulting design will be too conservative (Figure 1.2). Too conservative means that, for example, walls could be unnecessarily thick to withstand reasonable environmental loads.

Thus, to design a reliable yet lightweight offshore wind turbine, long-term environmental extremes need to be accurately predicted. Then, based on these extremes, loads can be estimated, which then can be used to optimize the turbine's structure to be as light as possible while withstanding these loads. In this work, we will develop a methodology that supports designers in estimating the long-term distribution of offshore environmental conditions and determining design loads based on this distribution. Since any kind of offshore structure – wind turbine, oil and gas platform, or wave energy converter – is subject to wind and wave loads and benefits from a systematic way of determining environmental loads in their design process, the methodology will be applicable to different kind of structures. However, throughout the thesis, we will pay special attention to the design of offshore wind turbines.

1 Introduction

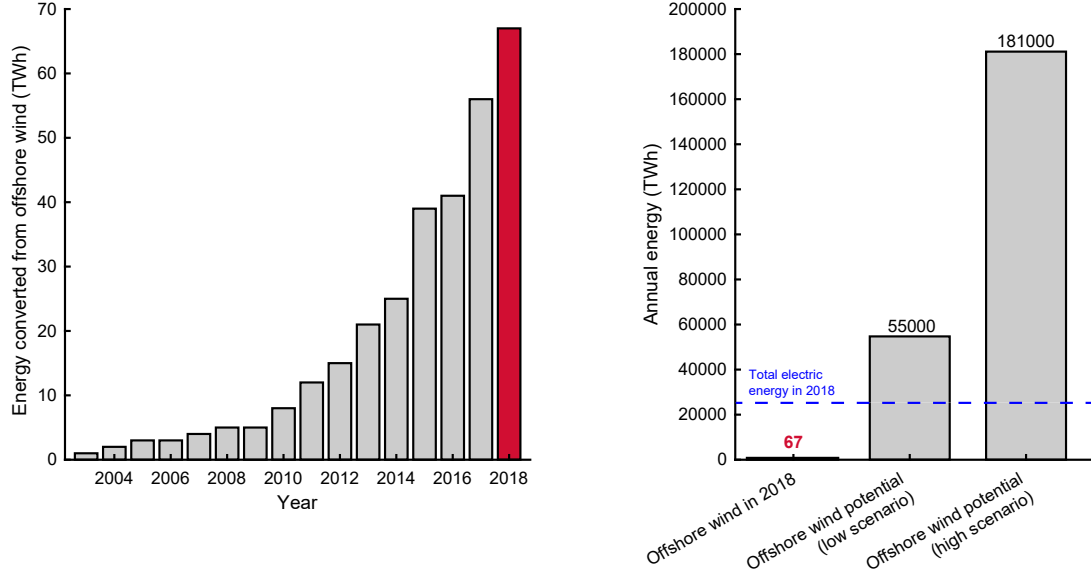


Figure 1.1: Energy converted from offshore wind has steadily increased in recent years. Despite this, it provided only 0.3% of the global electric energy supply in 2018. The potential for offshore wind exceeds the current global electricity demand. Data sources: Historical data from [131], energy potential from [43], total electric energy generation from [242].

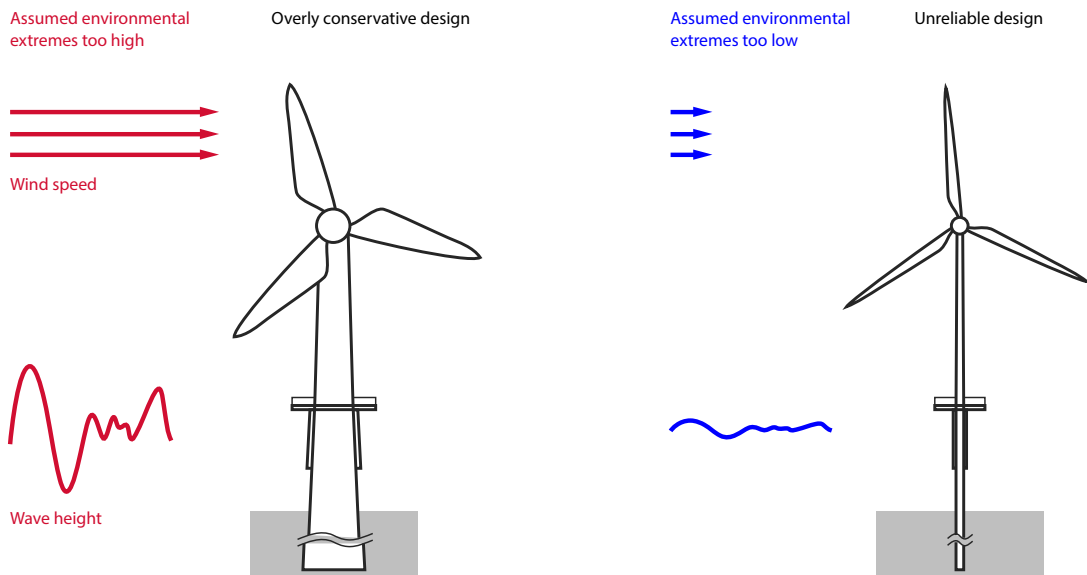


Figure 1.2: The design of an offshore structure is driven by assumed design loads, which are based on inferred long-term extreme values of wave height and wind speed. Overestimated design loads lead to an overly conservative design (left) and underestimated design loads to an unreliable design (right).

1.2 PROBLEM DESCRIPTION AND RESEARCH GOAL

Offshore structures have been designed for many decades and most of these structures appear to survive the typical environmental loads just fine. Does that mean that current design methodologies are complete and smoothly guide designers through the process of estimating extreme environmental conditions and determining design loads? Interestingly, current design guidelines and standards are relatively vague at important steps regarding this process.

An important step in determining design loads is to choose a model that represents the true long-term distribution of offshore environmental conditions. Engineering guidelines such as the widely used “recommended practices” on environmental conditions and environmental loads by the classification society DNV [47] lay out different options for modeling a single variable, like significant wave height or wind speed, without recommending one model over the other. Important standards such as the International Electrotechnical Commission’s (IEC) standard on the design of offshore wind turbines [129], recommend that a joint distribution of wind speed and wave height shall be estimated, but do not recommend which form this model shall have. Of course, an informal “common practice” exists, and this common practice – with its models and their problems – will be reviewed in Section 2.3. Nevertheless, caution and the lack of authoritative guidance that the authors of offshore standards and guidelines use, seems to be appropriate as it reflects the state of research in the field: The scientific literature does not contain a generally accepted model for the long-term distribution of the significant wave height and offers even less agreement for the joint distribution of variables like wind speed and wave height.

This lack of fundamental knowledge is likely responsible for the gaps in guidelines for the design process of offshore structures. Gaps concern (1) the choice of distribution for the significant wave height; (2) the choice of distribution for the joint distribution of wind speed, significant wave height, and wave period; and (3) which type of joint extremes of environmental variables should be used to estimate appropriate design loads.

The goal of this thesis is to address these three gaps in current design guidelines by providing new fundamental knowledge on the distribution of offshore environmental conditions and on the pitfalls of choosing joint extremes for the estimation of design loads. Then, this new knowledge shall be used to create a “design support” for engineers (Figure 1.3): A novel methodology to determine design loads for offshore structures will be proposed and its methods and models will be implemented as a software package. The goal of the methodology and the software is to provide support to engineers who design offshore structures. It should help them to better define extreme loads that an offshore structure must survive in order to reach a given target reliability. Finally, a case study on the design of an offshore wind turbine will be conducted.

1.3 RESEARCH APPROACH AND STRUCTURE OF THIS THESIS

As this research aims to develop a methodology and software that support engineers who design offshore structures, it can be characterized as “design research.” Blessing and Chakrabarti [19] proposed a methodology for design research projects that can be applied to any research that deals with design, where they describe design as “those activities that actually generate and develop a product from a need, product idea or technology to the full documentation needed to realize the product and to fulfill the perceived needs of the user and other stakeholders.” In their design research methodology (DRM) framework, they classify design research into four stages: research clarification, a first descriptive study stage, a prescriptive study stage, and a second descriptive study stage (Figure 1.4). They argue that different research projects could contain different combinations of these research

1 Introduction

stages. Within their framework, this thesis would be a type 5 research project: Based on a review-based research clarification, a comprehensive descriptive study is conducted with the goal being a better description of the offshore environment. Then, a comprehensive prescriptive study will be conducted, where the outcome is a design support (the methodology to determine design loads and the software that implements the methodology). Finally, an initial descriptive study that deals with designing an offshore wind turbine will be used to evaluate the design support.

The structure of this thesis is based on the four research stages that are apparent in this work: Chapter 2 comprises the research clarification; Chapters 3 and 4 present the first descriptive study which aims to generate understanding about the probability distribution of offshore environmental conditions; Chapter 5 investigates how joint extremes can be selected based on a given probability distribution; Chapter 6 describes the outcome of the prescriptive study, the developed methodology to determine design loads and its software implementation; and Chapter 7 comprises the second descriptive study: a case study on the structural design of an offshore wind turbine. Finally, Chapter 8 will provide conclusions for the overall findings and provide an outlook for future research. Thereby the macrostructure of this thesis follows the so-called “traditional: complex” theme that is described by Paltridge [204]. Under this theme, after a general introduction and literature review, multiple individual studies are presented, each of them containing an introduction, a methods section, a results section, and a discussion.

Some of these studies were published in journals (Chapters 3, 5, and 7, as well as parts of 6) or in conference proceedings (Chapter 4). While the author of this thesis is the first author of these publications, important contributions were made by co-authors. The acknowledgement section and a contribution section describe how other researchers contributed to this thesis. Note that many sections in this thesis have been largely left unchanged from the original publications to avoid unnecessary reformulations and to avoid having two conflicting versions of conducted studies in the scientific record. Brief statements at the beginning of chapters state upon which publications they are based.

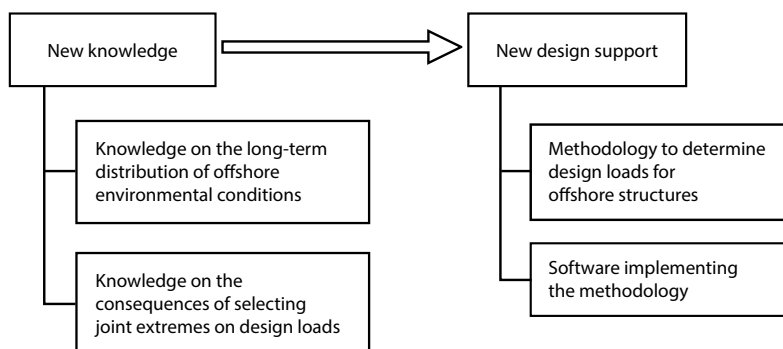


Figure 1.3: The goal of this research is to gain new knowledge on the long-term distribution of offshore environmental conditions and in selecting joint extremes of environmental variables. This knowledge shall be used to develop a “design support” for engineers, in particular, a methodology to determine design loads for offshore structures and software that implements this methodology.

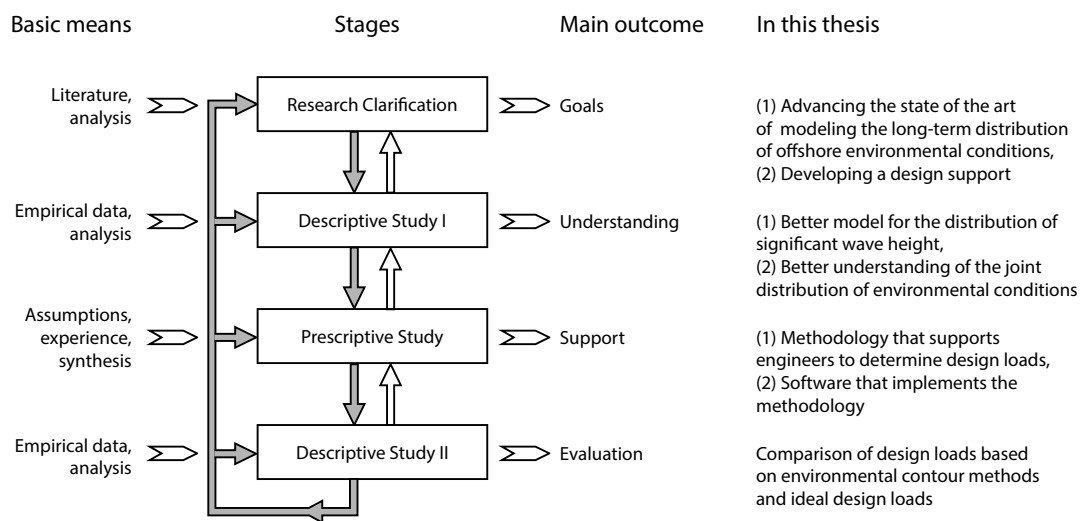


Figure 1.4: Design research methodology framework after Blessing and Chakrabarti [19] and the main outcomes of the research project described in this thesis.

2

THEORETICAL BACKGROUND AND LITERATURE REVIEW

This thesis deals with designing offshore structures that withstand extreme environmental loads. In this chapter we will lay out the theoretical background of the three main areas that are touched by the thesis: designing (Section 2.1), extreme values (Section 2.2), and offshore structures (Section 2.3).

2.1 ENGINEERING DESIGN THEORIES AND METHODOLOGIES

2.1.1 SYSTEMATIC ENGINEERING DESIGN

Engineering design deals with the creation of artifacts. The process of creating these artifacts, the design process¹, plays a vital role in the way companies bring new products to market. From a broad perspective, the design process has great importance how humans shape the world: Everything artificial – opposed to the natural – was created via some form of this process.

Design researchers have developed models of the process, either based on empirical studies or based on a prescriptive approach with the goal of supporting the process. A great variety of models of the design process have been published, including Pahl and Beitz's engineering design methodology (Figure 2.1; [203]), which arose from mechanical engineering, Gero's more abstract general-purpose design process model [72, 73], and the V-model [214], which is now often associated with systems engineering [36, 226]. Some models focus on specific aspects of designing, like Albert and Burzac's product generation engineering approach [3, 4] or Krause and coworkers' approach to develop modular product families [143]. Researchers have also proposed design methodologies for specific artifacts such as offshore wind turbines [33, 146] and the design process of offshore structures will be described in detail in Section 2.3. A recent extensive review on the wide range of general-purpose design process models is provided by Wynn and Clarkson [269].

In addition to research that focuses on the design process, researchers have attempted to create theories that deal with the description of artifacts and their creation more broadly. These theories include Hubka and Eder's theory of technical systems [120], Suh's axiomatic design [233, 234], and Hatchuel and Weil's C-K theory [105, 106]. Statistics-based approaches – a category to which this thesis will add to – include reliability-based design [165], robust design [29, 276] and design for six sigma [271]. A recent overview of theories and models of design is provided in a book edited by Chakrabarti and Blessing [28].

Usually, a design project starts with a high-level description of requirements, and it is considered a task within the design process to refine these requirements. In the popular engineering design methodology by Pahl and Beitz [203] the refinement of requirements is part of the stage “planning and clarifying the task.” The outcome of this stage is a “requirements list” that holds a set of individual requirements. Requirements describe desired properties of a product and might deal with such

¹Here, for simplicity, we use the term “design process” instead of the longer term “design and development process.” However, any activities that some might consider to be rather called “development” instead of “design” are meant to be included in our use of “design process.”

2 Theoretical background and literature review

diverse aspects as function, geometry, aesthetics, law conformance, manufacturing, and economics. The goal of the design process is to find a design solution that satisfies a set of requirements (see, for example, [230, 259]).

Note that requirements are usually not static during the design process, as for example shown by Almefelt et al. [5]. They found that in a design project in the car industry requirements were adjusted, new requirements were created, and old requirements were discarded regularly. Fernandes et al. [60] analyzed the causes for requirement changes at the aerospace company Rolls-Royce. The three most common causes were that a previous description of a requirement was incomplete, that traceability links or references changed, and that the customer changed the requirement.

McKay et al. [171] developed a representation scheme that can be used as a data structure for requirements. Their work is based on the structure for a requirements list that was proposed by Pahl and Beitz [203] and their representation can be summarized as follows: a requirements list has multiple groups of requirements, and each requirement comprises (among others) a requirement context and a requirement value. A requirement value can be either a quality, a quantity, or a reference to a standard [171].

Note that some authors use terms different than “requirement list” including “product specification” [171] and “product requirements document” [60] and these terms could have slightly different meanings. In this work, we use the term “requirements list” and define it simply as a list of all requirements, where a “requirement” is a condition that a design must fulfill to be satisfactory. We choose to represent requirements in a very simple form: each requirement has one or multiple requirement values and a textual description (Figure 2.2). Of course requirements could be represented using a more detailed structure as demonstrated, for example, by McKay et al. [171], Chen and Zeng [32], Chen et al. [31] and Weissman et al. [262], but these details are not relevant for the goal of this research.

In this work, we are concerned with a particular kind of requirement: the requirement that an offshore structure must withstand a particular combination of environmental conditions. The goal of the design process is to create a design that among others fulfills this kind of requirement. Methods that support designers in defining environmental conditions, estimating loads based on these conditions and designing a structure that withstands these loads are being developed and analyzed in the field of structural design.

2.1.2 STRUCTURAL DESIGN: LOAD, RESPONSE, AND RELIABILITY

The goal of structural design is to create a structure that withstands the loads that can be expected to occur during the structure’s lifetime. The structure’s “response” to these loads must be below a given response threshold, sometimes called the “response capacity.” Loads of many structures are dominated by environmental variables such as wind speed and wave height, which can be well described as random variables. Thus, structural design makes heavy use of probability theory and we shall introduce some mathematical notation before we describe the main concepts of structural design.

Throughout this thesis, we will use upper-case letters to describe random variables and lower-case letters for the realizations of random variables. Let X be a random variable and x its realization. Then

$$F(x) = \Pr(X \leq x) = p \quad (2.1)$$

is the variable’s distribution function, $f(x)$ its density function and $Q(p)$ its quantile function:

$$Q(p) = F^{-1}(x) = \min\{x : F(x) \geq p\}. \quad (2.2)$$

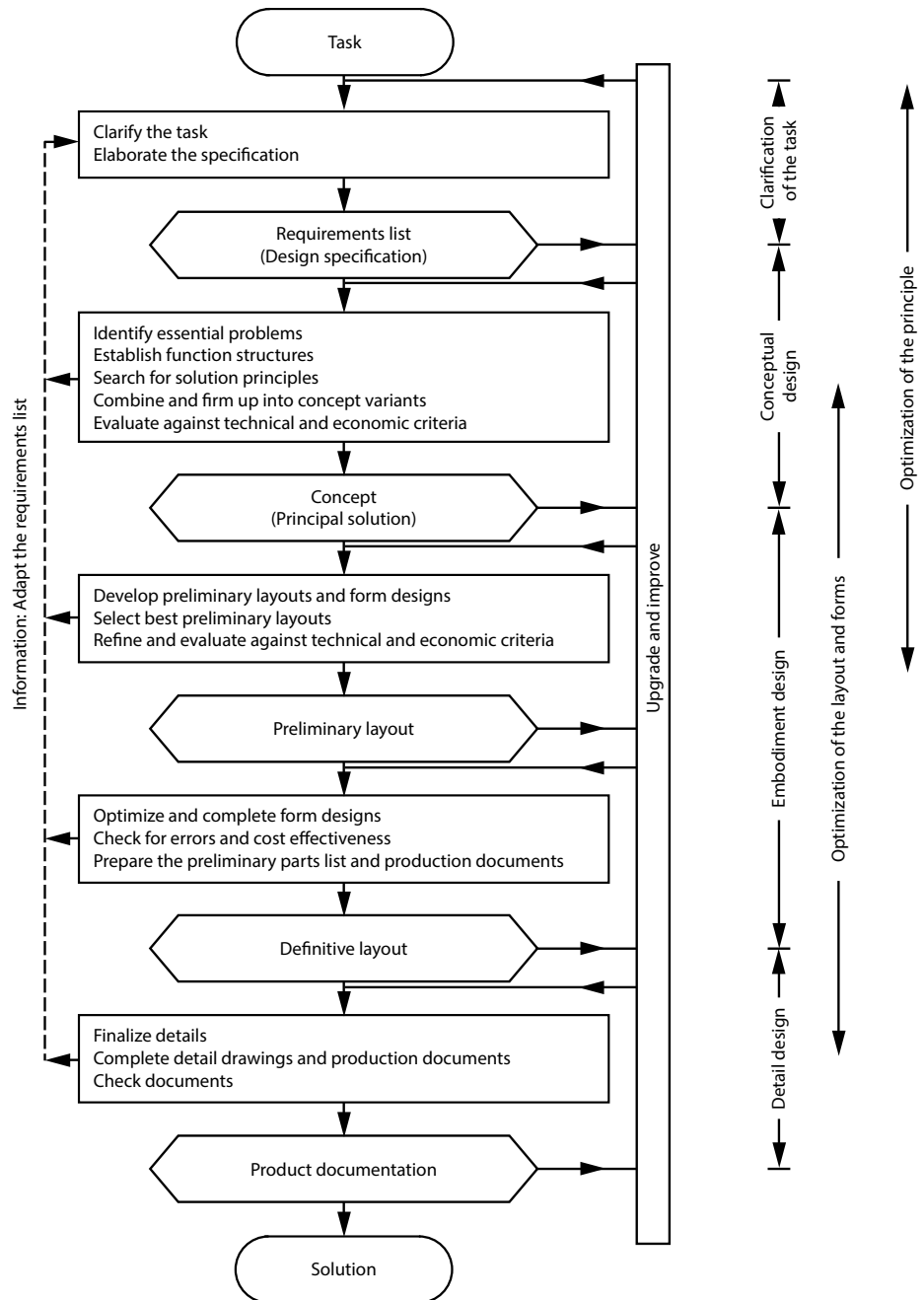


Figure 2.1: Pahl and Beitz's description of the design process (adapted from [203] and [173]).

2 Theoretical background and literature review

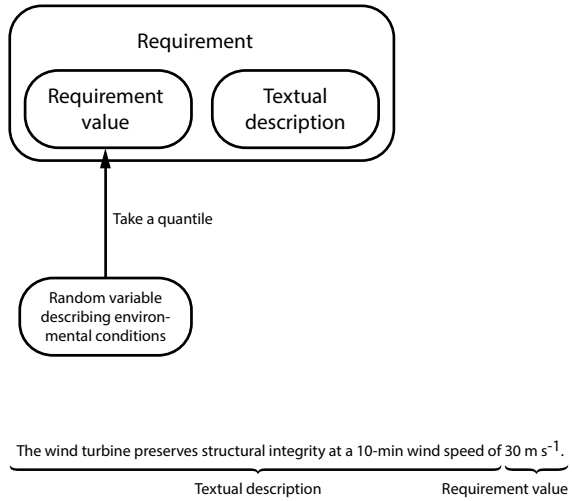


Figure 2.2: Representation of a requirement in this work. An environmental condition such as wind speed is described as a random variable. That means that a probability distribution function associated to wind speed needs to be established. To describe a requirement, a quantile of the environmental conditions is used by evaluating the inverse distribution function at a given exceedance probability. This quantile serves as a “requirement value.” A textual description and a requirement value constitute a requirement.

As described, environmental conditions like wind speed and wave height are often modeled as random variables. Let X represent an environmental variable that dominates the loads acting on a structure. Then, load and response can also be conveniently expressed as random variables such that the mathematics of structural design can be summarized as

$$R = h_1(L) = h_1[h_2(X)] \quad (2.3)$$

where R is the response, L is the load, X is the environmental variable, h_1 is the function that transforms L to R , and h_2 is the function that transforms X to L . Note that a response can be a variety of different quantities – it is simply the effect of a single load or a combination of loads on a structural component or system, for example, internal force, stress, strain, displacement or motion (following the definition used in IEC’s standard on offshore wind turbines [129], which uses the term “load effect” instead of “response”). Figure 2.3 presents an illustration of the three random variables: environment X , load L , and response R .

The relationship between the environment, the load, and the response can also be written for the random variable realizations such that the realized response r is:

$$r = h_1(l) = h_1[h_2(x)], \quad (2.4)$$

or rewriting $h_1[h_2(\cdot)]$ as a response function $h(\cdot)$ that directly relates an environmental variable to a response quantity:

$$r = h(x). \quad (2.5)$$

A structural design is considered good if the response r to a given environmental condition x is below the response capacity r_{cap} . Based on the response capacity, two states can be differentiated:

- If the response is less than the capacity, $r < r_{cap}$, the structure survives and

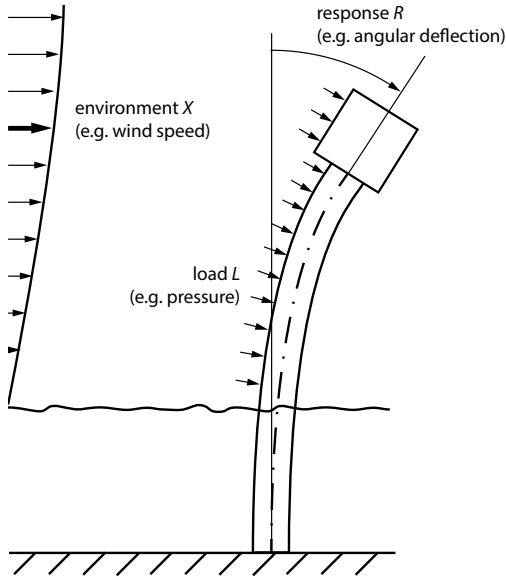


Figure 2.3: Illustration of the three random variables environment X , load L , and response R . In this example wind (the environment) causes pressure forces (the load) which leads to angular deflection of the tower (the response).

- if the response is greater than or equal to the capacity, $r \geq r_{cap}$, the structure fails.

Then the structure's reliability p_R can be calculated as the probability that the response to a random environmental condition is less than the response capacity:

$$p_R = \Pr(R < r_{cap}) = \Pr[h(X) < r_{cap}]. \quad (2.6)$$

Often a target reliability $p_{R,target}$ is prescribed as a requirement, meaning that the structure's reliability p_R must be greater than or equal to this target reliability value:

$$p_R \geq p_{R,target}. \quad (2.7)$$

Vice-versa the probability of failure in a random environmental condition, p_F , must be less than the target probability of failure $p_{F,target}$:

$$p_F = 1 - p_R < p_{F,target}. \quad (2.8)$$

The environmental random variable X usually describes environmental states, meaning that a realization x represents a characteristic value of an environmental phenomenon during a given state duration T_S . Since each realization has an associated duration, a reliability target also has an associated duration.

Generally, a “return period” or “recurrence period” describes the average time between two consecutive events that exceed a threshold. If one is interested in events that result in failure, the return period at which failures occur is defined as:

$$T_R = \frac{T_S}{p_F}, \quad (2.9)$$

2 Theoretical background and literature review

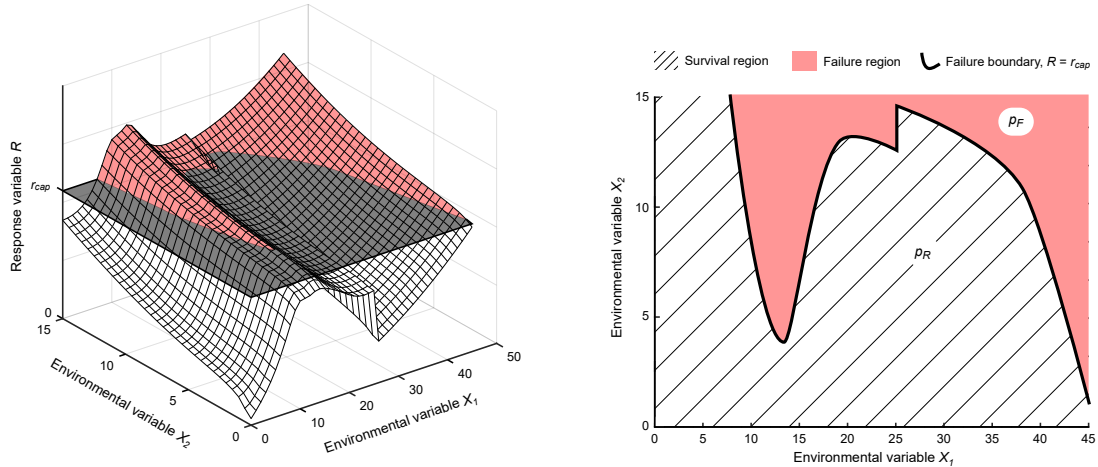


Figure 2.4: Environmental variable space (X_1, X_2) separated into failure and survival regions. At environmental states within the failure region the structure's response exceeds the structural response capacity r_{cap} resulting in failure. The probability content contained in the survival region is the structure's reliability p_R and the probability content contained in the failure region is the failure probability p_F .

where T_S and T_R are given in the same units of time and it is assumed that the environmental states of duration T_S are independent and identically distributed (this assumption will be discussed later). The return period is generally much larger than the sea state duration, $T_R \gg T_S$. Typically, the return period is in the order of years while the state duration is in order of minutes or hours. The probability of failure p_F is a probability and is dimensionless.

Similarly, the target return period, $T_{R,target}$, relates to the target probability of failure:

$$T_{R,target} = \frac{T_S}{p_{F,target}}. \quad (2.10)$$

Many structures experience loads that arise from a combination of environmental variables. For example, both, winds and waves, cause high loads on an offshore wind turbine. In such a case, it is typical to describe the environment using a random vector $\mathbf{X} = (X_1, X_2, \dots, X_d)^T$ with $d \in \mathbb{N}$ being the number of load-relevant environmental variables.

When at least two environmental variables are load-relevant, it is often interesting to analyze at which region in the environmental variable space a structure fails and at which it survives. The region that covers environmental states that cause structural failure is called “failure region” and the region that covers environmental states that lead to responses that are acceptable is called “survival region” [165, p. 9] (Figure 2.4). These two regions are separated by environmental states that cause a response of exactly the response capacity. The set of these states is called “failure surface” or “failure boundary.”

Often, the structural response increases as an environmental variable’s quantity increases – loads usually increase as wind speed or wave height increases – such that it is often assumed that an extreme environmental condition with a return period of N years leads to a structural response with a return period of N years. This assumption is often used to ensure that a structure fulfills a given reliability

target. Let α denote the exceedance probability of an environmental condition. Then the N -year environmental extreme $x_{[N]}$ – sometimes also called N -year “return value” – can be written as

$$x_{[N]} = Q(1 - \alpha), \quad (2.11)$$

where

$$\alpha = p_{F,target} = \frac{T_S}{T_{R,target}}. \quad (2.12)$$

In words, the above equation states that the probability that an environmental condition is exceeded in a random event of duration T_S is the same as the target probability that the structure fails in a random event of duration T_S . Thus α is chosen based on the target probability of failure $p_{F,target}$ and α determines the requirement value $x_{[N]}$. This relationship of $\alpha = p_{F,target}$, however, does not generally hold and the reasons will be explained in the next paragraphs.

Let $\hat{r}_{[N]}$ denote an estimate for the true N -year structural response $r_{[N]}$. The true long-term structural response can be obtained by evaluating the long-term distribution of the response, which can be calculated by integrating the environment’s probability density function $f_x(x)$,

$$r_{[N]} = r : \int_{h(x) < r} f_x(x) dx = 1 - \alpha. \quad (2.13)$$

Assuming that the N -year response occurs at the N -year environmental extreme, however, yields the relationship:

$$r_{[N]} \approx \hat{r}_{[N]} = h(x_{[N]}). \quad (2.14)$$

Sometimes this simplification holds true: for a deterministic response function, $\hat{r}_{[N]}$ is exactly $r_{[N]}$ if the response function monotonically increases (Figure 2.5). If the response is non-monotonic, however, $\hat{r}_{[N]} \neq r_{[N]}$. Thus, estimating the N -year response based on the N -year environmental extreme is only justified for monotonically increasing response functions. While many response quantities do increase with environmental quantities, there are important exceptions: For example, due to the controller, the forces acting on an offshore wind turbine do not monotonically increase with wind speed. The case study to be presented in Chapter 7 will describe this effect in detail. Figure 2.5 shows one monotonic and one non-monotonic response function and how it influences the estimate $\hat{r}_{[N]}$: For the monotonically increasing response function, the estimate of the response return value is equal to the true return value ($\hat{r} = r$; Figure 2.5d), but for the non-monotonic response function, the estimate of the response return value differs from the true return value at many exceedance probabilities ($\hat{r} \neq r$; Figure 2.5e). The response is overestimated for exceedance probabilities of about 10^{-1} and underestimated for very low exceedance probabilities such as 10^{-4} or 10^{-5} . This effect is due to the peak of the response function at medium wind speed. It peaks at a wind speed value, which has a non-exceedance probability of approximately 10^{-1} . Note that if $r_{[N]}$ cannot be estimated well as $h(x_{[N]})$, assuming that $\alpha = p_{F,target}$ will result in some bias: the true probability of failure will be under- or overestimated. While Figure 2.5 shows the univariate case (only one environmental variable is considered), similar problems apply in multivariate cases. The multivariate case will be described later in this chapter, when the environmental contour method is introduced (Section 2.3.2), and in Chapter 5 where a new contour method is proposed.

In structural design, the target return period is typically in the order of years while the environmental state’s duration is typically in the order of minutes or hours such that the exceedance probability α is very small. For example, if we are considering hourly sea states and if we are interested in

2 Theoretical background and literature review

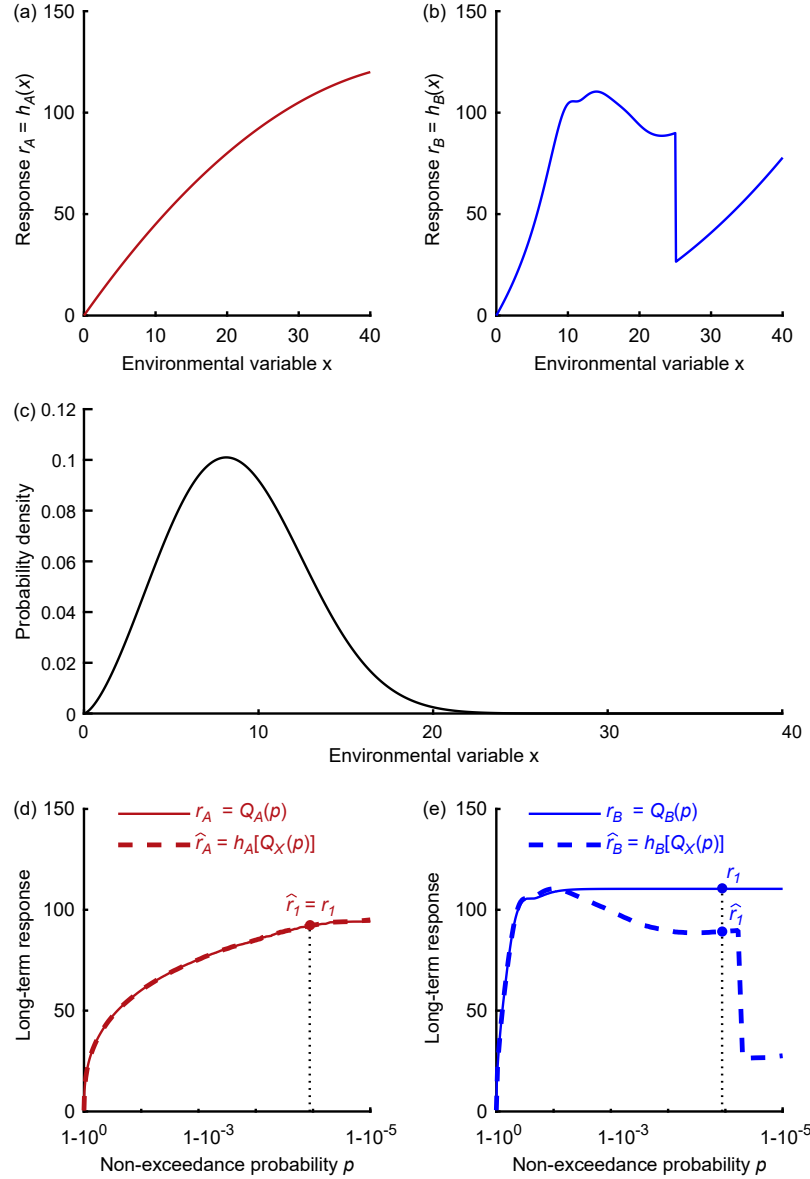


Figure 2.5: Estimating response return values from environmental return values. In this illustration, for simplicity, the short-term response functions h_A and h_B are deterministic (a, b) and the probability distribution of the environment is known (c). If the response function h monotonically increases, the long-term response's quantile $Q(p)$ equals the response of the environmental variable's quantile $h[Q_X(p)]$ (response A ; panels a, d). If the response function is non-monotonic, $Q(p)$ is not equal to $h[Q_X(p)]$ for some quantiles such as the 1-year return value r_1 (response B ; panels b, e). h_A and h_B = response functions, Q_A and Q_B = quantile functions of the long-term response functions of responses A and B , Q_X = quantile function of the environmental variable X , p = non-exceedance probability.

designing a structure with a target return period of 50 years, we would have a target probability of failure $p_{F,target}$ and consequently an exceedance probability α of

$$\alpha = p_{F,target} = \frac{1 \text{ hour}}{50 \times 365.25 \times 24 \text{ hours}} \approx 2.28 \times 10^{-6} \quad (2.15)$$

Then the 50-year environmental extreme x_{50} is

$$x_{50} = Q(1 - 2.28 \times 10^{-6}), \quad (2.16)$$

and the true 50-year response r_{50} could be approximated as the response that occurs at the 50-year environmental extreme \hat{r}_{50} :

$$r_{50} \approx \hat{r}_{50} = h(x_{50}). \quad (2.17)$$

Based on that approximation we can design a structure with a target probability of failure of $p_{F,target} = \alpha = 2.28 \times 10^{-6}$ by ensuring that it has a structural capacity of $r_{cap} = \hat{r}_{50}$. If the true 50-year response r_{50} is greater than the approximated \hat{r}_{50} , our structure will have a too high true probability of failure ($p_F > p_{F,target}$) and if the true 50-year response is less than \hat{r}_{50} , we will have a too low probability of failure ($p_F < p_{F,target}$). Thus, it is very important how r_{50} is estimated. In Section 2.3 we will describe in detail how the extreme response is typically estimated in the design process of offshore structures.

One important step in estimating the long-term extreme response of an offshore structure is modeling the probability distribution of environmental conditions. As rare environmental events often dominate the extreme response, modeling extreme values is especially important. Thus, the next chapter introduces extreme value theory.

2.2 EXTREME VALUES IN ENGINEERING DESIGN

2.2.1 UNIVARIATE EXTREMES

While many statistical methods focus on “typical” values of a variable, as described with the average or the median, extreme value theory deals with the tails of a probability distribution. It deals with very small and very large quantiles in the sense that it is concerned with $Q(p = \alpha)$ or $Q(p = 1 - \alpha)$ instead of any $Q(\alpha < p < 1 - \alpha)$ where α describes the probability of exceedance and $Q()$ the quantile function (Expression 2.2). Note that there is no generally accepted upper limit for α to call the quantile an “extreme value.” Instead, in statistics textbooks, extreme values are usually defined based on their broader meaning of being maxima or minima of time series or of subsamples (see, for example, [15, 26, 39]).

Important univariate extreme value models include distributions that arise when a sample holds maxima or minima from subsamples as well as distributions that arise when only observations above (or below) a particular threshold are considered (Figure 2.6). It can be mathematically shown that these extreme value distributions arise when the considered extremes are independent and identically distributed (IID). If the underlying data are time series that describe the dynamics of a system such as the response of an offshore structure, making sure that the extremes are indeed IID can be difficult. If maxima of subsamples are considered, it requires defining the block length of which maxima are taken and if peaks over a threshold are considered, it requires choosing an appropriate threshold. Both, selecting a block length and a threshold, represents a decision where one needs to balance the amount of data points one obtains from the original time series (longer blocks mean less data

2 Theoretical background and literature review

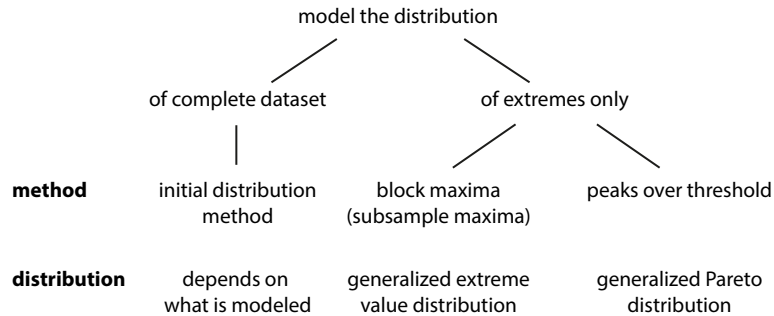


Figure 2.6: Approaches to model extreme values.

points) versus the degree of independence of the resulting extremes (longer blocks mean stronger independence).

Extremes of subsamples can be described using the generalized extreme value distribution:

$$F(x) = \begin{cases} \exp\left(-\exp\left(-\frac{x-\mu}{\sigma}\right)\right), & \xi = 0, \\ \exp\left(-\left(1 + \xi \frac{x-\mu}{\sigma}\right)_+^{-1/\xi}\right), & \xi \neq 0, \end{cases} \quad (2.18)$$

where $(\cdot)_+ = \max\{\cdot, 0\}$. The distribution has three parameters: a location parameter μ , a scale parameter σ and a shape parameter ξ . It generalizes the Gumbel distribution (which has $\xi = 0$) the Fréchet distribution ($\xi > 0$) and the reversed Weibull distribution ($\xi < 0$).

Observations above a threshold are typically described using the generalized Pareto distribution. This distribution also has three sub-families, which relate to the sub-families of the generalized extreme value distribution. For further reading, the reader is referred to the textbook by Castillo et al. [26] that introduces extreme value theory for engineers and scientists.

As an alternative to distributions that only describe extremes, “global models” that describe the full range of data can be used to estimate extreme values. Global models often provide worse model fit at the distribution’s tail, but avoid the problem of dealing with multiple, possibly deviating models for a single dataset when designers are interested in both, typical and extreme values. Currently, global models are widely used in engineering. For example, in structural engineering maximum values of the wind speed are often obtained by fitting a Weibull distribution to a global dataset (see, for example, [155]). This approach of modeling is sometimes called the initial distribution method (see, for example, [47, section 3.6.1.4]).

2.2.2 MULTIVARIATE EXTREMES

In multivariate cases $\mathbf{X} = (X_1, \dots, X_d)^T$, $d \in \mathbb{N}$ denotes the random vector that comprises d random variables. Its associated joint distribution function is $F(\mathbf{x})$ and its density function is $f(\mathbf{x})$. Like univariate extreme value theory, multivariate extreme value theory provides plenty of statistical models for extremes (see, for example, Beirlant et al. [15] for an overview).

However, while the distribution function and the density function – similar to the univariate setting – are uniquely defined, the multivariate quantile function can be defined in various ways. There is no single quantile function that is preferred by statisticians, and researchers are actively proposing definitions for quantiles [55, 87]. Because extreme values are defined with the quantile function [15] (Expression 2.2), no unique definition for multivariate extremes exists.

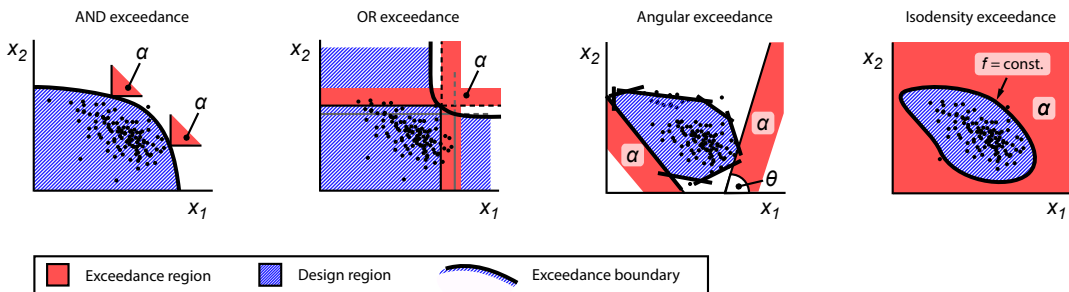


Figure 2.7: Sketches of possible definitions for bivariate exceedance. Although each exceedance region holds the same amount of exceedance probability α the resulting design regions (hatched areas) greatly differ.

Consider bivariate exceedance. In the bivariate case an “exceedance boundary”² separates the two-dimensional variable space into a non-exceedance region and an exceedance region (Figure 2.7). In this work, we call the region that is not exceeded by one or multiple exceedance regions “design region” (Figure 2.7). We can find several regions of exceedance that contain probability α , each based on a different definition. However, depending on the context one definition could fit better than another. Suppose we are interested in maximum ocean wave heights at different wave periods. Let the random variables X_1 and X_2 describe wave period and wave height respectively. In this context it might be useful to define a set of bivariate maxima – an exceedance boundary – by searching for the curve of constant probability density that is exceeded in X_2 -direction with a probability of α . Such a curve holds joint extremes of wave height and period – with high values of the wave height, X_2 , and associated values of the period, X_1 . A similar definition has been proposed by Haver [109, 110].

Now consider that we are not primarily concerned with high values of one variable, but of both variables. Then, it might be more advantageous to define bivariate maxima by defining exceedance using two thresholds, x_1 and x_2 : $\Pr(X_1 > x_1 \cap X_2 > x_2) = \alpha$ (AND exceedance in Figure 2.7). Serinaldi [227] presented an overview of common definitions for bivariate exceedance and proposed names for the various probabilities of exceedance.

Figure 2.7 shows four sketches of possible definitions for bivariate exceedance, which we consider to belong to the broader categories of “AND exceedance,” “OR exceedance,” “angular exceedance,” and “isodensity exceedance” (the mathematical definitions for these different exceedance probabilities are given in the appendix). Figure 2.8 presents exceedance boundaries where these four definitions were applied to the same joint distribution. Although each exceedance region holds the same amount of exceedance probability α the resulting exceedance boundaries and design regions greatly differ. In addition, the amounts of probability contained within the design regions differ: While in some bivariate concepts for exceedance the design region probability is $p_{DR} = 1 - \alpha$, other definitions yield design regions that contain less than $1 - \alpha$ probability content.

In summary, extreme value theory deals with the tails of a distribution. Models that are used to define extreme values might describe (1) the whole range of a dataset (global models), (2) the subset of a dataset that exceeds a particular threshold, or (3) the maxima (or minima) of multiple subsamples. In engineering design, extreme value theory can be used to define the boundary of a design region.

²We use the term “exceedance boundary” as it can be used irrespective of the number of dimensions of the probability distribution. The exceedance boundary can be a threshold (univariate distribution), a curve (bivariate joint distribution), a surface (three-dimensional distribution) or a hypersurface (distribution with $d > 3$ dimension). The term is used, for example, by Huseby et al. [124].

2 Theoretical background and literature review

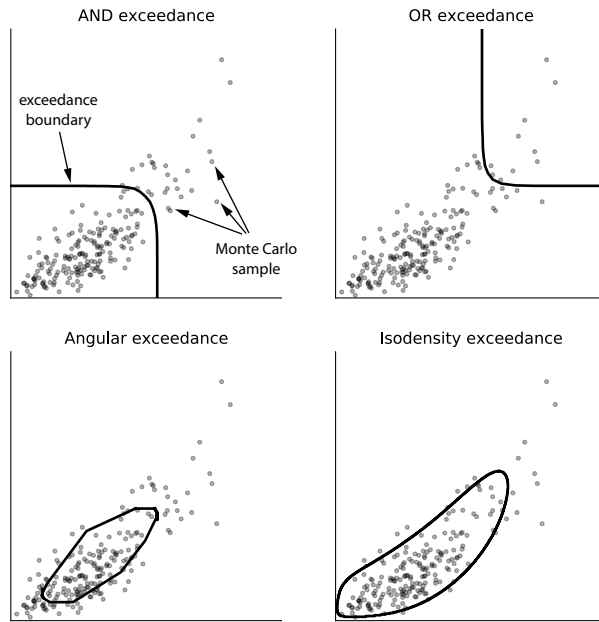


Figure 2.8: Example of different bivariate exceedance definitions and the resulting exceedance boundaries. Although all exceedance boundaries were calculated with the same value of $\alpha = 0.1$ and the same joint distribution, their shapes are vastly different.

A design region is defined in this thesis as the region in the environmental variable space that must be considered for loads. Defining the design region based on a univariate distribution is straightforward because the quantile function is uniquely defined. Defining the design region based on a multivariate distribution, on the other hand, requires further thought because alternative definitions for the multivariate quantile function exist.

2.3 DESIGNING OFFSHORE STRUCTURES

Offshore structures are structures located in the ocean, off shore. They can be grouped into (1) structures that, once installed, stay at one geographical place; and (2) structures that are in motion much of the time. Geographically fixed structures include bottom-fixed offshore wind turbines, floating offshore wind turbines, tidal energy converters, wave energy converters, bottom-fixed oil and gas platforms, floating production storage and offloading units (FPSO; these are structures used in the oil and gas industry), cross-sea suspension bridges, and floating bridges (Figure 2.9). Moving offshore structures are various kinds of vessels such as boats, container ships, bulk carriers, and oil tankers.

These offshore structures experience loads that arise from waves, currents, and – if they are not fully submerged – winds. While designing an offshore structure involves a great variety of tasks, estimating loads for the structural design is especially challenging as the ocean environment is difficult to model: Multiple environmental variables are load-relevant and these variables are quantities that describe outputs of complex physical processes. Meteorologists use today's most powerful computers to model these processes in weather and climate simulations.

As in any other design project, the process of designing an offshore structure starts with clarifying the design task and then – according to Pahl and Beitz's methodology – by defining a requirements list (Figure 2.1). If the offshore structure of interest is to be deployed at a fixed location, many requirements will be based on environmental variables at this location. For example, design standards

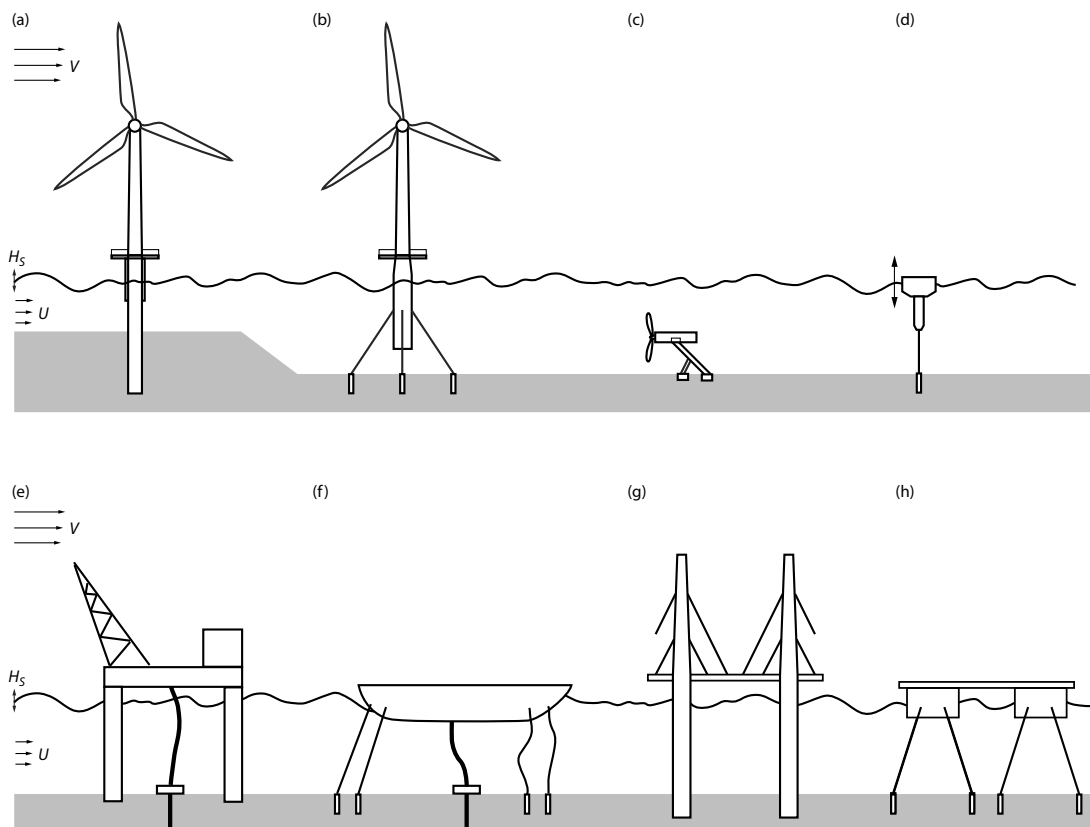


Figure 2.9: Offshore structures that, once installed, stay at one geographical place. (a) Bottom-fixed offshore wind turbine. (b) Floating offshore wind turbine. (c) Tidal energy converter. (d) Wave energy converter. (e) Bottom-fixed oil and gas platform. (f) Floating production storage and offloading unit (FPSO; an offshore structure that is used in the oil and gas industry). (g) Cross-sea suspension bridge. (h) Floating bridge.

2 Theoretical background and literature review

for offshore wind turbines [129] require structural design checks based on the site's 50-year extreme wave height. Thus, an important part of the design process is first describing the site-specific offshore environment and then deriving requirement values based upon this description. In IEC's standard on offshore wind turbines [129] these activities are summarized in the design process' step to define the "site-specific external conditions." These conditions, and other requirements, are then used to define a "design basis" for the offshore wind turbine (Figure 2.10a; [225, 260]). The term "design basis" describes a type of requirements list that is common in wind turbine structural design (see references [66, 208] for two published design bases). Then, the standard proposes that the designer creates a support structure design and a design for the rotor nacelle assembly (RNA). These designs are then evaluated using standardized load cases. Load and load affect calculations are performed and the results are used in a "limit state analysis" to check whether the support structure design and the RNA design preserve structural integrity. A limit state analysis describes the process of analyzing at which extreme environmental conditions a structure fails and which it survives using factored loads and material properties [165].

The steps of the design process of an offshore wind turbine can be generalized to describe the design process of an arbitrary offshore structure. We can organize the design process using six consecutive steps (Figure 2.10b):

1. Define the site-specific external conditions.
2. Define the design basis for the offshore structure.
3. Create a design for the offshore structure.
4. Use standardized design load cases.
5. Perform load and response calculations.
6. Perform a limit state analysis. In case structural integrity is ensured, the design is completed and in case it is not ensured the design must be altered.

The first step of this process, the definition of the site-specific external conditions, uses statistics to describe the offshore environment. The following section deals with this aspect.

2.3.1 STATISTICAL DESCRIPTION OF THE OFFSHORE ENVIRONMENT

The typical representation of the offshore environment is to assume that the long-term evolution of environmental conditions can be considered as a sequence of stationary processes [190]. That is, the random process associated with a certain environmental condition is assumed to be stationary for fixed time intervals of equal length. Common choices for the state duration are $T_S = 10 \text{ min}$, $T_S = 1 \text{ hour}$, or $T_S = 3 \text{ hours}$. The statistical description of the environment during the state duration is then referred to as "short-term statistics" while so-called "long-term statistics" are used to describe the environment on a timescale of years. Long-term statistics deal with parameters that are time-integrated over the state duration T_S like the significant wave height or the 1-hour mean wind speed. These time-integrated variables often parametrize spectra that describe the short-term statistics. The basis of the spectra could be the water surface elevation or the wind's instantaneous velocity. All environmental variables that are associated to meteorology and oceanography are often summarized as "metocean variables" in offshore structural design.

Offshore, ocean waves are the most prominent environmental phenomenon. In the statistical approach [200], for a duration of a few hours, waves are assumed to be well-described as a stationary

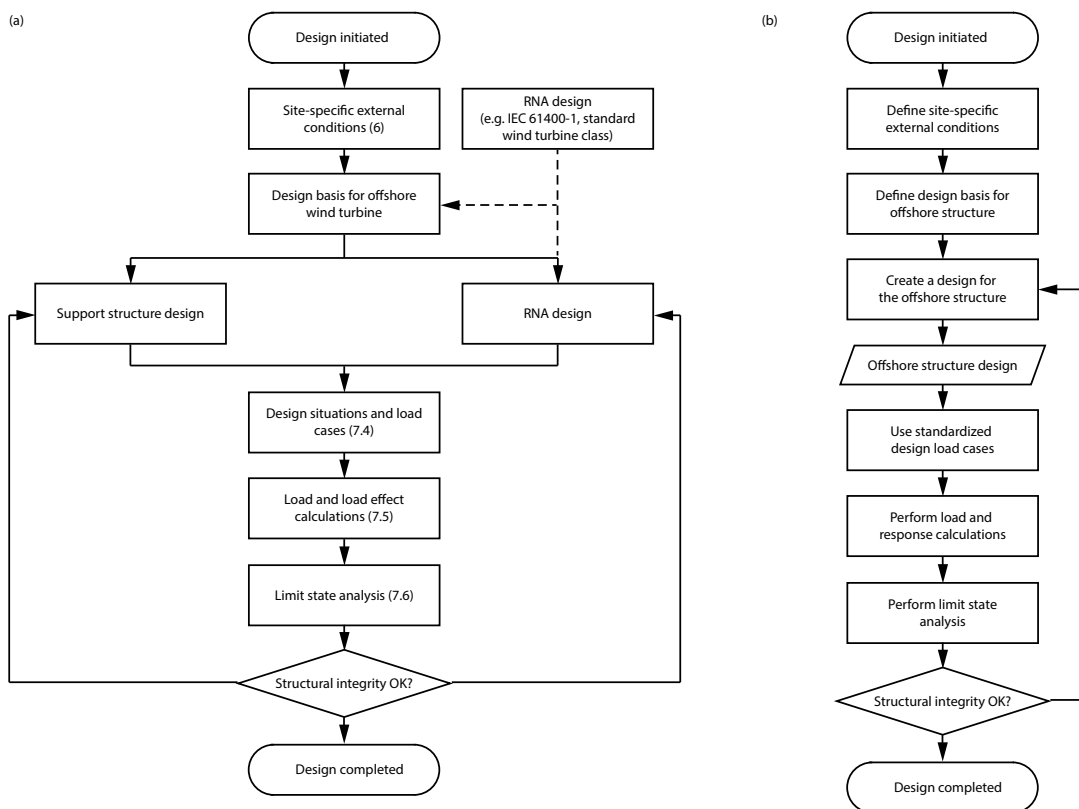


Figure 2.10: (a) The design process of an offshore wind turbine according to IEC's standard 61400-3-1 [129]. The numbers in parenthesis refer to chapters within the standard. RNA = rotor nacelle assembly. (b) Main steps when designing an arbitrary offshore structure according to the author of this thesis.

2 Theoretical background and literature review

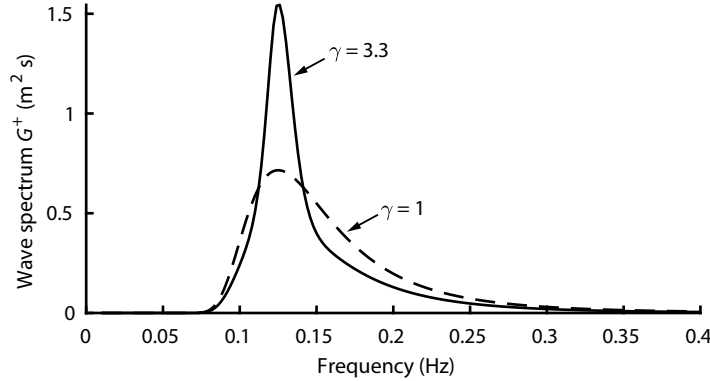


Figure 2.11: JONSWAP spectrum with different peak enhancement factors, γ . A peak enhancement factor of 3.3 is often assumed for sea states in the North Sea. If $\gamma = 1$ the spectrum becomes the modified Pierson-Moskovitz spectrum. Both plotted spectra have a peak period of $T_p = 8$ s (0.125 Hz peak frequency) and a significant wave height of $H_s = 1$ m.

process whose properties are summarized as a “sea state.” A sea state is represented using a spectrum that describes how the variance of the water surface elevation is distributed over different frequencies. Typical shapes of ocean wave spectra have been reported – among them the Pierson Moskovitz spectrum [205], which describes fully developed wind seas, and the JONSWAP spectrum [104], which describes typical sea states in the North Sea (Figure 2.11). If a spectrum is assumed to follow the Pierson Moskovitz or a JONSWAP spectrum with a given peak enhancement factor, it can be parameterized using only two variables: one variable that describes the amount of variance and one that describes a typical frequency of the sea state.

To interpret a “variance spectrum” (or as a synonym “energy spectrum,” “power spectral density,” “spectral density,” or just “spectrum” [191, p. 16]), it is useful to briefly introduce the fundamentals of what constitutes a “stationary process” and how the variance spectrum relates to properties of this process. A stationary process is a special kind of “stochastic process.” While the outcomes of a random variable are scalars, the realizations of a stochastic process are time series (Figure 2.12). Let $X(t)$ represent a stochastic process and $x(t)$ its realization. A stochastic process is (weakly) stationary if the expected value of the process $E[X(t)]$ and its autocorrelation function $E[X(t)X(t + \tau)]$ are both independent of time [191, p. 152], where τ represents a time delay, $\tau \in \mathbb{R}$. When ocean waves are described as a stationary process, $X(t)$ represents the water surface elevation.

The variance spectrum is often denoted as $S_X(\omega)$ and is defined as the Fourier transform of the autovariance function $C_X(\tau)$ [191, p. 161]:

$$S_X(\omega) = \frac{1}{2\pi} \int_{-\infty}^{\infty} C_X(\tau) e^{-i\omega\tau} d\tau, \quad (2.19)$$

where $C_X(\tau) = E[(X(t) - m_X)(X(t + \tau) - m_X)]$ with $m_X = E[X(t)]$.

Because $C_X(\tau)$ and $S_X(\omega)$ constitute a so-called Fourier transform pair, $C_X(\tau)$ can also be expressed as an integral of $S_X(\omega)$:

$$C_X(\tau) = \int_{-\infty}^{\infty} S_X(\omega) e^{i\omega\tau} d\omega. \quad (2.20)$$

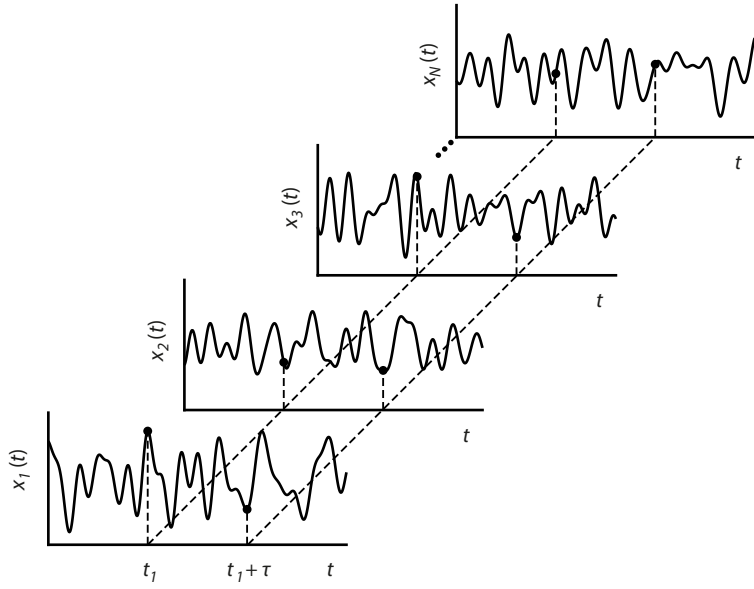


Figure 2.12: An ensemble of realizations of a stationary stochastic process. $X(t)$ is normally distributed and the expected value $E[X(t)]$ does not change over time. The process' autocorrelation function $E[X(t)X(t + \tau)]$ is independent of time as well. This figure is inspired by Figure 5.6 in Naess and Moan's textbook [191].

When $\tau = 0$ the autocovariance function returns the normal variance σ_X^2 :

$$\sigma_X^2 = C_X(0) = \int_{-\infty}^{\infty} S_X(\omega) d\omega, \quad (2.21)$$

which shows how the spectrum relates to the variance of the sea surface elevation. Consequently a variance spectrum can be interpreted as the variance's distribution over different frequencies.

Note that $S_X(\omega)$ is defined based on angular frequencies ranging from $-\infty$ to $+\infty$ and that the function is symmetric in the sense that $S_X(-\omega) = S_X(\omega)$ [191, p. 162]. Since physically, only positive frequencies exist and as many researchers prefer the frequency f over the circular frequency ω for ease of interpretation, the spectrum is often expressed as a one-sided variance spectrum as a function of the unit Hertz:

$$G_X^+(f) = \begin{cases} 4\pi S_X(\omega) & \text{if } \omega \geq 0, \\ 0 & \text{if } \omega < 0, \end{cases} \quad (2.22)$$

where $\omega = 2\pi f$.

As noted previously, if the form of the spectrum is known, two parameters are often sufficient to fully describe a spectrum. These parameters are usually defined based on the spectrum's statistical moments \tilde{m}_j :

$$\tilde{m}_j = \int_0^{\infty} f^j G_X^+(f) df, \quad j = 0, 1, 2, \dots \quad (2.23)$$

The most common variable to describe a sea state's intensity – a measure for the variance of the water surface elevation over time – is the “significant wave height” H_s :

$$H_s = 4\sqrt{\tilde{m}_0} = 4\sigma_X. \quad (2.24)$$

2 Theoretical background and literature review

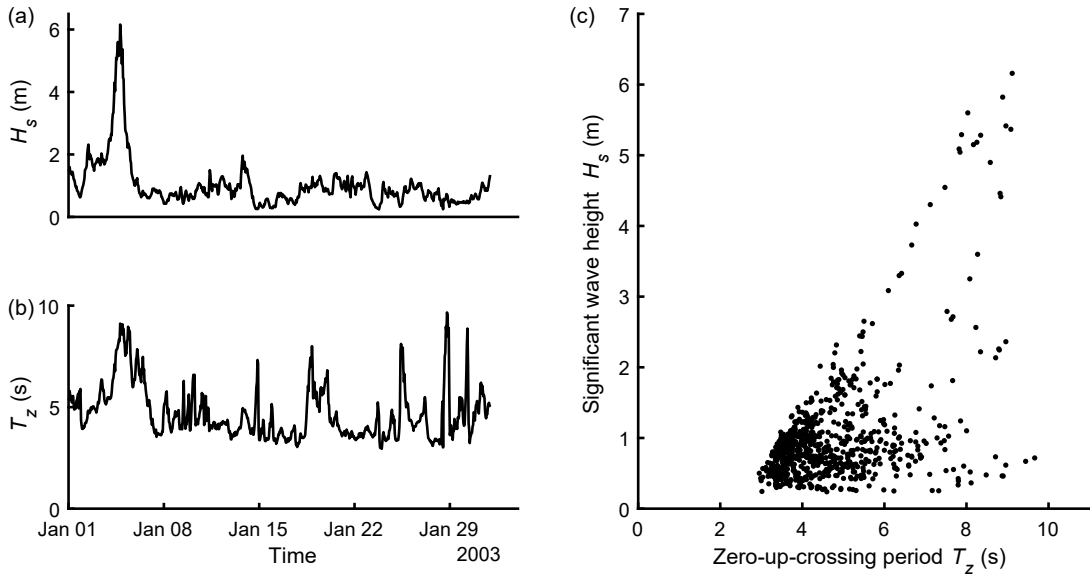


Figure 2.13: One month of metocean data measured with a buoy that is moored at the US East Coast (Buoy NDBC 44007).

To describe a characteristic frequency or period of the spectrum, multiple types of periods are common. A typical choice is the mean “zero-up-crossing period” T_z sometimes simply called “mean wave period,” which is the square root of the ratio of the zeroth moment over the second moment:

$$T_z = \sqrt{\frac{\tilde{m}_0}{\tilde{m}_2}}. \quad (2.25)$$

Other typical choices are the “energy period,” $T_e = \tilde{m}_{-1}/\tilde{m}_0$, and the “spectral peak period” T_p , which is the period with the highest spectral density.

The long-term distribution of sea states is therefore often represented by a joint probability distribution of variables such as significant wave height and zero-up-crossing period, $F_{H_s, T_z}(H_s, T_z) = \Pr(H_s \leq h_s, T_z \leq t_z)$. Figure 2.13c shows a scatter diagram of sea states, measured with a buoy that is moored at the US East Coast. To fully describe the offshore environment, one might be interested in additional variables, such as the mean wind speed V , which would lead to a three-dimensional joint distribution: $F_{V, H_s, T_z}(V, H_s, T_z) = \Pr(V \leq v, H_s \leq h_s, T_z \leq t_z)$.

To achieve a handy formal description of an offshore environment, parametric probability distribution models are often fitted to raw data such as the buoy measurements shown. Raw data can be derived either from measurements or from high-fidelity computer simulations, so-called “climatic reanalysis” or “hindcasts.” Depending upon the load case of interest, sometimes establishing a univariate probability distribution is sufficient, while at other times a multi-dimensional joint probability distribution is required.

Similar as already described for generic variables in Section 2.2.1, when univariate distributions of variables such as significant wave height or wind speed are modeled, two different approaches exist: “global models” and “event models.” In a global model, a distribution is fitted to the complete dataset. Often simple parametric distributions with 2 to 5 parameters are used, for example, the common 2-parameter Weibull distribution, the translated Weibull distribution, or the log-normal distribution. Event models, however, are only concerned with extreme events. Thus, these models do not describe the complete range of a dataset but only certain extremes. A review on modeling

extremes of metocean variables is provided by Jonathan and Ewans [133]. Two kinds of event models are commonly used: In the “annual maxima method,” a time series of metocean data is separated into yearly blocks, their maxima are identified and a distribution is fitted to these maxima (sometimes also shorter blocks with lengths of days or weeks are used [172, 223]). In the “peaks over threshold method,” only metocean data above a defined threshold is considered for modeling. Detailed reviews on the various models that are used to fit the marginal distributions of significant wave height and wind speed were presented by Muir and El-Shaarawi [183] and Jung and Schindler [140], respectively.

Global models and event models have different weaknesses and strengths: Global models use all data points and therefore use the maximum amount of information available. However, subsequent data points in a time series of a metocean variable are strongly correlated (Figure 2.14) such that the model assumption that observations are independent and identically distributed is violated. If one treats such correlated data as if they were independent, one introduces bias (see, for example, Mackay et al. [159]). The observations that are used to fit event models are much more independent, however, much information is lost by discarding the majority of data points when these models are fitted. Therefore, the uncertainty of estimates is higher.

The effect of serial correlation in offshore environmental conditions received much attention recently because global models are widely used and often serial correlation is not accounted for [91]. Extremes of environmental conditions typically occur in clusters. For example, in a hourly time series often multiple very high H_s values occur during a single storm. The effect of this serial correlation can be quantified with the extremal index (see, for example, [64, 147, 174]). The extremal index $\theta \in [0, 1]$ describes the inverse of the mean cluster size [174]. Thus, extremes of time series with $\theta = 1$ are independent while extremes in time series with $\theta < 1$ have some degree of serial dependence. While the extremal index describes correlation at asymptotically high levels, the sub-asymptotic extremal index θ_x can be used to characterize extremes at quantiles relevant to structural design [159]. Mackay et al. [159] showed that $\theta_x = \tilde{T}_R(x)/T_R(x)$, where $T_R(x)$ is the true return period of environmental condition x , and $\tilde{T}_R(x)$ is the return period of the equivalent independent time series. The equivalent independent time series is the sequence that would be obtained by randomizing the order of observations in the serially correlated time series. Thus, if correlated events are used as if they were independent events, the return period of the level x is underestimated. This implies that quantiles from a distribution function that was derived from serially correlated data overestimate the true return values. If θ_x is known, the effect can be compensated. Eastoe and Tawn [50] estimated θ_x to derive unbiased estimates of return values. Of course performing this compensation requires that θ_x is estimated accurately as the uncertainty of the estimate of θ_x is incorporated into the estimation of return values.

Multivariate models can be classified into global models and event models as well. In global models, a widely used model structure is the so-called “global hierarchical model” (some researchers also use the term “conditional modeling approach”; see, for example, [17, 156]). In these models one variable is independent while all other variables depend on at least one other variable. The dependence structure is usually modeled using simple dependence functions with 2 to 4 parameters (see, for example, [118, 151]). Currently, to model the long-term distribution of sea states, the classification society DNV recommends assuming that significant wave height follows a translated 3-parameter Weibull distribution, and that zero-up-crossing period follows a lognormal distribution that is conditional on significant wave height [47, p. 77]:

$$F_{H_s}(h_s) = 1 - e^{-[(x-\gamma)/\alpha]^\beta}, \quad (2.26)$$

2 Theoretical background and literature review

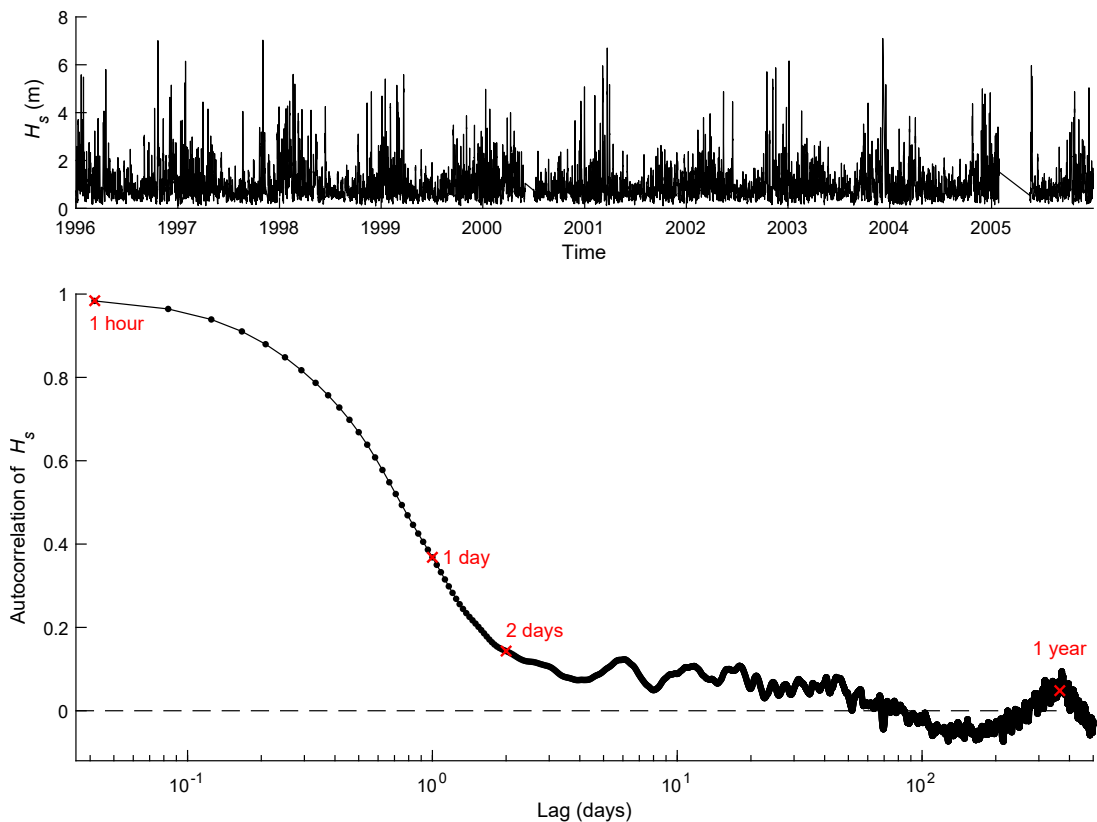


Figure 2.14: Serial correlation between hourly measurements of significant wave height H_s . Hourly observations are not independent but are strongly correlated. Seasonality is also apparent in the data: observations with a delay of about half a year are negatively correlated while observations with a delay of about a year are positively correlated. The data was measured with a buoy that is moored at the US East Coast (Buoy NDBC 44007).

$$F_{T_z|H_s}(t_z|h_s) = \frac{1}{2} + \frac{1}{2} \operatorname{erf}\left(\frac{\ln t_z - \mu}{\sqrt{2}\sigma}\right), \quad (2.27)$$

where erf is the error function and the parameters μ and σ are functions of the wave height h_s :

$$\mu = c_1 + c_2 h_s^{c_3}, \quad (2.28)$$

$$\sigma = c_4 + c_5 e^{c_6 h_s}. \quad (2.29)$$

The parameters α, β, γ , and c_1, \dots, c_6 are estimated by fitting the model structure to a dataset.

A similar distribution is recommended by DNV for the joint distribution of significant wave height and wind speed [47, p. 78]. These models, or slight adaptations of them, are also often used by academics who study the design of offshore wind turbines. In their study on design loads on an offshore wind turbine, Liu et al. [155] assumed that wind speed follows a 2-parameter Weibull distribution, significant wave height follows a 2-parameter Weibull distribution that is conditional on wind speed, and spectral peak period follows a log-normal distribution that is conditional on wind speed and wave height. They modeled the dependence structure with simple parametric functions with three parameters for each function.

Another way to define a global multivariate model is to utilize copulas. A copula is a multivariate joint distribution, which has uniform marginal distributions in the interval $[0, 1]$. It can be used to describe the dependence structure between variables such that a global multivariate model can be designed by using one marginal distribution for each environmental variable and a copula to describe the dependence between the variables. In the last 10 years Silva-González et al. [228], Montes-Iturriaga and Heredia-Zavoni [176], Vanem [244, 248], Montes-Iturriaga and Heredia-Zavoni [177], Manuel et al. [166], Fazeres-Ferradosa et al. [58], Zhang et al. [275], Heredia-Zavoni and Montes-Iturriaga [113], Lin et al. [154], and Huang and Dong [119] applied different types of copula models to metocean variables. Finally, global models based on kernel density estimation can be used as global models too [52, 62, 99].

Multivariate event models have been proposed more recently. Currently, they play a minor role in technical standards and studies on offshore structures, however, they are increasingly used in academic studies on joint extremes of metocean variables. In 2004, Heffernan and Tawn [111] proposed a conditional extreme value model that has gained popularity. Jonathan et al. [135] and Mackay and Jonathan [163] used the Heffernan and Tawn model to estimate the bivariate distribution of peak significant wave height and wave period. Mackay and Jonathan [163] also used it to estimate the bivariate distribution of peak wind speed and significant wave height. Extreme value models and models for the bulk of the data can be combined too: Such a blending of models has been demonstrated, for example, by Mackay and Jonathan [163] and Qiao and Myers [206]. The work of Mazas [170] presents a framework for assessing natural hazards where he carefully defines what multivariate environmental extremes are and how they relate to the physical processes that cause such extremes.

The typical approach to modeling the long-term distribution of environmental variables is based on the idea that future environmental conditions will be like past environmental conditions. However, as the climate is changing, the long-term distribution of variables such as wind speed and wave height will be affected as well. Young et al. [272] investigated global changes in oceanic wind speed and wave height using satellite altimeter measurements over a period of 23 years. They found that mean wind speed increased at most locations, while the trend for significant wave height was less clear. Extreme wind speeds and extreme significant wave heights, in their paper defined as the 90th percentile, both increased stronger than the mean values. Hemer et al. [112] studied how wave cli-

2 Theoretical background and literature review

mate changed between a 30-year period in the recent past and a projected 30-year period in the future using climatic computer models. The period that was considered to represent present climate covered the years between 1979 and 2009 and the future period was from 2070 to 2100. They found that – between the two periods – mean significant wave height increases at 7% of the ocean's area, but decreases at 26% of the area.

Modeling future wind-wave climate is subject to high uncertainty. Much of the uncertainty is due to differences in modeling approaches. By comparing projections from different wave models, Morim et al. [181] found that 50% of the uncertainty is due to modeling differences. Despite the uncertainty, they identified statistically robust changes in many regions of the world. For both, mean significant wave height and the 99th percentile significant wave height, they found some regions where these variables increase and some regions where these variables decrease. Overall, the studies on climate change show that (1) metocean variables such as wind speed and wave height are affected by a changing climate; (2) extreme values might be affected stronger than mean values; and (3) wind speeds are expected to increase in most regions of the world while wave heights are expected to increase at some regions, but decrease at other regions.

Researchers have developed approaches on how climatic trends can be accounted for in probabilistic models of metocean variables. One approach that was proposed to apply to significant wave height [251], is to first identify the yearly trend of how the wave height's expected value changes and how its variance changes. Then, one uses the trend to alter a parametric distribution that was previously fitted to a metocean dataset [251]. Vanem [249] applied various methods to derive extreme values of significant wave height and considered a scenario without climatic changes and two scenarios with climatic changes. His study shows that, both the extreme value modeling approach and the modeling of the climatic trend greatly contribute to the uncertainty of 20-year and 100-year return values of the significant wave height. Climate change also affects the joint distribution of environmental variables. Vanem [248] explored how different bivariate models of significant wave height and zero-up-crossing period can be used to model climatic changes.

Climate changes over many years, changes in shorter timescales such as the seasons [247], and in general the complexity of the physical process that are involved in how winds and waves evolve in time, contribute to the uncertainty of a statistical model of offshore environmental conditions. Consequently, univariate and multivariate return values, which are derived from these statistical models are subject to uncertainty too. Researchers analyzed how a joint model's uncertainty affects joint extremes derived from the model [175, 229] and how the sampling uncertainty due to the finite length of a metocean dataset affects joint extremes [79, 252]. In a benchmarking study co-organized by the author of thesis [92], the uncertainty associated to joint extremes was analyzed as well. In this study uncertainty was classified into different sources:

- uncertainty associated with the quality of the metocean dataset, for example, due to systematic biases in measurements or hindcast models;
- uncertainty due to limited sample size and sampling variability;
- uncertainty associated with choosing a model for the joint distribution (all statistical models that describe wind and wave can be considered to have some degree of model misspecification);
- uncertainty associated with choosing a type of parameter estimation technique (for example, maximum likelihood estimation versus the method of moments or least squares estimation);
- uncertainty associated with setting hyper-parameters in the parameter estimation technique (for example, the number of intervals that are used when data are binned);

- uncertainty associated with how the climate will change;
- uncertainty associated with the numerical methods used in deriving joint extremes, for example, due to the used numeric integration method or due to the applied Monte Carlo method; and
- uncertainty associated with which definition for multivariate extremes shall be used for the application of interest (this type of uncertainty refers to the so-called environmental contour method and its approximation of the failure region; the contour method will be introduced later in this chapter).

Unfortunately, these sources are often difficult to quantify in design projects. However, procedures such as using safety factors are meant to compensate for the possibility that loads are underestimated, due to uncertainty.

In summary, when the offshore environment is modeled, it is common to differentiate between two timescales: Short-term statistics describe how the environment behaves within a timescale of minutes or hours, while long-term statistics describe how the environment behaves within a timescale of years. The short-time statistics are described using variance spectra while long-term statistics are described using probability distributions of parameters that describe these variance spectra. Sometimes it is useful to describe the long-term distribution of a single variable while at other times joint distributions are required. Models for long-term distributions might be classified as global models or as event models. Some environmental variables are affected by robust trends due to a changing climate. If such a trend can be quantified it can be used to alter the distribution that has been fitted to a metocean dataset.

Next, we will focus on what to do after a satisfying model for the offshore environmental conditions has been established – that is, using this model to derive the requirement values of environmental variables, that must be used to derive design loads. Requirement values must be derived as part of defining a design basis (step 2 in Figure 2.10b).

2.3.2 DETERMINING REQUIREMENT VALUES OF ENVIRONMENTAL VARIABLES

Offshore structures usually have multi-decade design lives. For example, offshore wind turbines are usually designed to safely operate 20 to 25 years [21]. Based on this design life, requirement targets are formulated. For example, one might set the target reliability based on the idea that within a design life of 20 years structural failure shall occur with a probability of less than 1%, $p_{F,target,DL} = 0.01$. If environmental states with state durations of 1 hour are considered as independent events, this idea would translate to a target probability of failure per environmental event, $p_{F,target}$, of

$$p_{F,target} = 1 - (1 - p_{P,target,DL})^{1/n} \quad (2.30)$$

where n is the number of environmental states that occur during the design life, $n = 20 \times 365.25 \times 24 = 175,320$. Thus

$$p_{F,target} = 1 - (1 - 0.01)^{1/175,320} \approx 5.7 \times 10^{-8}. \quad (2.31)$$

This target probability of failure would translate to a target return period of approximately 2000 years:

$$T_{R,target} = \frac{T_S}{p_{F,target}} = \frac{1 \text{ hour}}{5.7 \times 10^{-8}} \approx 1.74 \times 10^7 \text{ hours} \approx 2000 \text{ years} \quad (2.32)$$

2 Theoretical background and literature review

Such return periods, however, would require extensive extrapolation because datasets from hindcasts or buoys typically cover between 10 and 50 years. Therefore, such high return periods are usually not calculated for structures such as offshore wind turbines.

Instead, many standards do not prescribe a value for the probability that failure occurs during the structure's lifetime. Instead, they prescribe various target return periods for environmental conditions with the aim that these environmental conditions lead to the N -year response (see, for example, [129, p. 24]). For offshore wind turbines, designers are often asked to ensure that the turbine survives the 50-year response by ensuring that it survives loads from environmental conditions with a return period of 50 years (see, for example, [129]). This process is criticized by Serinaldi [227] as these return periods somewhat distract the attention from the true variable of interest, which is the probability of failure during the design life. Furthermore, as described in Section 2.2.2, there are different definitions for multivariate exceedance and these different definitions lead to different environmental extremes.

Since standards usually present a common design practice and many companies are required to design their products to comply with standards, their methods of deriving requirement values for environmental variables are described in the following. Offshore design standards such as the International Electrotechnical Commission's (IEC) standards on offshore wind turbines [129, 130] organize the design process using so-called "design load cases" (DLCs). A DLC describes an operating condition of a wind turbine, together with the environmental conditions during the operating conditions. In IEC's standard 61400-3-1 [129] the DLCs are numbered, such that, for example, DLCs starting with the number 1 describe the turbine during power production and DLCs starting with the number 6 represent the turbine in parked mode (Table 2.1). The DLCs regulate which type of extreme values shall be assumed for different environmental variables. For example, in DLC 6.1 the marginal 50-year return value of significant wave height, H_{s50} , must be estimated. Some DLCs, however, also require the estimation of joint extremes: DLC 1.6 demands the estimation of so-called severe sea states, which are defined as the joint 50-year extremes of wind speed and significant wave height.

To estimate joint wind speed - wave height extremes, designers must first estimate the joint distribution of wind speed and significant wave height with methods described in Section 2.3.1. Then joint extremes are defined based on that distribution resulting in a curve that, based on a given definition of exceedance, represents 50-year extremes. In the realm of designing offshore structures the curve that holds joints extremes is known as an "environmental contour" and the method of constructing the curve is known as the "environmental contour method" (Figure 2.15). The environmental contour method deals with the challenge of how joint extremes shall be defined (Section 2.2.2) and how to deal with the differentiation between short-term and long-term statistics, which is commonly used in offshore engineering. Ultimately, it aims to provide a computationally efficient approximation of the N -year structural response. It has been applied in the structural analysis of a wide range of marine structures such as wind turbines [30, 141, 155, 185, 220, 221, 236, 256], wave energy converters [37, 184, 194], an integrated wind-wave-tidal energy converter[150], floating structures for oil and gas production [229, 261, 265], bridges [75, 270], and vessels [6].

This method's roots can be traced back to Haver's publication from 1985 [110] where he described how a curve of joint extremes of H_s and T_p can be constructed to derive requirement values. He called this curve "design curve" (Table 2.2). His proposed environmental contour is constructed by first selecting an appropriate interval for spectral peak period and then calculating the corresponding H_s value by enforcing two conditions: The conditional probability distribution $H_s|T_p$ has constant exceedance probability for each T_p value within the predefined interval and the total exceedance probability must equal a given value. In 1993, Winterstein et al. [263] proposed constructing envi-

Design situation	DLC	Wind condition	Waves	Wind and wave directionality	Sea currents	Water level	Type of analysis	Partial safety factor
1) Power production	1.1	NTM $V_{in} < V_{hub} < V_{out}$ rotor-nacelle assembly	NSS $H_s = E[H_s V_{hub}]$	COD, UNI	NCM	MSL	U	N (1.25)
	1.2	NTM $V_{in} < V_{hub} < V_{out}$	NSS Joint probability distribution of H_s, T_p, V_{hub}	MIS, MUL	No currents	NWLR or \geq MSL	F	*
	1.3	ETM $V_{in} < V_{hub} < V_{out}$	NSS $H_s = E[H_s V_{hub}]$	COD, UNI	NCM	MSL	U	N
	1.4	ECD $V_{hub} = V_r - 2 \text{ m/s}, V_r,$ $V_r + 2 \text{ m/s}$	NSS $H_s = E[H_s V_{hub}]$	MIS, wind direction change	NCM	MSL	U	N
	1.5	EWS $V_{in} < V_{hub} < V_{out}$	NSS $H_s = E[H_s V_{hub}]$	COD, UNI	NCM	MSL	U	N
	1.6	NTM $V_{in} < V_{hub} < V_{out}$	SSS $H_s = H_{s,SSS}$	COD, UNI	NCM	NWLR	U	N
	.							
	.							
	.							
6) Parked (standing still or idling)	6.1	EWM Turbulent wind model $V_{hub} = V_{ref}$	ESS $H_s = H_{s50}$	MIS, MUL	ECM $U = U_{50}$	EWLR	U	N
	.							
	.							
	.							
8) Transport, assembly, maintenance, and repair	8.2	EWM $V_{hub} = V_1$	ESS $H_s = H_{s1}$	COD UNI	ECM $U = U_1$	NWLR	U	A

Table 2.1: Design load cases from the standard IEC 61400-3-1 [129], which regulates designs of bottom-fixed offshore wind turbines. For simplicity, the column “other conditions” is not shown. COD = co-directional, ECD = extreme coherent gust with direction change, ESS = extreme sea state, ETM = extreme turbulence model, EWM = extreme wind speed model, MIS = misaligned, MSL = mean sea level, MUL = multi-directional, NCM = normal current model, NSS = normal sea state, NTM = normal turbulence model, NWLR = normal water level range, SSS = severe sea state, UNI = uni-directional, F = fatigue, U = ultimate strength, N = normal, * = partial safety factor for fatigue, numbers written as subscripts of V , H_s and U denote the return period in years.

2 Theoretical background and literature review

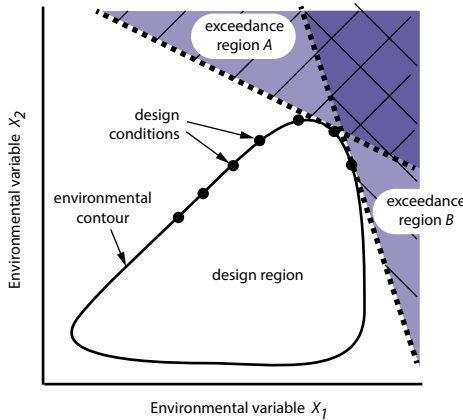


Figure 2.15: Illustration of an environmental contour and the associated terminology. As an example, a direct sampling contour, which is defined with angular exceedance regions in the original variable space, is shown.

ronmental contours in a general way that is not specific to H_s and T_p . They proposed binding the design region by multiple exceedance regions that are bound by a line that has an angle θ relative to the abscissa (in 2D). The design region, however, is not constructed in the physical variable space, but only after transforming the variables into standard normal space, which allows for easier mathematical expressions. In 2D, the exceedance boundary describes a circle in standard normal space. In higher dimensions, the design region becomes a sphere ($d = 3$) or a hypersphere ($d > 3$) in standard normal space, bound by (hyper)planes. Winterstein et al. [263] carefully embedded their environmental contour method in reliability theory and called it the “inverse first-order reliability method” (IFORM; Figure 2.16). In the IFORM, the exceedance regions relate to the possible failure region of the structure that is being designed. Many marine structures will have a failure boundary that can be approximated as a straight line (in two dimensions) or as a (hyper)plane if $d > 2$. Thus, if a structure is designed based on an IFORM contour with exceedance probability α , it will often have a failure probability of approximately $p_F \approx \alpha$. The work by Winterstein et al. [263] also introduced a way to deal with the effect that, due to the response’s short-term variability, the highest response could also occur at a high quantile of a low environmental condition. They suggested that contours can be “inflated” by using a higher return period than intended when constructing the contour. Alternatively, short-term response variability can be compensated by using the original return period, but evaluating the response at a higher quantile [8, 184] or by multiplying an additional safety factor to the environmental load [197].

Yet another way to construct an environmental contour was proposed in the standard NORSO K N-003 in 2007³ [197]: In the so-called constant probability density approach, first the marginal N -year return value, $H_{s[N]}$, is estimated. Then the mean conditional T_p value for $H_{s[N]}$ is estimated. Finally, the contour is constructed as the contour of constant probability density going through the point $(H_{s[N]}, E[T_p|H_{s[N]}])$. In 2013, Huseby et al. [124] proposed constructing environmental contours using angular exceedance in the original variable space. In 2014, Jonathan et al. [134] explored using different joint exceedance regions to construct environmental contours.

In this thesis, a novel way of constructing a N -year environmental contour will be proposed. This contour method, called highest density contour method, will be introduced in detail in Section 6.1.

³Anecdotally, this approach has been proposed and used earlier, however, the author of this thesis is not aware of an earlier reference.

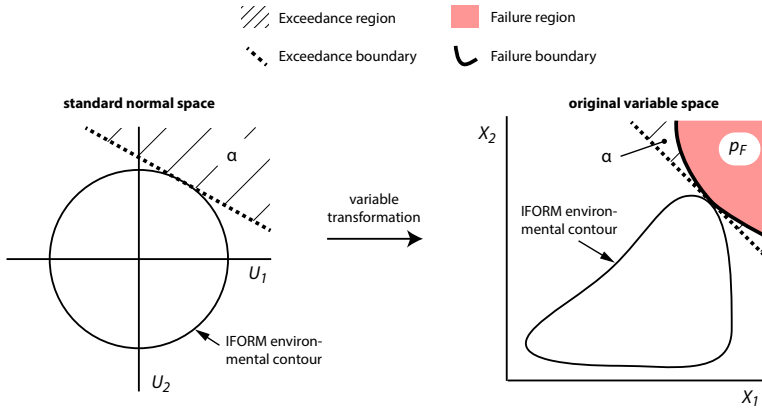


Figure 2.16: Concept of an IFORM environmental contour. Contours are derived by first constructing a circle in standard normal space, where all variables are normally distributed with a mean of 0 and a standard deviation of 1, and then transforming this circle to the original variable space. One of the exceedance regions, that holds probability α , approximates the failure region. If the failure region is convex the probability of failure p_F will be smaller than the exceedance probability α .

In this section, the related contour methods will also be described in detail. The highest density method was published in 2017 [100]. It influenced a method based on similar ideas, the inverse second-order reliability method (ISORM; [27]). In addition, after 2017, Derbanne and Hauteclocque [44] proposed a “direct IFORM” contour method, which has similarities with the direct sampling contour method and Dimitrov [46] proposed a contour method that he called “inverse directional simulation.” While working on this thesis, reviews and comparison studies on the environmental contour method were published: Ross et al. [216] provided a broad review on the environmental contour method, Eckert et al. [51] proposed a comparison framework for contours and the author of this thesis co-organized a benchmarking study on contour methods [92, 93].

After the values of all environmental variables that are required as part of a design load case have been determined – using univariate methods or using the environmental contour method – simulations can be set up to analyze which loads these environmental conditions cause and how the structure of interest responds to these loads. The next section describes this process.

Method	Year	First publication
Design curve method	1985	Haver [110]
Inverse first-order reliability method (IFORM)	1993	Winterstein et al. [263]
NORSOK’s constant probability density approach	2007*	NORSOK [197]
Direct sampling contour method	2013	Huseby et al. [124]
Joint exceedance contour method	2014	Jonathan et al. [134]
Highest density contour method	2017	Haselsteiner et al. [100]
Inverse second-order reliability method (ISORM)	2018	Chai and Leira [27]
Direct IFORM	2019	Derbanne and Hauteclocque [44]
Inverse directional simulation	2020	Dimitrov [46]

Table 2.2: Environmental contour methods. The highest density contour method was proposed by the author of this thesis and will be introduced in detail in Chapter 5. * Anecdotally, this approach has been proposed and used earlier, however, the author of this thesis is not aware of an earlier reference.

2 Theoretical background and literature review

2.3.3 EVALUATING OFFSHORE STRUCTURES WITH DESIGN LOADS

The combinations of environmental conditions that are defined via a particular load case are typically used to initialize the boundary conditions of a multi-physics time-domain simulation. For example, let $\mathbf{x} = (v, h_s, t_p, \theta_{wind}, \theta_{wave}, u, w)^T$ describe the environmental conditions that correspond to one of the DLCs in IEC 61400-3-1 [129] (Table 2.1; with v representing wind speed, h_s significant wave height, t_p spectral peak period, θ_{wind} the wind's main direction, θ_{wave} the wave's main direction, u the sea current and w the water level). Then, the designer of an offshore wind turbine is interested in the amount of load l that the combination of environmental conditions \mathbf{x} cause and eventually which response r the load causes. To determine the response, usually codes that couple aerodynamic, hydrodynamic, control, and structural models are used – so-called aero-hydro-servo-elastic codes. Popular codes that are used to simulate offshore wind turbines are Bladed (DNV AS, Norway), HAWC2 (DTU Wind Energy, Denmark), and OpenFast (NREL, USA). These – and other codes – have been used in offshore code comparison projects OC3 [138], OC4 [139] and OC5 [213]. An overview about aeroelastic wind turbine codes is given by Ahlström [2] and by Zhang and Huang [274]. While Bladed, HAWC2, and OpenFast are specific to wind turbines, general-purpose codes can be used to simulate the dynamics of vessels and other offshore structures. Popular general purpose codes are among others the panel codes Ansys Aqwa (Ansys Inc, USA) and WAMIT (WAMIT Inc, USA). A comparison among these codes is presented by Gourlay et al. [77].

If a DLC, as for example DLC 1.6, requires the estimation of joint extremes, the set of environmental conditions that must be evaluated in simulations depends upon the environmental contour method used. For example, loads that result from environmental conditions derived from a direct sampling contour method might be higher than the loads derived from an IFORM contour. Current guidelines and standards allow the use of different contour methods. Consequently, even if we had a joint distribution that perfectly describes the long-term statistics of the offshore environment, the requirements that constitute DLCs are insufficient in determining unique design loads and – if one designs the structure to survive the design loads – a definitive reliability.

The true reliability of a structure can only be determined using a so-called “full long-term analysis,” which – when only sea states are evaluated – is also known as “all sea states approach.” In a full long-term analysis, a structure’s response over the complete variable space is evaluated to determine its reliability. Assuming that environmental states are independent and identically distributed, the long-term response function of the response variable R can be written as (see, for example, [33])

$$F_R(r) = \int_{\mathbf{x}} F_{S,R|\mathbf{X}}(r|\mathbf{x}) f_{\mathbf{x}}(\mathbf{x}) d\mathbf{x}, \quad (2.33)$$

where $F_{S,R|\mathbf{X}}$ is the short-term response function (the distribution function of the response at a given environmental condition) and $f_{\mathbf{x}}$ is the long-term joint density function of the environmental conditions.

Then, based on the structure’s response capacity r_{cap} its true reliability is

$$p_R = \Pr(R < r_{cap}) = F_R(r_{cap}). \quad (2.34)$$

The problem is that in practice the short-term response function, $F_{S,R|\mathbf{X}}$, is not known and estimating it at every possible realization of \mathbf{X} is infeasible as performing aero-hydro-servo-elastic simulations is computationally expensive. Consequently, the whole process of evaluating several DLCs could be interpreted as a method to reduce computational costs by evaluating only a reduced number of realizations \mathbf{x} . Indeed, IEC’s standard on offshore wind turbines states that the extreme environmental conditions that are defined using the standard’s procedures are “intended to produce N -year ($N=1$

or 50) return period load effects” [129, p. 24] where their use of “load effect” is like this thesis’s use of “response.” Thus, the standard’s procedures are intended to estimate the 50-year response r_{50} without deriving the long-term response function (Expression 2.33).

2.3.4 PROBLEMS IN THE DESIGN PROCESS THAT ARE ADDRESSED

This thesis addresses the first two steps of the overall design process of offshore structures: how site-specific external conditions are determined and how they are used in the formulation of a design basis (Figure 2.17). These two main steps are comprised of many individual detailed process steps. Specifically, this thesis addresses three of these detailed steps:

1. Modeling the long-term probability distribution of H_s with a parametric distribution;
2. Modeling the long-term wind and wave joint distribution F_{V,H_s,T_p} ; and
3. Determining joint wind speed - wave height extremes that have a joint return period of 50 years with an environmental contour method.

The current practice for these steps has problems that this thesis tries to solve.

Currently, it is common to model the long-term distribution of H_s assuming that significant wave height data follows a translated Weibull distribution (see, for example, the recommendations by DNV [47, p. 76] or a recent study on wind turbine design by Velarde et al. [256]). However, if a translated Weibull distribution is fitted to H_s data, extreme values are often underestimated (Figure 2.18 top). Researchers have proposed more complex distributions (in terms of number of variables, [63, 110, 198]) or to use an event model instead of a global model to solve the problem (see, for example, [25, 61]). However, because these solutions have other drawbacks, currently many researchers still use the translated Weibull distribution to model significant wave height (see, for example, [16, 17, 35, 202, 248, 256]). In this thesis, it will be explored, whether the exponentiated Weibull distribution can describe empirical H_s data better than the translated Weibull distribution.

To model the joint wind speed - wave height distribution, engineers and researchers often follow the recommendations given in DNV’s “recommended practice” on environmental conditions and environmental loads [47]. There, DNV recommends a model for the wind speed - wave height joint distribution F_{V,H_s} and a model for F_{H_s,T_p} . Unfortunately, when the recommended structure for F_{V,H_s} is fitted to wind and wave data, the model does not represent the empirical dependence structure well at many offshore sites (Figure 2.18 middle): Usually, in the region of high wave heights for a given wind speed, the model has lines of constant density with positive curvature, while the empirical distribution has lines of constant density with negative curvature. In this thesis, a novel model structure for F_{V,H_s} and for F_{H_s,T_p} will be introduced and analyzed.

Finally, it is common practice to use the inverse first-order reliability method (IFORM) to determine joint extremes of wind speed and significant wave height that have a joint return period of 50 years. IFORM contours incorporate an assumption about the topology of the structural response: It is assumed that the failure region has a convex shape. However, this is not always the case, and this thesis will show that especially, for offshore wind turbines, this is usually not the case in the $V - H_s$ space (Figure 2.18 bottom). Thus, if wind-wave joint extremes are determined using an IFORM environmental contour, resulting loads and consequently the resulting responses might be underestimated. Then, it could happen that the estimated 50-year response is lower than the true 50-year response. In this thesis, an alternative environmental contour method will be proposed, which does not require a convex failure region and therefore will also be conservative if the failure region is non-convex.

2 Theoretical background and literature review

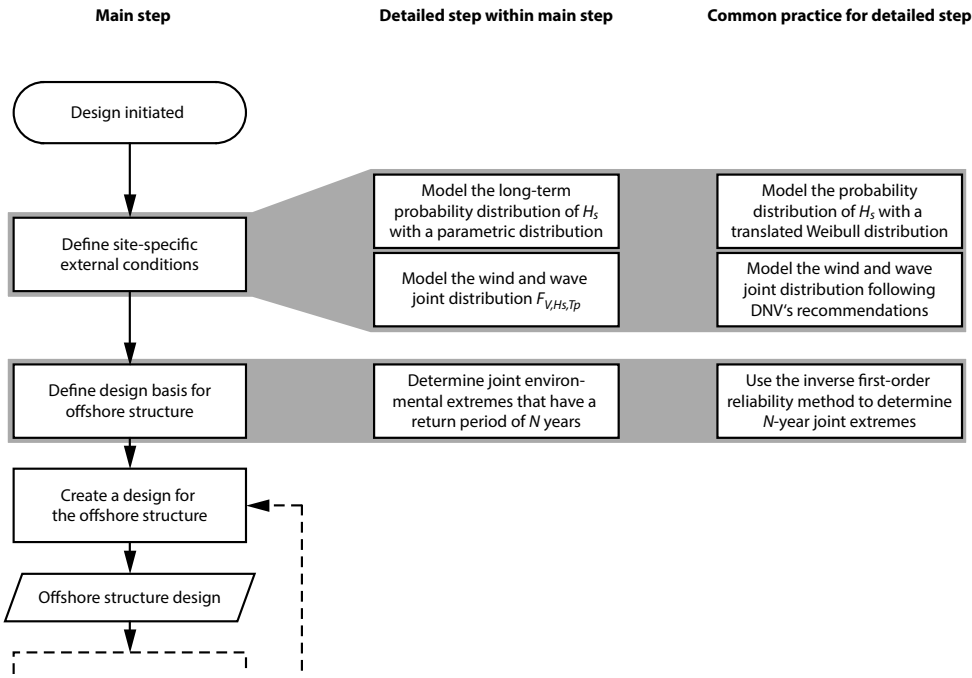


Figure 2.17: Detailed steps in the design process of an offshore structure that are addressed in this thesis.

Based on these novel models and methods, a methodology for designing offshore structures will be proposed. Compared to the state of the art, this design methodology shall increase the likelihood that a structure that was designed according to it meets its target reliability. The next chapters will comprise descriptive studies on modeling the offshore environment (Chapters 3 and 4) and on selecting joint extremes (Chapter 5) so later chapters can use these models and methods to introduce a novel design support for engineers who work on offshore structures (Chapter 6).

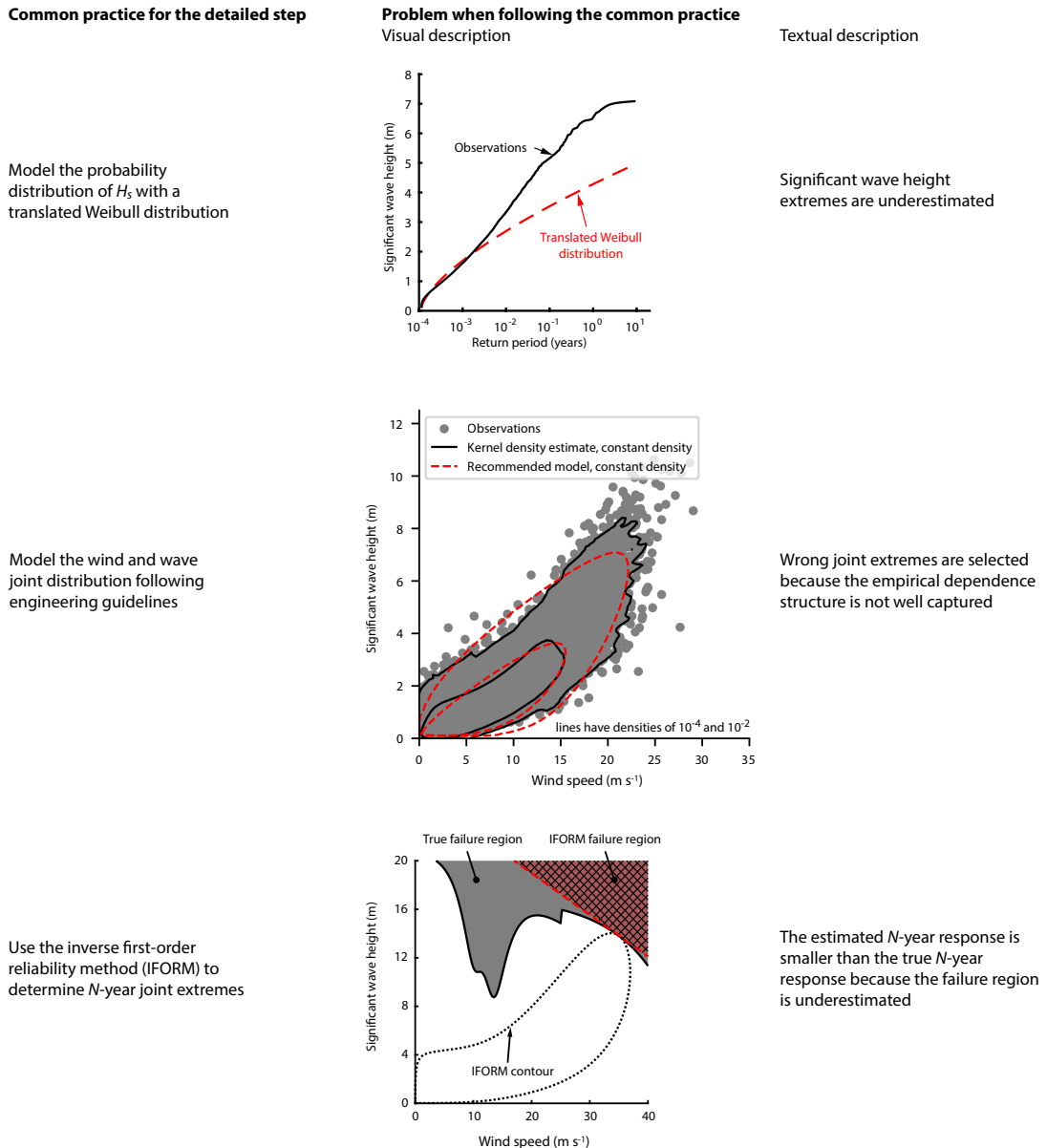


Figure 2.18: Problems in the design process that are addressed in this thesis: (1) When the probability distribution of significant wave height H_s is modeled using the translated Weibull distribution, extreme values are usually underestimated; (2) when the joint wind speed - wave height model that is advocated in DNV's "recommended practice" [47] is used, the fitted joint distribution usually does not capture the empirical dependence structure well, resulting in wrong joint extremes being selected; and (3) when wind speed - wave height joint extremes are determined using the inverse first-order reliability method (IFORM), the long-term extreme response can be underestimated.

3

LONG-TERM DISTRIBUTION OF THE SIGNIFICANT WAVE HEIGHT

PREVIOUSLY PUBLISHED This chapter is based on a publication by Haselsteiner and Thoben [103]. The chapter will introduce a new parametric model for the distribution of the significant wave height. This model represents one of three suggested improvements of the overall design process of offshore structures.

PUBLICATION'S FULL CITATION A. F. Haselsteiner and K.-D. Thoben. "Predicting wave heights for marine design by prioritizing extreme events in a global model". *Renewable Energy* 156, 2020, pp. 1146–1157. DOI: [10.1016/j.renene.2020.04.112](https://doi.org/10.1016/j.renene.2020.04.112)

3.1 INTRODUCTION

To estimate the loads on a marine structure like an offshore wind turbine, the long-term distribution of environmental variables that describe wave characteristics needs to be modeled. Especially important is significant wave height, which describes the intensity of a sea state. The long-term distribution of significant wave height is typically estimated by fitting a parametric probability distribution to measured or simulated wave data. Then, based on this probability distribution different quantiles are derived and used as design conditions for structural integrity calculations for the marine structure of interest. For example, standards for offshore wind turbines [129, 130], require designers to estimate the 1-year and 50-year return value of significant wave height – extreme values that are exceeded, on average, every 1 and 50 years, respectively. To calculate these values, designers might use a global model or an event model. As described in Section 2.3.1, global models are derived using all available data from a long series of subsequent observations while event models are derived from selected extremes of the original dataset [47, p. 75].

These two approaches have different strengths and weaknesses. Global models utilize the complete original dataset and consequently make use of all available information. Further, no preprocessing is required, and common parametric distributions can be used. However, time series of significant wave height show strong autocorrelation such that individual data points are not independent and identically distributed. Additionally, common fitting approaches like maximum likelihood estimation (MLE) and least squares estimation weight every data point equally and thus do not consider that in structural design high values of significant wave height are especially important.

Event models are typically fitted using the peak over threshold method or the block maximum method such as the annual maxima method. In both cases, the original time series are preprocessed and individual peaks are identified. These peaks are more independent than the data points of the raw time series. However, much less information is used when fitting a distribution to these peaks. Furthermore, event models only describe the upper – or as a synonym right – tail of the global distribution of significant wave height. In design, also quantiles within the bulk of the distribution sometimes need to be estimated such that a second model that covers lower quantiles is required.

3 Long-term distribution of the significant wave height

Distribution	Nr. of parameters	References that used it for H_s	Proposed in
Lognormal	2	[132, 199]	1956 [132]
2-parameter Weibull	2	[13, 75, 199, 249]	1972 [13]
Translated Weibull	3	[17, 195, 202, 248, 249, 252, 256]	1973 [195]
Generalized gamma	3	[198]	1992 [198]
3-parameter beta	3	[63]	1999 [63]
Ochi distribution	4	[199]	1980 [199]
Lonowe distribution	4-5	[110, 151]	1985 [110]

Table 3.1: Distributions that have been used to model the long-term distribution of significant wave height.

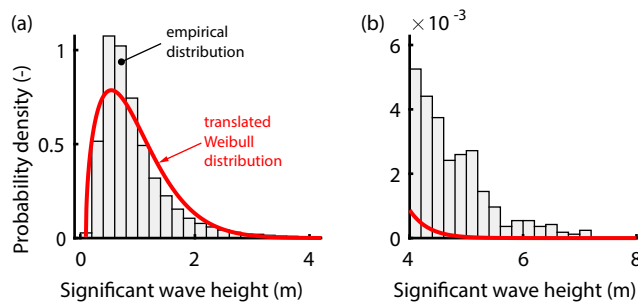


Figure 3.1: Typical model fit of the translated Weibull distribution. The distribution fits the data relatively well at its body (a), but poorly at its tail (b).

Often, this second model is a global model so as, in one design project, two diverging models for high quantiles might exist.

Here, we focus on global models. In the past, significant wave height has been modeled using various parametric distributions with two to five parameters: The lognormal distribution [132, 199], the 2-parameter Weibull distribution [13, 199], the translated Weibull distribution (sometimes simply called “3-parameter Weibull distribution”) [195, 252], the generalized gamma distribution [198], a 3-parameter beta distribution of the second kind (and two similar distributions, which showed worse model fit) [63], Ochi’s four-parameter distribution [199] and the “Lonowe distribution” [110, 151, 267] (Table 3.1). Now, probably the most used distribution to model significant wave height is the Weibull distribution. While some researchers use the 2-parameter Weibull distribution (for example [75, 249]), most researchers use the translated Weibull distribution (for example [16, 17, 83, 202, 248, 249, 252, 256]). Certifying organizations also recommend assuming that significant wave height follows a translated Weibull distribution unless data indicate otherwise [47, p. 76].

However, the translated Weibull distribution often does not fit well at its upper tail and underestimates high quantiles (Figure 3.1). Moreover, some authors have criticized that the distribution’s location parameter, which represents a minimum non-zero value, lacks physical meaning since sea states of significant wave height zero exist and represent the calm sea [199].

In this study, it will be shown that a similar distribution, the exponentiated Weibull distribution, provides better model fit to significant wave height data than the translated Weibull distribution. The exponentiated Weibull distribution has three parameters as well and consequently does not increase model complexity. Instead of a location parameter, the distribution has a second shape parameter, which offers the flexibility that is required to ensure good model fit at both, the distribution’s bulk and the tail.

3.2 THE EXPONENTIATED WEIBULL DISTRIBUTION

The exponentiated Weibull distribution is a generalization of the common 2-parameter Weibull distribution. It has been proposed by Mudholkar and Srivastava [182] to model nonmonotone failure rates and has subsequently been used in a variety of contexts (for a review, see Nadarajah et al. [186]). It extends the 2-parameter Weibull distribution with a second shape parameter, δ , that comes as an exponent of the cumulative distribution function (CDF):

$$F(x) = \left[1 - e^{-(x/\alpha)^\beta}\right]^\delta \quad (3.1)$$

for $x > 0, \alpha > 0, \beta > 0$ and $\delta > 0$. In the case of $\delta = 1$ the exponentiated Weibull distribution becomes the 2-parameter Weibull distribution. For comparison, the translated Weibull distribution's CDF, which has a location parameter, γ , instead of a second shape parameter reads

$$F(x) = 1 - e^{-[(x-\gamma)/\alpha]^\beta}. \quad (3.2)$$

Because adding an exponent to a distribution does not change a distribution's max-domain of attraction [211], the exponentiated Weibull distribution has the same max-domain of attraction as the 2-parameter Weibull distribution: the Gumbel distribution.

3.3 RESEARCH METHODOLOGY

To assess whether the exponentiated Weibull distribution represents a better model for significant wave height, we analyzed hourly time series of wave data of six locations. We considered three models: (1) the translated Weibull distribution with its parameters estimated using maximum likelihood estimation; (2) the exponentiated Weibull distribution, fitted using maximum likelihood estimation; and (3) the exponentiated Weibull distribution, fitted using weighted least squares (WLS) estimation. To assess the goodness of fit of the three models, we computed the mean absolute error (MAE) between the models' predictions and the observations. Additionally, we computed 1-year and 50-year return values and visually inspected quantile-quantile (QQ) plots. In the following, we describe the datasets, the parameter estimation, and the goodness of fit assessment in detail.

3.3.1 DATASETS

We used six datasets of significant wave height (Table 3.2). Three datasets (A, B, C) were derived from moored buoys off the US East Coast and three datasets were gathered from a hindcast that covers the North Sea (D, E, F ; Figure 3.2). The three buoy datasets were recorded by the National Data Buoy Center (NDBC; [192]) and were downloaded from www.ndbc.noaa.gov. They cover the time between January 1, 1996 and December 31, 2005. However, the buoys did not measure the complete duration such that these datasets hold between 81,749 (dataset C) and 83,917 (dataset A) hourly measurements. Datasets D, E and F were simulated in the hindcast "coastDat-2" [80, 81] and cover the complete time between January 1st, 1965 and December 31st, 1989. Additionally, for each location, we retained some data (datasets $A_r, B_r, C_r, D_r, E_r, F_r$) to assess how well fitted distributions can predict a future time period. The NDBC datasets were preprocessed: we filtered out time periods when no measurements have been conducted, calculated significant wave height from the spectral energy, and created consistent hourly time series by combining 30-minute sea states to hourly sea states when sea states with a duration of 30 minutes instead of 60 minutes were recorded. No preprocessing has been performed on the coastDat-2 datasets. This study's datasets were also

3 Long-term distribution of the significant wave height

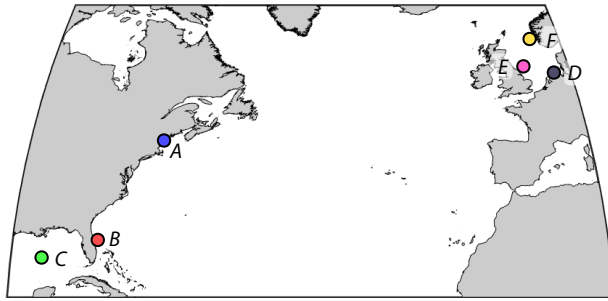


Figure 3.2: Locations of the used datasets.

used in a benchmarking exercise on estimating extreme environmental conditions for engineering design [92, 93]. In addition, they were used in this thesis' study on bivariate models that will be presented in Chapter 4.

Dataset	Duration	<i>n</i>	Site	Data source
<i>A</i>	Jan. 1996 to Dec. 2005	82,805	43.525 N 70.141 W (off Maine coast)	buoy 44007
<i>A_r</i>	Jan. 2006 to Oct. 2017	92,515		
<i>B</i>	Jan. 1996 to Dec. 2005	83,917	28.508 N 80.185 W (off Florida coast)	buoy 41009
<i>B_r</i>	Jan. 2006 to Jul. 2017	91,403		
<i>C</i>	Feb. 1996 to Dec. 2005	81,749	25.897 N 89.668 W (Gulf of Mexico)	buoy 42001
<i>C_r</i>	Jan. 2006 to Jun. 2018	93,571		
<i>D</i>	Jan. 1965 to Dec. 1989	219,144	54.000 N 6.575 E (off German coast)	hindcast
<i>D_r</i>	Jan. 1990 to Dec. 2014	219,144		
<i>E</i>	Jan. 1965 to Dec. 1989	219,144	55.000 N 1.175 E (off UK coast)	hindcast
<i>E_r</i>	Jan. 1990 to Dec. 2014	219,144		
<i>F</i>	Jan. 1965 to Dec. 1989	219,144	59.500 N 4.325 E (off Norwegian coast)	hindcast
<i>F_r</i>	Jan. 1990 to Dec. 2014	219,144		

Table 3.2: Used datasets of significant wave height. The buoy data were downloaded from the website of the National Buoy Data Center, www.ndbc.noaa.gov, and the hindcast samples were derived from the coastDat-2 hindcast [81]. *n* = Number of observations.

3.3.2 PARAMETER ESTIMATION METHODS

We estimated the parameters of the translated Weibull distribution using maximum likelihood estimation (MLE). MLE is a standard parameter estimation technique [57] and is commonly used in the context of estimating the distribution of significant wave height (see, for example, [252]). We used Matlab's (Mathworks, USA, version 2019a) function `MLE.m` to perform the MLE computation. For the second model, an exponentiated Weibull distribution fitted using MLE, we used Matlab's function `MLE.m` as well. The third model, the exponentiated Weibull distribution whose parameters are fitted using weighted least squares estimation, represents a less typical parameter estimation technique and is therefore explained in detail.

The goal of this approach is to minimize the sum of the weighted squared deviations between observed quantiles and predicted quantiles. Let the set $\{x_i\}_{i=1}^n$ represent the ordered values of a significant wave height sample with x_1 representing the lowest measured value and x_n representing the highest measured value, where n represents the length of the sample. Each ordered value, or sample quantile, x_i , has an associated probability $p_i = (i - 0.5)/n$ where i is the index of the

ordered value, $i \in [1, n]$. Further, let \hat{x}_i denote the predicted quantile based on an exponentiated Weibull distribution with the parameters α, β, δ . Then, the set of parameters that minimizes the sum of the weighted squared deviations between the sample quantiles and the predicted quantiles can be expressed as

$$\{\hat{\alpha}, \hat{\beta}, \hat{\delta}\} = \underset{\alpha, \beta, \delta}{\operatorname{argmin}} \sum_{i=1}^n w_i (x_i - \hat{x}_i)^2, \quad (3.3)$$

$$\text{where } \hat{x}_i = F^{-1}(\alpha, \beta, \delta; p_i) \quad (3.4)$$

and F^{-1} denotes the inverse cumulative distribution function (ICDF), also known as the quantile function (see Section 2.1.2). While in principle many functions for the weights, w_i , are possible, here we chose to weight the error based on the squared wave height,

$$w_i = \frac{x_i^2}{\sum_{i=1}^n x_i^2}. \quad (3.5)$$

Thus, errors between observation and prediction at high wave heights contribute much stronger to the overall error than errors at low wave heights ensuring that extreme events are prioritized in the parameter estimation procedure. Alternative choices that prioritize high wave heights could be, for example, linearly increasing weights, $w_i = x_i / \sum x_i$, or cubically increasing weights, $w_i = x_i^3 / \sum x_i^3$. We briefly tested these alternatives and, based on visual inspection of the estimated distributions, decided to weight errors quadratically. The outlined estimation method was implemented in Matlab.¹ In the appendix, in Section A.2, we describe the mathematics and algorithms used to solve Expression 3.3.

To assess the uncertainty of the estimated parameters, we used bootstrapping with replacement (see, for example, [54]). We estimated standard errors based on 100 bootstrap samples.

3.3.3 GOODNESS OF FIT ASSESSMENT

We assessed each model's goodness of fit by computing the mean absolute error and by comparing each model's predicted 1-year return value with the empirical 1-year return value. Both assessments were first performed with the original datasets (A, B, C, \dots) and then with the retained datasets (A_r, B_r, C_r, \dots).

Mean absolute error, \bar{e} , was first computed for the whole dataset:

$$\bar{e} = \frac{\sum_{i=1}^n |x_i - \hat{x}_i|}{n}, \quad (3.6)$$

Then, to assess the goodness of fit at high quantiles, we computed mean absolute error for quantiles with $p_i > 0.99$ (“the tail”) and for quantiles with $p_i > 0.999$ (“the very tail”). The two errors, $\bar{e}_{0.99}$ and $\bar{e}_{0.999}$ read

$$\bar{e}_{[p_i]} = \frac{\sum_{i=j}^n |x_i - \hat{x}_i|}{n - j + 1} \quad (3.7)$$

where j is the index of the first empirical quantile whose p_i value is above the threshold of 0.99 or 0.999.

¹The code is available at <https://github.com/ahaselsteiner/exponentiated-weibull>.

3 Long-term distribution of the significant wave height

For the assessment of the predicted 1-year return value, we computed the normalized return value, H_{s1}^* , by dividing the predicted return value, \hat{H}_{s1} , by the empirical return value, H_{s1} :

$$H_{s1}^* = \frac{\hat{H}_{s1}}{H_{s1}} \quad (3.8)$$

where H_{s1} is the smallest empirical quantile whose probability, p_i , is greater than $(1 - \alpha)$, with α being the probability of exceedance, $\alpha = 1/(365.25 \times 24)$ for hourly sea states. For consistency, \hat{H}_{s1} is computed using this empirical p_i value too, instead of the exact value, which is $1 - \alpha$. Then $H_{s1}^* = 1$ represents perfect agreement, $H_{s1}^* < 1$ a too low prediction and $H_{s1}^* > 1$ a too high prediction.

3.4 RESULTS

3.4.1 ESTIMATED PARAMETERS AND VISUAL ASSESSMENT

The fitted translated Weibull distributions (Table 3.3) provide decent model fit within the bulk of the data, but fit poorly at the tail. This is apparent both, in density plots (Figure 3.3 and 3.4) and in QQ-plots (Figure 3.5). In all datasets, the translated Weibull distribution predicts too low probability densities in the tail ($p_i > 0.99$; Figure 3.4) and consequently also too low quantiles in the tail (Figure 3.5a).

Density plots suggest that the fitted exponentiated Weibull distributions (Table 3.4) provide good model fit at both, the body and the tail (Figure 3.3 and 3.4). At the tails, the densities of the MLE-fitted exponentiated Weibull distributions provide better model fit than the translated Weibull distributions. However, for dataset *D* and *F* the MLE-fitted exponentiated Weibull distribution predicts too high densities. The densities of the WLS-fitted distributions seem to better fit these datasets. Overall, at the tail, the WLS-fitted exponentiated distributions match the empirical density values the closest.

The QQ-plots show results similar to density plots: The MLE-fitted exponentiated Weibull distributions match the data better than the translated Weibull distributions at high quantiles (Figure 3.5). However, at four datasets they predict too high values (datasets *A*, *D*, *E*, *F*). The WLS-fitted distributions provide good model fit over the complete range of the datasets. Only at the highest few observations deviations between the ordered values and the theoretical quantiles are apparent.

In summary, the density plots and the QQ-plots suggest that the exponentiated Weibull distribution is a better global model for significant wave height than the translated Weibull distribution. However, the QQ-plots show that in some datasets the MLE-fitted exponentiated Weibull distributions predict too high wave heights at high quantiles. There, the WLS-fitted distributions represent an improvement over the MLE-fitted distributions.

3.4.2 QUANTITATIVE ASSESSMENT

The two models of the exponentiated Weibull distribution provide the best fit in terms of mean absolute error (Figure 3.6). When the whole range of the datasets is considered, the MLE-fitted distributions have the lowest mean absolute error in five of six datasets. In the tail ($p_i > 0.99$) the WLS-fitted exponentiated Weibull distributions have the lowest mean absolute errors in five of six datasets. In the very tail ($p_i > 0.999$) the WLS-fitted exponentiated Weibull distributions have the lowest errors in all datasets. There, the averaged mean absolute errors of the three models are 0.24 ± 0.14 m, 1.08 ± 0.67 m and 1.80 ± 0.50 m (WLS-fitted exponentiated Weibull distribution, MLE-fitted expo-

3.4 Results

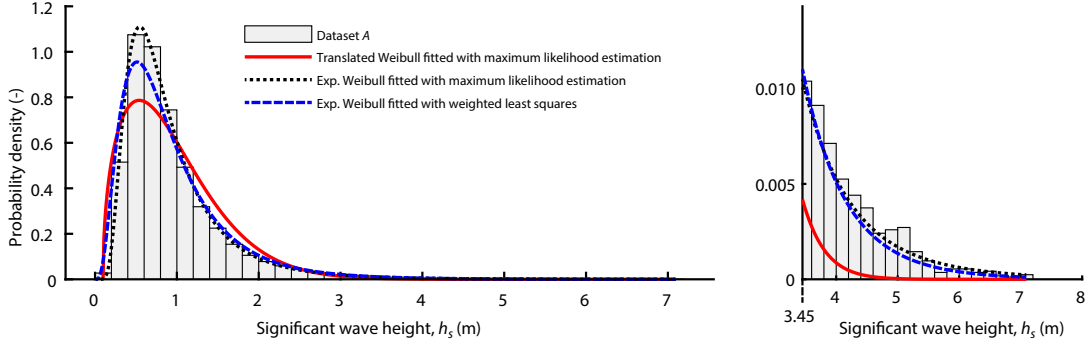


Figure 3.3: Model fit between dataset A and the three considered models. Left: Complete range of the distribution. Right: Tail of the distribution ($p_i > 0.99$). The three models fit decently at the distribution's body, but at the tail the translated Weibull distribution underestimates the observed probability density. This behavior is present in all six datasets.

Dataset	α (scale)	β (shape)	γ (location)
A	0.9445 ± 0.0055	1.4818 ± 0.0097	0.0981 ± 0.0039
B	1.1413 ± 0.0118	1.5990 ± 0.0140	0.1878 ± 0.0030
C	1.1645 ± 0.0124	1.5562 ± 0.0166	0.0566 ± 0.0097
D	1.5797 ± 0.0032	1.4067 ± 0.0029	0.1024 ± 0.0014
E	1.8608 ± 0.0027	1.4925 ± 0.0028	0.1222 ± 0.0007
F	2.5693 ± 0.0059	1.5466 ± 0.0046	0.2248 ± 0.0008

Table 3.3: Estimated parameters of the translated Weibull distributions. Values after the \pm -sign represent the bootstrap estimate of the standard error.

Dataset	Method	α (scale)	β (shape)	δ (shape)	$E[]$	Variance
A	MLE	0.0373 ± 0.0041	0.4743 ± 0.0094	46.6078 ± 3.8433	0.9428	0.4089
	WLS	0.2069 ± 0.0149	0.6844 ± 0.0142	7.7863 ± 0.6239	0.9387	0.4287
	Observed				0.9444	0.4121
B	MLE	0.1731 ± 0.0077	0.6563 ± 0.0085	17.3927 ± 0.7582	1.2063	0.4924
	WLS	0.0988 ± 0.0259	0.5835 ± 0.0316	36.5747 ± 9.7319	1.2139	0.4550
	Observed				1.2054	0.4696
C	MLE	0.3026 ± 0.0085	0.7445 ± 0.0077	6.4434 ± 0.1762	1.0984	0.5455
	WLS	0.2269 ± 0.0735	0.6973 ± 0.0636	9.8461 ± 4.2791	1.1086	0.4970
	Observed				1.0975	0.5163
D	MLE	0.4728 ± 0.0072	0.7452 ± 0.0042	5.1186 ± 0.0743	1.5354	1.2373
	WLS	0.9801 ± 0.0278	1.0077 ± 0.0147	2.1787 ± 0.0805	1.5291	1.1938
	Observed				1.5345	1.1751
E	MLE	0.7889 ± 0.0098	0.8842 ± 0.0052	3.7615 ± 0.0513	1.7972	1.4387
	WLS	1.2387 ± 0.0249	1.0991 ± 0.0120	2.0867 ± 0.0601	1.7918	1.4211
	Observed				1.7968	1.4011
F	MLE	0.7180 ± 0.0117	0.7663 ± 0.0046	6.5994 ± 0.1112	2.5263	2.6630
	WLS	1.6237 ± 0.0387	1.0941 ± 0.0141	2.4034 ± 0.0824	2.5197	2.5336
	Observed				2.5248	2.5014

Table 3.4: Estimated parameters of the exponentiated Weibull distributions. Parameters were estimated either using maximum likelihood estimation (MLE) or weighted least squares (WLS). Values after the \pm -sign represent the bootstrap estimate of the standard error. While there are strong differences between MLE and WLS parameters, expected values $E[]$ and variances are similar.

3 Long-term distribution of the significant wave height

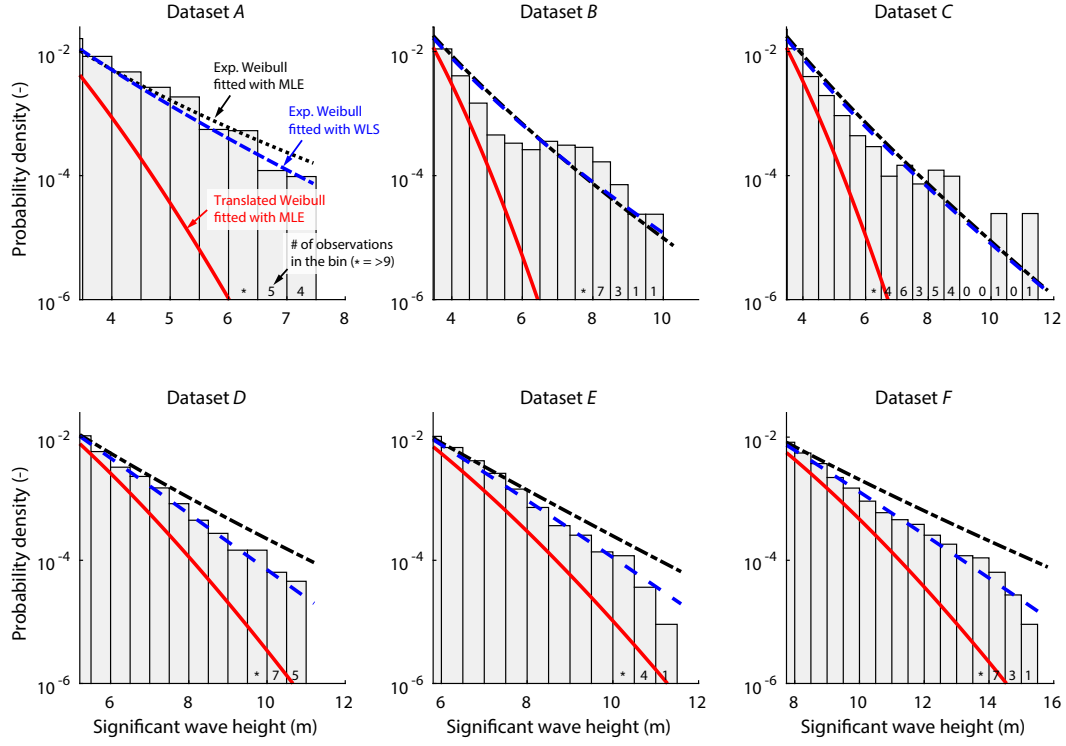


Figure 3.4: Tail plots of all datasets ($p_i > 0.99$). The translated Weibull distributions predict too low probability densities in all datasets. In datasets D, E, and F, the MLE-fitted exponentiated Weibull distributions predict too high probability densities.

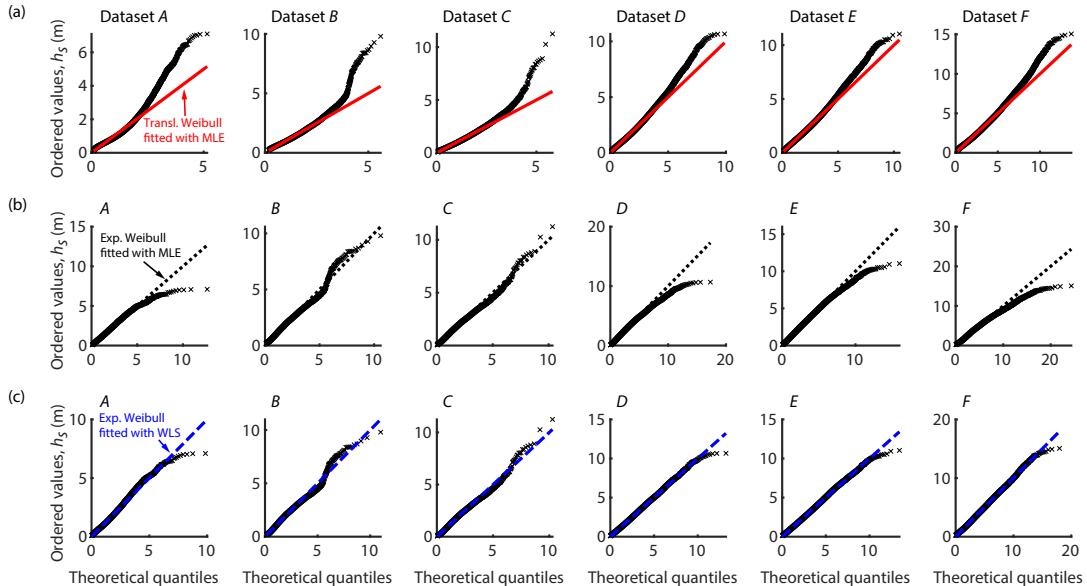


Figure 3.5: QQ-plots of all datasets. (a) Translated Weibull distributions. (b) Exponentiated Weibull distributions fitted with maximum likelihood estimation (MLE). (c) Exponentiated Weibull distributions fitted with weighted least squares (WLS) estimation.

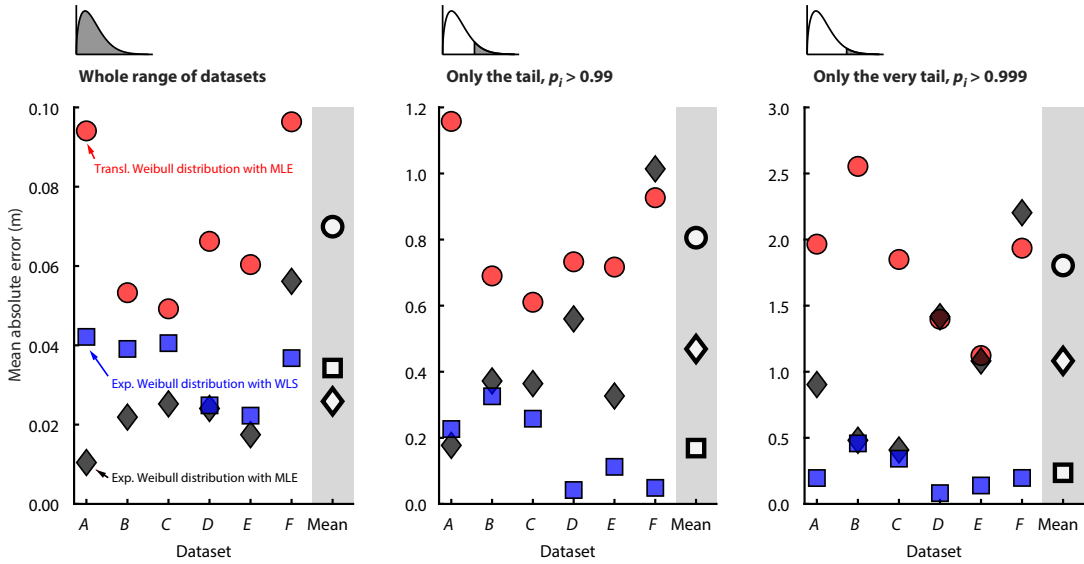


Figure 3.6: Mean absolute error of the predicted significant wave height for different parts of the distribution. Mean absolute error is a measure for the goodness of fit. It is calculated from the deviations between sample quantiles and predicted quantiles (see Equations 3.6 and 3.7). Circles = translated Weibull distributions, diamonds = MLE-fitted exponentiated Weibull distributions, squares = WLS-fitted exponentiated Weibull distributions.

nentiated Weibull distribution and translated Weibull distribution, respectively; $\bar{e}_{0.999}$ values are averaged over the six datasets, $N = 6$; values after the \pm -sign represent standard deviations).

The empirical return values are best predicted by the WLS-fitted exponentiated Weibull distribution (Figure 3.7). Its averaged normalized 1-year return value is 0.985, its standard deviation 0.054 ($N = 6$). The translated Weibull distribution predicts too low 1-year return values in all datasets ($H_{s1}^* = 0.714 \pm 0.122$, $N = 6$) and the MLE-fitted exponentiated Weibull distribution predicts too high return values in four datasets ($H_{s1}^* = 1.112 \pm 0.151$, $N = 6$).

The three types of models lead to big differences when 50-year return values are predicted (Figure 3.8). For example, for dataset A the translated Weibull distribution predicts $H_{s50} = 5.43$ m, the MLE-fitted exponentiated Weibull distribution predicts $H_{s50} = 14.35$ m and the WLS-fitted distribution predicts $H_{s50} = 10.86$ m. For comparison, in dataset A, which covers a duration of only 10 years, the highest measured H_s value is 7.10 m.

As a possibly more direct assessment of how well the fitted distributions predict future wave heights, we used some retained parts of the used data sources. The results obtained with these retained datasets are similar to the results with the original datasets: QQ-plots show that the WLS-fitted exponentiated Weibull distributions provide a good model fit at low, medium and high quantiles (Figure 3.9). Also, the translated Weibull distributions predict too low wave heights at high quantiles and the MLE-fitted exponentiated Weibull distributions sometimes predict too high wave heights at very high quantiles.

Among all models and datasets, the overall mean absolute error is between 0.01 and 0.14 m and no model is best or worst among all datasets (Figure 3.10). In the very tails ($p_i > 0.999$), the WLS-fitted exponentiated Weibull distributions have the lowest averaged mean absolute error, 0.37 ± 0.08 m ($N = 6$). The averaged mean absolute error of the MLE-fitted exponentiated Weibull distributions is 0.93 ± 0.63 m ($N = 6$) and the averaged mean absolute error of the translated Weibull distributions is 1.79 ± 0.49 m ($N = 6$; both also for $p_i > 0.999$).

3 Long-term distribution of the significant wave height

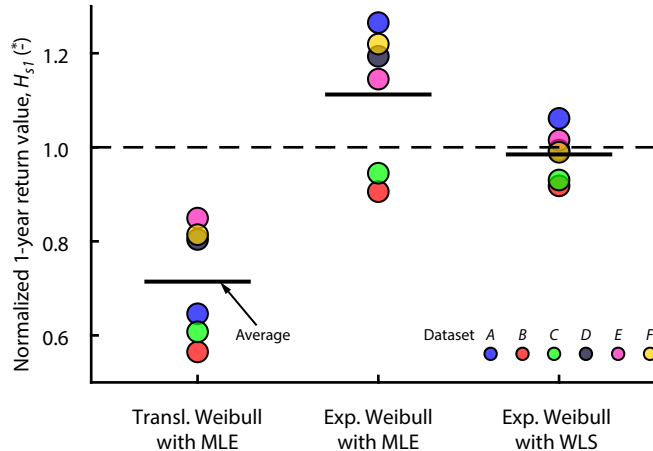


Figure 3.7: Comparison of the 1-year return values predicted by the three considered models. Normalized return values were calculated by dividing each model's return value by the empirical return value such that a value of 1 describes perfect agreement. The average of the normalized 1-year return values is too low for the translated Weibull distribution and too high for the MLE-fitted exponentiated Weibull distribution. The 1-year return values of the WLS-fitted exponentiated Weibull distribution agrees best with the empirical return values.

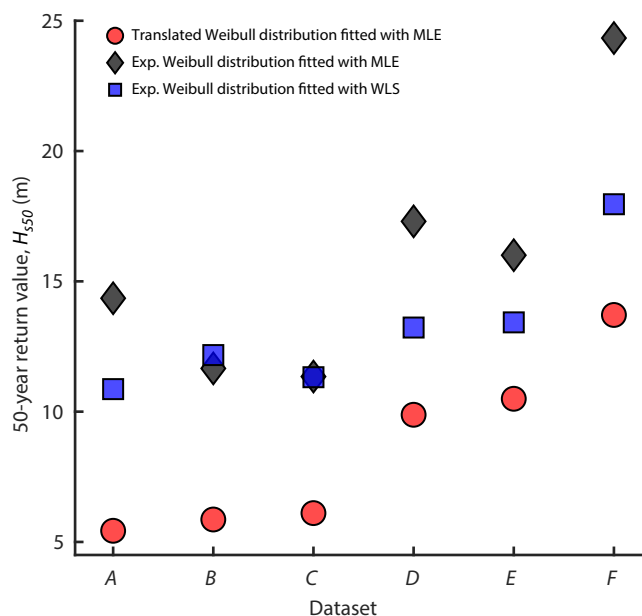


Figure 3.8: Predictions of the 50-year return values. The translated Weibull distribution predicts the lowest return value in all considered datasets.

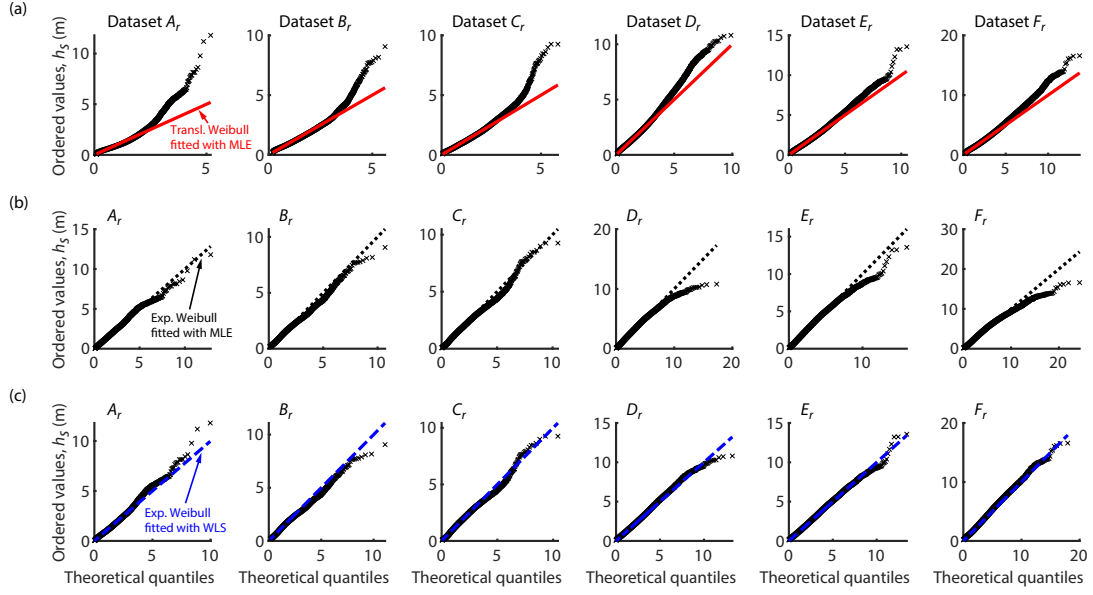


Figure 3.9: QQ-plots of the fitted distributions and the retained datasets. (a) Translated Weibull distributions. (b) Exponentiated Weibull distributions fitted with maximum likelihood estimation. (c) Exponentiated Weibull distributions fitted with weighted least squares estimation.

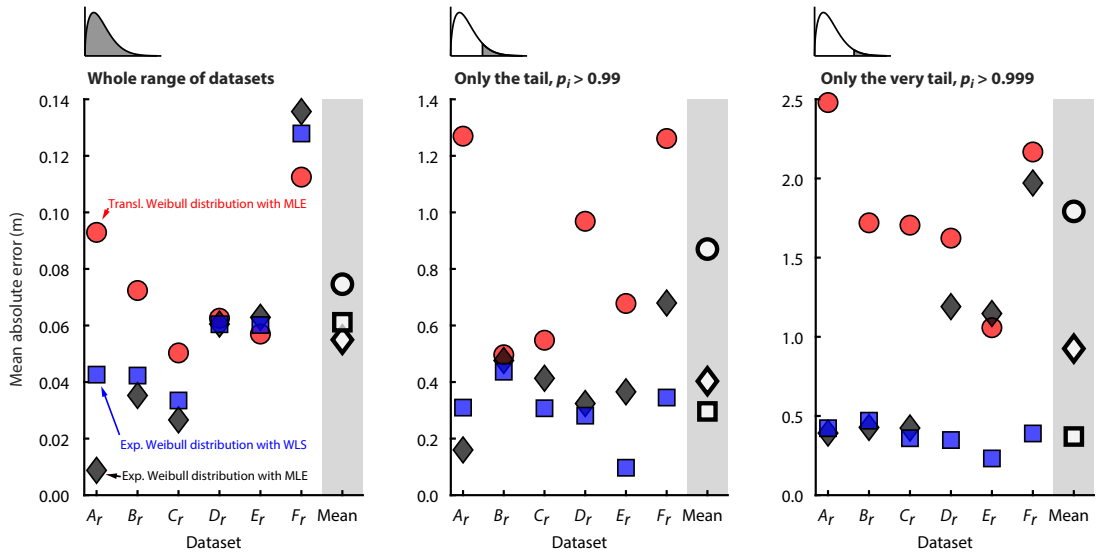


Figure 3.10: Mean absolute error between the fitted distributions and the retained datasets. In the very tail ($p_i > 0.999$) the WLS-fitted exponentiated Weibull distribution has the lowest error. Circles = translated Weibull distributions, diamonds = MLE-fitted exponentiated Weibull distributions, squares = WLS-fitted exponentiated Weibull distributions.

3 Long-term distribution of the significant wave height

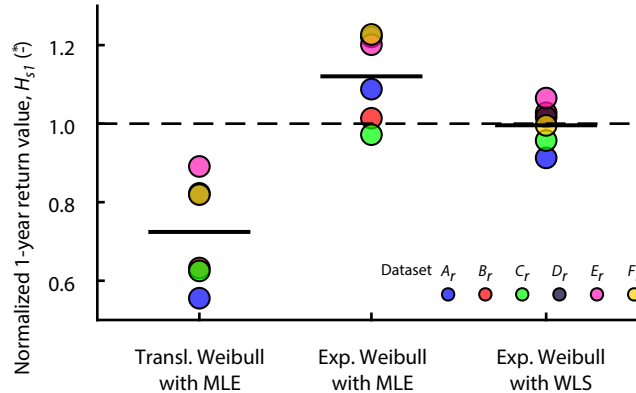


Figure 3.11: Comparison of the predicted 1-year return values and the return values of the retained datasets. Normalized return values are calculated by dividing each model's return value by the empirical return value such that a value of 1 describes perfect agreement.

When the predicted 1-year return values are compared with the empirical 1-year return values of the retained datasets, the results are similar as in the comparison with the values of the original datasets (Figure 3.11): The translated Weibull distributions predict too low wave heights ($H_{s1}^* = 0.724 \pm 0.137$, $N = 6$), the MLE-fitted exponentiated Weibull distributions predict mostly too high wave heights ($H_{s1}^* = 1.120 \pm 0.112$, $N = 6$) and the WLS-fitted distributions match the empirical return values best ($H_{s1}^* = 0.996 \pm 0.054$, $N = 6$).

In summary, the quantitative assessment showed that the three models have overall mean errors in the same order of magnitude. Among all datasets, all models and both in-sample predictions (datasets A, B, \dots) and out-of-sample predictions (datasets A_r, B_r, \dots), the overall mean error was between 0.01 and 0.14 m. Overall mean error and QQ-plots suggest that the three models perform relatively similar for typical H_s values. In the very tail ($p_i > 0.999$), however, a clear ranking of model performance is apparent: The WLS-fitted exponentiated Weibull distribution has the lowest averaged mean absolute error (0.24 m in-sample prediction, 0.37 m out-of-sample prediction) and the translated Weibull distribution has the highest error (1.80 m in-sample, 1.79 m out-of-sample).

3.5 DISCUSSION

3.5.1 COMPARISON BETWEEN THE TESTED AND OTHER MODELS

Our analysis suggests that the exponentiated Weibull distribution is a better model for significant wave height than the translated Weibull distribution. The exponentiated Weibull distribution matches the empirical data better especially at the tail. However, when the distribution is fitted using maximum likelihood estimation, the estimated parameters are mainly driven by the bulk of the data and not by the data in the very tail. Consequently, in our analysis, considerable errors remained for high quantiles such as the 1-year return value. In the design process of offshore structures, high quantiles of significant wave height are especially important. Thus, to improve model fit at the tail, we estimated the distribution's parameters by minimizing the sum of the weighted squared errors between data and model. To prioritize high values, we weighted the errors based on the squared wave height value.

The strongest possible prioritization of observations of high wave heights would be to ignore observations up to a particular threshold. In this case one would fit a distribution solely to the tail. To create a global model, a second distribution could be fitted to the bulk of the data. The combina-

tion of these two distributions creates a “two-part model,” which would serve as a global model. In such a model, the tail could be modeled with a generalized Pareto distribution and the body could be modeled, for example, with a Weibull distribution. The generalized Pareto distribution is often used to model the tails of other distributions and has been considered for wave heights (see, for example, [235, 237]). We expect that a two-part model could estimate the tail even better than the model that we proposed, however, that is expected for a model that has more parameters (2-3 parameter for the tail and 2-3 parameter for the body). Besides, two-part models either have a discontinuity in the PDF at the transition between the two distributions or they enforce continuity as another boundary condition, which might weaken the goodness of fit to the data (for a review on extreme value threshold estimation, see Scarrott and MacDonald [222]).

Other models that have been proposed as global models for the significant wave height are the log-normal distribution [132], the 2-parameter Weibull distribution [13], the generalized gamma distribution [198], the 3-parameter beta distribution of the second kind [63], the “Ochi distribution” [199] and the “Lonowe distribution” [110]. The 2-parameter Weibull distribution and the log-normal distribution have only two parameters and – to justify that we propose to use a distribution with three parameters – should fit the data much worse. These 2-parameter distributions are considered to be insufficient by other authors (see, for example, [151, 199]) and the brief inspection we performed suggested the same thing for this study’s datasets.

To understand why the exponentiated Weibull distribution provides a much better model fit than the common 2-parameter Weibull distribution, plotting the data on “Weibull paper” is illuminating (Figure 3.12). On Weibull paper, the wave data does not follow a straight line, but a continuously bending curve. The exponentiated Weibull distribution’s second shape parameter, δ , enables the distribution to follow this bend: $\delta > 1$ will lead to a curve that bends to the right and $\delta < 1$ will lead to a curve that bends to the left. The translated Weibull distribution’s location parameter also leads to a slight bend when plotted on Weibull probability paper. However, its location parameter does not control the shape directly and consequently, the translated Weibull distribution cannot match the empirical wave data to a similar degree as the exponentiated Weibull distribution.

The Ochi distribution and the Lonowe distribution have more parameters than the exponentiated Weibull distribution: The Ochi distribution has four parameters and the Lonowe distribution has four or five (depending on whether one counts the threshold between the Weibull-part of the model and the lognormal-part of the model as a parameter or not). Since we consider the performance of the exponentiated Weibull distribution as sufficiently good, we did not consider these more complex distributions in this study.

The generalized gamma distribution [198], and the 3-parameter beta distribution of the second kind [63], however, have similar model complexity in terms of number of parameters. Thus, we tested these distributions by fitting them to the six datasets using maximum likelihood estimation and by computing the overall mean absolute error (details are provided in Section A.2). The generalized gamma distributions and the 3-parameter beta distributions had errors of 0.0317 ± 0.0203 m and 0.0294 ± 0.0177 m, respectively ($N = 6$). These averaged errors are higher than the averaged error of the MLE-fitted exponentiated Weibull distributions (0.0259 ± 0.0158 m, $N = 6$), however, in the same order of magnitude. In two datasets, the exponentiated Weibull distribution had the lowest error, and in four datasets, the generalized gamma distribution had the lowest error. Thus, these three models seem to perform roughly equally well. Future research based on more datasets could help to learn more about the detailed differences between these three distributions.

In summary, among the variety of possible global models for significant wave height, the exponentiated Weibull distribution represents a good compromise between model complexity and model accuracy: It performs better than the current mostly used model – the translated Weibull distribution

3 Long-term distribution of the significant wave height

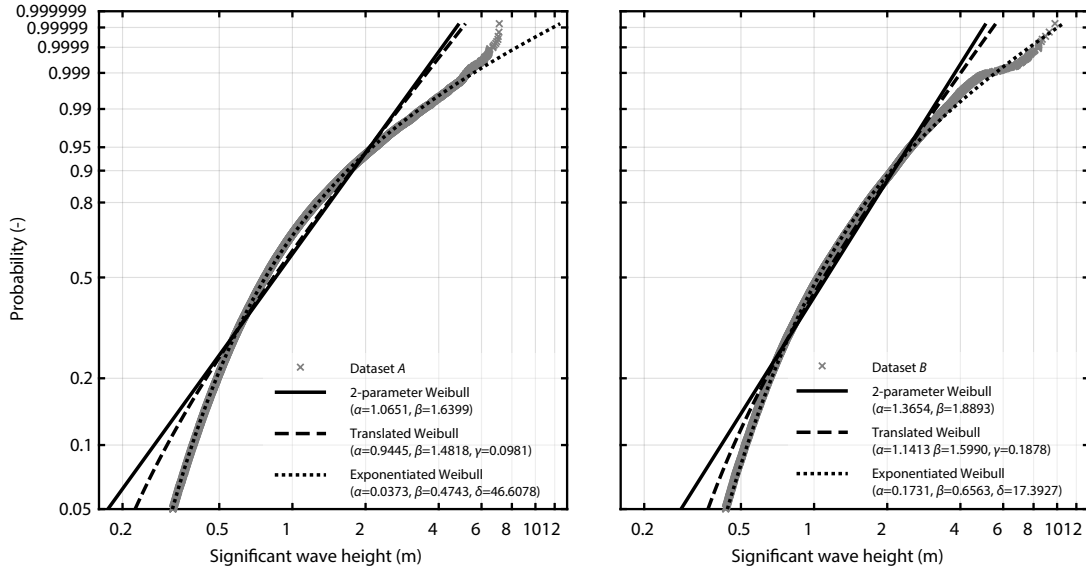


Figure 3.12: Weibull probability plot of datasets *A* and *B*. The shape parameter δ enables the exponentiated Weibull distribution to represent a curved line that is similar to the empirical data. The parameters of the shown distributions were fitted using maximum likelihood estimation.

– without increasing model complexity. The good performance of the exponentiated Weibull distribution can be explained by its second shape parameter, δ , which allows the distribution to represent a bending curve when plotted on Weibull paper.

3.5.2 IMPLICATIONS ON DESIGN LOADS

Current international standards that regulate the design of fixed and floating offshore wind turbines [129, 130] require designers to estimate the 1-year and 50-year return values of the significant wave height. These return values are used in standardized design load cases (DLCs). A design load case describes an operating condition of a wind turbine, together with the environmental conditions during this operating condition. They are used to check whether a wind turbine design preserves structural integrity under all future environmental and operating conditions that can reasonably be expected. DLCs are developed and maintained by standardization organizations. The International Electrotechnical Commission's standard IEC 61400-3 [129] is widely used by turbine manufacturers, certifying organizations and by academics who study wind turbine design (see, for example, [178, 212]). Estimating the 1-year wave height return value, H_{s1} , is required for the design load cases 6.3, 7.1 and 8.2, while the 50-year return value, H_{s50} , is required for DLC 6.1 and 6.2 [129]. In each of these design load cases, the estimated wave height return value determines a design load that is used to evaluate structural integrity. Consequently, the model used to describe the distribution of significant wave height influences wind turbine design via these design load cases.

Our results show that the current common technique of fitting a translated Weibull distribution to significant wave height data using maximum likelihood estimation strongly underestimates the 1-year return value. At the six tested sites, the 1-year return value is underestimated on average by about 30%. In some cases, the underestimation is even more severe. For example, in dataset *A*, the empirical 1-year return value is about 6.7 m, but the fitted translated Weibull distribution predicts a wave height of only 4.3 m.

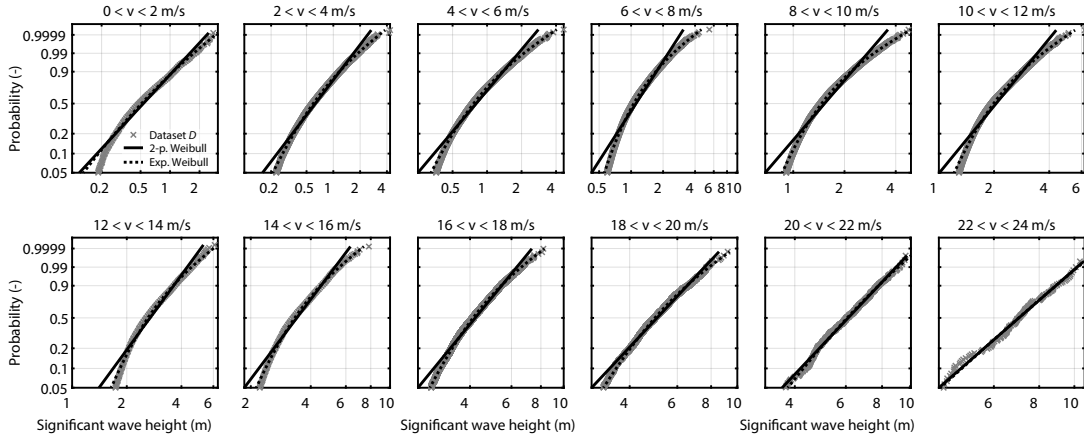


Figure 3.13: Weibull probability plots of conditional wave height distributions. Dataset D was sorted into wind speed intervals (v = wind speed). Due to the shape parameter δ the exponentiated Weibull distributions (dotted lines) can follow the curved lines of the empirical data. The displayed exponentiated Weibull distributions were fitted using weighted least squares estimation.

In structural design, uncertainties are partly taken care of with safety factors, which are multiplied with design loads (for details, see, for example, [129, pp. 66-68]). The normal safety factor for offshore wind turbines is 1.35 ([129]; see Table 3 in [128]), which is of similar magnitude as the typical error when H_{s1} is estimated based on a fitted translated Weibull distribution. This suggests that the found errors can be critical for the safety of a wind turbine design, especially if a turbine is particularly wave-sensitive (for a discussion on wave-sensitive turbine design, see, for example, [256]). The differences in the estimated 50-year return values are potentially even greater: For example, for dataset B , the translated Weibull distribution predicts a 50-year return value of about 6 m, while the WLS-fitted exponentiated Weibull distribution predicts a return value of about 12 m.

Besides the marginal distribution of H_s , the offshore wind standard IEC 61400-3-1 [129] requires designers to estimate joint 50-year extremes of wind speed and wave height. In the standard's DLC 1.6, designers need to estimate the conditional wave height distribution for a given wind speed, that is $F(h_s|v)$. The standard does not prescribe which distribution should be assumed for $F(h_s|v)$, however, researchers usually assume that conditional wave height follows a 2-parameter Weibull distribution (see, for example, [151, 155]). We tested how the 2-parameter Weibull distribution and the exponentiated Weibull distribution fit to conditional wave height data, using dataset D (the hindcast coastDat-2 also contains hourly wind data). Visual inspection of Weibull probability paper plots suggest that the exponentiated Weibull distribution fits better (Figure 3.13). In this thesis' following chapter, we will analyze the joint distribution of wind speed and significant wave height in detail. We will model the conditional distribution of H_s with an exponentiated Weibull distribution and we will explore, which expressions could be used to model the dependence functions of the parameters α , β and γ .

3.6 CONCLUSIONS

In this chapter, it was shown that the exponentiated Weibull distribution matches the empirical distribution of significant wave height data better than the commonly used translated Weibull distribution. Since the exponentiated Weibull distribution does not add complexity when compared with the translated Weibull distribution, we argue that it represents a better global model for significant

3 Long-term distribution of the significant wave height

wave height. In the six analyzed datasets, the translated Weibull distribution always predicted too low 1-year return values. When the exponentiated Weibull distribution was fitted using maximum likelihood estimation, it predicted too high 1-year return values in four of six cases. To improve its fit at the tail, we estimated its parameters by minimizing the weighted squared error between the model and the observations. The weights were chosen to quadratically increase with wave height. These WLS-fitted distributions showed good fit over the complete range of the datasets. Overall mean absolute error was in the order of 0.1 m and at the very tails ($p_i > 0.999$) mean absolute error was in the order of 0.5 m. Based on these results, we argue that if data do not indicate otherwise, the exponentiated Weibull distribution should be fitted to wave data instead of the translated Weibull distribution.

DATA AVAILABILITY AND MATLAB IMPLEMENTATION

The complete analysis performed in this study and the creation of the presented figures can be reproduced by running the file `CreateAllFigures.m` that is available in the repository <https://github.com/ahaselsteiner/2019-paper-predicting-wave-heights>. This repository also contains all datasets – preprocessed and structured as they were used in this study. Alternatively, the raw data of this study can be downloaded from the NDBC website, www.ndbc.noaa.gov, and from the coastDat-2 repository, doi: https://doi.org/10.1594/WDCC/coastDat-2_WAM-North_Sea.

The considered distributions were implemented in custom Matlab code. We created a Matlab class for each distribution. These classes provide functions to assess the PDF, the CDF, the ICDF, to estimate the distribution's parameters and draw samples from the distribution. They are publicly available:

- <https://github.com/ahaselsteiner/exponentiated-weibull>
- <https://github.com/ahaselsteiner/translated-weibull>
- <https://github.com/ahaselsteiner/generalized-gamma>
- <https://github.com/ahaselsteiner/beta-3p-second-kind>

4

JOINT DISTRIBUTION OF WIND SPEED, WAVE HEIGHT, AND WAVE PERIOD

PREVIOUSLY PUBLISHED This chapter is based on a publication by Haselsteiner et al. [102]. The chapter will introduce novel parametric models for the joint distribution of wind speed and wave height as well as for the joint distribution of wave height and wave period. The wind speed - wave height model represents one of three suggested improvements for the overall design process of offshore structures.

PUBLICATION'S FULL CITATION A. F. Haselsteiner, A. Sander, J.-H. Ohlendorf, and K.-D. Thoben. "Global hierarchical models for wind and wave contours: Physical interpretations of the dependence functions". In: *Proc. 39th International Conference on Ocean, Offshore and Arctic Engineering (OMAE 2020)*. American Society of Mechanical Engineers (ASME), 2020. doi: 10.1115/OMAE2020-18668

4.1 INTRODUCTION

Most joint distributions that are used to describe the metocean environment are not based on physical models. As discussed in the previous chapter, the marginal distribution of the significant wave height is sometimes modeled with a 2-parameter Weibull distribution [13], a 3-parameter Weibull distribution [195], a gamma distribution [198] or a hybrid log-normal-Weibull distribution ("Lonowe model") [110] and there is no physical model that supports the use of any particular distribution. Similarly, the state-of-the-art dependence structures between the metocean variables do not offer direct physical interpretation.

In engineering, probably the most used model type for the joint distribution of metocean variables is the global hierarchical model [47, 92]. In this model type, joint distributions are built up using conditional parametric distributions. For example, significant wave height H_s might be modeled with a marginal 3-parameter Weibull distribution and wind speed V with a 2-parameter Weibull distribution whose parameters depend on the value of H_s [47, p. 78]. Then so-called dependence functions are used, which in the wind speed - wave height case might be $\alpha_V(h_s) = c_1 + c_2 h_s^{c_3}$ where α_V represents the wind distribution's scale parameter. Such a dependence function might fit well to a particular dataset, however, it does not provide direct physical insights. As one cannot physically interpret such a dependence function, reasoning how well a particular fitted dependence function extrapolates outside a dataset could be called statistically informed guessing.

To describe the offshore environment, two bivariate joint distributions are commonly used: the distribution of sea states, F_{H_s, T_z} , and the distribution of wind speed - wave height states, F_{V, H_s} . The classification society DNV recommends the use of hierarchical model structures, each with 9 parameters, for these two joint distributions [47]. Their model structures are also widely used in academic publications (see, for example, [92, 246, 255]). In a recent benchmark study [93] co-organized by the author of this thesis, the authors used the recommended model structures and intentionally applied them without checking whether the models were appropriate for a particular offshore site. This

4 Joint distribution of wind speed, wave height, and wave period

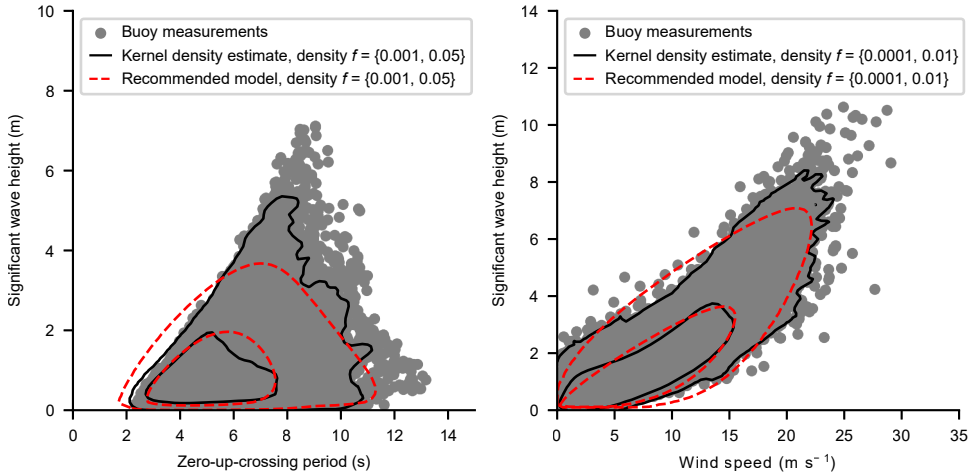


Figure 4.1: Problems in state-of-the-art joint models for sea states and for wind speed - wave height states.

Left: The fitted recommended sea state model has too low probability density at high wave heights.
 Right: The fitted recommended wind-wave model has too high density at the region of high wave heights and medium wind speeds. There, lines of constant density have negative curvature while empirical (kernel density estimation) lines of constant density have positive curvature. The plots are based on datasets A and D, respectively.

task was conducted to provide baseline results for the exercise. The fitted joint distributions did not match the empirical distributions properly: The sea state joint model F_{H_s, T_z} underestimated the occurrence of high wave heights and the dependence structure of the wind-wave joint model F_{V, H_s} described an incorrect relationship between the two variables (Figure 4.1).

This work was motivated by the potential advantages that dependence functions that can be interpreted physically could offer. Much is known about how winds and waves behave: how wind generates waves, when waves break and how wind sea and swell mix. If we can utilize this knowledge in the formalization of the joint model of environmental variables we should be able to design models that extrapolate better and whose parameters can be interpreted physically. In this study, we will design a novel dependence structure for the joint distribution of significant wave height and zero-up-crossing period, F_{H_s, T_z} , and a novel dependence structure for wind speed and wave height, F_{V, H_s} . We will focus on using physically interpretable expressions that describe how T_z depends on H_s and how H_s depends on V . Then, we will estimate the parameters of these distributions by fitting the models to six datasets describing metocean conditions in the Atlantic and in the North Sea.

4.2 RESEARCH METHODOLOGY

4.2.1 DATASETS

To test our models, we used six datasets: three datasets that describe sea states (H_s - T_z , datasets A, B, C) and three datasets that describe wind-wave states (V - H_s , datasets D, E, F; Table 4.1). These are the same datasets that were also used in Chapter 3. Additionally, these datasets were used in a benchmarking study on estimating extreme environmental conditions [92, 93]. Datasets A, B and C are from buoys of the National Data Buoy Center [192] and cover 10 years of hourly sea state conditions. Datasets D, E and F were retrieved from the hindcast coastDat-2 [80] and cover 25 years of hourly wind and wave data. The wind data represent a 10-minute mean value, measured 10 m above sea level.

Dataset	Variables	Site	Data source
A	H_s, T_z	off Maine coast	buoy 44007 [192]
B	H_s, T_z	off Florida coast	buoy 41009 [192]
C	H_s, T_z	Gulf of Mexico	buoy 42001 [192]
D	V, H_s	off German coast	hindcast [80]
E	V, H_s	off UK coast	hindcast [80]
F	V, H_s	off Norwegian coast	hindcast [80]

Table 4.1: Used datasets. These are the same locations and data sources as in the study presented in Chapter 3.

4.2.2 GLOBAL HIERARCHICAL MODELS

As described in Section 2.3.1, global hierarchical models are joint distribution models that cover the complete range of an environmental variable (“global”) and which follow a particular hierarchical dependence structure. In a global hierarchical model, if the joint density function is factorized, simple terms for the univariate density functions exist. Let X_1 and X_2 represent random variables, for example $X_1 = V$ and $X_2 = H_s$, and let $f_{X_1, X_2}(x_1, x_2)$ represent its joint density function. Then the factorization

$$f_{X_1, X_2}(x_1, x_2) = f_{X_1}(x_1)f_{X_2|X_1}(x_2|x_1) \quad (4.1)$$

describes a hierarchy where a random variable with index i can only depend upon random variables with indices less than i . In the two-dimensional case, random variable X_1 is independent and random variable X_2 is conditional on X_1 ($X_i|X_{i-1}$ with $i = 2$). Usually, simple parametric distributions are assumed for the random variables and the dependence of X_2 under X_1 is modeled using simple dependence functions with 2 to 4 parameters (see, for example, [17, 34, 116, 118, 151, 168]). Let α_2 and β_2 represent the parameters of the second distribution. Then these parameters might be modeled with dependence functions $h_{[\text{parameter}]}$ with n parameters (denoted as c_i and d_i , $i = 1, \dots, n$):

$$\begin{aligned} \alpha_2 &= h_\alpha(x_1; c_1, c_2, \dots, c_n), \\ \beta_2 &= h_\beta(x_1; d_1, d_2, \dots, d_n). \end{aligned} \quad (4.2)$$

Typical expressions are a power function, $h_\alpha(x_1) = c_1 + c_2x_1^{c_3}$, or an exponential function, $h_\alpha(x_1) = d_1 + d_2e^{d_3x_1}$ [47].

We assumed the following model for sea states: Significant wave height follows an exponentiated Weibull distribution and zero-up-crossing period follows a log-normal distribution that depends on the value of H_s . The exponentiated Weibull distribution has been proposed to model H_s in Chapter 3 and the log-normal distribution is a usual choice for modeling $T_z|H_s$ [47]. The two distributions read

$$\begin{aligned} F(h_s) &= \left(1 - \exp\left[-(h_s/\alpha)^\beta\right]\right)^\delta, \\ F(t_z|h_s) &= \frac{1}{2} + \frac{1}{2}\operatorname{erf}\left(\frac{\ln t_z - \mu_{tz}}{\sqrt{2}\sigma_{tz}}\right). \end{aligned} \quad (4.3)$$

We modeled the log-normal distribution’s parameter μ_{tz} with a two-parameter dependence function:

$$\mu_{tz} = \ln\left(c_1 + c_2\sqrt{\frac{h_s}{g}}\right), \quad (4.4)$$

4 Joint distribution of wind speed, wave height, and wave period

where g is the acceleration due to gravity, $g = 9.81 \text{ m s}^{-2}$ and c_1 and c_2 are parameters that will be estimated. The parameter μ_{tz} can be directly related to the period's median, $\tilde{t}_z = e^{\mu_{tz}}$. Thus, the dependence function implies

$$\tilde{t}_z = c_1 + c_2 \sqrt{\frac{h_s}{g}}, \quad (4.5)$$

which is an expression that is physically consistent if $[\tilde{t}_z] = \text{s}$, $[h_s] = \text{m}$ and $[g] = \text{m s}^{-2}$ if $[c_1] = \text{m}$ and c_2 is unitless. The parameter σ_{tz} is modeled with an asymptotically decreasing dependence function:

$$\sigma_{tz} = c_3 + \frac{c_4}{1 + c_5 h_s}. \quad (4.6)$$

For the wind speed - wave height joint distribution, the following model is assumed: Wind speed follows an exponentiated Weibull distribution and significant wave height follows an exponentiated Weibull distribution that is conditional on the value of V :

$$\begin{aligned} F(v) &= \left(1 - \exp\left[-(v/\alpha)^\beta\right]\right)^\delta, \\ F(h_s|v) &= \left(1 - \exp\left[-(h_s/\alpha_{hs})^{\beta_{hs}}\right]\right)^{\delta_{hs}}. \end{aligned} \quad (4.7)$$

Weibull distributions are a typical choice for both, wind speed and wave height. However, wave height is usually modeled with a translated Weibull distribution and wind speed with a 2-parameter Weibull distribution depending on the value of H_s (see, for example, [47, 93]) instead of the exponentiated Weibull distribution. Here, we used the exponentiated Weibull distribution for wind speed, as the 2-parameter Weibull distribution provided bad model fit for one of the datasets.

We modeled the dependence structure between the two variables by assuming two relationships:
1) the median of H_s increases with wind speed,

$$\tilde{h}_s = c_6 + c_7 v_*^{c_8}, \quad (4.8)$$

where the non-dimensional wind speed $v_* = v/v_c$, with $v_c = 1 \text{ m s}^{-1}$; and 2) the shape parameter β_{hs} follows a logistics function,

$$\beta_{hs} = c_9 + \frac{c_{10}}{1 + e^{-c_{11}(v - c_{12})}}. \quad (4.9)$$

We used non-dimensional wind speed in Expression 4.8 to ensure that the units of the equation are correct if $[\tilde{h}_s] = \text{m}$, $[c_6] = \text{m}$, $[c_7] = \text{m}$, and $[c_8]$ is unitless.

Because exponentiated Weibull's quantile function reads

$$Q(p) = \alpha \left[-1 \ln(1 - p^{1/\beta_{hs}}) \right]^{1/\beta_{hs}}, \quad (4.10)$$

the median wave height can also be expressed as

$$\tilde{h}_s = Q(0.5) = \alpha_{hs} \left[-1 \ln(1 - 0.5^{1/\beta_{hs}}) \right]^{1/\beta_{hs}}. \quad (4.11)$$

In our model, the exponent of the exponentiated Weibull distribution is set to $\delta_{hs} = 5$ such that

$$\begin{aligned}\tilde{h}_s &= \alpha_{hs} \left[-1 \ln(1 - 0.5^{1/5}) \right]^{1/\beta_{hs}}, \\ \tilde{h}_s &= \alpha_{hs} 2.0445^{1/\beta_{hs}}.\end{aligned}\quad (4.12)$$

Rearranging this equation to express the dependence function of α_{hs} and substituting \tilde{h}_s with (4.8), we obtain

$$\alpha_{hs} = (c_6 + c_7 v^{c_8}) / 2.0445^{1/\beta_{hs}}. \quad (4.13)$$

This structure has the advantage that the relationship between typical (median) wave height values and wind speed values is modeled with a simple expression that can be interpreted physically. The estimated exponent c_8 might imply that \tilde{h}_s increases linearly, quadratically or something in between with increasing wind speed and its value can be compared with theories on wind-generated seas (see, for example, [115])

4.2.3 PARAMETER ESTIMATION

The eight parameters of the sea state model and the ten parameters of the wind speed - wave height model were estimated by fitting the described model structure to each of the datasets. All computations were performed using the open-source Python software viroconcom in version 1.3.9 [95].

We fitted the sea state model by following a stepwise process: First the marginal distribution of H_s was fitted by using the weighted least squares method that was presented in Chapter 3. Second, zero-up-crossing period was sorted into H_s intervals. We used an interval size of 0.5 m. Third, distributions were fitted to zero-up-crossing period in each interval that held at least 50 data points using maximum likelihood estimation. Finally, the dependence functions were fitted using nonlinear least squares.

Similarly, the parameters of the wind speed - wave height models were estimated following a stepwise process: The marginal distribution of V and the distribution of H_s in each interval were fitted using the weighted least squares method (Chapter 3). The interval size was 2 m s^{-1} and the required number of data points within each bin was set to 50 as well. Dependence functions were fitted using nonlinear least squares with weights of $(1 / \text{parameter value})$. As a consequence, the estimated dependence function will fit the observations at small parameter values better, at the expense of a higher error at large parameter values (compared to if no weights were used).

4.3 RESULTS

4.3.1 OVERALL MODEL FIT

Table 4.2 presents the estimated parameters of the joint distribution models and Figure 4.2 and Figure 4.3 show the joint models' density functions. Both, the sea state, and the wind speed - wave height models appear to catch the two-dimensional structure of the datasets. Constant density lines of the joint model describe smooth versions of empirical density lines, which are estimated using kernel density estimation (Figure 4.2 and Figure 4.3). Conditional median values of the model and the original datasets compare well too: In the sea state model they match well, except at very low wave heights ($H_s < 0.5 \text{ m}$); in the wind speed - wave height model the fit of the conditional median value is good across the complete wind speed range.

Dataset	Significant wave height			Zero-up-crossing period, log-normal distribution						
	Exponentiated Weibull distribution			$\mu_{tz}(h_s) = \ln\left(c_1 + c_2\sqrt{\frac{h_s}{g}}\right)$			$\sigma_{tz}(h_s) = c_3 + \frac{c_4}{1 + c_5 h_s}$			
	α (scale)	β (shape)	δ (shape)	c_1	c_2		c_3	c_4	c_5	
A	0.207	0.684	7.79	3.62	5.77		0	0.324	0.404	
B	0.0988	0.584	36.6	3.54	5.31		0	0.241	0.256	
C	0.227	0.697	9.85	2.71	6.51		0.0109	0.147	0.236	
Wind speed			Significant wave height, exponentiated Weibull distribution with $\delta_{hs} = 5$							
Exponentiated Weibull distribution			$\alpha_{hs}(v) = (c_6 + c_7 v_*^{c_8}) / 2.0445^{1/\beta_{hs}(v)}$			$\beta_{hs}(v) = c_9 + \frac{c_{10}}{1 + e^{-c_{11}(v - c_{12})}}$				
α (scale)			c_6	c_7	c_8	c_9	c_{10}	c_{11}	c_{12}	
D	10.0	2.42	0.761	0.488	0.0114	2.03	0.714	1.70	0.304	8.77
E	10.8	2.48	0.683	0.617	0.0174	1.87	0.724	2.01	0.309	9.59
F	11.5	2.56	0.534	1.09	0.0251	1.80	0.726	1.89	0.194	13.4

Table 4.2: Fitted sea state (datasets A, B, C) and wind speed - wave height (datasets D, E, F) joint models. g = acceleration due to gravity, v_* = non-dimensional wind speed ($v_* = v/v_c, v_c = 1 \text{ m s}^{-1}$)

Another way to assess overall model fit is to compare the marginal distributions of the original dataset and the fitted joint model. Figure 4.4 and Figure 4.5 show quantile-quantile plots of the marginal distributions of the sea state and wind-wave models, respectively. At the highest quantiles, notable deviations are apparent for significant wave height in dataset *A* and for zero-up-crossing period in dataset *B*. In dataset *A* higher wave heights are predicted by the model and in dataset *B* lower periods are predicted by the model.

The results presented in this chapter were also submitted to a benchmarking exercise on environmental contours. In the manuscript that presented the results of this exercise [92] further analysis for the model is provided. Additionally, it provides a comparison with eight other contributions to the benchmark, which used different types of joint distribution models. Because this benchmarking study was a joint work with 21 colleagues, its results are not presented in this thesis. A similar benchmarking study, that focused on modeling the marginal distribution of significant wave height and the influence of a changing climate was announced in 2021 [91, 157]. This study will make use a recently published 700-year long hindcast dataset [11, 231] such that estimates for the 50-year wave height return value can be better analyzed than with common hindcast datasets that cover less than 100 years.

4.3.2 DEPENDENCE FUNCTIONS

The estimated parameter values suggest that dependence structures of the sea state models have common characteristics (Figure 4.6). The dependence functions for the parameter μ_{tz} imply a relationship for the median T_z given H_s

$$\tilde{t}_z(h_s) = [2.7 \text{ s}, 3.6 \text{ s}] + [5.3, 6.5] \sqrt{h_s/g}, \quad (4.14)$$

where values within the brackets hold the lowest and highest parameter values among the three datasets (parameters c_1 and c_2 in Table 4.2). For high sea states, $h_s = 10 \text{ m}$, these dependence functions predict $\tilde{t}_z = \{9.5 \text{ s}, 8.9 \text{ s}, 9.3 \text{ s}\}$ for datasets *A*, *B* and *C*, respectively. Visually comparing these predicted sea states with the datasets suggest that the dependence functions are reasonable (Figure 4.2).

These dependence functions can also be used to analyze what they imply for steepness. Steepness, s_z , is a non-dimensional variable that describes a sea state [115, p. 88]:

$$s_z = \frac{2\pi h_s}{gt_z^2}. \quad (4.15)$$

Using our expression for \tilde{t}_z , we can derive a model for expected median steepness, \tilde{s}_z :

$$\tilde{s}_z = \frac{2\pi h_s}{g(c_1 + c_2 \sqrt{h_s/g})^2}. \quad (4.16)$$

A plot of steepness over significant wave height suggests that the predicted median steepness is reasonable (Figure 4.7). Interestingly, the used datasets contain many data points whose steepness exceeds 1/15, which is sometimes seen as an upper limit due to wave breaking (see, for example, [115, p. 88]).

Similarly, dependence functions of fitted wind speed - wave height models show similarities among the three datasets and can be physically interpreted (Figure 4.8). The

4 Joint distribution of wind speed, wave height, and wave period

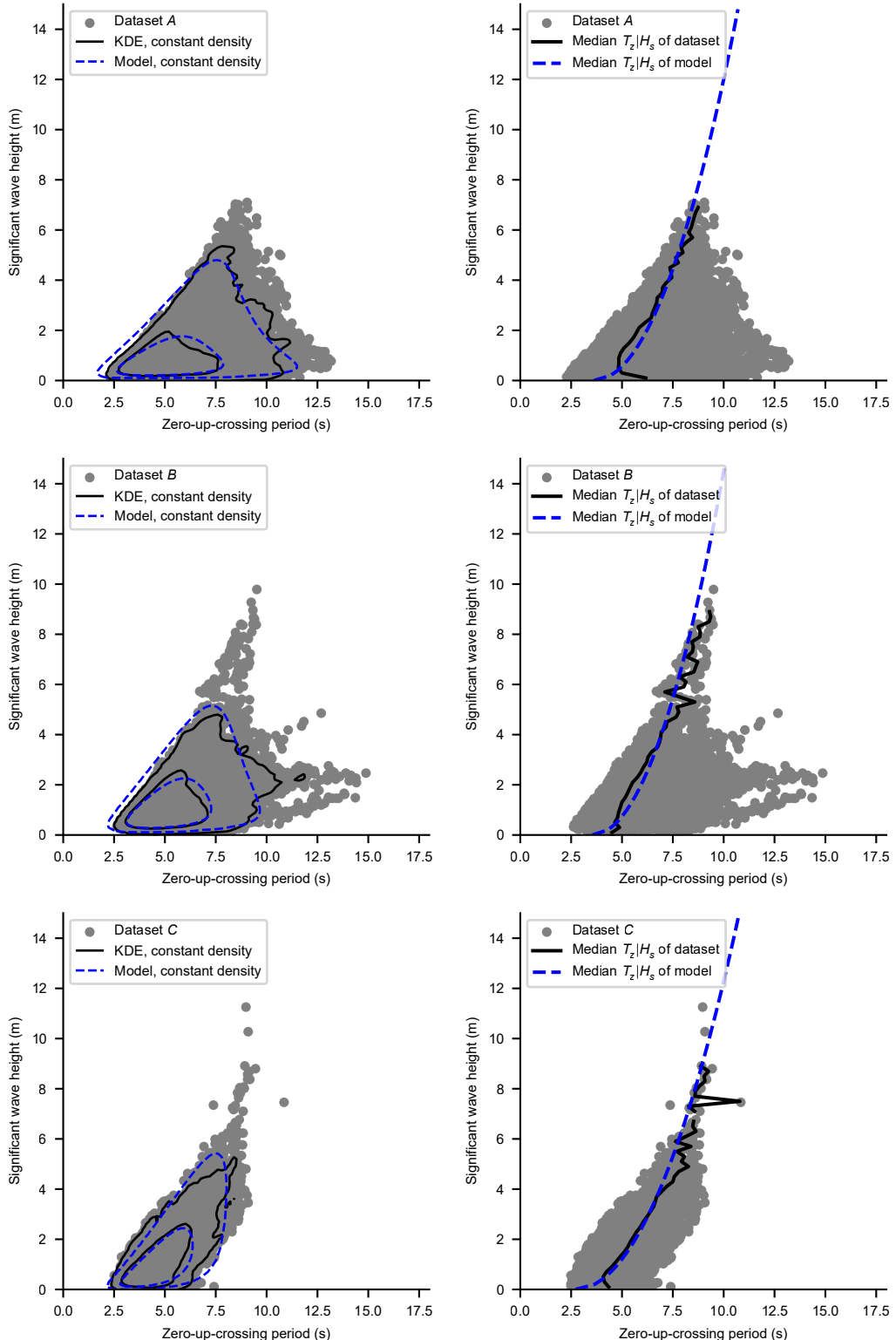


Figure 4.2: Overall model fit of the sea state joint model. Left: Lines of constant probability density $f = \{0.001, 0.05\}$ of a kernel density estimate (KDE), which represents empirical density, and of the proposed global hierarchical model. Right: Comparison of the conditional median zero-up-crossing period given significant wave height.

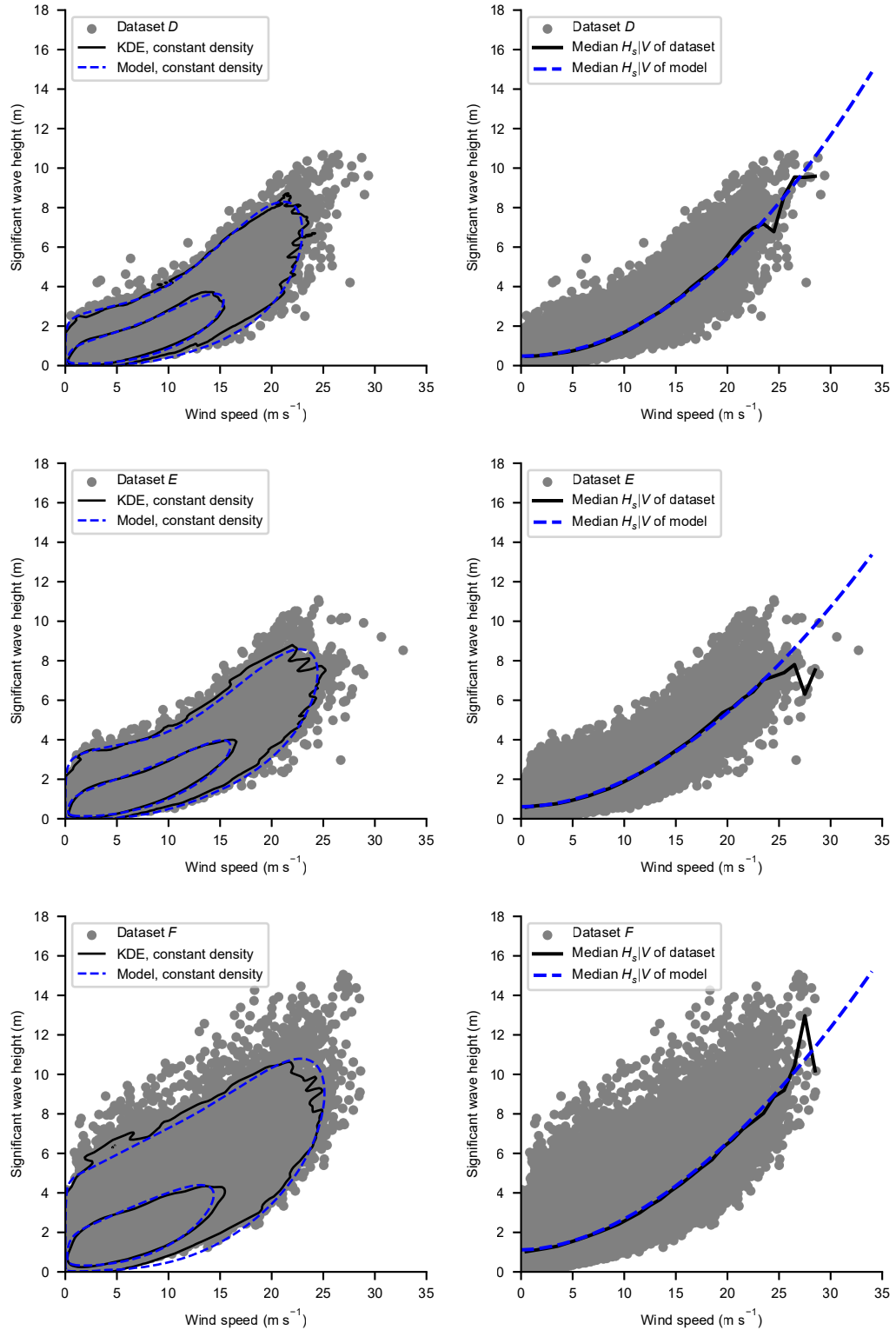


Figure 4.3: Overall model fit of the wind speed - wave height joint model. Left: Lines of constant probability density $f = \{0.0001, 0.01\}$ of a kernel density estimate (KDE), which represents empirical density, and of the proposed global hierarchical model. Right: Comparison of the conditional median significant wave height given wind speed.

4 Joint distribution of wind speed, wave height, and wave period

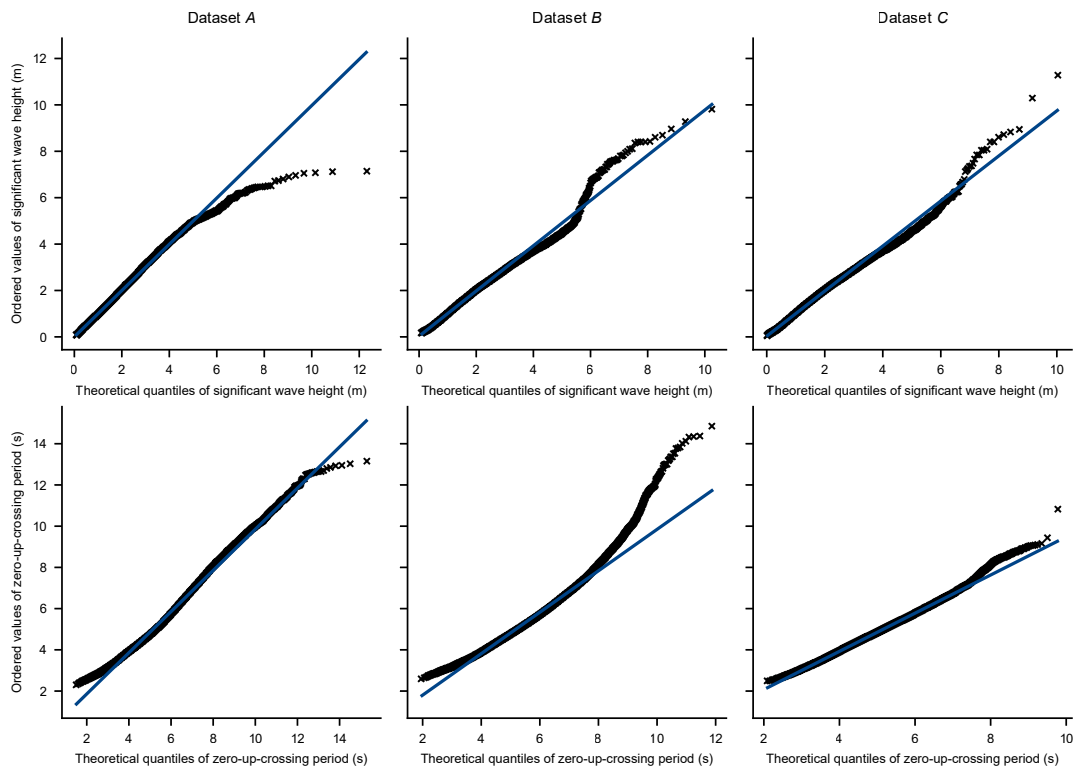


Figure 4.4: Quantile-quantile plots of the marginal distributions of the sea state joint distribution model. Straight lines indicate a perfect fit between the empirical distribution and the model distribution.

4.3 Results

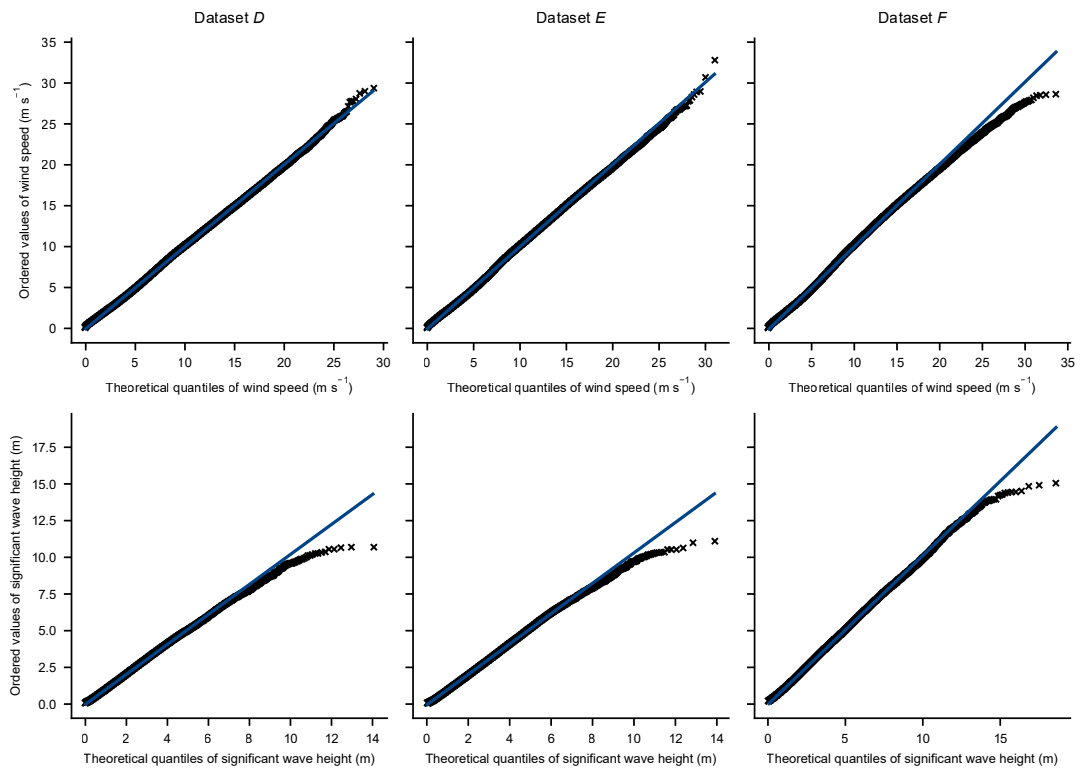


Figure 4.5: Quantile-quantile plots of the marginal distributions of the wind speed - wave height joint distribution model. Straight lines indicate a perfect fit between the empirical distribution and the model distribution.

4 Joint distribution of wind speed, wave height, and wave period

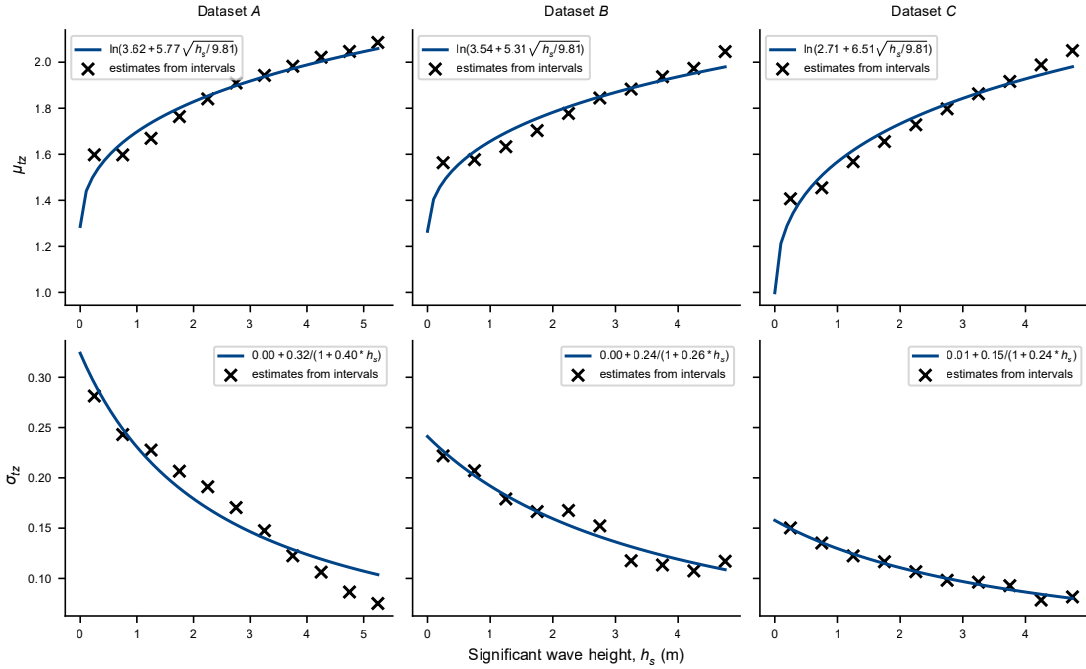


Figure 4.6: Sea state joint model. The dependence function of μ_{tz} is designed such that the median of the zero-up-crossing period increases with $\sqrt{h_s/g}$ where h_s represents significant wave height and g represents the acceleration due to gravity at Earth's surface.

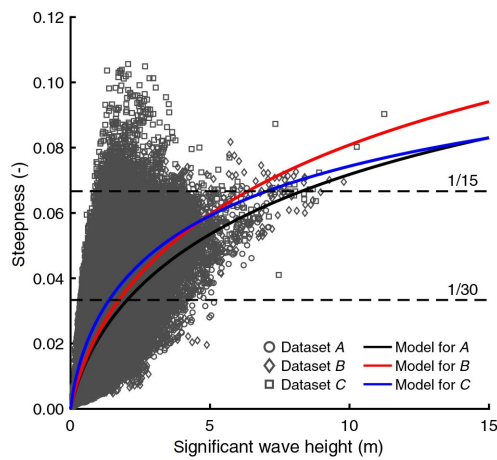


Figure 4.7: The dependence function for median zero-up-crossing period given wave height can be used to derive the predicted relationship for the median of steepness as a function of wave height.

4.3 Results

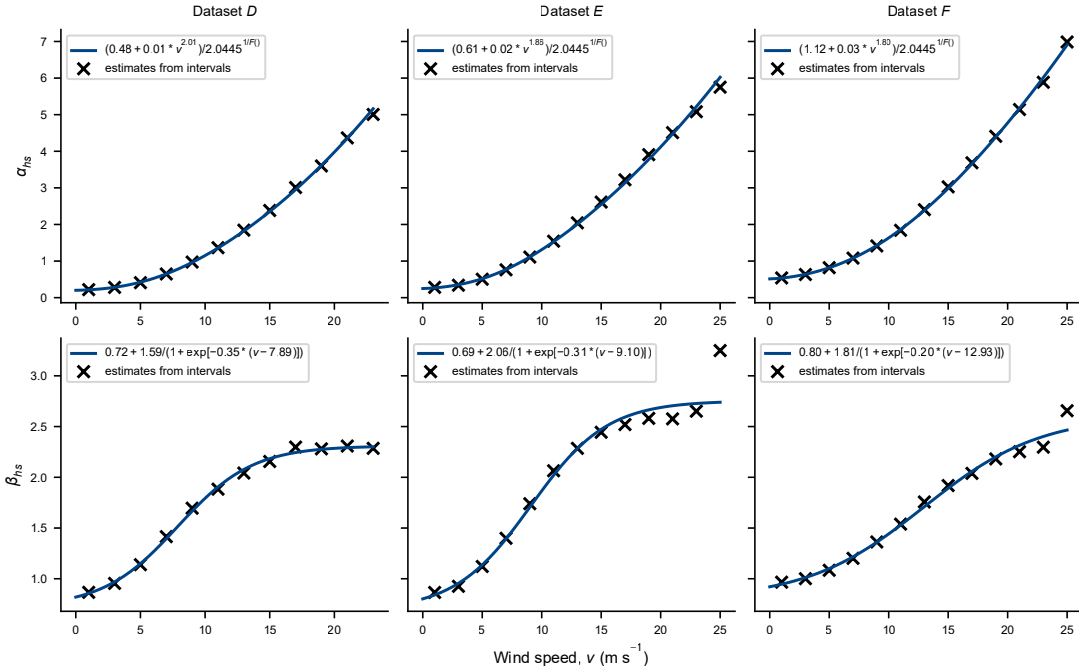


Figure 4.8: Wind speed - wave height joint model. The dependence function of the scale parameter α_{hs} is based on the median of significant wave height \tilde{h}_s , which is modeled as $\tilde{h}_s = c_6 + c_7 v^{c_8}$ where v represents wind speed.

median of significant wave height increases with wind speed in the following manner:

$$\tilde{h}_s = [0.5 \text{ m}, 1.1 \text{ m}] + [0.011 \text{ m}, 0.025 \text{ m}] v_*^{[1.8, 2.0]}, \quad (4.17)$$

where values within the brackets hold the lowest and highest coefficient values among the three datasets (parameters c_6 , c_7 , and c_8 in Table 4.2).

This suggests that there are two parts to significant wave height: one part that is independent of local wind speed and is in the order of 1 m and one part that increases with wind speed, where the increase is more than linear, but at two sites also less than quadratic. The first part could be interpreted as either a swell component or as waves that were generated locally, but in the past. The second part is especially interesting as it might offer insights into the nature of the sea state. The found exponents between 1 and 2 lie between the limits of two different kind of seas: In fully developed wind-generated seas that follow a Pierson-Moskowitz spectrum, significant wave height quadratically increases with wind speed [200, p. 35]. In seas, which are not fully developed, significant wave height might increase linearly (if they are fetch-limited) or with $v^{9/7}$ if they are duration-limited [240, p. 360].

4.3.3 EXPONENTIATED WEIBULL DISTRIBUTION

The exponentiated Weibull distribution is a novel distribution choice for sea state joint models and for wind-wave joint models. The marginal distribution of H_s was modeled well with the exponentiated Weibull distribution and a detailed analysis on its goodness of fit for datasets A, B and C was presented in Chapter 3.

In the wind speed - wave height models, we used the exponentiated Weibull distribution to model the marginal distribution of wind speed. Usually, a 2-parameter Weibull distribution is used instead, which is an exponentiated Weibull distribution with $\delta = 1$. Thus, thanks to its additional parameter, an exponentiated Weibull distribution will fit any dataset at least as good as a 2-parameter Weibull

4 Joint distribution of wind speed, wave height, and wave period

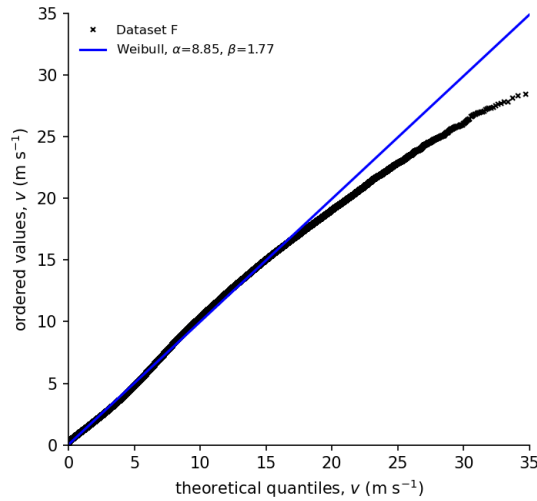


Figure 4.9: In dataset F wind speed does not follow a two-parameter Weibull distribution at high quantiles.

distribution. However, the additional parameter adds complexity and therefore its use over the 2-parameter Weibull distribution should be justified. The distribution of wind speed in datasets D and E can be described well with a 2-parameter Weibull distribution, however, in dataset F the data do not follow a 2-parameter Weibull distribution at high wind speeds (Figure 4.9). A fitted 2-parameter Weibull distribution would predict too high wind speeds in dataset F while a fitted exponentiated Weibull distribution can follow the shape of the empirical distribution and thus can predict wind speeds better (Figure 4.5). Interestingly, the estimated values for the second shape parameter, δ , were less than 1 in all three datasets (Table 4.2). This is in contrast to the δ values that were estimated for the marginal distribution of significant wave height: they were greater than 1 in all datasets.

Finally, we used the exponentiated Weibull distribution to model the distribution of significant wave height within given wind speed intervals. To keep model complexity – measured in numbers of free parameters – in balance, we used an exponentiated Weibull distribution with a fixed exponent of $\delta = 5$. This choice was based on first fitting exponentiated Weibull distributions with free exponents to binned wave data. We found that δ varied between 2 and 23 and that it followed a bell-like curve (Figure 4.10). Based on these results we decided to set $\delta = 5$ and to fit these fixed-exponent distributions again such that we would get the parameter values of α and β that lead to the best fit with $\delta = 5$.

The exponentiated Weibull distributions with $\delta = 5$ showed good model fit at all wind speed intervals (Figure 4.11). Plotting the distribution on Weibull paper illustrates that a 2-parameter Weibull distribution is insufficient to describe the empirical distribution. The second shape parameter of the exponentiated Weibull distribution, $\delta = 5$, however, enables the distribution to follow the shape of the data. These results suggest that if data do not indicate otherwise, conditional significant wave height data should be assumed to follow an exponentiated Weibull distribution.

4.3.4 EXTRAPOLATION

To derive extreme loads with return periods of 50 years or higher, we would need to extrapolate beyond the duration of the datasets. Figure 4.12 shows lines of very low constant density plotted on top of the datasets. Although we do not have enough data to allow a direct comparison between

4.3 Results

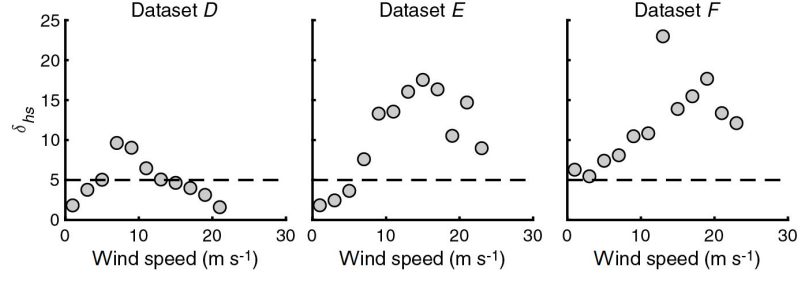


Figure 4.10: Estimates for the second shape parameter, δ_{hs} , of the exponentiated Weibull distribution at different wind speed intervals. Although the exponent changes, in our model, we set $\delta_{hs} = 5$ to reduce model complexity.

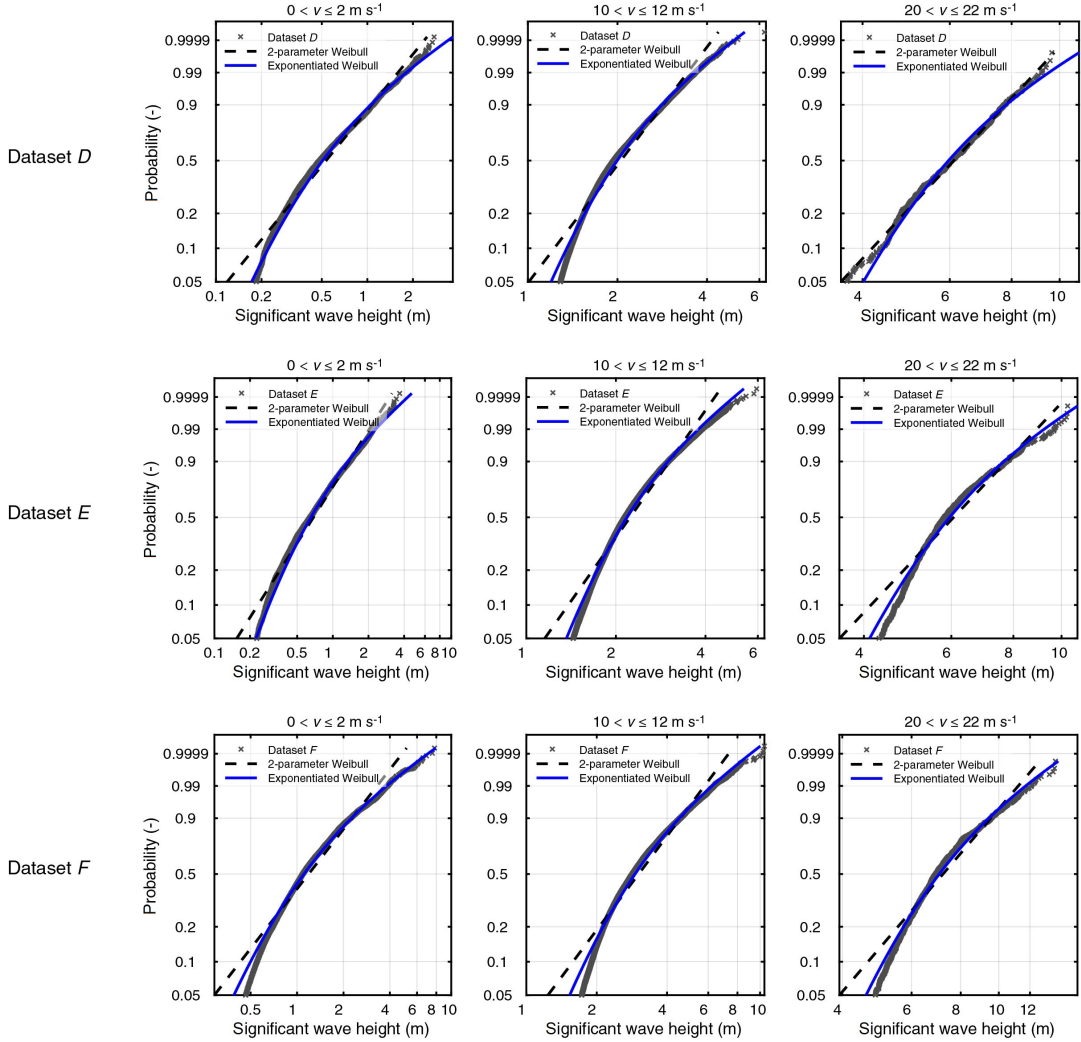


Figure 4.11: Weibull probability plots for significant wave height at different wind speeds. The exponentiated Weibull distribution with $\delta = 5$ describes the data better than a 2-parameter Weibull distribution.

4 Joint distribution of wind speed, wave height, and wave period

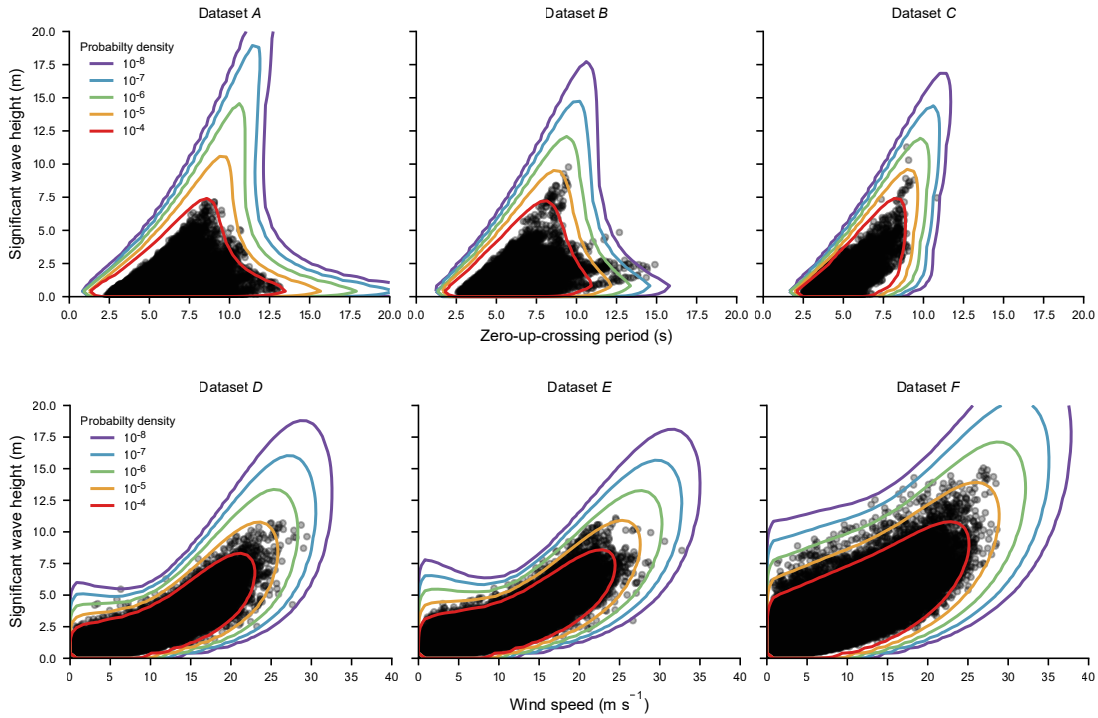


Figure 4.12: Extrapolation outside the dataset. Lines of very low probability density of fitted joint models are shown. Top: The behavior of typical periods for a given wave height seems reasonable, but the wave breaking limit is not respected by the joint model. Bottom: The way the joint model extrapolates at joint extreme wind speeds and wave heights appears reasonable, but at dataset E the region of joint low wind speeds and wave heights appears questionable.

empirical density values and model density values at levels below $\sim 10^{-5}$, we can reason whether the model's behavior in the tail appears logical.

In the sea state model, the H_s peaks of isodensity curves appear at higher T_z values as the probability density decreases (Figure 4.12). This behavior seems reasonable as it is caused by the dependence function that dictates that the median $t_z|H_s$ increases with $\sqrt{h_s}$. Unfortunately, the sea state model seems to ignore the wave breaking limit: For a given significant wave height value there is a lower T_z limit which is not exceeded as waves would otherwise break. Consequently, in the joint model the lower tail of $T_z|H_s$ seems to be too long. Future work could explore how sea state joint models can better respect the wave breaking limit. One promising possibility for that is to fit a distribution to steepness instead of zero-up-crossing period (see, for example, reference [163] and the environmental model used in Chapter 7).

In the wind speed - wave height model the behavior at joint extreme wind speeds and wave heights appears reasonable. Driven by the dependence function of the median $h_s|v$ typical significant wave heights increase with $v^{[1.8,2]}$. In deep waters, this relationship should hold for higher wind speeds. In shallower waters, however, significant wave height may be additionally limited such that median h_s might increase with less than $v^{[1.8,2]}$. The fitted joint model for dataset E has an unphysical artifact at the region of low wind speeds and high wave heights. At the 10^{-9} probability density level, higher wave heights occur at 1 m s^{-1} than at 10 m s^{-1} . This seems unlikely. Future work could explore how such model behavior can be avoided.

4.4 CONCLUSIONS

In this chapter, it was shown how models for the long-term joint distribution of sea states F_{H_s, T_z} and wind speed - wave height states F_{V, H_s} can be designed in a manner that the dependence function of the conditional variable offers physical interpretation. We modeled the median of the zero-up-crossing period to increase with $\sqrt{h_s}$ and the median of the significant wave height to increase with v^c where the exponent c was estimated to be between 1.8 and 2. The relationship $\tilde{t}_z \propto \sqrt{h_s}$ ensures that the wave period increases in a physically interpretable manner and the relationship $\tilde{h}_s \propto v^c$ offers insights into which kind of sea the joint distribution describes.

In comparison with the joint models that are currently recommended in engineering guidelines, the two proposed model structures appear to be an improvement: (1) Significant wave height is not underestimated anymore; and (2) the dependence structure between wind speed and wave height is improved. While the state-of-the-art wind speed - wave height model described constant density lines with positive curvature, both the empirical data and the newly proposed model described constant density lines with negative curvature. The author of this thesis believes that the proposed model for the joint distribution of wind speed and wave height F_{V, H_s} is a useful model for engineering, however, he thinks that the joint model for wave height and wave period, F_{H_s, T_z} should be further improved. The conditional distribution of zero-up-crossing period does not capture the wave breaking limit well and might also underestimate or overestimate the right tail. Likely, a different distribution than the log-normal distribution is required to achieve improvement (the state-of-the-art model also assumes a log-normal distribution for $T_z | H_s$ and this assumption was not challenged in this study).

While the two new joint models performed well within the support of the metocean dataset, it is unclear how good they extrapolate outside the samples that were used to fit them. The models were designed by focusing on the relationship of the conditional median value. As these relationships are physically interpretable and have shown good model fit within the samples, we have higher confidence in the extrapolation of these conditional median values than in the extrapolation at other regions of the variable space. Future research could aim to build models, which are also physically interpretable for non-median values. For example, the knowledge of the wave breaking limit, which can be expressed using the non-dimensional parameter steepness, could be incorporated into a sea state model.

5 ENVIRONMENTAL CONTOURS FROM HIGHEST DENSITY REGIONS

PREVIOUSLY PUBLISHED This chapter is based on publications by Haselsteiner et al. [96, 100] and Mackay and Haselsteiner [158]. The chapter proposes a novel contour construction method, whose approximation of the failure region is conservative for any deterministic response function. The method is an alternative to the currently widely used IFORM contour method and represents one of three suggested improvements to the overall design process of offshore structures.

PUBLICATION THAT INTRODUCED THE HIGHEST DENSITY CONTOUR METHOD A. F. Haselsteiner, J.-H. Ohlendorf, W. Wosniok, and K.-D. Thoben. “Deriving environmental contours from highest density regions”. *Coastal Engineering* 123, 2017, pp. 42–51. doi: [10.1016/j.coastaleng.2017.03.002](https://doi.org/10.1016/j.coastaleng.2017.03.002)

PUBLICATION THAT PRESENTED THE DIRECTIONAL DESIGN CONDITION EXAMPLE E. Mackay and A. F. Haselsteiner. “Marginal and total exceedance probabilities of environmental contours”. *Marine Structures* 75, 2021. doi: [10.1016/j.marstruc.2020.102863](https://doi.org/10.1016/j.marstruc.2020.102863)

PUBLICATION THAT INTRODUCED “MILD REGIONS” A. F. Haselsteiner, E. Mackay, and K.-D. Thoben. “Reducing conservatism in highest density environmental contours”. *Applied Ocean Research* 117, 2021, p. 102936. doi: [10.1016/j.apor.2021.102936](https://doi.org/10.1016/j.apor.2021.102936)

5.1 INTRODUCTION

5.1.1 PURPOSE OF ENVIRONMENTAL CONTOURS

Engineers must design any marine structure in such a way that it is able to withstand the loads induced by the environment. As the environment, that is wind, waves and currents, continually change and cannot be predicted for long periods of time, the environment is often modeled statistically by focusing on the probability distribution of variables like the 10-minute average wind speed or the significant wave height. Then, the structure is designed to withstand all but some extremely rare environmental states, for example, all waves with significant wave heights, H_s , less than a threshold, h_s , with a cumulative probability of $1 - \alpha$ or an “exceedance probability” of α , that is $\Pr(H_s \leq h_s) = 1 - \alpha$ or $\Pr(H_s > h_s) = \alpha$. In general notation for any random variable, X_1 , there exists a threshold, x_1 , which fulfills

$$F(x_1) = \Pr(X_1 \leq x_1) = \int_{-\infty}^{x_1} f(x)dx = 1 - \alpha, \quad (5.1)$$

where $F(x)$ is the distribution function and $f(x)$ is the density function.

The exceedance probability α corresponds to a “recurrence” or “return period” of the environmental conditions which describes the average time period between two consecutive environmental

5 Environmental contours from highest density regions

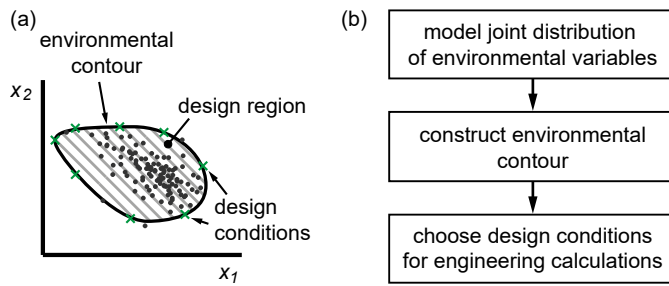


Figure 5.1: Concept of an environmental contour. (a) The environmental contour encloses all variable combinations which must be considered in the design process (the design region). (b) Flowchart describing the design process utilizing an environmental contour.

states above the threshold, x_1 . The threshold is called “return value.” For example, to comply with standards, a marine structure such as an offshore wind turbine is required to withstand significant wave heights, H_s , with a return period of 50 years [129].

Often, however, structural safety depends not only on one variable but on the occurrence of combinations of d variables, $\{X_j\}_{j=1}^d$. When two variables are of importance, for example, significant wave height, H_s , and spectral peak period, T_p , a joint probability density function can be defined and an environmental contour can be calculated which encloses the subset (or region) of environmental states that the structure must be designed for. Here, we call this region “design region” (Figure 5.1). Often the most critical structural response is associated with very high or low values of environmental variables, that is with environmental conditions located at the boundary of the design region. Consequently, standards allow engineers to calculate structural responses for a limited set of environmental “design conditions” along the contour instead of requiring engineering calculations based on a high number of possible variable combinations spread over the complete design region [47]. If there are more than two variables the concept of environmental contours leads to environmental surfaces (3 variables) or environmental manifolds (> 3 variables). Here, for simplicity, we also refer to these as environmental contours. In practice, environmental contours are often calculated for sea states (see, for example, [53, 194, 263]) and wind speed - wave height states [129], but sometimes also for other variables such as wave direction [7, 85], wind direction [254] or wind turbulence [88].

5.1.2 DIFFERENT EXCEEDANCE REGIONS LEAD TO DIFFERENT CONTOURS

As there are different mathematical definitions for environmental contours one has to further specify which kind of environmental contour is being constructed. Different concepts of environmental contours lead to different design loads and consequently to different structural responses [6]. The different concepts of environmental contours arise from different definitions of multivariate exceedance. As described in Section 2.2.2, in contrast to univariate statistics, there exist no unique definition for the multivariate quantile function and consequently also no unique definition for multivariate exceedance. Section 2.2.2 introduced some commonly used concepts for multivariate exceedance, namely AND exceedance, OR exceedance, angular exceedance and isodensity exceedance. These types of exceedances – and in principle, any other definition for exceedance – can be used to construct an environmental contour.

Originally, environmental contours arose from the concept of return values in univariate statistics, which are calculated based on one-sided exceedance over a threshold (Figure 5.2a). Consequently, a logical definition for an environmental contour is constant one-sided exceedance in all directions of the d -dimensional variable space, $\Pr(X_1 > x_1, X_2 > x_2, \dots, X_d > x_d) = \alpha$. The bottom

panel in Figure 5.2a shows the contour for the two-dimensional joint distribution of X_1 and X_2 . However, for design purposes not only the highest values of a variable can be of interest, but also the lowest. When designing an offshore structure whose characteristics are not known beforehand, low values of the peak period, T_p , have to be considered as the structure's natural frequencies can be either higher or lower than the average peak period. Accordingly, another possible definition for an environmental contour is two-sided exceedance over threshold (Figure 5.2b; for example, [134]). A third possibility is to define an environmental contour to have constant probability density, f_m , along its path enclosing the most likely environmental states (Figure 5.2c). In this case an N -year return period means that on average every N years an environmental state with a probability density less than f_m occurs. In the broader statistics literature the variable region enclosed by such a contour is called a “highest density region” (HDR) [126]. Although HDRs are a logical concept for environmental contours, no author has yet strictly followed this definition.

The constant probability density approach described in NORSO’s standard N-003 [197] and in DNV’s recommended practices [47], defines a fully closed contour of constant probability density. However, it is defined in such a way that it is unclear how much probability is enclosed by the contour. Instead, the contour’s probability density, f , is chosen to be the joint probability density of the (x_1, x_2) -variable combination with $x_1 = \text{return value}$ based on the marginal x_1 -distribution and $x_2 = \text{an associated } x_2 \text{ value}$ (Table 5.1). Leira [148]¹, however, has indeed used a highest density region with a defined probability content, but only after a transformation of the original variables into standard normal space. When transforming the contour back to the original variable space, the constant probability density is not preserved so that the resulting contour is not the boundary of a highest density region in the original variable space. Here we will compute contours strictly following the highest density region definition.

Table 5.1 presents an overview of all environmental contour methods that have been proposed. Currently, the most used definition to construct an environmental contour is based on “angular exceedance” (as introduced in Section 2.2.2). Either angular exceedance is applied in the standard normal space – then the contour method is known as the “inverse first-order reliability method” (IFORM) [108, 263] – or angular exceedance applied in the original variable space – then the contour method is known as the direct sampling contour method [124, 125]. Engineering guidelines and standards recommend the use of IFORM contours [47, 129, 197] and isodensity contours where the density value is chosen based on the marginal distribution of the primary variable [197] (referred to as “NORSO’s constant probability density approach” in Table 5.1).

Following IFORM to construct a contour, one first defines a circle with radius β in the standard normal space (Table 5.1). The radius corresponds to the return period and increases with longer periods. Then one transforms the points along the circle to the original variable space leading to the environmental contour. This transformation is done via the inverse Rosenblatt transformation [215]. As its name implies IFORM is a reliability method and is based on the idea that the “exceedance region” approximates the “failure region” of a structure (and the exceedance probability α approximates the structure’s “failure probability” p_F ; see [165]). Contours based on IFORM are widely used and have been published, for example, by Baarholm et al. [8], Eckert-Gallup et al. [53], Leira [148], Li et al. [151], Liu et al. [155], Myers et al. [185], Saranyasoontorn and Manuel [219], and Valamanesh et al. [243].

¹In 2018 Chai and Leira [27] fully introduced the contour method that was firstly roughly formulated by Leira in 2008 [148]. As we proposed the highest density contour method in a *Coastal Engineering* article [100] in 2017, this chapter uses only the literature that was available at that time as otherwise the motivation would be unclear. Another important publication after 2017 was the extensive review on environmental contours by Ross et al. [216].

5 Environmental contours from highest density regions

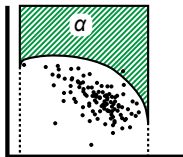
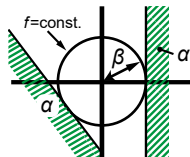
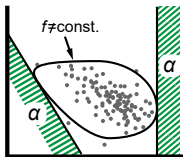
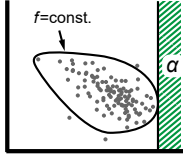
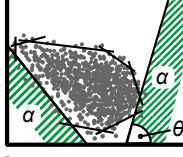
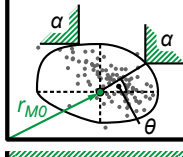
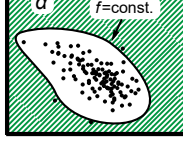
Method	Year	Standard normal variable space	Original variable space
Haver's design curve method [110]	1985		
Inverse first-order reliability method (IFORM) [263]	1993		
NORSOK's constant probability density approach [197]	2007*		
Direct sampling contour method [124]	2013		
Joint exceedance contour method [134]	2014		
Highest density contour method (this work; first published in [100])	2017		

Table 5.1: Illustration of established contour construction methods. The methods use different definitions for bivariate exceedance. α is the exceedance probability that is used to construct the contour, $\alpha = T_S/T_{R,target}$. In most methods, the contour is constructed in the original variable space. IFORM contours, however, are constructed in standard normal space and are then transformed into the original variable space. * Anecdotally, this approach has been proposed and used earlier, however, the author of this thesis is not aware of an earlier reference.

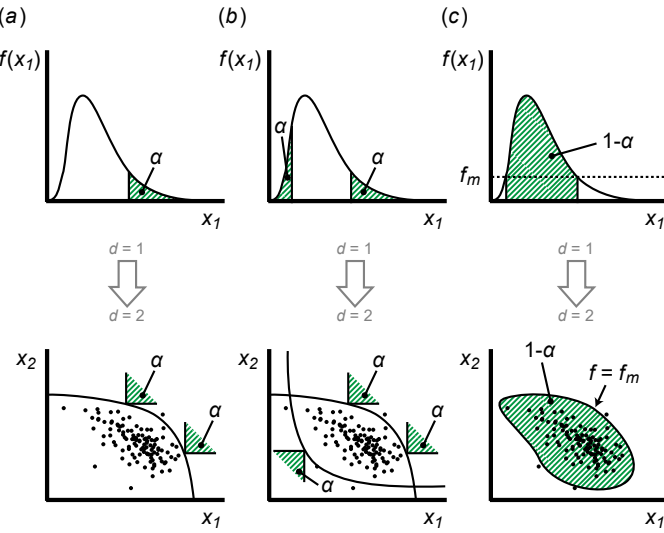


Figure 5.2: Environmental contours and their basis in univariate probability distributions. Top: Univariate probability distributions ($d = 1$). Bottom: Example data and contours based on two-dimensional joint probability distributions ($d = 2$). (a) One-sided exceedance based on AND exceedance. (b) Two-sided exceedance based on AND exceedance. (c) Highest density regions with a minimum probability density, f_m .

Huseby et al. [124], however, pointed out that the Rosenblatt transformation introduces errors as failure probabilities, p_F , can be underestimated or overestimated on a case by case basis. Therefore, they introduced an alternative method, the “direct sampling environmental contour method,” to calculate environmental contours in the original variable space. Following their method, one first carries out a Monte Carlo simulation to randomly draw a high number of environmental states from a given joint probability distribution model. Then one chooses an angle θ defining a line (in two dimensions, $d = 2$) and varies its position so that it divides the variable space into one halfspace containing most data points and the other halfspace containing the data points representing the exceedance probability, $\alpha \times n$ (with n being the total number of simulated environmental states, Table 5.1). By iterating this procedure over a finite number of angles, $\theta \in [0, 360]$, the resulting lines can be connected to an environmental contour. This new approach has been picked up in several recent publications, for example, to compare the approach to the traditional IFORM method [250], to compare different statistical models [248] or to decrease the required process time [122]. While the direct sampling environmental contour method overcomes the problems associated to the variable transformation, it requires the Monte Carlo simulation of environmental states, which is typically computationally more expensive than the simple IFORM calculations.

Jonathan et al. [134] defined environmental contours yet differently. They proposed to construct contours with constant AND exceedance probability, $\Pr(X_1 > x_1, X_2 > x_2) = \alpha$ (notation for two dimensions, $d = 2$). Thus, instead of finding halfspaces which are tangential to the contour, their exceedance regions have finite boundaries for each variable leading to outwards radiating rectangles in a two-dimensional Cartesian coordinate system (Table 5.1). As a result, contrary to IFORM and the direct sampling method the method does not try to match the exceedance region with the failure region. Following this method one first chooses a reference point, r_{M0} , then defines a line which passes through that point at an angle, θ , to the abscissa. Lastly the position along the line which is exceed with probability α using the AND exceedance definition is found. Repeating this procedure over a full circle, $\theta \in [0, 360]$, one finds the environmental contour. The method can be

5 Environmental contours from highest density regions

applied in any variable space, in the original variable space or in the standard normal variable space. Further, besides fully closed contours, one-sided exceedance was also considered by Jonathan et al. [134].

Here, contours enclosing highest probability density regions are introduced. Such contours enclose the most likely environmental states, which together make up a defined probability of $1 - \alpha$. The probability that such a contour is exceeded anywhere, the total exceedance probability, is α . The use of this definition is motivated by the fact any structure that is designed to withstand the environmental conditions contained in the contour, will have a probability of failure less than α (for deterministic responses). This is in contrast to the IFORM and direct sampling contour, where the important condition of $\alpha = p_{F,target} \geq p_F$ is only fulfilled if the failure region is fully contained in one of the exceedance regions. Similarly, AND contours such as those presented by Jonathan et al. [134] will have a total exceedance probability of more than α in that they also lead to the undesired case that the structure's probability of failure can be greater than α for some response functions.

Because IFORM contours are so widely used and their underlying idea of approximating the failure boundary with a straight line (in $d = 2$) is often accurate, it is worth pointing out some examples where the IFORM approximation is non-conservative. In these cases, if design loads are derived from an IFORM contour and the structure is designed to withstand only these loads, the true probability of failure will be higher than the target probability of failure. This problem occurs if the failure region is concave at the point that touches the environmental contour. This can happen, for example,

- for contours in the significant wave height - wave period variable space if the structure has two distinct eigenfrequencies (such an example is presented in a joint publication with Ed Mackay [158]),
- for contours in the wind speed - wave height variable space if offshore wind turbines are analyzed [152, 153, 220] (such an example will be presented in a case study in Chapter 7), and
- for directional environmental contours where contours are defined for the x and y component of wind speed [254] or significant wave height [85] (such an example will be presented later in this chapter).

Figure 5.3 shows three such examples. Another way in which IFORM's approximation of the failure region can become non-conservative is if a single structure has multiple response variables that have their highest response at different regions of the environmental variable space and consequently at different regions along the contour. This is for example the case in offshore wind turbine design (to be analyzed in detail in Chapter 7). Consider the bending moment of a turbine's support structure, a monopile, at various water depths, for example at 5 m water depth and at 30 m water depth (Figure 5.4 right). The bending moment is mainly caused by wind and wave forces, which act at different heights and consequently with different levers (moment = lever \times force). As a simplification, all wave forces and all wind forces can be summarized as two point forces. Because the center of pressure of wave forces is at a much lower height than the center of pressure of wind forces, the relative contribution of wave forces on the overall bending moment increases as the water depth increases (at a water depth of 0 m, wave forces have a lever of approximately 0 m, but at the ocean floor, wave forces have a lever of approximately the total water depth). Thus, the highest value along the contour of the 5 m moment occurs ca. at 15 m s^{-1} wind speed, but for the 30 m moment, it occurs at ca. 35 m s^{-1} wind speed (Figure 5.4 left). If the monopile's wall thickness is optimized based on the highest bending moment values along the contour at both heights, two individual failure regions will touch the contour at two distinct wind speed values. The monopile's overall failure region is the

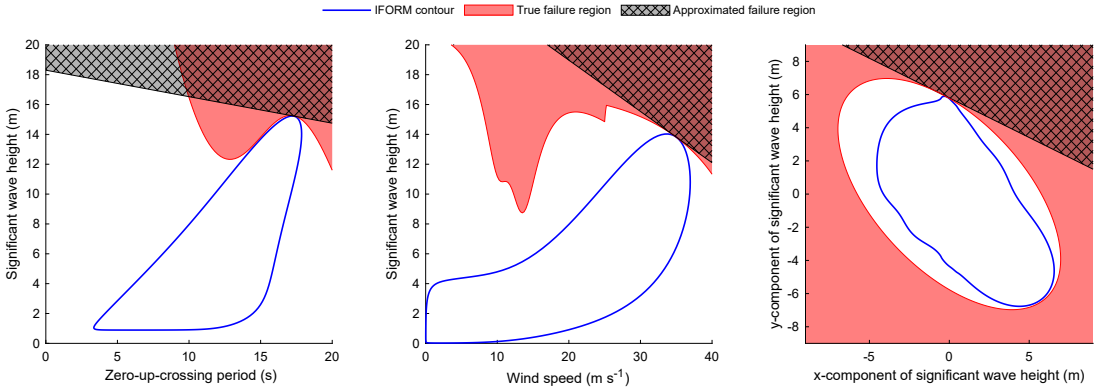


Figure 5.3: Examples of single responses where the approximation of the failure region of an IFORM [263] or direct sampling [124] environmental contour is non-conservative. In all three cases, the true failure region extends beyond the approximated failure region. Left: A response with two distinct eigenfrequencies [158]. Middle: The 10 m bending moment of an offshore wind turbine (Chapter 7). Right: A response of a structure that is designed to be stronger in the direction of the highest waves (example will be introduced in detail later in this Chapter).

union of the individual failure regions of the two (or more) response variables. Hence, the overall failure region is non-convex and contains a probability greater than α .

If one is not sure whether the IFORM contour definition is conservative in a particular application, a highest density contour can be constructed instead. A highest density contour will always yield conservative design conditions (for deterministic responses) as its total exceedance probability is α . By definition a highest density contour is surrounded by an exceedance region that contains α probability. Consequently, the failure region of any structure that is designed based on a highest density contour is a subset of the exceedance region and contains less than α probability (Figure 5.5).

Here, we will construct highest density contours in the original variable space and we will compute them using numerical integration. Although only simple two-dimensional examples will be presented, the concept generalizes to more than two dimensions and a three-dimensional example will be given in a case study presented in Chapter 7.

5.2 HIGHEST DENSITY CONTOUR

5.2.1 ANALYTICAL DEFINITION

The goal is to find a contour of constant probability density that encloses a probability of $1 - \alpha$. Such a contour surrounds a so-called highest density region, which is a statistical concept that is used in various contexts (see, for example, [126]). A highest density region R is the smallest possible region in the variable space that contains a given probability content. Mathematically, it can be expressed as the set of all \mathbf{x} whose probability density is greater than a threshold f_m :

$$R(f_m) = \{\mathbf{x} \in \mathbb{R}^d : f(\mathbf{x}) \geq f_m\}, \quad (5.2)$$

where $f(\mathbf{x})$ is the joint density function and f_m is chosen as the largest threshold that yields a region, which contains a probability of at least $1 - \alpha$, that is

$$f_m = \operatorname{argmax}_{f \in [0, \infty)} \Pr[\mathbf{X} \in R(f)] \geq 1 - \alpha. \quad (5.3)$$

5 Environmental contours from highest density regions

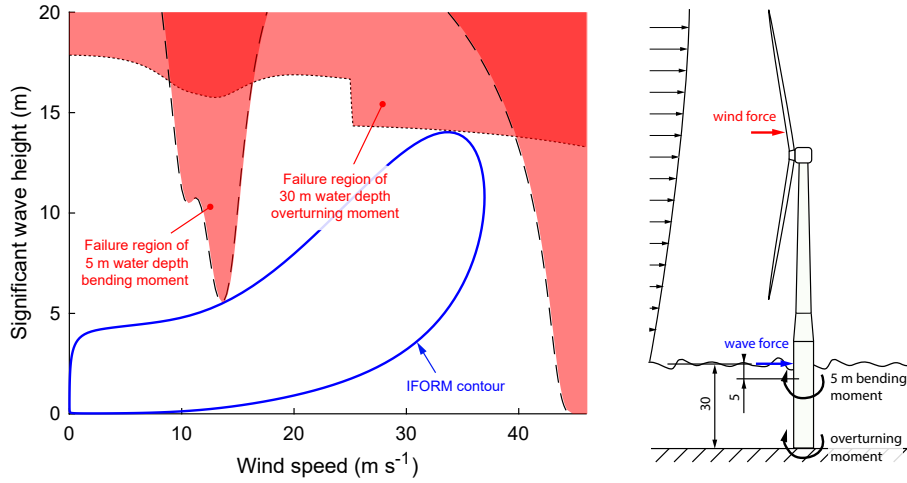


Figure 5.4: Example of how the combination of multiple response variables can cause the IFORM approximation to become non-conservative. Shown are failure surfaces from response variables relevant to the design of offshore wind turbine foundations. The relative contribution of wave forces is greater for the moment at 30 m than for the moment at 5 m water depth (will be shown in detail in Chapter 7). Consequently, their failure regions have different shapes and touch the contour at different positions. The overall failure region is the union of the two individual failure regions. It contains more than α probability.

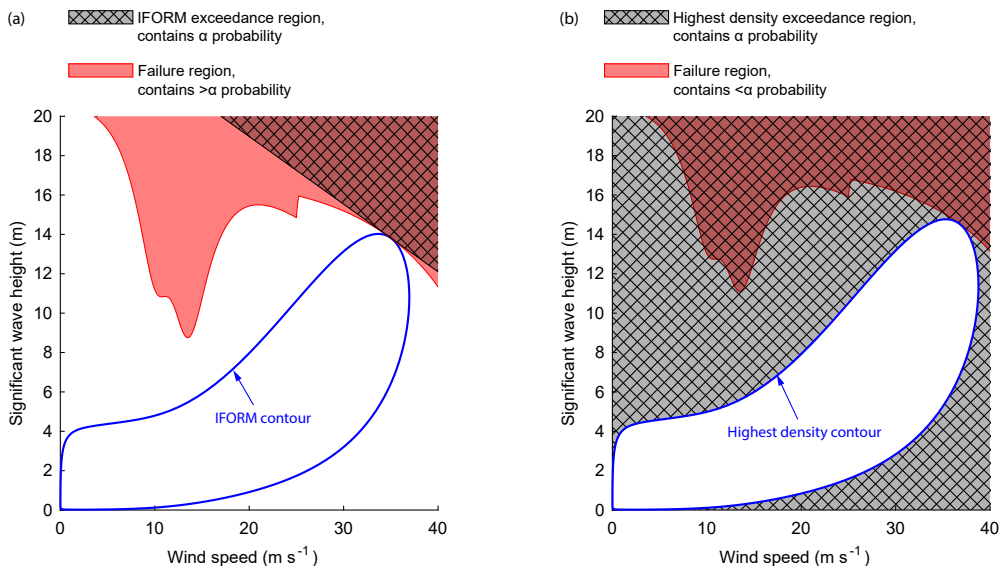


Figure 5.5: While a concave failure region can be problematic for an IFORM contour, it is not problematic for a highest density contour. Because a highest density contour is fully surrounded by an exceedance region of α probability, the failure region of any structure that is designed based on that contour is a subset of the exceedance region and consequently contains less than α probability. Thus, the reliability target is also met if the failure region is concave. Note that due to the definition of exceedance, the highest density contour is larger than the IFORM contour and consequently its design conditions lead to higher loads and responses.

5.2 Highest density contour

Then, the α -exceedance highest density contour is defined as the set $C(\alpha) \subset R(f_m)$ that contains the environmental states where the probability density equals f_m :

$$C(\alpha) = \{\mathbf{x} \in \mathbb{R}^d : f(\mathbf{x}) = f_m\}. \quad (5.4)$$

This contour C encloses the highest density region R . Therefore we call C “highest density contour” (HDC). A highest density region fulfills two interesting properties: (1) the probability density of every point inside is at least as large as the probability density of any point outside and (2) for a given probability content the region occupies the smallest possible volume in the variable space [23]. There is no general analytic solution to find the HDR or HDC, that is solving for C or R in (5.2) or (5.4).

HDRs, however, can be computed based on numerical integration approaches [268] or Monte Carlo techniques [126]. Environmental contours involve very low α values and are usually based on low-dimensional probability models. Accordingly, we choose numerical integration over Monte Carlo simulation to compute the highest density contour C . However, if a probability model, which incorporates many environmental variables (high d value), is evaluated, numerical integration might become infeasible and Monte Carlo approaches should be used. In the next section, the two-dimensional case will be evaluated, but in the journal publication that this chapter is mainly based on [100] the equations for d dimensions are given too.

5.2.2 NUMERICAL IMPLEMENTATION

First, a region in the variable space that contains almost the complete probability content is separated into n cells, where each cell has a unique index $i \in [1, n]$ (Figure 5.6).

The probability contained in cell i , p_i , is approximated by multiplying the marginal probabilities contained within this cell:

$$p_i = [F_x(x_i^u) - F_x(x_i^l)] \times [F_{y|x}(y_i^u|x_i^c) - F_{y|x}(y_i^l|x_i^c)], \quad (5.5)$$

where x_i^l, x_i^c, x_i^u represent the x coordinates of the cell’s lower boundary, center and upper boundary, respectively, and y_i^l and y_i^u upper and lower boundary of the y coordinate. F_x represents the marginal distribution function of the first variable X and $F_{y|x}$ represents the conditional distribution function of the second variable Y given X . For briefer notation, we use $X = X_1$, $x = x_1$, $Y = X_2$, and $y = x_2$ here.

Based on this probability, the average probability density for each cell is calculated by dividing by the cell size:

$$\bar{f}_i = \frac{p_i}{\Delta x \Delta y}. \quad (5.6)$$

After having calculated p_i and \bar{f}_i for all cells with indices $i = \{1, \dots, n\}$, equation 5.3 is numerically solved by first defining a function that returns the probability contained in $R_{HD}(f)$,

$$G(f) = \Pr[\mathbf{X} \in R_{HD}(f)] \approx \sum_i^n p_i : \bar{f}_i \geq f, \quad (5.7)$$

and then finding the value f that fulfills $G(f) = 1 + \alpha$:

$$f_m \approx f : G(f) = 1 + \alpha. \quad (5.8)$$

5 Environmental contours from highest density regions

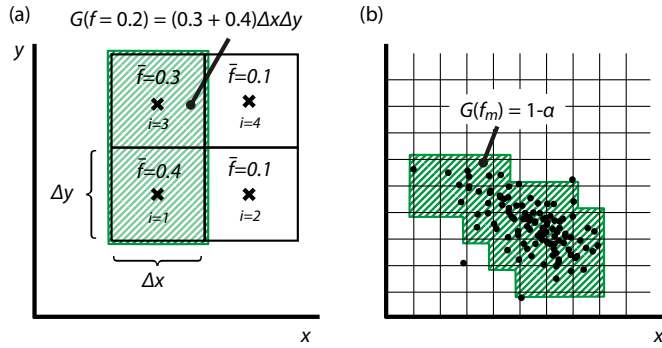


Figure 5.6: Computation of the highest density contour (HDC) using a numerical grid. Shaded area = highest density region (HDR), outline = HDC. (a) The variable space is discretized into equally sized grid cells and the average probability density \bar{f} is calculated for each cell. The probability enclosed by the highest density contour of f_m probability density is calculated by first finding all cells whose probability density \bar{f} is greater than or equal to the minimum probability density f_m and then summing up the individual probabilities of these cells. (b) An environmental contour is computed by finding the probability density f_m that satisfies $G(f_m) = 1 - \alpha$.

f_m can either be found by solving the root finding problem $G(f) - 1 + \alpha = 0$, for example with Matlab's function `fzero`, or by first sorting the cells by their f_i values and then adding cells – starting with the cell with the highest f_i value and adding them in descending order – until $G(f_i) \geq 1 - \alpha$. The last cell's f_i value is then taken as an estimate for f_m .

The outlined scheme to compute a highest density contour is sensitive to the used grid resolution and position, and it is necessary to check the cell size is small enough to ensure grid independence. Consequently, a grid study will be included in one of the examples presented here.

5.3 EXAMPLES

5.3.1 SEA STATE ENVIRONMENTAL CONTOUR

In this example, the construction of contours that describe sea states with the variables significant wave height H_s and zero-up-crossing period T_z will be considered. A joint distribution model that has been used in many previous studies on the environmental contour method will be used. IFORM and highest density contour will be constructed and compared.

JOINT DISTRIBUTION

We use the joint distribution proposed by Vanem and Bitner-Gregersen [251]. Here, we assume that the model represents the long-term distribution of 3-hour stationary processes². Vanem and Bitner-Gregersen [251] used the model to construct environmental contours using both the traditional IFORM and the newer direct sampling contour method [124]. In this global hierarchical

²The model, however, was derived by fitting its structure to sea state data from the ERA interim dataset [42], which provides one data point per 6-hour interval. Nevertheless, it is assumed to represent 3-hour sea states in this work. That the model was derived from 6-hour sea states was overlooked in the original study that was published in *Coastal Engineering* [100]. As the model only served as an example and the comparison between contours is not affected by assuming whether the joint distribution represents 3-hour or 6-hour sea states, the author of this thesis kept the way the model was used in the *Coastal Engineering* publication also in this Chapter.

model significant wave height H_s is modeled as a 3-parameter Weibull distribution with the parameters α (scale), β (shape), and γ (location):

$$f_{H_s}(h_s) = \frac{\beta}{\alpha} \left(\frac{h_s - \gamma}{\alpha} \right)^{\beta-1} \exp \left[- \left(\frac{h_s - \gamma}{\alpha} \right)^\beta \right]; \quad h_s \geq \gamma. \quad (5.9)$$

Based on a least squares fit the parameters are $\alpha = 2.776$, $\beta = 1.471$ and $\gamma = 0.8888$ [251].

The zero-up-crossing period T_z is modeled to follow a log-normal distribution:

$$f_{T_z|H_s}(t_z|h_s; \tilde{\mu}, \tilde{\sigma}) = \frac{1}{t_z \tilde{\sigma} \sqrt{2\pi}} \exp \left[\frac{-(\ln t_z - \tilde{\mu})^2}{2\tilde{\sigma}^2} \right]. \quad (5.10)$$

The distribution's parameters, $\tilde{\mu}$ and $\tilde{\sigma}$, are conditional on significant wave height and are modeled as 3-parameter functions:

$$\tilde{\mu}(h_s) = a_1 + a_2 h_s^{a_3}, \quad (5.11)$$

$$\tilde{\sigma}(h_s) = b_1 + b_2 \exp(b_3 h_s). \quad (5.12)$$

In this case they are estimated to be $a_1 = 0.1000$, $a_2 = 1.489$, $a_3 = 0.1901$, $b_1 = 0.0400$, $b_2 = 0.1748$, $b_3 = -0.2243$ [251].

Multiplying the marginal distribution of the significant wave height and the conditional distribution of the zero-up-crossing period the joint distribution can be calculated:

$$f_{H_s, T_z}(h_s, t_z) = f_{H_s}(h_s) f_{T_z|H_s}(t_z|h_s). \quad (5.13)$$

Because it is assumed that the data represents independent 3-hour sea states, exceedance probability α for a N -year return period is calculated as

$$\alpha = \frac{1}{N \times 365.25 \times 24/3}. \quad (5.14)$$

COMPUTED CONTOURS

As in previous work based on the described sea state model [124, 251] we computed the 1-, 10- and 25-year environmental contours (Figure 5.7). The corresponding exceedance probabilities were $\alpha_1 = 3.42 \times 10^{-4}$, $\alpha_{10} = 3.42 \times 10^{-5}$ and $\alpha_{25} = 1.37 \times 10^{-5}$ respectively. The highest density contours computed have constant probability densities of $f_{m1} = 4.4 \times 10^{-5}$ (1-year), $f_{m10} = 4.3 \times 10^{-6}$ (10-year) and $f_{m25} = 1.7 \times 10^{-6}$ (25-year). Figure 5.8a shows how the enclosed probability G monotonically decreases with increasing f_m until it reaches $G = 0$. Since the probability functions used here (Weibull and log-normal) are unbounded, G asymptotically approaches 1 as f_m approaches 0. Figure 5.8b presents the maximum H_s and T_z values along a contour of constant f_m -probability density ($H_s f_m$, $T_z f_m$). Longer return periods lead to smaller f_m values and consequently to bigger contours with higher $H_s f_m$ and $T_z f_m$ values.

As discretization in general is sensitive to step size, we evaluated the contour's robustness with respect to grid cell size $\Delta x = \Delta H_s$, $\Delta y = \Delta T_z$. We analyzed how minimum probability density f_m changes with grid cell size. In all three tested return periods, (1-, 10- and 25-year contour) minimum probability density f_m was roughly constant at small cell sizes and started to fluctuate with increasing cell size indicating a grid-independent solution can be reached (Figure 5.9a). Oversized grid cells can lead to minimum probability density being half or double than the converged minimum prob-

5 Environmental contours from highest density regions

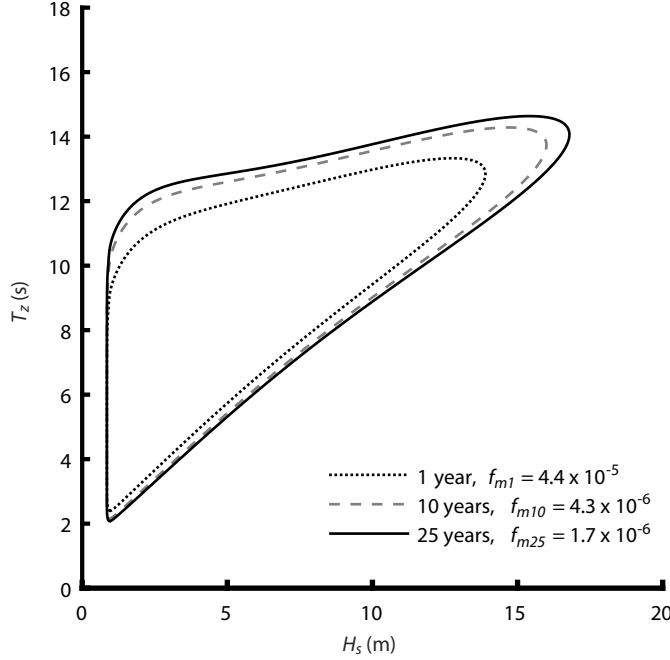


Figure 5.7: Computed highest density contours. Along the contour probability density f_m is constant and the enclosed region has a probability of $1 - \alpha$ with α corresponding to a given target return period ($T_{R,\text{target}}=1, 10$ or 25 years). Grid cell size is $0.05\text{ m} \times 0.05\text{ s}$.

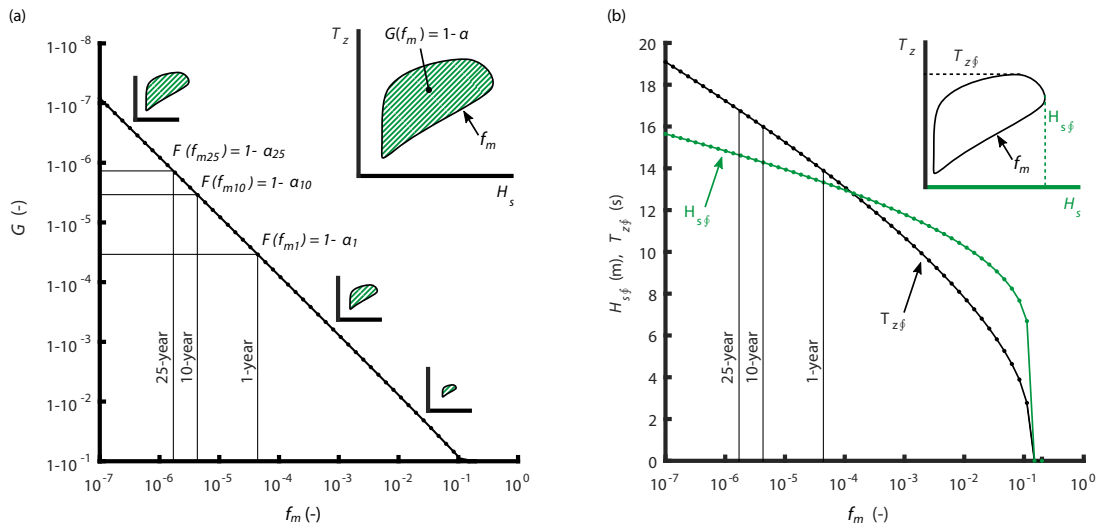


Figure 5.8: Expansion of the highest density contour. (a) The probability enclosed by the contour, $G(f_m)$, is 1 at a minimum probability density of $f_m = 0$ and monotonically decreases to $G(f_m \approx 0.12) = 0$. Probabilities corresponding to the 1-, 10- and 25-year contour are shown. The inset illustrates the definition of G and f_m . (b) Maximum variable values along the contour, $H_{s,\phi}$ and $T_{z,\phi}$, as a function of minimum probability density, f_m . The inset illustrates that there is no $(H_{s,\phi}, T_{z,\phi})$ -sea state along the contour. Instead, the $(H_{s,\phi}, T_z)$ -sea state has a T_z value different from $T_{z,\phi}$ and vice versa.

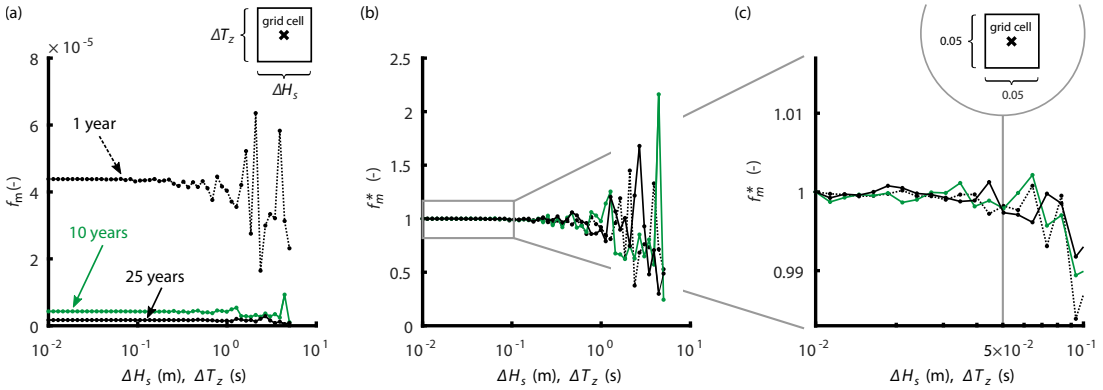


Figure 5.9: Grid independence study. Quadratic grid cells with sizes ranging from 0.01 to 10 units of grid cell length are tested to evaluate grid convergence. (a) The contour's minimum probability density f_m for a given return period is sensitive to grid cell size ΔH_s , ΔT_p . Sensitivity increases with grid cell length. (b) If grid cell size is too big minimum probability density f_m can be half or double than the converged minimum probability density. Plotted is f_m^* which is the minimum probability density, f_m , normalized by the converged f_m value. (c) Aiming for grid convergence with an error of less than 1 % we used grid cells with dimensions of $0.05 \text{ m} \times 0.05 \text{ s}$ (marked with a vertical line).

ability density (Figure 5.9b). For the given probability model convergence was reached at a grid cell size of $H_s = 0.05 \text{ m}$ and $T_z = 0.05 \text{ s}$. There, deviation to the smallest tested grid cell size was less than 1%, $0.99 < f_m^* < 1.01$, with f_m^* being minimum probability density, f_m , normalized by the converged f_m value (Figure 5.9c). For comparison, we also computed environmental contours using IFORM based on the same joint distribution. The highest density contours had shapes similar as the contours calculated with IFORM and the direct sampling method (Figure 5.10c,d). However, we defined a highest density contour to enclose a probability of $1 - \alpha$ while an IFORM contour and a direct sampling contour each enclose a probability less than $1 - \alpha$ since by their definitions multiple regions outside the contour have a probability of α (Figure 5.10a). Consequently, the highest density contour's dimensions in terms of H_s and T_z are bigger in comparison. For a more direct comparison we can inflate an IFORM contour and find the N -year contour which encloses exactly $1 - \alpha$ probability. Leira [148] showed that this can be done by utilizing the inverted Rayleigh distribution (for two dimensions). Leira [148] called these contours "equi-shape contours."³ Here, it is found that such a 25-year equi-shape contour corresponds to a 308.8-year IFORM contour. The contour's shape and size is roughly similar to the 25-year highest density contour. These similarities suggest that the 308.8-year IFORM contour has approximately constant probability density along the contour.

To visualize a typical dataset, we Monte Carlo simulated 25 years of 3-hour sea states ($n = 73050$; gray dots in Figure 5.10c). In this particular dataset, one data point exceeds the highest density contour while there are multiple data points exceeding the 25-year IFORM contour. The different contour dimensions can also be expressed in terms of maximum H_s - and T_z values along the N -year contour ($H_{s \frac{f}{N}}$, $T_{z \frac{f}{N}}$). Here we find $H_{s \frac{f}{25}} = 16.79 \text{ m}$ and $T_{z \frac{f}{25}} = 14.64 \text{ s}$ for the highest density contour and $H_{s \frac{f}{25}} = 15.23 \text{ m}$ and $T_{z \frac{f}{25}} = 13.96 \text{ s}$ for the IFORM contour (Figure 5.10d). Thus, the highest density contour $H_{s \frac{f}{25}}$ value is 10.2 % higher than the IFORM contour's value. Consequently, from an engineering design point of view, highest density contours yield more conservative requirements for design loads.

³In 2018, Chai and Leira [27] fully worked out the idea of constructing a contour that encloses $1 - \alpha$ probability in standard normal space. They called this method inverse second-order reliability method.

5 Environmental contours from highest density regions

This does not only apply to the considered distribution but is a generic property based on the different definitions of these contours. IFORM and direct sampling contours are defined to contain the return value of the marginal distribution of the primary variable X_1 as their highest variable value, that is $H_{s \notin 25} = H_{s25}$ (Figure 5.10a). On the other hand, a highest density contour is defined to enclose $1 - \alpha$ probability. Since it does not contain all H_s - T_z sea states fulfilling $H_s < H_{s25}$ (which together would make up $1 - \alpha$ probability) it must contain some sea states with $H_s > H_{s25}$.

By the highest density contour's definition of an enclosed probability of $1 - \alpha$, in an uncorrelated random 25-year dataset the probability that at least one data point exceeds a 25-year contour is about 63.2 %, $1 - (1 - \alpha_{25})^n \approx 0.632$ with $n = 25 \times 365.25 \times 24/3 = 73050$. Here, exceedance precisely means that this sea state realization is anywhere outside the region enclosed by the contour. Such a sea state occurs on average every 25 years. This simple and clear interpretation is why we have chosen the definition of constant probability density and a probability of $1 - \alpha$, that is defining the contour to enclose the highest density region. We believe that this definition offers an intuitive and meaningful concept for an N -year environmental contour in the engineering design process. If an engineer designs a structure to withstand all sea states inside an N -year contour, the structure will be designed for the most likely (extreme) sea states which are expected to occur in N years. Then on average every N years a sea state will occur for which the structure is not designed. Some of these values might lead to failure and some not.

Alternative concepts with multiple α -exceedance regions (see Table 5.1) are based on the idea of known failure regions in the context of structural reliability methods (see [165]). IFORM assumes that a structure's failure region has a convex shape. It defines the α -halfspace exceedance regions in its way because in that case the true failure surface can be linearized such that the variable space is separated by a straight line at an angle θ into a survival region and a failure region (in two dimensions). Then, this failure region overlaps with IFORM's exceedance region. It has the failure probability $p_F = \alpha$ and the survival region the survival probability $1 - p_F$ (for a deterministic response). Here, however, we do not intend to align the α -probability exceedance region with a particular failure region.

Nevertheless, the exceedance probability α can be compared with failure probabilities p_F from potential structures. If the structure survives all environmental conditions along (and within) a highest density environmental contour, it will have a probability of failure less than the exceedance probability. $p_F < \alpha$ (for a deterministic response).

As described IFORM leads to a contour that encloses less than $1 - \alpha$ probability and consequently results in less conservative design conditions compared to a highest density contour. If the structural design, which is developed based on these environmental conditions, has a convex failure region, the theoretical precondition of IFORM is met. Then in comparison, a highest density contour can be seen as overly conservative. Thus, if the designer knows that a structure responds with a convex failure region choosing an IFORM contour is advantageous in the sense that it yields less conservative but still safe design conditions.

In a publication by Ed Mackay and the author of this thesis [158], we analyzed how design conditions from IFORM, direct sampling and highest density contours lead to different responses by using two simple deterministic response models. In the study, we used the same joint distribution to represent sea states. In our first response model, a function that peaks at a particular period – such a response function could represent a single degree of freedom system – all contour methods were conservative. The response of the highest density contour was overly conservative. In our second response model, a bimodal function, IFORM and direct sampling contours led to non-conservative design conditions, while design conditions from the highest density contour were conservative.

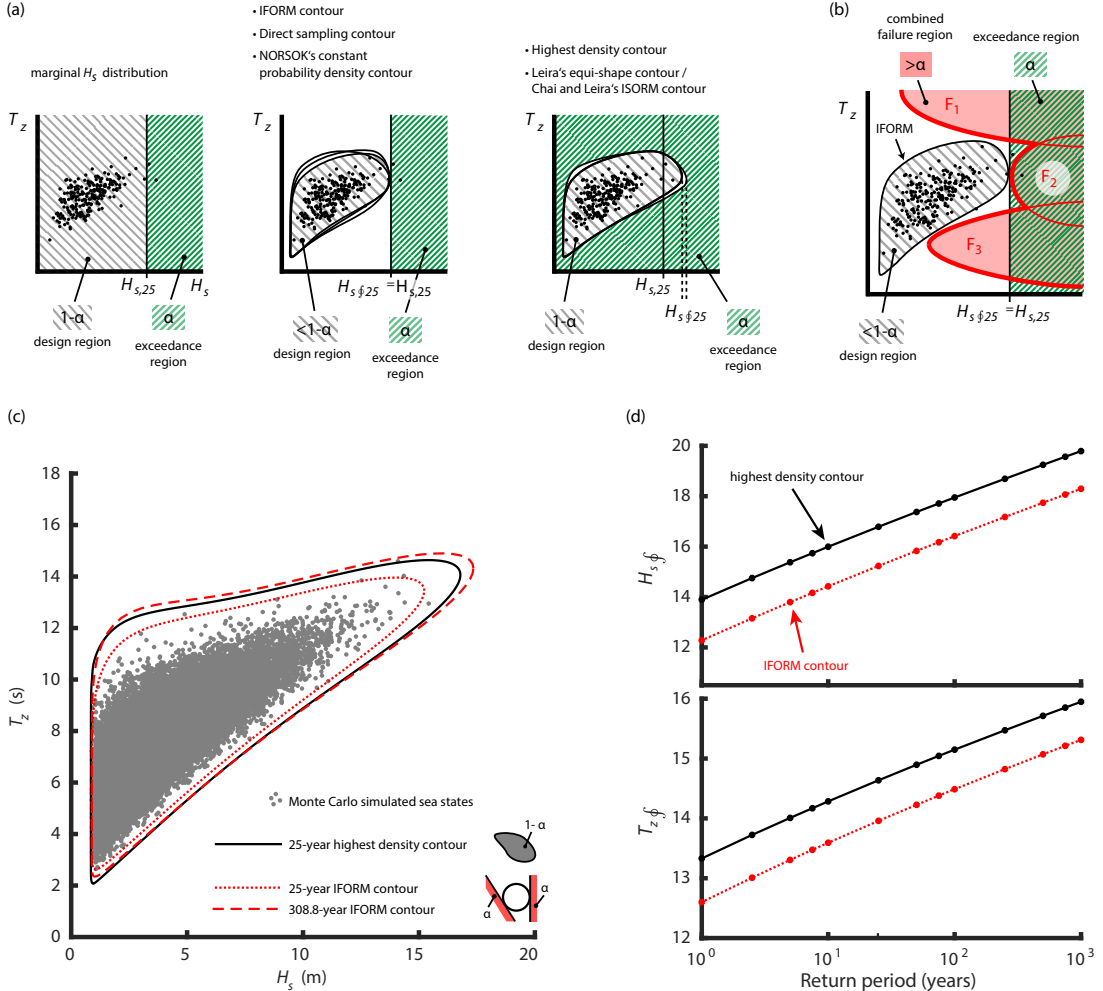


Figure 5.10: Comparison of environmental contours derived using different methods. (a) Sketches showing expected differences in contour size due to different definitions. Some contours are defined in such a way that the maximum value along the contour, $H_{s,f}$, is equal to the return value of the marginal distribution, $H_{s,25}$, (middle). The highest density contour (HDC), however, is defined to enclose $1 - \alpha$ probability and thus has a maximum value along the contour which is higher than the return value of the marginal distribution, $H_{s,f} > H_{s,25}$, (right). (b) Sketch illustrating an IFORM contour and possible failure regions of a linear system of three components, \mathcal{F}_1 , \mathcal{F}_2 , \mathcal{F}_3 . Since the contour contains less than $1 - \alpha$ probability the system's failure probability can be greater than α . (c) A total of $n = 73050$ sea state data points have been Monte Carlo simulated representing a 25-year dataset (scatter plot). The 25-year HDC (solid line) and the 25-year IFORM contour (short dashes) have similar shapes, but as expected the HDC is bigger. The 308.8-year IFORM contour or 25-year “equi-shape contour” (long dashes; [148]) encloses the same amount of probability as the 25-year HDC. (d) Comparison of maximum values along the contour, $H_{s,f}$ and $T_{z,f}$. As expected by the different definitions, the HDC has higher maximum significant wave height $H_{s,f}$ and maximum zero-up-crossing period $T_{z,f}$ than the IFORM contour.

5 Environmental contours from highest density regions

While many structures respond with a convex failure region in the $H_s - T_p$ space, this precondition for IFORM connects the environmental contour to a certain class of structures. The shape of the failure surface might be unknown beforehand and only becomes apparent during the design process. If it turns out that the failure surface is non-convex and therefore violates IFORM's precondition the designer would need to go one step backwards and define new design conditions by inflating the IFORM contour. By not making use of the properties of possible structural responses, the highest density contour is more conservative, but also more general in its application. It would avoid the need of the described iteration loop in the design process.

Further, a highest density contour is advantageous in the design process of a structural problem of a system consisting of multiple components. Consider a “series structure” consisting of z different components with z different failure functions. In a series structure a failure of one component results in failure of the system [12]. Suppose that each component fulfills IFORM's precondition of having a convex failure region. Nevertheless, the probability contained by the union of all z failure regions, $\mathcal{F}_1 \cup \mathcal{F}_2 \dots \cup \mathcal{F}_z$, could exceed α (Figure 5.10b). In that case it would be expected that more frequent than every N years an environmental state occurs which leads to failure of some of the components and consequently failure of the system. If on the other hand an environmental contour containing $1 - \alpha$ probability were used to design the components, by definition the system's probability of failure would be less than α . Consequently, the system would be expected to survive longer than N years.

A similar example can be given for a single component with multiple failure modes. The three failure regions shown in Figure 5.10b would then correspond to different failure modes and the same conclusions as for the series structure could be drawn. These two examples explain why IFORM is primarily aimed at assessing the reliability of one component failing in one failure mode. A highest density contour, on the other hand, can be used in these two cases without worrying that any assumptions might be violated.

5.3.2 CONTOURS FOR DIRECTIONAL DESIGN CONDITIONS

In this example the specification of directional design conditions for the design or assessment of a marine structure is considered. In many locations, the severity of wave conditions exhibits a dependence on wave direction. Specifying the design wave height as a function of direction can allow the optimization of an asymmetrical structure. Directional return values are often estimated in discrete directional sectors. However, it is becoming more common to use extreme value models where the model parameters vary smoothly with direction (for example [136, 209]). In these cases, environmental contours can be used to define directional design conditions. In this example a previously published joint distribution is used and three types of contours are considered: IFORM, direct sampling, and highest density contours.

JOINT DISTRIBUTION

We use a simple description of the joint distribution of H_s and wave direction Θ based on the joint distribution of wind speed and direction given by Haghayeghi and Katabdari [86] and studied further by Vanem et al. [254] (Figure 5.11). Its joint density function f_{Θ, H_s} can be written as a hierarchical model:

$$f_{\Theta, H_s}(\theta, h_s) = f_\Theta(\theta) f_{H_s|\Theta}(h_s|\theta). \quad (5.15)$$

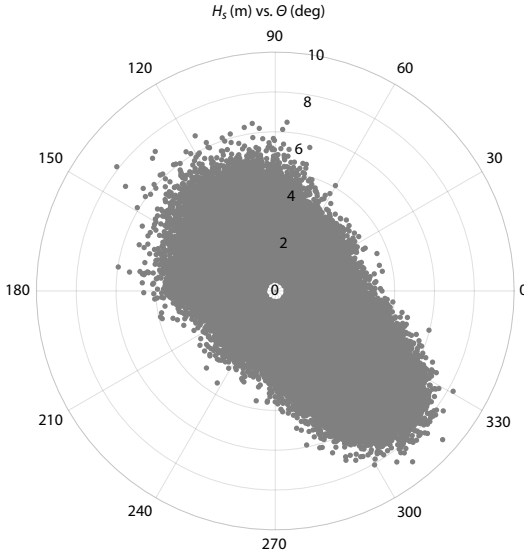


Figure 5.11: A Monte Carlo sample of the joint distribution of significant wave height H_s and direction Θ .

i	w_i	μ_i	κ_i
1	0.21	2.10	0.74
2	0.79	5.54	13.11

Table 5.2: Parameters for distribution of wave direction.

The marginal distribution of wave direction is expressed as a mixture of von Mises distributions,

$$f_\Theta(\theta) = \sum_{i=1}^n w_i f_i(\theta), \quad (5.16)$$

where $w_i \in [0, 1]$ are weights and $\sum_{i=1}^n w_i = 1$. The PDF of the von Mises distribution is

$$f_i(\theta) = \frac{\exp[\kappa_i \cos(\theta - \mu_i)]}{2\pi I_0(\kappa_i)}, \quad (5.17)$$

where I_0 is the zero-order modified Bessel function of the first kind, κ_i is a concentration factor and μ_i is the location parameter. The model for H_s conditional on direction is a three-parameter Weibull distribution, with parameter dependence on direction given in terms of a Fourier series:

$$\lambda(\theta) = a_0 + \sum_{j=1}^m a_j \cos(j\theta) + b_j \sin(j\theta), \quad (5.18)$$

$$k(\theta) = c_0 + \sum_{j=1}^m c_j \cos(j\theta) + d_j \sin(j\theta). \quad (5.19)$$

The model presented in Haghayeghi and Katabdari [86] uses $m = 8$ harmonics for the Fourier series. In this example we assume the Weibull location parameter is constant at $\gamma = 0.5$. The other distribution parameters are defined in Tables 5.2 and 5.3.

5 Environmental contours from highest density regions

j	a_j	b_j	c_j	d_j
0	1.875		1.910	
1	0.345	-0.140	0.240	-0.130
2	-0.210	-0.820	-0.080	-0.170
3	-0.160	-0.200	-0.010	-0.030
4	-0.265	0.095	-0.110	0.030
5	-0.090	0.110	0.0004	0.003
6	0.070	0.070	0.060	0.020
7	0.030	0.020	0.060	0.020
8	0.030	-0.015	0.004	-0.010

Table 5.3: Fourier coefficients for distribution of H_s conditional on wave direction.

When constructing contours for directional distributions it is important to be clear about what coordinate system is used. If IFORM or direct sampling contours are constructed in the H_s - Θ coordinate system, then the contours will have upper and lower bounds for Θ for any directional distribution, which does not make sense from the perspective of structural reliability. Whether highest density contours have upper and lower bounds on Θ depends on the shape of the joint PDF. The construction of IFORM contours based on applying the Rosenblatt transformation in the form $\Phi(U_1) = F_\Theta(\theta)$, $\Phi(U_2) = F_{H_s|\Theta}(h_s|\theta)$, was discussed in references [85, 86, 254]. The IFORM contours presented in these works exhibit a discontinuity in the transition between 0 and 2π , due to the upper and lower bounds for θ .

To address this issue, Vanem et al. [254] proposed deriving contours in terms of the x and y components of significant wave height, defined as

$$h_x = h_s \cos(\theta), \quad h_y = h_s \sin(\theta). \quad (5.20)$$

The joint density function of h_x and h_y in Cartesian coordinates can be written as

$$f_{H_x, H_y}(h_x, h_y) = f_{\Theta, H_s}(\theta, h_s) \left| \frac{\partial(h_s \cos(\theta), h_s \sin(\theta))}{\partial(h_s, \theta)} \right|^{-1} = \frac{f_{\Theta, H_s}(\theta, h_s)}{h_s}. \quad (5.21)$$

Note that since the Weibull location parameter γ is greater than zero in this example, the transformed density function is non-singular at the origin since $f_{\Theta, H_s}(\theta, 0) = 0$. In the following, all considered contours are constructed in H_x - H_y space. This means that direct sampling contours assume that the failure surface is linear in this space. For IFORM contours, the assumed failure surface is not necessarily linear in H_x - H_y space, due to the use of the Rosenblatt transformation. However, this is a common feature of the IFORM method for any parameter space, as discussed in references [121, 122, 124].

CONTOURS AND RESPONSES

The 1-year IFORM, direct sampling and highest density environmental contours are shown in Figure 5.12 together with the 1-year omnidirectional return value (assuming that observations are at 3-hour intervals as before). As the isodensity contours of the joint distribution are close to convex in (h_x, h_y) coordinates, the direct sampling and IFORM contours are in close agreement. The highest density contour gives a maximum value of H_s approximately 1 m larger than the direct sampling and IFORM contours. The IFORM contour exhibits a small ridge at around 90° . This is a result

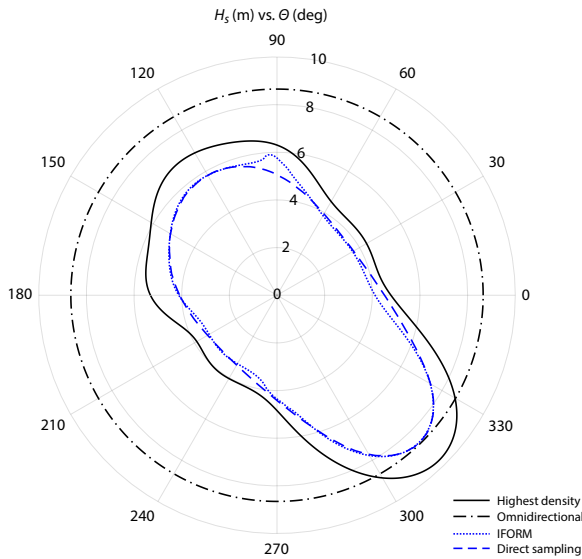


Figure 5.12: 1-year environmental contours for joint distribution of H_s and wave direction Θ and 1-year omnidirectional return value.

of the use of the Rosenblatt transformation. The location of the ridge is dependent on the order of variables used in the transformation, as discussed by Mackay and Haselsteiner [158].

Note that marginal probabilities in Cartesian $H_x - H_y$ space do not correspond to marginal probabilities of H_s . The set of points with $H_s \leq r$ is contained in the set of points with $H_x \leq r$ (see Figure 5.13). Since this is true under any rotation of the axes, the maximum radius of a direct sampling contour constructed in the $H_x - H_y$ space will be less than the omnidirectional return value. In the example considered here, the 1-year omnidirectional return value is 8.65 m and the maximum H_s on the direct sampling contour is 8.58 m. The maximum H_s on the IFORM contour is slightly higher, at 8.59 m, due to the effects of the Rosenblatt transformation (for a discussion on this effect, see Mackay and Haselsteiner [158]).

Suppose that a structure has a deterministic omnidirectional response and is designed so that it fails if the wave height exceeds the maximum value along an N -year IFORM or direct sampling contour. Since the N -year omnidirectional return value of H_s is greater than the maximum value of H_s along the contour, the structure will have a higher failure probability than intended. Now suppose that the omnidirectional structure is designed using the omnidirectional return value at exceedance probability α , denoted h_α , so that the failure surface is located at h_α and is independent of direction. In this case, the probability of failure will be equal to α , by definition, since h_α is the value of H_s that is exceeded with probability α , independent of direction. If the structure is asymmetric and designed so that the failure surface is located at a value greater than or equal to h_α in each direction, then the probability of failure will be less than or equal to α . So the use of omnidirectional criteria gives the target failure probability, but may lead to a less efficient design as the potential to optimize the design with respect to direction is not exploited.

Now suppose that an asymmetric structure is optimized based on directional extreme conditions from an environmental contour. For example, the stiffness of a fixed structure in a particular direction could be optimized with respect to direction or similarly the mooring response of a floating structure could be optimized to allow larger responses in directions where the wave conditions are less severe.

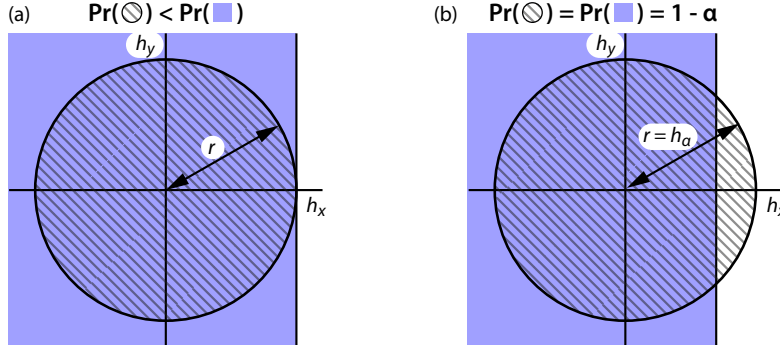


Figure 5.13: (a) Significant wave height $h_s = \sqrt{h_x^2 + h_y^2}$. Thus, the set of points with $H_s \leq r$ (hatched area) is contained in the set of points with $H_x \leq r$ (blue area). This explains why the maximum H_s on an N -year direct sampling contour is smaller than the N -year omnidirectional H_s return value. (b) For the hatched area to contain the same probability as the shaded area, radius r must be greater than the bound of the blue area on h_x .

Consider a hypothetical marine structure that is fully optimized to directional values of H_s , such that failure occurs immediately if the directional value of H_s is exceeded. In such a case it can be seen from the results by Mackay and Haselsteiner [158] that if the directional values of H_s are specified based on IFORM or direct sampling contours then the failure probability will be approximately 10 times higher than the exceedance probability of the contour. So for this application, the use of IFORM or direct sampling contours is not conservative. A similar argument was made by Forristall [70]. He noted that if a structure is designed based on directional return values in discrete sectors, each at exceedance probability α , then the failure probability of the structure is greater than α . Highest density contours at exceedance probability α have a total exceedance probability of α . Therefore, if the hypothetical, fully optimized structure is designed using directional criteria derived from highest density contours then the failure probability will be equal to the contour exceedance probability (under the assumption of a deterministic response).

The highest density contour as well as the omnidirectional return value contour all enclose a region of parameter space containing total probability $1 - \alpha$. From Figure 5.14 it is evident that the highest density contour offers the potential for considerable directional optimization compared to the omnidirectional contour, but at the cost of requiring a greater capacity in the sector between 300° and 330° . Feld et al. [59] note that there are infinitely many ways to define directional criteria which achieve the target reliability for the structure. Among the set of possible regions, a highest density region defines the smallest area containing probability $1 - \alpha$. Similarly, one way to interpret the omnidirectional return value is that it is the contour with the smallest radius containing probability $1 - \alpha$.

In reality, no structure will be fully optimized in each direction. Instead, there can be a single direction where exceeding the directional values leads to failure, but in other directions, a non-zero margin exists until failure occurs. In such a case the probability of failure of a structure that is designed based on design conditions from a highest density contour will be smaller than the target failure probability. Consider the simple example that the structure is designed to have a smaller response in the x' -direction than the y' -direction (where x' and y' represent a local coordinate system of the structure). In this example we consider the following simple response function

$$r(h_{x'}, h_{y'}) = \sqrt{ah_{x'}^2 + bh_{y'}^2}, \quad (5.22)$$

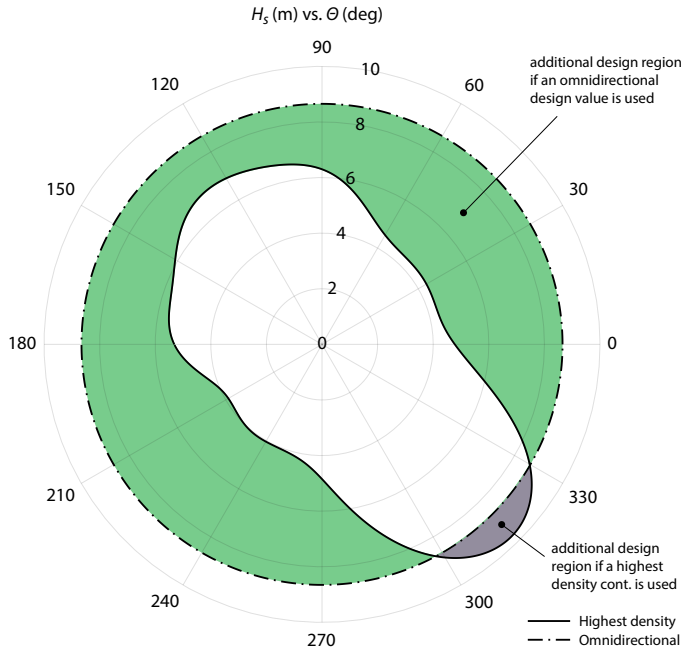


Figure 5.14: Both, the region within an omnidirectional contour and the region within a highest density contour contain probability of $1 - \alpha$ such that a structure that is designed based on such contours will have a probability of failure $p_F < \alpha$ (for a deterministic response). The highest density contour offers the potential for considerable directional optimization compared to the omnidirectional contour, but at the cost of requiring a greater capacity in the sector between 300° and 330°

where $a = 1.4$ and $b = 5$. Or expressing this in the global coordinates, x, y , which are rotated by an angle ϕ to the local coordinate system:

$$r(h_x, h_y) = \sqrt{a(h_x \cos \phi + h_y \sin \phi)^2 + b(-h_x \sin \phi + h_y \cos \phi)^2}. \quad (5.23)$$

Based on the distribution of H_s and Θ we are considering here, suppose the structure is designed in such a manner that its response per unit wave height is smallest in the direction where the highest waves occur, such that $\phi = 315^\circ$. The 1-year response of this structure was calculated using a full long-term analysis and using the three environmental contour methods. The results are listed in Table 5.4. The failure surface corresponding to Expression 5.23 is shown in Figure 5.15, where the response capacity corresponds to the 1-year response estimated using the full long-term analysis.

As expected, the IFORM and direct sampling contours underestimate the 1-year response, since the methods assume that the failure region is convex in H_x - H_y space. Conversely, the highest density contour overestimates the 1-year response. The underestimation is approximately 3-5% for the IFORM and direct sampling contours and the overestimation is approximately 7-16% for the highest density contour.

Suppose that the structure is designed so that its capacity is exactly the 1-year response estimated by a particular contour method in that, for example, the case that an IFORM contour is used the capacity is 10.33, but if a highest density contour is used the capacity is 11.49. In this case the probability of failure for IFORM and direct sampling contours are roughly double the target probability of failure and the probability of failure for the highest density contour is lower than the target probability of failure (roughly four times lower; Table 5.4). So, in this example, the use of IFORM or

5 Environmental contours from highest density regions

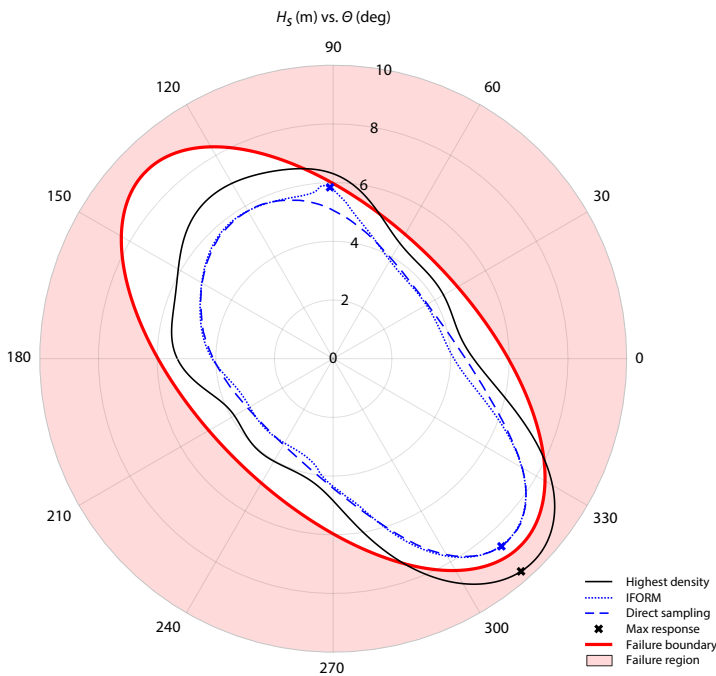


Figure 5.15: 1-year environmental contours for joint distribution of H_s and direction Θ , with failure surface for structure with response given by Expression 5.23. It is assumed that the structure fails at a response that leads to a probability of failure of $p_F = \alpha$.

Method	1-year response	Sea state causing 1-year response (h_s, θ)	p_F
IFORM contour	10.33	5.8 m, 91°	1.80α
Direct sampling contour	10.20	8.6 m, 311°	2.28α
Highest density contour	11.49	9.7 m, 311°	0.23α
Full long-term analysis	10.7	-	α

Table 5.4: Structural responses from different contour methods for a system whose response depends on wave direction, with response given by Expression 5.23. p_F is the probability of failure of a structure that is designed to have a capacity of the 1-year response.

direct sampling contours would be non-conservative, while using a highest density contour would achieve the target reliability.

The directional response function given in Expression 5.23 is not intended to represent a particular structure but is intended to illustrate the differences between the various contour methods considered. The response of a particular structure will fall somewhere between the two limiting cases considered above: (1) a fully optimized structure whose failure surface coincides with the environmental contour that was used to design it; and (2) an omnidirectional structure whose capacity is designed to withstand the highest response along the contour. Table 5.5 lists the failure probabilities of these two structures when designed using each contour method. Interpreting these cases as the boundaries of the set of reasonable direction-sensitive structures, for the joint distribution of H_s and Θ considered here, a structure designed using an IFORM or direct sampling contour will have a probability of failure between ca. 1.1 and 9.2 α and a structure designed using a highest density contour will have a probability of failure between ca. 0.07 and α .

Method	p_F of fully optimized structure	p_F of omnidirectional structure
IFORM contour	9.16α (see Mackay and Haselsteiner [158])	1.16α
Direct sampling contour	ca. 9α (similar to IFORM)	1.11α
Highest density contour	α	0.07α

Table 5.5: Structural responses from different contour methods for the two limiting cases of directionally optimized structures: a hypothetical structure that is fully optimized to wave direction and a structure whose response is independent of wave direction (computed by setting $a = b$ in Expression 5.23). p_F is the probability of failure of a structure that is designed to have a capacity of the environmental contour method's estimated 1-year response.

This example shows that in the derivation of directional design conditions, the highest density contour method's inherent conservatism is necessary to ensure that the assumed design loads are conservative. Using IFORM and the direct sampling contour method led to non-conservative design conditions. However, the highest density contour method led to significant conservatism ($p_F = 0.23\alpha$) in the somewhat optimized structure highlighting that in a practical structure, the failure probability will likely be much smaller than α .

In other variable spaces, for example $H_s - T_z$ there are even regions in the variable space, which cannot lead to structural failure if a structure is designed based on a contour: If a structure is optimized for the contour's upper H_s value of a given T_z value, it will not fail for any H_s at this T_z that is below the contour's lower boundary. To avoid over-conservatism in such cases a method to remove such regions from the exceedance set is described in the following subsection.

5.3.3 REMOVING NON-SEVERE REGIONS FROM THE EXCEEDANCE SET

Sometimes it is clear that a certain region in the variable space will not lead to high loads and consequently will not be part of the failure region of the response of any structure that is designed based on an environmental contour. For example, if a (H_s, T_z) -contour is constructed, the region in the variable space below the contour's lower boundary, will not be part of the failure region. Therefore, to avoid that a highest density contour leads to overly conservative design loads such regions could be specifically treated. Let R_M denote a region in the variable space whose environmental conditions cannot lead to loads, which result in structural failure. Its environmental conditions are “non-severe” or “mild.” Therefore, we call this region “mild region” (Figure 5.16).

Expression 5.2 and Expression 5.3 defined the design region as the highest density region that includes $1 - \alpha$ probability. Its complement is the exceedance region. To avoid having non-severe conditions in the α -exceedance region, we define the design region R_D as the union of a highest density region R_{HD} and a predefined mild region R_M :

$$R_D = R_{HD} \cup R_M. \quad (5.24)$$

The complement of the design region, the α -exceedance region, does not contain the mild region's non-severe environmental conditions. To construct such a design region, first the mild region R_M is defined based on case-specific engineering judgement, which the analyst uses to define ranges of variables. Then, a highest density region must be found, which – in union with the mild region – contains $1 - \alpha$ probability:

$$f_a = \underset{f \in [0, \infty)}{\operatorname{argmax}} \Pr(\mathbf{X} \in R_{HD}(f) \cup R_M) \geq 1 - \alpha. \quad (5.25)$$

5 Environmental contours from highest density regions

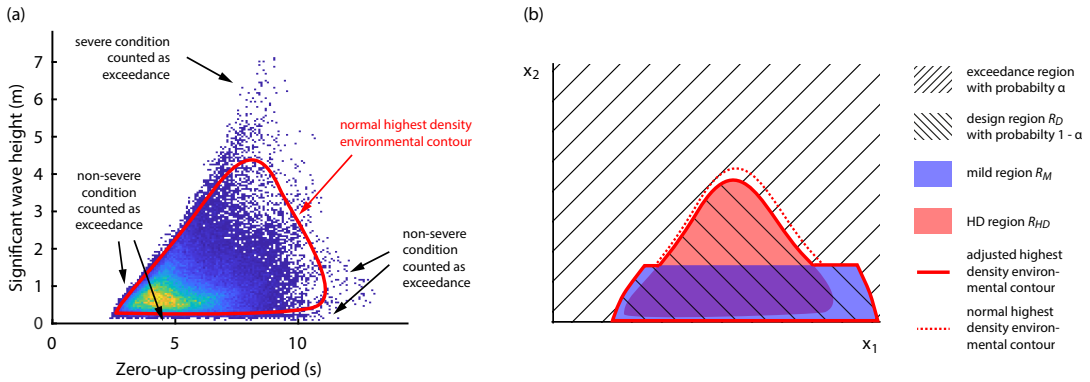


Figure 5.16: Motivation for adjusting a highest density contour. (a) In some variable spaces it is clear that the environmental conditions in certain regions will not cause structural failure because they hold non-severe or “mild” environmental conditions. When these regions are part of the exceedance region that holds a probability of α , a normal highest density contour will be overly conservative. (b) Non-severe conditions can be excluded from the exceedance region by defining a “mild region.” Then the exceedance region must spread to additional regions in the variable space to hold a probability of α . Consequently, a contour adjusted based on a mild region holds less severe environmental conditions – in the illustrated case a lower maximum wave height – than a normal highest density contour.

As defined in (5.24) the design region is then found by calculating the union of the highest density region R_{HD} and the mild region R_M . The adjusted highest density environmental contour is the boundary of the design region. Note that the density value f_a of the adjusted contour will be higher than the density value of an unadjusted highest density contour f_m (compare equations 5.3 and 5.25).

Based on this definition, the variable space is divided into two regions: A design region that holds $1 - \alpha$ probability and an exceedance region that holds α probability. The definition will result in a contour that is smaller in the non-mild region than a pure highest density contour such that its design conditions will be less conservative. However, as long as a structure’s failure region is contained in the exceedance region, N -year design conditions will lead to a conservative estimation of the N -year response (assuming a deterministic response). For brevity, no examples with a mild region are presented in this thesis. However, in a publication by Haselsteiner et al. [96] where the mild region concept was introduced as a stand-alone paper, a full example is available.

5.4 CONCLUSIONS

In this chapter, we presented environmental contours, which enclose regions of highest probability density. A highest density contour has constant probability density along its path and occupies the smallest possible volume in the variable space for a given probability content. We computed the contour using numerical integration based on a grid, iteratively finding the minimum probability density which leads to a contour containing the most likely environmental states that together have a probability of $1 - \alpha$. Defined this way an N -year environmental contour is exceeded on average every N years anywhere along the contour. This means precisely that such an environmental state is realized anywhere outside the environmental contour (and not in a further limited exceedance region). Highest density contours can be computed based on any probability density function, for example global hierarchical models, kernel density based models or joint extreme value models.

5.4 Conclusions

We presented examples for highest density environmental contours and compared them with IFORM and direct sampling contours. In the first example contours were constructed in the H_s - T_z space and in the second example in the H_x - H_y space. The examples highlight when a highest density contour is an appropriate choice and when it would lead to overly conservative design conditions. In cases where a pure highest density contour would be too conservative, the contour can be adjusted by removing a predefined region of non-severe environmental conditions from the exceedance region. It is argued that to choose an appropriate contour method, some understanding about the shape of a structure's failure surface is required. Overall, the method's simple definition based on constant probability density and total exceedance probability provides an alternative in cases where it is unclear whether IFORM and direct sampling contours provide conservative design conditions.

6

SUPPORT FOR THE DESIGN PROCESS

In this chapter, new knowledge that resulted from the studies presented in the previous chapters will be used to propose changes to the current design process of offshore structures. Additionally, a software implementation will be presented that shall support engineers who design or analyze offshore structures.

6.1 METHODOLOGY TO DETERMINE DESIGN LOADS

The new models for the long-term distribution of offshore environmental conditions and the new method to determine joint extremes can be used to formulate an improved methodology to determine design loads. Section 2.3 presented a representation of the design process of offshore structures and identified problematic individual steps. Figure 6.1 shows how the new models and the new method can improve the design process.

Specifically, changes to three detailed steps of the design process are proposed:

1. The long-term probability distribution of H_s shall be modeled with an exponentiated Weibull distribution;
2. The long-term wind speed - wave height joint distribution shall be modeled as a hierarchical model whose dependence functions are physically interpretable; and
3. A contour method shall be used that ensures that, based on its environmental loads, the structure's estimated N -year response will be greater than the true N -year response.

Chapter 3 demonstrated how the exponentiated Weibull distribution can be used to model the distribution of H_s at various sites. Similarly, Chapter 4 presented a hierarchical model for the joint distribution of sea states, F_{H_s, T_z} , and a hierarchical model for wind speed - wave height states, F_{V, H_s} . These models could easily be combined into a three-dimensional wind-wave model, F_{V, H_s, T_z} . Similarly, the same model structure should apply to other parameters that describe a sea state's frequency content, such as the spectral peak period T_p or the energy period T_e . Chapter 5 presented a contour method which – under the assumption of a deterministic response – will always lead to conservative design loads. However, sometimes its assumption of a failure region that surrounds the contour will be overly conservative. Thus, the proposed step of using a contour method that ensures that the estimated N -year response is conservative will be laid out in more detail in the following.

As discussed in Chapter 5, different contour methods are based on different concepts of multivariate exceedance. As an N -year environmental contour is used to estimate an N -year structural response, its definition of exceedance must approximate the shape of the failure region. Because in structural engineering the consequences of underestimating and overestimating a load are asymmetrical, generally, the approximated failure region shall be bigger than the true failure region. In principle, a structure's failure region can have any shape and when defining the design basis its shape is usually not known. Nevertheless, one can often anticipate its approximate shape. For example, the response of a single degree of freedom systems can be conservatively approximated by assuming

6 Support for the design process

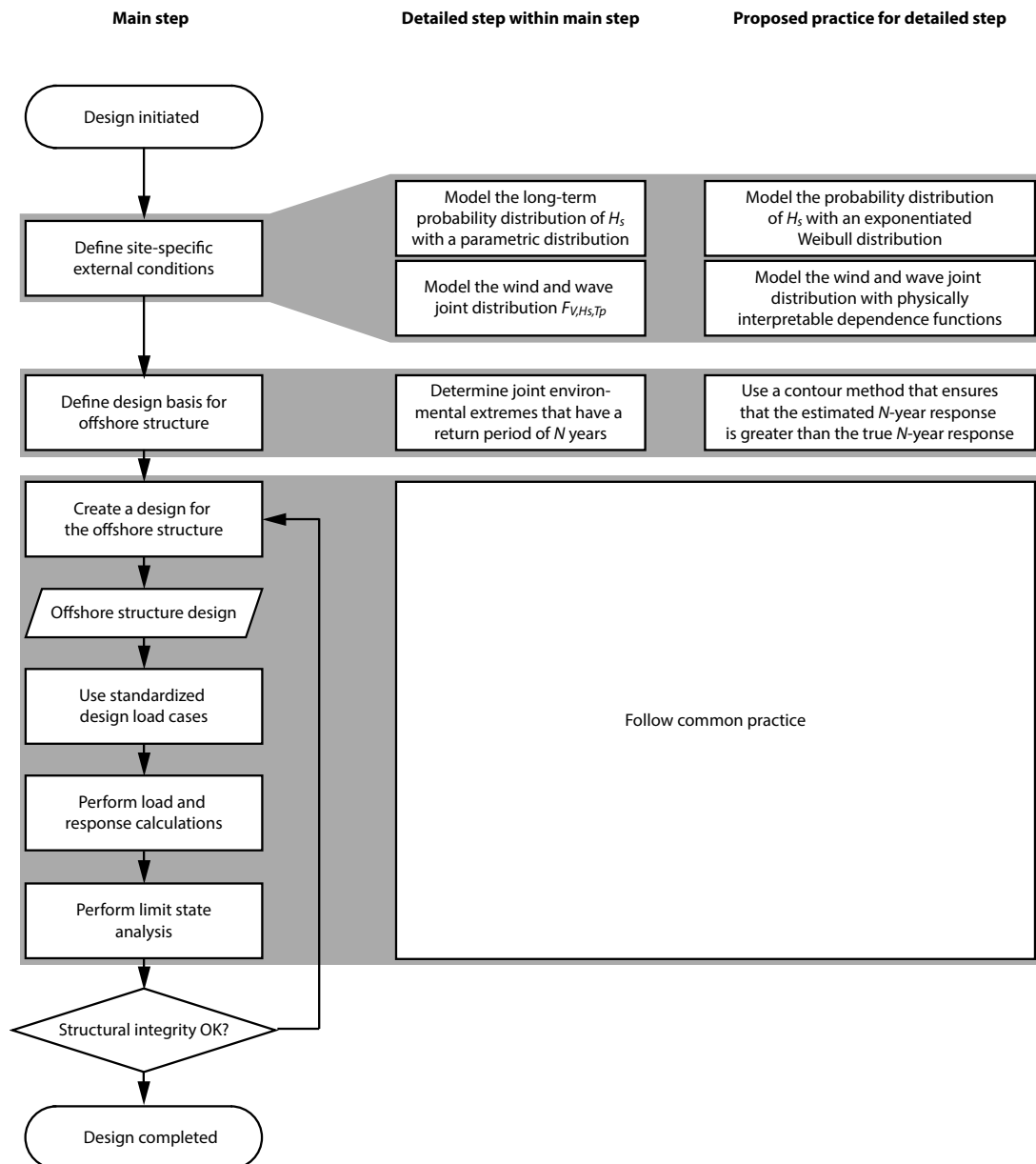


Figure 6.1: Proposed process to design an offshore structure. To determine design loads that lead to the intended reliability, three changes to the common practice are proposed.

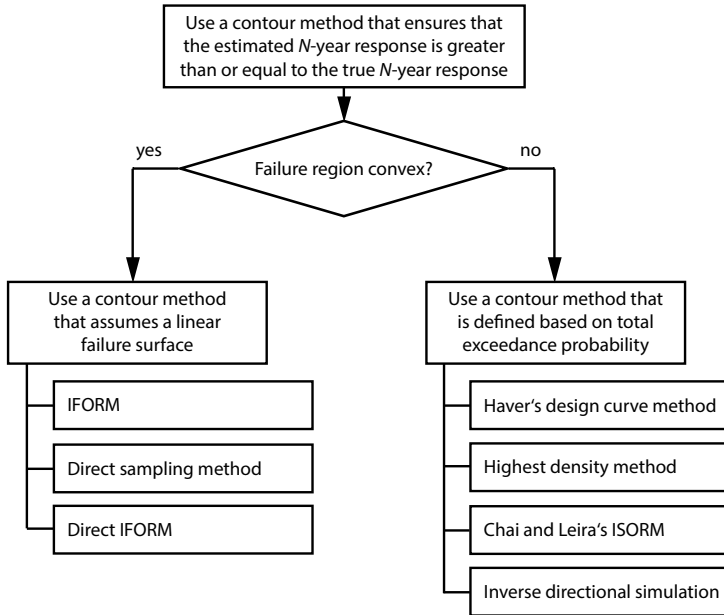


Figure 6.2: To choose a contour method that ensures that the estimated loads and responses will be conservative, one must anticipate whether the structure's failure region will be convex.

a linear failure surface [158] such that using an IFORM [263], a direct IFORM [44], or direct sampling contour [124] is appropriate (Figure 6.2). If it is unclear, however, whether the failure region is convex, a contour that is defined based on total exceedance probability should be used instead. Such contour methods are Haver's design curve method [110], the highest density method that was developed within this thesis, the inverse second-order reliability method proposed by Chai and Leira [27] and the inverse directional simulation contour method by Dimitrov [46]. Figure 6.2 presents a flow chart that illustrates in which cases which type of contour should be used.

To support researchers and engineers in applying the novel models for the long-term distribution and the proposed practice to determine joint extremes, a software implementation was developed. The software focuses on the three detailed steps that are addressed in this thesis, is written in Python and is publicly available under the popular, permissive MIT open-source license¹. Its functionality and architecture are described in the following chapter.

¹<https://opensource.org/licenses/MIT>

6.2 SOFTWARE IMPLEMENTATION

PREVIOUSLY PUBLISHED This section is based on a publication by Haselsteiner et al. [95]. It describes a Python software package that implements the models and methods that were proposed in previous chapters.

PUBLICATION'S FULL CITATION A. F. Haselsteiner, J. Lehmkuhl, T. Pape, K.-L. Windmeier, and K.-D. Thoben. "ViroCon: A software to compute multivariate extremes using the environmental contour method". *SoftwareX* 9, 2019, pp. 95–101. doi: 10.1016/j.softx.2019.01.003.

6.2.1 INTRODUCTION

To support engineers in practice and in academia the models and methods developed in this thesis shall be provided as an easy-to-use open-source software. Such a software could also contain the state-of-the-art methods that are currently widely used. An open-source software with broad functionality to estimate the joint distributions of the offshore environmental conditions and to construct environmental contours could provide significant value. Such a software currently does not exist and if created could provide the methods and models from previous chapters as a subset of its total functionality.

As described, the environmental contour method is widely used to define extreme environmental loads for marine structures like offshore wind turbines, vessels and wave energy converters. Because the environmental contour method is recommended in various engineering guidelines and standards [47, 129, 197] one can assume that practitioners often use the method also.

Currently, obviously, no publicly available software exists that offers the novel methods and models developed in this thesis. Additionally, to the author's knowledge, there exists no publicly available software package that supports multiple environmental contour methods. The author is aware of two open-source implementations of the environmental contour method: (1) a Python implementation of the inverse first-order reliability method in the WEC Design Response Toolbox [38] and (2) a Matlab implementation of the highest density contour method developed by the author of this thesis [90]. In addition, the author is aware of two closed-source implementations: (3) "Proban" offers the inverse first-order reliability method [241] and (4) "Riscue," which is free for noncommercial purposes, offers the direct sampling contour method [123, 124]. All these implementations are focused on a single contour construction method. Here, we present the software "virocon" (from **envi**ronmental **c**ontour), which allows users to define joint distributions and to compute environmental contours with an importable Python package.

6.2.2 SOFTWARE DESCRIPTION

Virocon is written in Python 3. It is designed as a lightweight, importable software package that support users, who are fluent in Python, to compute environmental contours. It can be found on the GitHub repository <https://github.com/virocon-organization/virocon>. Here virocon version 2.0.2 is described, the current version during the writing of this thesis.

SOFTWARE FUNCTIONALITY

Virocon supports the so-called conditional modeling approach [18] to define joint distributions. Thus, distributions follow the global hierarchical model structure described in Section 2.3.1. A joint distribution can be defined by using normal, log-normal, and various forms of Weibull distributions

Element	Available options
Marginal distribution	Normal, log-normal, 2-parameter Weibull, translated Weibull, exponentiated Weibull
Dependence function	Any parametric Python function
Predefined joint models	Sea state model recommended by DNV [47, p. 77], Wind speed - wave height model recommended by DNV [47, p. 78], OMAE2020 sea state model (Chapter 4 and [102]), OMAE2020 wind-wave model (Chapter 4 and [102])
Parameter estimation	Maximum likelihood, least squares, weighted least squares
Contour	IFORM [263], ISORM [27], direct sampling [124], highest density [100]

Table 6.1: Implemented models and methods for various elements of the environmental contour method.

for individual variables and by modeling the dependence structure between the variables with dependence functions (Table 6.1). Dependence functions can be freely defined by the user such that the dependence functions proposed in Chapter 4 and the functions that are currently recommended in DNV's recommended practice RP-C205 [47] can be used to define joint distributions. The joint distribution models proposed in this thesis and the models recommended in RP-C205 are available as predefined models in *virocon*.

The majority of *virocon*'s methods are implemented for an unlimited number of dimensions in that 2-dimensional, 3-dimensional or higher dimensional contours can be computed. Users can choose the methods for fitting a model to measurement data. The implemented standard procedure is to use maximum likelihood estimation when marginal distributions are fitted and least squares when dependence functions are fitted. Users can compute environmental contours based on the inverse first-order reliability method (IFORM; [263]), the inverse second-order reliability method (ISORM; [27]), the direct sampling method [124] and the highest density contour method [100].

SOFTWARE EVALUATION

The implemented environmental contour methods were evaluated by calculating similar environmental contours as those presented by Vanem and Bitner-Gregersen [251], Huseby et al. [124], and Chai and Leira [27]. These contours are based on the joint distribution model of significant wave height H_s and zero-up-crossing period T_z that was also used in Chapter 5. The model's parameters were estimated by fitting it to a dataset of sea states with a duration of 6 hours. For evaluation, we computed environmental contours with return periods of 25 years. Consequently, the exceedance probability was $\alpha = 1/(25 \times 365.25 \times 24/6) \approx 2.74 \times 10^{-5}$. We report the maximum values for significant wave height and zero-up-crossing period along the contour (Table 6.2). Note that these two values do not represent a single sea state because the maximum value of H_s occurs at a different sea state than the maximum value of T_z .

The values calculated with *virocon* compare well with the results from the publications by Vanem and Bitner-Gregersen [251], Huseby et al. [124], and Chai and Leira [27] (Table 6.2). For IFORM and ISORM contours, the deviation between the results from the literature and from *virocon* was less than 1%. For the highest density contours, the deviation to results generated with a Matlab code that was previously published by this author [90], was much less than 1%. For the direct sampling contour, the difference was in the order of 1%.

6 Support for the design process

Contour method	Source	max. H_s (m)	max. T_z (s)
IFORM	Vanem and Bitner-Gregersen [251]	14.62	ca. 13.5*
	virocon	14.62	13.68
ISORM	Chai and Leira [27]	ca. 16.8*	ca. 14.7*
	virocon	16.75	14.63
Direct sampling	Huseby et al. [124]	14.66	13.68
	virocon	14.81	13.73
Highest density	Haselsteiner [90]	16.18	14.37
	virocon	16.15	14.33

Table 6.2: Evaluation of the implemented environmental contour methods. Contours with a return period of 25 years were compared (exceedance probability $\alpha \approx 1.37 \times 10^{-5}$). Shown are the maximum values along computed and published environmental contours. IFORM = inverse first-order reliability method, ISORM = inverse second-order reliability method, * = estimated from a published figure.

6.2.3 ILLUSTRATIVE EXAMPLES

This section presents examples on how to use `virocon`. We will start with a simple example that illustrates the complete process of loading a dataset, fitting a distribution and computing an environmental contour. Then we will show one example for each of the three suggested improvements to the design process: (1) how significant wave height can be modeled using the exponentiated Weibull distribution; (2) how the proposed joint distributions with physically interpretable dependence functions can be used; and (3) how a contour method that ensures that the estimated N -year response is conservative can be used.

FITTING A MODEL AND COMPUTING A CONTOUR BY IMPORTING VIROCON

The package `virocon` is designed as a Python package that users can import to access its methods. Listing 6.1 gives an example on how a user can import the `GlobalHierarchicalModel` and `IFormContour` classes to first fit a distribution to buoy measurements and to then compute an environmental contour. In this example, the global hierarchical model for wind speed and wave height that was presented in Chapter 4 was applied. By importing `virocon`, defining this novel model structure and fitting it to measurement data is achieved with three lines of code (lines 9,10 and 13 in Listing 6.1). Then, in the example, an IFORM contour is constructed based on the estimated joint distribution. If the user concludes that another kind of contour (ISORM, direct sampling or highest density) is more appropriate, changing the command for contour construction is sufficient (line 19 in Listing 6.1). The code shown in Listing 6.1 will produce the plot shown in Figure 6.3.

```

1 import matplotlib.pyplot as plt
2 from virocon import (read_ec_benchmark_dataset, get_OMAE2020_V_Hs,
3 GlobalHierarchicalModel, IFORMContour, plot_2D_contour)
4
5 # Load wind speed - wave height hindcast dataset.
6 data = read_ec_benchmark_dataset("datasets/ec-benchmark_dataset_D.txt")
7
8 # Define the structure of the joint distribution model.
9 dist_descriptions, fit_descriptions, semantics = get_OMAE2020_V_Hs()
10 model = GlobalHierarchicalModel(dist_descriptions)
11
12 # Estimate the model's parameter values (fitting).
13 model.fit(data)
14
15 # Compute an IFORM contour with a return period of 50 years.
16 tr = 50 # Return period in years.
17 ts = 1 # Sea state duration in hours.
18 alpha = 1 / (tr * 365.25 * 24 / ts)
19 contour = IFORMContour(model, alpha)
20
21 # Plot the contour.
22 plot_2D_contour(contour, data, semantics=semantics)
23 plt.show()

```

Listing 6.1: Example showing how to use `virocon` to estimate the long-term joint distribution of wind speed and wave height and how to compute an environmental contour.

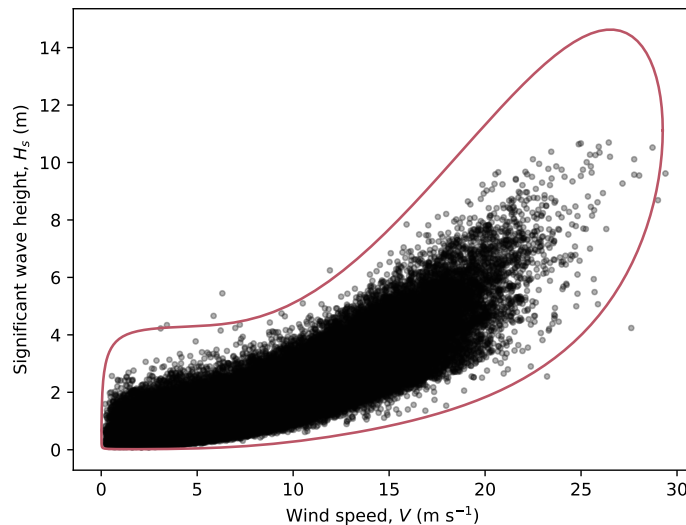


Figure 6.3: Plot of an IFORM environmental contour with a return period of 50 years that was produced by running the code shown in Listing 6.1 .

6 Support for the design process

THE EXPONENTIATED WEIBULL DISTRIBUTION

The exponentiated Weibull distribution is implemented as a class called `ExponentiatedWeibullDistribution`. If the parameters of the distribution are known, a distribution object can be created by calling the constructor with the parameter values, for example:

```
dist = ExponentiatedWeibullDistribution(alpha=2, beta=3, delta=1.5)
```

If the parameter values are not known, but should be estimated, an `ExponentiatedWeibullDistribution` object can be created without specifying parameter values. Then, the method `fit()` can be called to estimate the parameters based on a given dataset. The implementation uses the parameter estimation method based on weighted least squares that is described in Chapter 3. Listing 6.2 shows a full example on how the exponentiated Weibull distribution can be used to model wave height data.

```
import numpy as np
from virocon import ExponentiatedWeibullDistribution, read_ec_benchmark_dataset

# Load sea state measurements from the NDBC buoy 44007.
data = read_ec_benchmark_dataset("datasets/ec-benchmark_dataset_A_1year.txt")
hs = data["Significant wave height (m)"].to_numpy()

# Fit the exponentiated Weibull distribution to the measurements.
dist = ExponentiatedWeibullDistribution()
dist.fit(hs)

# Print the distribution object, which outputs the estimated parameters.
print(dist)
```

Listing 6.2: Example showing how to use `virocon` to fit an exponentiated Weibull distribution to wave height measurements.

PHYSICALLY INTERPRETABLE DEPENDENCE FUNCTIONS

The model structures for significant wave height and zero-up-crossing period as well as for wind speed and significant wave height that were presented in Chapter 4 are implemented in `virocon`. These model structures can be constructed – like any other global hierarchical model – by using the implemented parametric distributions and by defining parametric dependence functions. Listing 6.3 presents an example on how the model structure for sea states is defined using `virocon`'s syntax and how it is fitted to buoy data. Similarly, Listing 6.4 presents an example with the model structure for wind speed - wave height states. Running these codes creates the plots presented in Figure 6.4.

Note that in the code listings shown joint model structures were intentionally defined explicitly. Alternatively, we could have imported these model structures because they are already predefined by writing:

```
from virocon import get_OMAE2020_Hs_Tz
dist_descriptions, fit_descriptions, semantics = get_OMAE2020_Hs_Tz()
model = GlobalHierarchicalModel(dist_descriptions)
```

for the sea state model and

```
from virocon import get_OMAE2020_V_Hs
dist_descriptions, fit_descriptions, semantics = get_OMAE2020_V_Hs()
model = GlobalHierarchicalModel(dist_descriptions)
```

for the wind speed - wave height model.

```

import numpy as np
import matplotlib.pyplot as plt
from virocon import (read_ec_benchmark_dataset, GlobalHierarchicalModel,
                     ExponentiatedWeibullDistribution, LogNormalDistribution,
                     DependenceFunction, WidthOfIntervalSlicer, plot_2D_isodensity)

# Load sea state measurements from NDBC buoy 44007.
data = read_ec_benchmark_dataset("datasets/ec-benchmark_dataset_A.txt")

# Define the marginal distribution for Hs.
dist_description_hs = {
    "distribution": ExponentiatedWeibullDistribution(),
    "intervals": WidthOfIntervalSlicer(width=0.5, min_n_points=50),
}

# Define the conditional distribution for Tz.
def _asymdecrease3(x, a, b, c):
    return a + b / (1 + c * x)
def _lnsquare2(x, a, b, c):
    return np.log(a + b * np.sqrt(np.divide(x, 9.81)))
bounds = [(0, None), (0, None), (None, None)]
sigma_dep = DependenceFunction(_asymdecrease3, bounds=bounds)
mu_dep = DependenceFunction(_lnsquare2, bounds=bounds)
dist_description_tz = {
    "distribution": LogNormalDistribution(),
    "conditional_on": 0,
    "parameters": {
        "sigma": sigma_dep,
        "mu": mu_dep,
    },
}

# Create the joint model structure.
dist_descriptions = [dist_description_hs, dist_description_tz]
model = GlobalHierarchicalModel(dist_descriptions)

# Define how the model shall be fitted to data and fit it.
fit_description_hs = {"method": "wlsq", "weights": "quadratic"}
fit_descriptions = [fit_description_hs, None]
model.fit(data, fit_descriptions)

# Analyze the model's goodness of fit with an isodensity plot.
semantics = {
    "names": ["Significant wave height", "Zero-up-crossing period"],
    "symbols": ["H_s", "T_z"],
    "units": ["m", "s"],
}
plot_2D_isodensity(model, data, semantics, swap_axis=True)
plt.show()

```

Listing 6.3: Example shows how to use virocon to fit the model structure proposed in Chapter 4 to sea state data.

6 Support for the design process

```

import numpy as np
import matplotlib.pyplot as plt
from virocon import (read_ec_benchmark_dataset, GlobalHierarchicalModel,
                     ExponentiatedWeibullDistribution, DependenceFunction,
                     WidthOfIntervalSlicer, plot_2D_isodensity)

# Load wind speed - wave height measurements from the coastDat-2 hindcast.
data = read_ec_benchmark_dataset("datasets/ec-benchmark_dataset_D.txt")

# Define the marginal distribution for wind speed.
dist_description_v = {
    "distribution": ExponentiatedWeibullDistribution(),
    "intervals": WidthOfIntervalSlicer(2, min_n_points=50),
}

# Define the conditional distribution for Hs.
def _logistics4(x, a=1, b=1, c=-1, d=1):
    return a + b / (1 + np.exp(c * (x - d)))
def _alpha3(x, a, b, c, d_of_x):
    return (a + b * x ** c) / 2.0445 ** (1 / d_of_x(x))
logistics_bounds = [(0, None), (0, None), (None, 0), (0, None)]
alpha_bounds = [(0, None), (0, None), (None, None)]
beta_dep = DependenceFunction(_logistics4, logistics_bounds, weights=lambda x, y: y)
alpha_dep = DependenceFunction(_alpha3, alpha_bounds, d_of_x=beta_dep, weights=lambda x, y: y)
dist_description_hs = {
    "distribution": ExponentiatedWeibullDistribution(f_delta=5),
    "conditional_on": 0,
    "parameters": {
        "alpha": alpha_dep,
        "beta": beta_dep,
    },
}

# Create the joint model structure.
dist_descriptions = [dist_description_v, dist_description_hs]
model = GlobalHierarchicalModel(dist_descriptions)

# Define how the model shall be fitted to data and fit it.
fit_description_v = {"method": "wlsq", "weights": "quadratic"}
fit_description_hs = {"method": "wlsq", "weights": "quadratic"}
fit_descriptions = [fit_description_v, fit_description_hs]
model.fit(data, fit_descriptions)

# Analyze the model's goodness of fit with an isodensity plot.
semantics = {
    "names": ["Wind speed", "Significant wave height"],
    "symbols": ["V", "H_s"],
    "units": [
        "m ${}^{-1}$",
        "m",
    ],
}
plot_2D_isodensity(model, data, semantics)
plt.show()

```

Listing 6.4: Example showing how to use `virocon` to fit the model structure proposed in Chapter 4 to wind speed - wave height data.

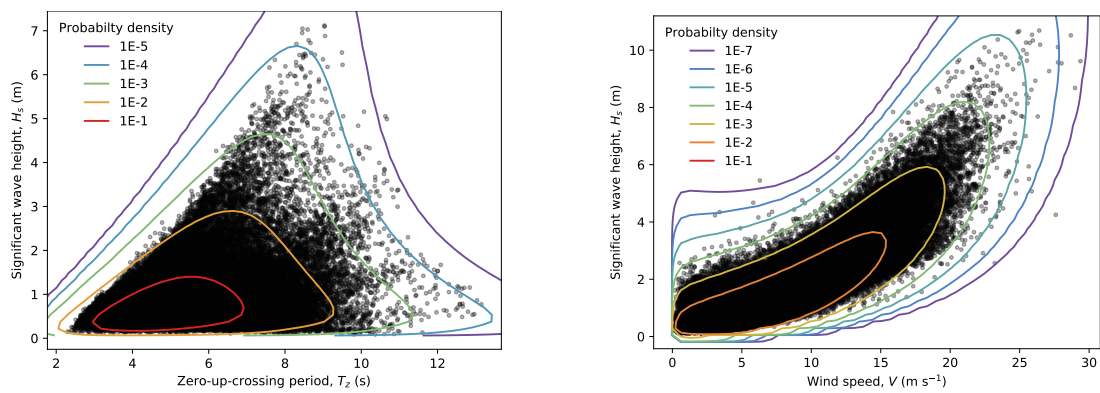


Figure 6.4: Isodensity lines of the joint distribution models on top of the datasets that were used to fit these models. The left and right subplots were produced by running the scripts shown in Listing 6.3 and in Listing 6.4, respectively.

6 Support for the design process

CONTOUR METHODS THAT ENSURE CONSERVATIVE LOADS

Based on a given joint distribution, different contour methods can be applied. As shown in Chapter 5 these contours can differ greatly. Depending on the structural response, some contours might lead to non-conservative or to overly conservative design loads. In *virocon* the four implemented contour methods can be applied similarly to a `GlobalHierarchicalModel` object. The classes `IFORMContour`, `ISORMContour`, `DirectSamplingContour` and `HighestDensityContour` are initialized with a joint distribution (`GlobalHierarchicalModel`) and a probability of exceedance. Listing 6.5 shows an example where, based on a joint distribution model for wind speed and wave height proposed in Chapter 4, four different environmental contours are constructed. Figure 6.5 shows the plot that is generated if the listing's code is executed.

6.2.4 IMPACT

The purpose of *virocon* is to act as a design support, supporting engineers to design or analyze off-shore structure such as wind turbines or ocean bridges. The software can be used by academics too. *virocon* can help researchers pursuing research questions concerning the design and analysis of marine structures. Researchers can start with a metocean dataset and work towards a set of extreme environmental design conditions in an easy, quick, and reproducible manner. That way researchers can define design conditions much quicker and more reliably than if they would implement the fitting and contour methods themselves. In addition, researchers can easily reproduce design conditions that peers have used in their research if both use the standard methods that are implemented in *virocon*. This way studies on marine structures under extreme environmental loads can gain reproducibility and comparability.

Virocon was released in 2019. The software has since been used by researchers and practitioners. As of autumn 2021, seventeen external persons have openly interacted with the software package. They asked questions via emails, via the GitHub repository or “starred” the repository, which is a way to recommend software. Eleven of these persons are associated with academic institutions and six with companies. Users are associated with organizations in the United States, in Europe, China and Australia. They work at universities, research centers, wind turbine manufacturers, ship building companies and consulting companies. The author intends to continue maintaining the software after finishing this doctoral research project.

6.2.5 CONCLUSIONS

Here, a software called *virocon* was presented. *virocon* was developed as a “design support” for engineers. It implements methods to model the joint distribution of metocean data and to compute an environmental contour based on that distribution. All new methods and models that were proposed within this thesis are implemented in *virocon*. Additionally, the software provides a variety of other models and methods that are commonly used. *virocon* is used by researchers and practitioners and is maintained by the author of this thesis.

```

import matplotlib.pyplot as plt

from virocon import (
    read_ec_benchmark_dataset,
    GlobalHierarchicalModel,
    get_OMAE2020_V_Hs,
    IFORMContour,
    ISORMContour,
    DirectSamplingContour,
    HighestDensityContour,
    plot_2D_contour,
)
)

# Load a wind speed - significant wave height dataset.
data = read_ec_benchmark_dataset("datasets/ec-benchmark_dataset_D.txt")

# Define the structure of the joint distribution model.
dist_descriptions, fit_descriptions, semantics = get_OMAE2020_V_Hs()
model = GlobalHierarchicalModel(dist_descriptions)

# Fit the model to the data (estimate the model's parameter values).
model.fit(data, fit_descriptions)

# Compute four types of contours with a return period of 50 years.
state_duration = 1 # hours
return_period = 50 # years
alpha = state_duration / (return_period * 365.25 * 24)
iform = IFORMContour(model, alpha)
isorm = ISORMContour(model, alpha)
direct_sampling = DirectSamplingContour(model, alpha)
highest_density = HighestDensityContour(model, alpha)

# Plot the contours on top of the metocean data.
fig, axs = plt.subplots(4, 1, figsize=[4, 12], sharex=True, sharey=True)
plot_2D_contour(iform, sample=data, semantics=semantics, ax=axs[0])
plot_2D_contour(isorm, sample=data, semantics=semantics, ax=axs[1])
plot_2D_contour(direct_sampling, sample=data, semantics=semantics, ax=axs[2])
plot_2D_contour(highest_density, sample=data, semantics=semantics, ax=axs[3])
titles = ["IFORM", "ISORM", "Direct sampling", "Highest density"]
for i, (ax, title) in enumerate(zip(axs, titles)):
    ax.set_title(title)
    if i < 3:
        ax.set_xlabel("")
plt.tight_layout()
plt.show()

```

Listing 6.5: Example showing how to use `virocon` to construct different types of environmental contours.

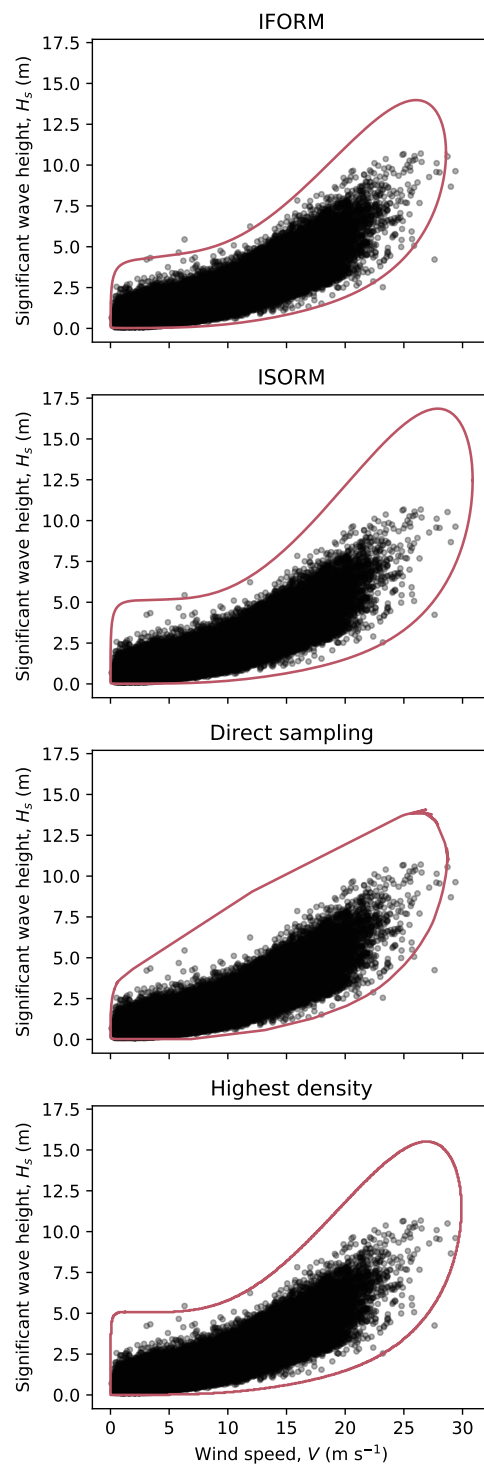


Figure 6.5: Different types of contours constructed with `virocon`. This plot was produced by running the code shown in Listing 6.5 .

7

CASE STUDY: STRUCTURAL DESIGN OF AN OFFSHORE WIND TURBINE

PREVIOUSLY PUBLISHED This chapter is based on a publication by Haselsteiner et al. [94]. It will present a case study on the design of an offshore wind turbine. That way the models and methods proposed in previous chapters will be put into a practical context. In addition, the case study focuses on the question of how accurate load estimates from contours are.

PUBLICATION'S FULL CITATION A. F. Haselsteiner, M. Frieling, E. Mackay, A. Sander, and K.-D. Thoben. "Long-term response of an offshore turbine: How accurate are contour-based estimates?" *Renewable Energy* 181, 2021, pp. 945–965. DOI: [10.1016/j.renene.2021.09.077](https://doi.org/10.1016/j.renene.2021.09.077)

7.1 INTRODUCTION

This chapter will present a comprehensive case study on how environmental contours are used to design the type of offshore structure that the author is most interested in, an offshore wind turbine. The study will compare different contour methods and will analyze the type of bias that contour-based estimates of the structural response have. In the previous chapter, it was always assumed that environmental conditions are independent and identically distributed. In addition, only deterministic responses were considered. In this chapter, none of these assumptions will be made. On the contrary, the biases that result from these assumptions will be explored.

As described in Section 2.3, a major task in the design process of an offshore wind turbine is to evaluate the structural integrity of a candidate design. This evaluation covers fatigue and extreme loads. The widely used international standard IEC 61400-3-1 [129] describes the design process for offshore wind turbines and formulates requirements for structural reliability. Concerning extreme loads, it requires that loads that have a return period of 50 years are assessed by environmental conditions that cause such loads.

To analyze a turbine's response, simulations in the time domain are typically performed (see, for example, [178]). These simulations are computationally expensive and thus it is important to decide which combinations of environmental conditions should be assessed. Some environmental conditions, such as air density or the type of sea state spectrum, can be kept constant over all simulations, under the assumption that the extreme responses are more sensitive to other environmental variables that exhibit large changes over time, such as wind speed, wave height and wave period. The number of simulations required to cover the full range of combinations of environmental conditions expected over the lifetime of the turbine can be very large. Thus, choosing sensible combinations of environmental variables in which to assess the turbine response is an important part of the design process.

The environmental contour method [110, 158, 216, 263] is an approach to define such combinations of environmental variables. The method provides a set of environmental conditions, which are assumed to cause an extreme response with a given target return period. The method is acknowledged to be a simplified approach, providing an estimate of the true long-term response. Using a full

7 Case study: Structural design of an offshore wind turbine

long-term analysis (FLTA) method (see, for example, [67, 191, 217, 257]) can provide more accurate estimates. However, FLTA methods require the turbine response to be estimated for all combinations of environmental variables, and are therefore not practical for wind turbine design, due to the high computational costs.

The authoritative design standard IEC 61400-3-1 [129] requires designers to estimate extreme responses using an environmental contour, and does not require the use of FLTA. Researchers, however, have pointed out that applying an environmental contour method to a wind turbine is challenging [117, 152, 220, 256]. The turbine's controller actively aims to minimize loading, resulting in non-monotonic responses for many design variables, such as bending moments on the tower and blades. This violates one of the key assumptions underpinning the commonly used inverse first-order reliability method (IFORM) contour approach – that the failure region is convex [263]. Moreover, since the response is sensitive to both wind and wave conditions, reducing the design conditions to a two-dimensional contour of wind speed and wave height introduces further uncertainty, since it neglects the stochastic nature of other variables. Previous studies have proposed modifications to the contour method described in IEC 61400-3-1, mainly based on theoretical arguments. However, it is yet unclear how contour-based estimates compare to the true long-term response of an offshore wind turbine and how different effects contribute to overall bias of the estimate. Although previous research has tackled this question [117, 152, 220, 256], the FLTA methods used in these studies did not account for the serial correlation in environmental data, which causes an overestimation of the response [159]. Furthermore, the research methodology of these studies did not allow to identify the individual sources of bias of a contour-based estimate of the response: Serial correlation, the used definition to construct a contour and a response's short-term variability all contribute to overall bias.

Here, we aim to answer the question: How accurate are contour-based estimates of the long-term response, and how much do different sources of bias contribute to the overall bias of a contour-based estimate of the extreme response? Due to the research methodology applied in this study – applying different types of full long-term analysis based on a 1000-year artificial time series of environmental conditions – we can tackle these questions to gain new insights.

This chapter is organized as follows. In Section 7.2 we review the various FLTA methods proposed for estimating the long-term extreme response of an offshore structure. We discuss the environmental contour method and the various approximations that are involved, relative to FLTA. We also review previous studies on the environmental contour method applied to offshore wind turbines. Section 7.3 describes the study's research methodology and explains how we isolate the various sources of bias introduced by the environmental contour approximation. Then, Section 7.4 presents a comparison between the true long-term response and contour-based estimates. Finally, conclusions are presented in Section 7.5.

7.2 ESTIMATING THE LONG-TERM EXTREME RESPONSE

To estimate the long-term extreme response of a structure to environmental loading, three things are required: (1) an environmental dataset; (2) a description of the short-term response as a function of environmental conditions; and (3) a method for combining the short-term response function with the environmental data to estimate the long-term extreme response. There are various methods available for calculating the long-term extreme response. We start by briefly discussing the most accurate types of methods for this task, various methods for “full long-term analysis” (FLTA). These methods account for the variation of the stochastic short-term response function over the full range of environmental conditions. In Section 7.2.1 we consider which type of FLTA method is most appropriate

to consider as a reference to compare contour-based estimates to. In Section 7.2.2, we discuss environmental contour methods, and the various approximations introduced relative to FLTA methods.

7.2.1 FULL LONG-TERM ANALYSIS METHODS

The approach taken for FLTA will depend on the return period of interest and the length of environmental data available. If the return period of interest is much less than the length of environmental dataset, then the short-term response function can be evaluated for each condition in the environmental dataset to obtain a time series of the response, from which the empirical quantile of interest can be obtained. Typically, this requires the environmental dataset to be at least one order of magnitude longer than the return period of interest to keep sampling uncertainties to a reasonable level (see, for example, [162]). If the return period of interest is similar or larger than the length of environmental record, then a way of fitting a model for the long-term distribution to extrapolate outside the range of observations is needed. There are two options for this:

- **Environment-based models:** A probabilistic model of the environmental data is constructed and used to extrapolate outside the range of observations. The extrapolated environmental conditions are then combined with the short-term response function to estimate the long-term extreme response.
- **Response-based models:** The environmental data is combined with the response function to obtain a time series of response. A probabilistic model is fitted to the response data and used to extrapolate to the return period of interest.

The advantage of response-based methods is that the problem of predicting long-term extremes is reduced to a univariate problem. However, the disadvantage is that a separate probabilistic analysis needs to be conducted for each response of interest. Moreover, response-based methods make the tacit assumption that the behavior of the response function does not change significantly outside the range of observations. As discussed further below, this assumption may not be appropriate for a wind turbine response, such as tower or blade bending moments. For example, at some locations, the largest responses in short environmental records may occur in operational conditions, whereas for longer return periods the largest responses may occur when the turbine is parked or idling. As the form of the response function can differ in operational and parked conditions, extrapolating based on observed responses over a short time period may lead to errors.

Environment-based extrapolation can be more complex to implement, since it typically involves a multivariate problem, such as fitting a model for the joint distribution of wind and wave conditions. However, it has the advantage that a single extreme value analysis of environmental conditions can be conducted and used to estimate multiple extreme responses. Moreover, no assumptions are required about how the response function behaves outside the range of observations, since the response function is evaluated explicitly for the extreme environmental conditions.

Another key distinction between FLTA methods is the treatment of serial correlation. Table 7.1 presents some examples of FLTA methods using environment-based and response-based extrapolation, categorized by whether they assume (a) individual response peaks (“all-peaks”); (b) short-term maxima; or (c) storm-peak values are independent. Here, “short-term maxima” refers to the maxima in each record of the environmental dataset, typically over time-scales of 10 minutes - 3 hours, whereas “all-peaks” methods consider all response peaks within each record as independent (typically there will be several hundred response cycles per hour). The correlation time-scales in the short term response function are typically much shorter than the time-scales of the environmental records. This means that if the environmental conditions were stationary, then it would be reasonable to assume

Events considered independent	Environment-based models	Response-based models
All response peaks	Nordenström [196] Battjes [14] Tucker [239] Guedes Soares [82] Naess [189]	
Short-term maxima	Krogstad [145] Videiro and Moan [257] Moriarty et al. [180] Fogle et al. [67] Sagrilø et al. [217] Muliawan et al. [184] Videiro et al. [258] Gramstad et al. [78]	Marshall et al. [167] Standing et al. [232] Mazaheri and Downie [169] Fontaine et al. [68] Vanem et al. [253]
Storm-peak values	Brown et al. [24] Hansen et al. [89] Mackay and Jonathan [163]	Tromans and Vanderschuren [238] Bowers et al. [22] Incecik et al. [127] Mackay and Johanning [160] and Mackay and Johanning [164] Koohi Kheili et al. [142]

Table 7.1: Examples of full long-term analysis methods used for estimating extreme responses.

that extreme responses separated by, for example, 1 hour, are independent. However, since the size of the response depends on the environmental condition, and time series of environmental conditions are serially correlated, time series of extreme responses will also exhibit serial correlation. Table 7.1 also includes some examples of methods for estimating long-term extremes of individual wave or crest heights, since these can be considered as FLTA methods, where the response function is the short-term wave or crest height distribution. The list of works cited in Table 7.1 is far from exhaustive, and there is a large volume of literature on this topic. The purpose of the table is to illustrate the types of methods proposed and the key assumptions made.

Comparisons between all-peaks, short-term maxima and storm-peak methods have been presented in references [69, 159, 161, 217]. All-peaks and short-term maxima methods neglect the serial correlation in environmental conditions. Mackay et al. [159] showed that this can lead to significant positive biases in estimates of long-term extreme responses, with the bias being larger when the distribution of storm-peak values has a longer tail. Nevertheless, environment-based short-term maxima FLTA methods are widely used in ocean engineering as reference methods for estimating extreme loads on offshore wind turbines [117, 152, 220, 256]. Moreover, they are the basis for the first- and second-order reliability methods (FORM and SORM) [165] and inverse FORM and SORM methods [74, 76].

Based on the discussion above, storm-based methods with environment-based extrapolation are considered most accurate for estimating the long-term extreme response of an offshore wind turbine. This method will therefore be used as the reference method in this study.

7.2.2 ENVIRONMENTAL CONTOURS FOR WIND TURBINE DESIGN

Compared to storm-based FLTA methods, the environmental contour method introduces three simplifying assumptions:

1. The maximum responses in each short-term condition are independent

2. The N -year response occurs at an N -year environmental extreme
3. The response in each environmental condition can be evaluated at a fixed quantile of the short-term distribution function

As discussed in the previous section, the first simplification is also applied in some commonly used FLTA methods. The second simplification is related to the assumption about the failure surface, made in the construction of the contour. IFORM contours [263] (and various alternative formulations [44, 124], which we also refer to here as IFORM methods) are based on the assumption that a structure's failure surface can be linearized at the design point (the point on the failure surface with the highest probability of occurrence). Under this assumption, multivariate extreme sets are defined as half-plane regions, corresponding to the linearized failure surface, which contain a fixed probability level α . The environmental contour is then defined as the boundary of the region consisting of the intersection of all such extreme sets. The alternative assumption is to assume that structural failure occurs anywhere outside the design region (see, for example, [27, 100]). Under this assumption, an environmental contour is defined as the boundary to a region containing probability $1 - \alpha$. Differences between these two types of contour are discussed in reference [158].

The third simplification is equivalent to assuming the short-term response function is deterministic rather than random, with the deterministic response defined as the response at the fixed quantile of the short-term distribution function. As the response of the structure is only evaluated in environmental conditions along the contour, this neglects the probability that the 50-year response could be caused by a high response in less extreme environmental condition or a low response in a more extreme condition. The effect of short-term variability is usually accounted for by evaluating the short-term response at a quantile higher than the median value [263].

In addition to the three simplifying assumptions listed above, the accuracy of the environmental contour method is dependent on three additional factors:

4. The reduction of a high-dimensional multivariate problem to a 2D or 3D problem
5. The accuracy of the joint probability model for the environmental variables
6. The accuracy of the response model

These factors also influence the accuracy of FLTA methods. The response of many offshore structures is dependent on multiple environmental variables (see the discussion in Section 7.3.1). However, due to the difficulty in estimating joint distributions in high dimensions and the number of simulations required to characterize the response in a high dimensional space, it is normally assumed that certain variables are either fixed or in fixed relation to other variables, so that only two or three variables need to be considered.

The environmental contour method is used to establish design loads for offshore wind turbines (see, for example, [1, 30, 117, 152, 153, 155, 220, 256]; Table 7.2). In design load case (DLC) 1.6 in IEC 61400-3-1 [129], it is required that the design is checked for combinations of wind speed and significant wave height along a 50-year environmental contour (Figure 7.1). Compared to other marine structures, applying a contour method to offshore wind turbine design presents particular challenges. The environmental contour method was developed mainly for structures where the wave height and period have a dominant influence on the response. For an offshore wind turbine both wind and wave loads are equally important. Thus, the effect of reducing the wind turbine design problem to a 2D contour may have a greater impact than for other structures.

The IEC standard recommends using IFORM contours for DLC 1.6. As discussed above, the IFORM approach assumes that a structure's failure surface can be linearized at the design point.

Source and year	Contour variables	Additional deterministic variable	Contour type	Analyzed here
Saranyasoontorn and Manuel [220], 2006	V, H_s	-	50-year IFORM	-
Li et al. [152, 153], 2016, 2017	V, H_s, T_p	-	Modified IFORM that restricts the contour to wind speeds $< 25 \text{ m s}^{-1}$	-
Horn and Winterstein [117], 2018	$V \cdot H_s \& H_s \cdot T_p$	T_p and V , respectively	Four 50-year IFORM contours, one per variable space sub-population	-
Velarde et al. [256], 2019	H_s, T_p	V	Multiple N -year IFORM contours, value of N determined based on V	-
Liu et al. [155], 2019	V, H_s	T_p , median $T_p V, H_s$ is used	50-year IFORM	X
IEC 61400-3-1, DLC 1.6 [128], 2019	V, H_s	T_p , highest load $T_p V, H_s$ is used ¹	50-year IFORM	X
Chen et al. [30], 2020	V, TI, H_s, T_p	-	50-year IFORM and modified IFORM	-
This work	V, H_s	T_p , median $T_p V, H_s$ is used	50-year highest density	X
This work	V, H_s	T_p , highest load $T_p V, H_s$ is used	50-year highest density	X
This work	V, H_s, T_p	-	50-year highest density	X

1 Guidance on choosing values is not definitive. The standard's text reads "The severe sea state shall include the extreme individual wave height that, in combination with the associated wave period and the mean wind speed, has a return period of 50 years. The designer shall take account of the range of wave period, T , appropriate to each extreme wave height. In the absence of a more sophisticated probabilistic assessment, design calculations shall assume values of wave periods within this range that results in the highest loads acting on an offshore wind turbine." [129]

Table 7.2: Environmental contour methods proposed for analyzing offshore wind turbine reliability. V = wind speed, TI = turbulence intensity, H_s = significant wave height, T_p = spectral peak period. Five of the listed methods are analyzed in this study.

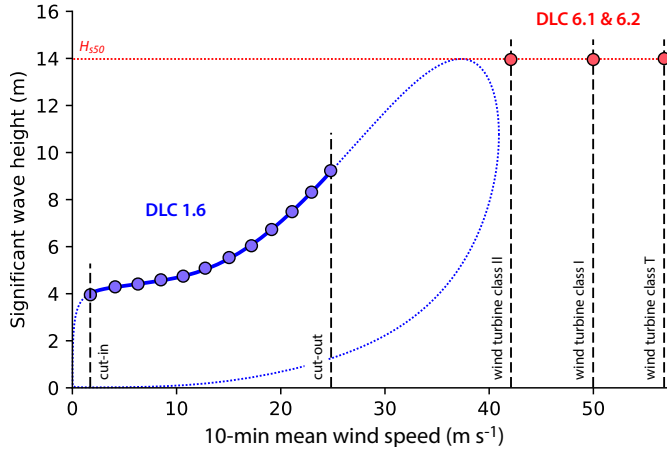


Figure 7.1: Design approach in IEC 61400-3-1 [129]. In design load case (DLC) 1.6, loads are evaluated at points along a 50-year wind-wave environmental contour, for wind speeds between cut-in and cut-out. At higher wind speeds, DLCs 6.1 and 6.2 require that the 50-year marginal significant wave height value, H_{s50} , and the reference wind speed value are combined. Reference wind speeds are based on the turbine classes defined in IEC 61400-1 [128] and must be higher than a site's 50-year wind speed. Circles show environmental conditions that must be considered based on the three load cases. Note that H_{s50} does not necessarily coincide with the highest point along the contour in a 50-year IFORM contour, but it depends on the order of the variable transformation [158].

While the linearization is reasonable for many marine structures, it is problematic for many wind turbine response variables. Modern wind turbines have control systems that optimize power output while reducing loads. The controller is designed to extract as much power as possible from the wind until the power output reaches the rated capacity, at the rated wind speed, which is typically around 11 to 13 m s^{-1} . Above this wind speed, the blades are progressively pitched to reduce loads while maintaining constant power output. Finally, at the cut-out wind speed, turbines stop producing power and the blades are fully pitched out of the wind to minimize loads. Consequently, some response variables such as the mudline overturning moment do not increase monotonically with wind speed (see Figure 7.2; [10, 152, 153]).

Thus, researchers have pointed out that an IFORM contour should not be applied directly in offshore wind turbine design (see, for example, [117, 152, 256]). Essentially, the non-monotonic response over wind speed leads to two distinct regions of high response along the environmental contour such that the failure surface cannot be well approximated by linearizing it at a single point (Figure 7.2). As a solution, Li et al. [152] proposed to use a procedure that involves checking multiple environmental contours with different return periods. Horn and Winterstein [117] also acknowledged the problem and proposed to divide the wind-wave variable space, with the turbine in power production and parked mode, into four sub-populations and to construct one contour per sub-population. Velarde et al. [256] focused on the sea state's frequency variation and proposed an environmental contour method to assess the wave peak period that causes the highest response.

The factors that are relevant for all marine structures have already been analyzed to a great extent in the literature. The uncertainty of choosing a joint model has been analyzed in a recent benchmarking study on environmental contours [92, 107]. Different definitions for contour exceedance have been analyzed [96, 134, 158, 250]. Short-term variability has been discussed in an early paper by Winterstein et al. [263] and since then been analyzed for various structures [8, 184]. Practical methods for accounting for short-term variability in contour methods are discussed in [45, 263]. The

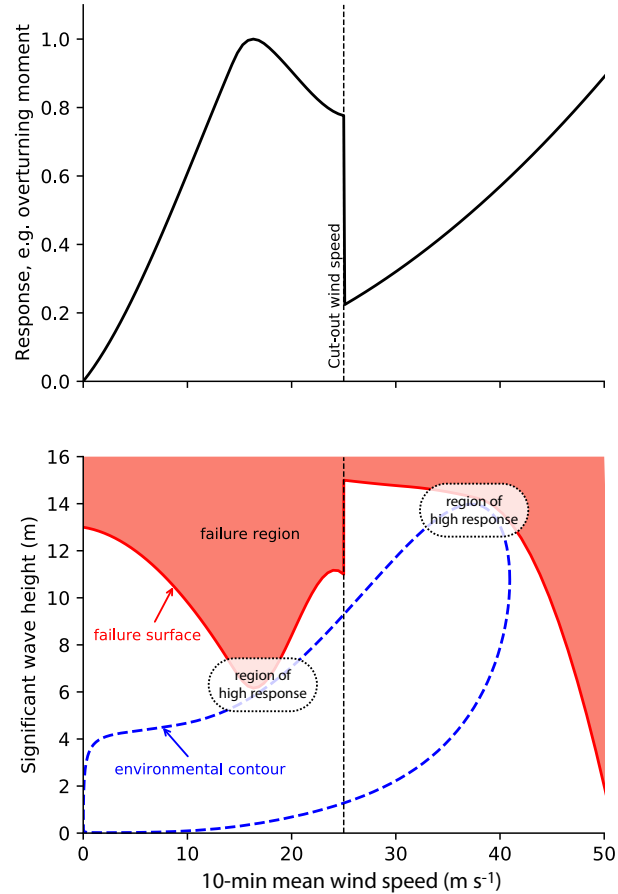


Figure 7.2: Non-monotonic response of an offshore wind turbine (top) and the associated problem when an environmental contour is used for structural design (bottom). Top: Due to a turbine's control system, response variables such as the overturning moment or the fore-aft shear force are non-monotonic (see, for example, [10, 152, 153]). Bottom: As a consequence, the failure region is non-convex and the contour has two regions of high response. This can be problematic for IFORM contours, which approximate failure surfaces as a hyperplanes, which is only conservative if the failure region is convex.

effect of serial correlation on environmental contours and estimates of long-term extreme loads has been discussed in [44, 159]. The two challenges associated with offshore wind turbines, dealing with the non-monotonic response and jointly dealing with wind and wave variables, are less understood.

The problem of the non-monotonic response violating the assumptions of IFORM contours can be addressed by using a contour that is defined based on the total exceedance probability outside the contour. For such contours a non-monotonic response does not violate any assumptions [27, 100, 158]. Non-monotonic responses are problematic for IFORM contours because they can lead to non-convex failure regions and IFORM is only conservative for convex failures regions. Total exceedance contours, such as highest density contours [100] and Chai and Leira's inverse second-order reliability method (ISORM; [27]) contours yield always conservative environmental design conditions (provided that short-term variability is accounted for).

For addressing the relevant variables – wind speed, wave height, wave period and potentially turbulence intensity (see [30]) – in a contour method, no clear solution is given in the literature. The design standard IEC 61400-3-1 [129] suggests that a 2D wind speed - wave height contour should be constructed, and that spectral peak period should be chosen as the period that causes the highest loads at the particular combination of wind speed and wave height. While this approach sounds somewhat sensible, this combination of probabilistic and deterministic choices of variables cannot be interpreted consistently in terms of failure probability and implied reliability. Velarde et al. [256], however, proposed that the joint distribution of wind speed, significant wave height (H_s) and spectral peak period (T_p) shall be used to construct multiple $H_s - T_p$ contours instead. Horn and Winterstein [117] proposed using multiple 2D contours, both wind speed - wave height and wave height - wave period to deal with the three-dimensional variable space. In principle, environmental contour methods generalize to higher dimensions [100, 245, 263] such that one could also construct a single three-dimensional wind speed, wave height, wave period surface, (which we also refer to as a “contour”, for consistency). Currently, it is unclear which of these approaches is best suited to deal with the environmental variables that are relevant to offshore wind turbine design.

Past works have analyzed the design loads on wind turbines using various contour methods [30, 152, 153, 155, 220, 256] and have proposed new contour methods based on theoretical arguments. Where the environmental contour method for wind turbines has been compared to FLTA, the FLTA method applied has been based on the assumption that hourly environmental extremes are independent. As discussed in Mackay et al. [159], hourly observations are strongly serially correlated and neglecting serial correlation can result in positive biases in estimates of long-term extreme response. Thus, no study has yet compared response estimates from contours with the true unbiased long-term response of an offshore wind turbine. This study aims to provide such a comparison.

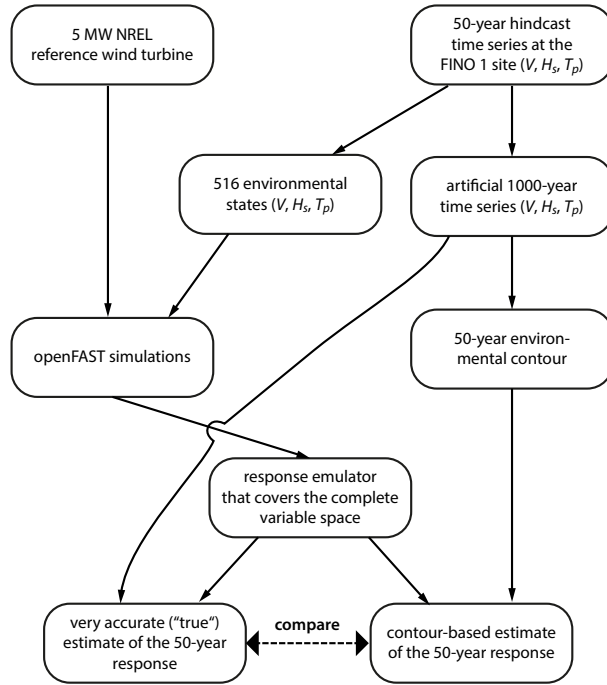


Figure 7.3: Research methodology. This study’s goal is to compare the “true” long-term response with an estimate based on an environmental contour. To enable this comparison a response emulator and an artificial 1000-year time series of environmental conditions were created.

7.3 RESEARCH METHODOLOGY

This study’s overall design is summarized in Figure 7.3. The goal is to compare the “true” 50-year long-term response with an estimate based on an environmental contour. Of the factors affecting the accuracy of the long-term response estimates, discussed in Section 7.2.2, the accuracy of the response model or the accuracy of the statistical model for environmental conditions are not taken under consideration, since these factors influence both contour and FLTA methods. Instead, we focus on isolating the influence of the approximations made in the environmental contour method relative to FLTA.

We use the 5 MW NREL reference wind turbine [137] and consider the FINO 1 research platform site in the German North Sea [65]. Because performing dynamic multiphysics simulations of a wind turbine with a state-of-the-art code such as openFAST requires CPU computation time in the same or a higher order of magnitude as the simulation time, simulating times series that cover multiple years is impractical. Thus, we created a response emulator based on 516 1-hour multiphysics simulations. This response emulator is a parametric statistical model that outputs a random 1-hour maximum response for a given environmental condition. Additionally, to estimate the 50-year response accurately, a much longer time series than measurements or hindcasts offer is required. Consequently, we created an artificial 1000-year time series. This time series and the response emulator were used to accurately estimate the 50-year response. Finally, we also used the response emulator and the empirical joint distribution derived from the artificial time series to calculate contour-based estimates of the 50-year response. The methodology is described in detail in the following subsections.

7.3.1 ENVIRONMENTAL CONDITIONS

To enable a comparison between a very accurate estimate, (which we refer to as the “true” long-term response), and estimates from contour methods, we needed to consider a time series that is several orders of magnitude longer than the return period of interest. Typical site-specific datasets of wind speed and wave height, however, only cover periods of the order of 10 - 100 years. To circumvent this problem, here, we generated an artificial time series, based on the statistical characteristics of a 50-year dataset from the coastDat-2 hindcast [80, 81] at the location of the FINO 1 research platform in the German North Sea (Figure 7.4). This 50-year dataset was also used in a recent benchmarking exercise on environmental contours [92].

The artificial time series was created using a block resampling method [163]. The method involves three steps. In the first step, the time series is divided into non-overlapping blocks, where the peaks of each variable of each block can be considered approximately independent from adjacent blocks (in a similar manner to a peaks-over-threshold analysis). In the second step, a joint distribution model is fitted to the block-peak values. In the third step, random vectors of peak values are simulated from the fitted model and measured blocks with peak values closely-matching the simulated values are selected at random and rescaled so that the resampled and simulated peak values coincide. The artificial time series is composed of the resampled and rescaled blocks from the original time series. The idea is that, provided that the measured blocks are only scaled by a small amount, the resampled time series should be physically realistic and closely match both the temporal and joint dependence structure of the measured time series. The resampled time series is not continuous at the block boundaries. However, the blocks are defined so that the peak values do not occur near the block boundaries, so that the temporal correlation structure around the peak values is preserved. Further details of the procedure used to generate the artificial time series are presented in the research article that this chapter is based on [94].

The artificial time series covers 1000 years. The model comprised a joint distribution for block maxima of wind speed, V , significant wave height, H_s , and wave steepness, $S = 2\pi H_s/gT_p^2$ (where g is the acceleration due to gravity). Comparisons of measured and simulated values of these variables are shown in Figure 7.4.

In the present work, we have only considered the variation of wind speed, significant wave height and wave steepness. The environmental variables that were assumed to remain constant over time are listed in Table 7.3.

Property	Value
Air density	1.225 kg m^{-3}
Wind speed profile	$V(z) = V_{hub}(z/z_{hub})^{0.14}$
Turbulence intensity	During power production: ca. 14% - 50% (wind turbine class B; IEC 61400-1 normal turbulence model) Above 25 m s^{-1} : 11% (IEC 61400-1 normal turbulence model)
Water density	1025 kg m^{-3}
Wave spectrum	JONSWAP spectrum with $\gamma = 3.3$
Wave directional spread	0 deg
Wave mean direction	0 deg
Wind mean direction	0 deg
Current velocity	0 m s^{-1}
Water depth	30 m

Table 7.3: Environmental variables that are constant over all simulations.

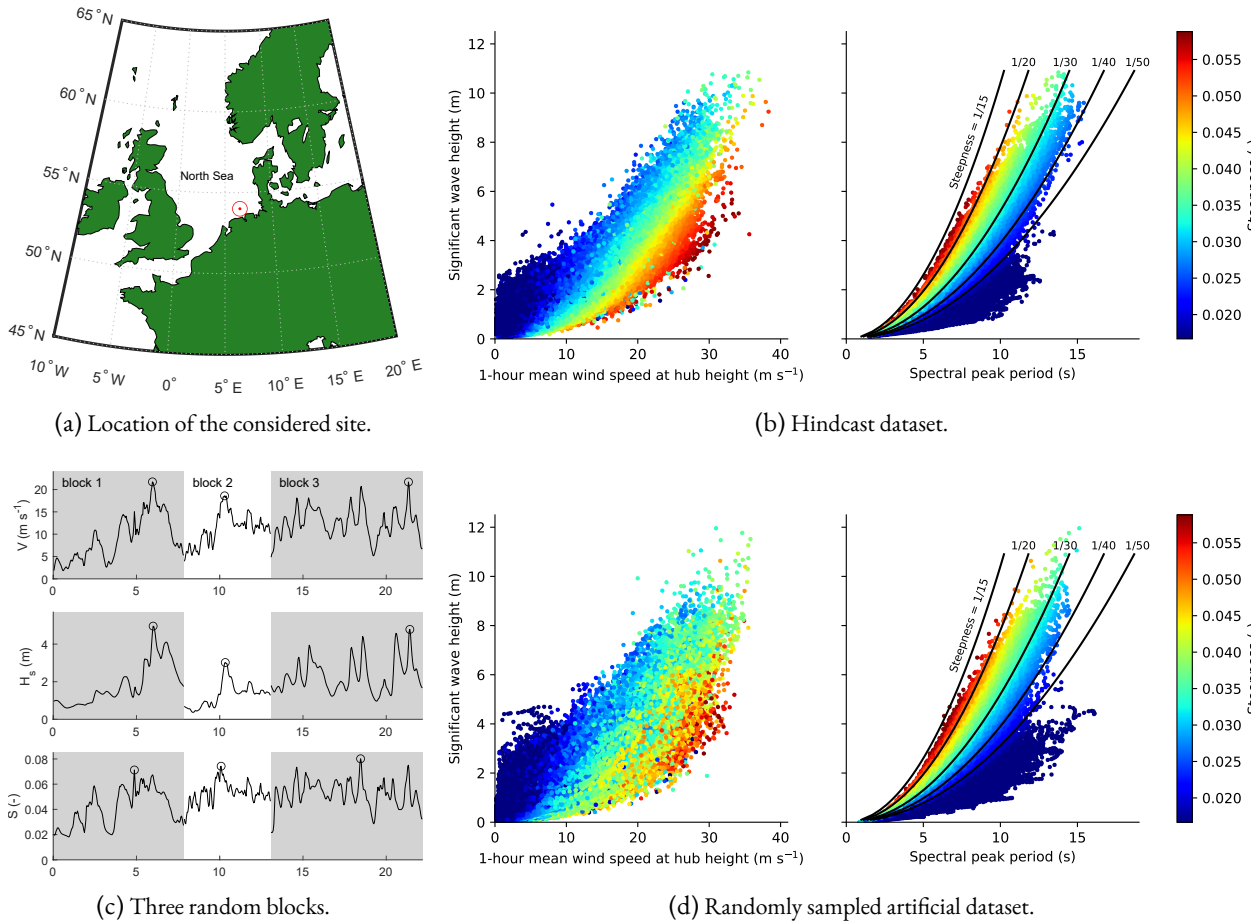


Figure 7.4: Metocean dataset. (a - b) A 50-year period of the coastDat-2 dataset [81] at the location of the FINO 1 research platform was used to build a statistical model. The three variables considered were 1-hour mean wind speed at hub height, 1-hour significant wave height and 1-hour spectral peak period. (c-d) An artificial dataset was created that spans 1000 years (the first 50 years are shown here), with statistical characteristics matching the coastDat-2 dataset. The dataset was created using a block-resampling method, where block-peak values (shown as circles) were drawn randomly from a joint model and measured blocks are resampled and rescaled so that the peak values match the simulated values.

7.3.2 WIND TURBINE RESPONSE

TURBINE PROPERTIES

We used the 5 MW NREL reference wind turbine [137] with the monopile design that was proposed by Bachynski et al. [9]. The 5 MW NREL reference turbine is widely used in academic studies (see, for example, [20, 48, 49, 84, 210, 273]). Figure 7.5 shows the turbine’s main dimensions, the three variables that were varied among simulations – wind speed, significant wave height, and spectral peak period – and the response variables that were analyzed, the bending moment at 10 m water depth and the mudline overturning moment. The turbine is controlled via a variable-speed-variable-pitch scheme, with a cut-in wind speed of 3 m s^{-1} and a cut-out wind speed of 25 m s^{-1} .

MULTIPHYSICS SIMULATIONS

We performed aero-hydro-servo-elastic simulations using the code openFAST ([193], version 2.2.0). OpenFAST is a multiphysics simulation code that allows the coupled simulation of aerodynamics (“aero”), hydrodynamics (“hydro”), structural dynamics (“elasto”) and a controller (“servo”). The code consists of several software modules that deal with different types of physics. The software module AeroDyn [179] handles the aerodynamics and is based on the principle of actuator lines. We used its implementation of the blade element momentum method. The software module HydroDyn handles the hydrodynamics. We used its implementation of strip theory that is based on Morison’s equation and linear wave theory to simulate wave loads. Structural mechanics were handled by the modules ElastoDyn (rotor blades, tower and transition piece) and SubDyn ([41]; monopile).

Simulations were run for a total duration of 1 hour and 30 s, however, the first 30 s were discarded because they were only intended to initialize the simulation to a dynamic state. The time step size was 12.5 ms. We performed simulations which covered the range of observed wind speeds, wave heights and wave periods (Figure 7.6). Thus, simulations were performed for wind speeds between 1 and 45 m s^{-1} , significant wave heights between 0 and 15 m and spectral peak periods between ca. 3 s and 18 s. The variable space was evaluated by performing simulations at four different T_p values per $V - H_s$ combination. These four “slices” of T_p through the 3-dimensional variable space were defined as:

$$\begin{aligned} t_{p1} &= \sqrt{\frac{2\pi h_s}{g \cdot 0.066}}, \\ t_{p2} &= \sqrt{\frac{2\pi h_s}{g \cdot 0.04}}, \\ t_{p3} &= t_{p2} + \frac{8}{1 + \sqrt{h_s + 2}}, \\ t_{p4} &= t_{p2} + \frac{20}{1 + \sqrt{h_s + 2}}, \end{aligned} \tag{7.1}$$

where $g = 9.81 \text{ m s}^{-2}$ is the acceleration due to gravity. In total 516 simulations were performed to cover the variable space.

STATISTICAL RESPONSE EMULATOR

We built a response emulator that returns a random 1-hour maximum moment at 30 m water depth for a given combination of 1-hour mean wind speed v , significant wave height h_s and peak period

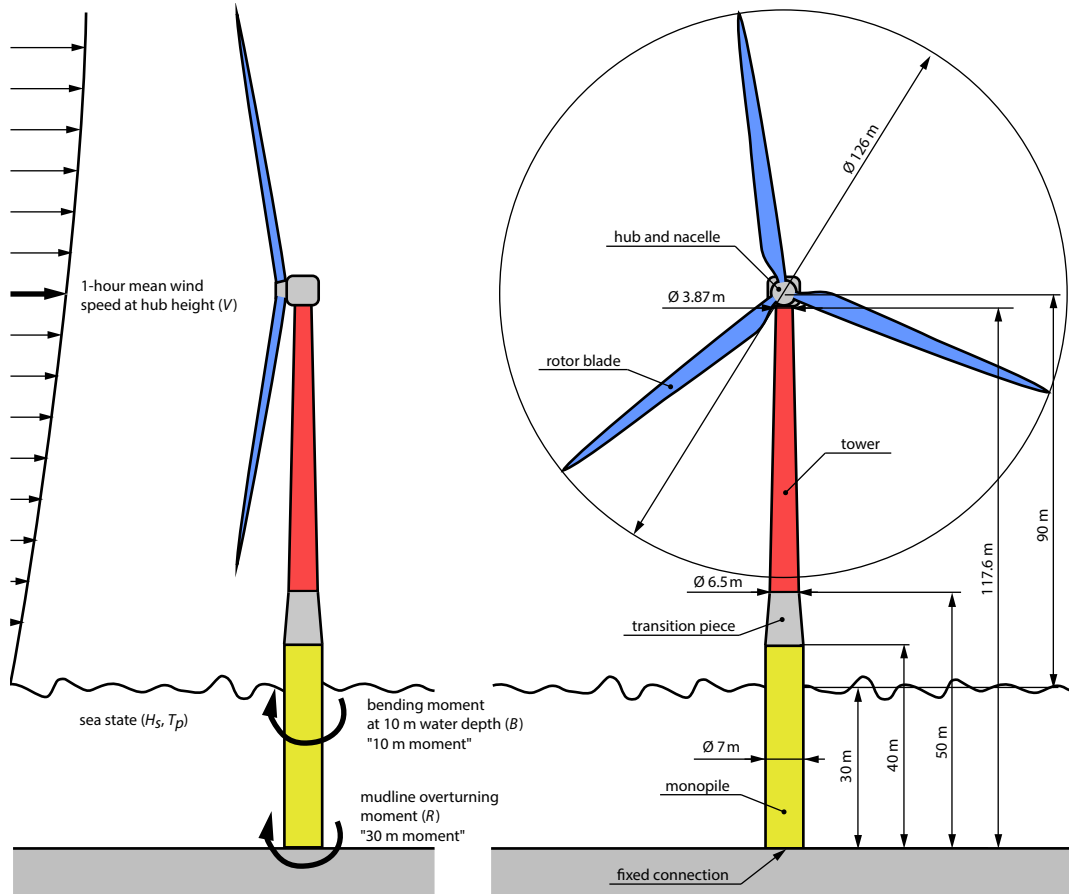


Figure 7.5: 5 MW NREL reference wind turbine [137] with the monopile foundation presented by Bachynski et al. [9]. In this study, we varied the three environmental conditions 1-hour mean wind speed V , significant wave height H_s , and spectral peak period T_p . For simplicity, only two response variables, the mudline overturning moment R and the bending moment at 10 m water depth B , were analyzed.

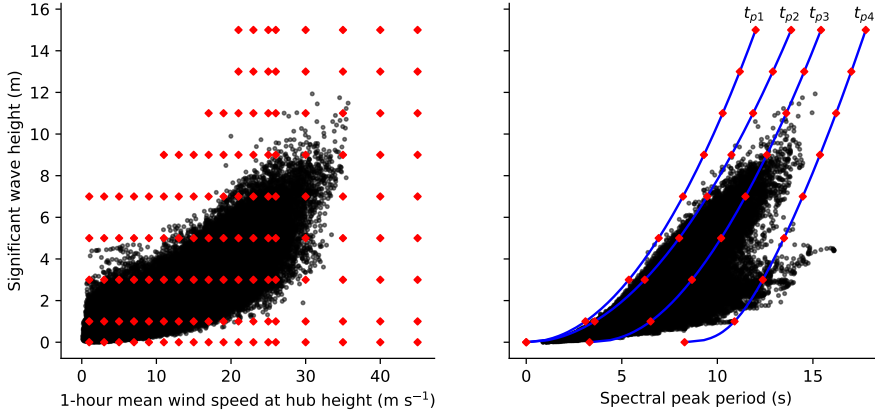


Figure 7.6: Environmental conditions at which multiphysics simulations were performed and which were used to build the statistical response emulator (red diamonds). A total of 516 different environmental conditions were evaluated (129 wind speed - wave height combinations and for each wind - wave combination four different spectral peak period values; $t_{p1}, t_{p2}, t_{p3}, t_{p4}$). Black dots show the environmental conditions within the first 50 years of the dataset for the FINO 1 site.

t_p . In principle, such a response emulator can be defined in various ways. Here, we chose to define the emulator as a parametric distribution of the short-term response maxima such that a random 1-hour maximum can be drawn by calling the distribution's inverse cumulative distribution function. Let $F_{1h}(r|v, h_s, t_p)$ denote the conditional distribution function of the 1-hour maximum mudline overturning moment. Thus the 1-hour maximum overturning moment is a random variable R and its realization is denoted r . Then the response emulator is the inverse distribution function:

$$F_{1h}^{-1}(p|v, h_s, t_p), \quad (7.2)$$

which can be called with a value for $p \in [0, 1]$ to evaluate a given quantile of interest. To draw a random 1-hour response realization, we simulated uniformly distributed random variables $p \in [0, 1]$ and then calculated $F_{1h}^{-1}(p|v, h_s, t_p)$.

The distribution of short-term response maxima can be estimated using various techniques, such as block-maxima, peaks-over-threshold, or up-crossing rate methods [187, 188, 207, 264]. Here, we used a block-maxima method, with F_{1h} modeled using the generalized extreme value (GEV) distribution. The location, scale, and shape parameters, (μ, σ, ξ) , were modeled as parametric functions of wind speed, wave height and wave period. The cumulative distribution function for the 1-hour maximum response is then given by

$$F_{1h}(r|v, h_s, t_p) = \begin{cases} \exp\left(-\exp\left(-\frac{r-\mu}{\sigma}\right)\right), & \xi = 0, \\ \exp\left(-\left(1 + \xi \frac{r-\mu}{\sigma}\right)_+^{-1/\xi}\right), & \xi \neq 0, \end{cases} \quad (7.3)$$

where $(\cdot)_+ = \max\{\cdot, 0\}$, and, for simplicity, the dependence of the parameters (μ, σ, ξ) on (v, h_s, t_p) has not been written explicitly. Various methods can be used to estimate the models for (μ, σ, ξ) as functions of (v, h_s, t_p) , such as radial basis function models or Gaussian process regression (Kriging). In this work we have opted to use simple parametric models. These models may not provide the optimal fit, but do allow the results of the study to easily be replicated. As described

further below, the response emulator was found to be sufficiently representative for the purpose of the study. The fitted functions for μ , σ and ξ are given in Section A.3 and contain a total of 33 parameters.

The process to establish the response emulator involved the following steps:

1. 1-hour simulations were conducted across the wind speed, wave height, peak period variable space.
2. Each 1-hour simulation was divided into 1-minute blocks (Figure 7.7).
3. GEV distributions were fitted to the block maxima in each simulation.
4. The continuous dependence functions $\mu(v, h_s, t_p)$, $\sigma(v, h_s, t_p)$ and $\xi(v, h_s)$ were fitted based on the various estimates of the parameters at discrete points of the variable space.
5. The 1-min maxima distribution was transformed into a 1-hour maxima distribution:

$$F_{1h}(r) = [F_{1min}(r)]^{60}.$$

Fogle et al. [67] found that the maxima of 40-60 s blocks can be considered independent in wind turbine load responses. While we did not test for independence here, in some time series the 1-minute maxima appears to be independent while other time series have some low-frequency modes that suggest that 1-minute maxima are not truly independent.

The parameter values of the GEV vary across the variable space, with discontinuities at the cut-out wind speed (figures are shown in Section A.3). While the estimates of the location and scale parameters vary relatively smoothly over the discrete simulation points, the shape parameter is more erratic, due to sampling variability.

The parametric response emulator captures important characteristics of the multiphysics simulations. This can be seen by comparing the GEV's parameter values over the variable space and by comparing realized 1-hour responses within the multiphysics simulations with random samples drawn from the emulator (Figures 7.8, 7.9, 7.10). At calm sea ($h_s = 0$ m), the multiphysics simulations describe a characteristic curve when the realized 1-hour maximum overturning moment is plotted over wind speed (Figure 7.8):

- The response increases roughly linearly until the rated wind speed of 11.4 m s^{-1} ;
- then it increases slower and with reduced short-term variability;
- at ca. 17 m s^{-1} the response starts to decrease with increasing wind speed, with high short-term variability; and
- finally, starting at 25 m s^{-1} , when the turbine switches into parked mode, the response drops and then increases quadratically with wind speed.

The response emulator reproduces these features of the response curve.

Overall, the response emulator for the overturning moment at 30 m water depth showed good agreement with the realizations of the multiphysics simulation. Differences were mostly below 20% (Figure 7.9) and scatter plots suggested that there was no systematic over- or under-estimation from the emulator (Figure 7.10).

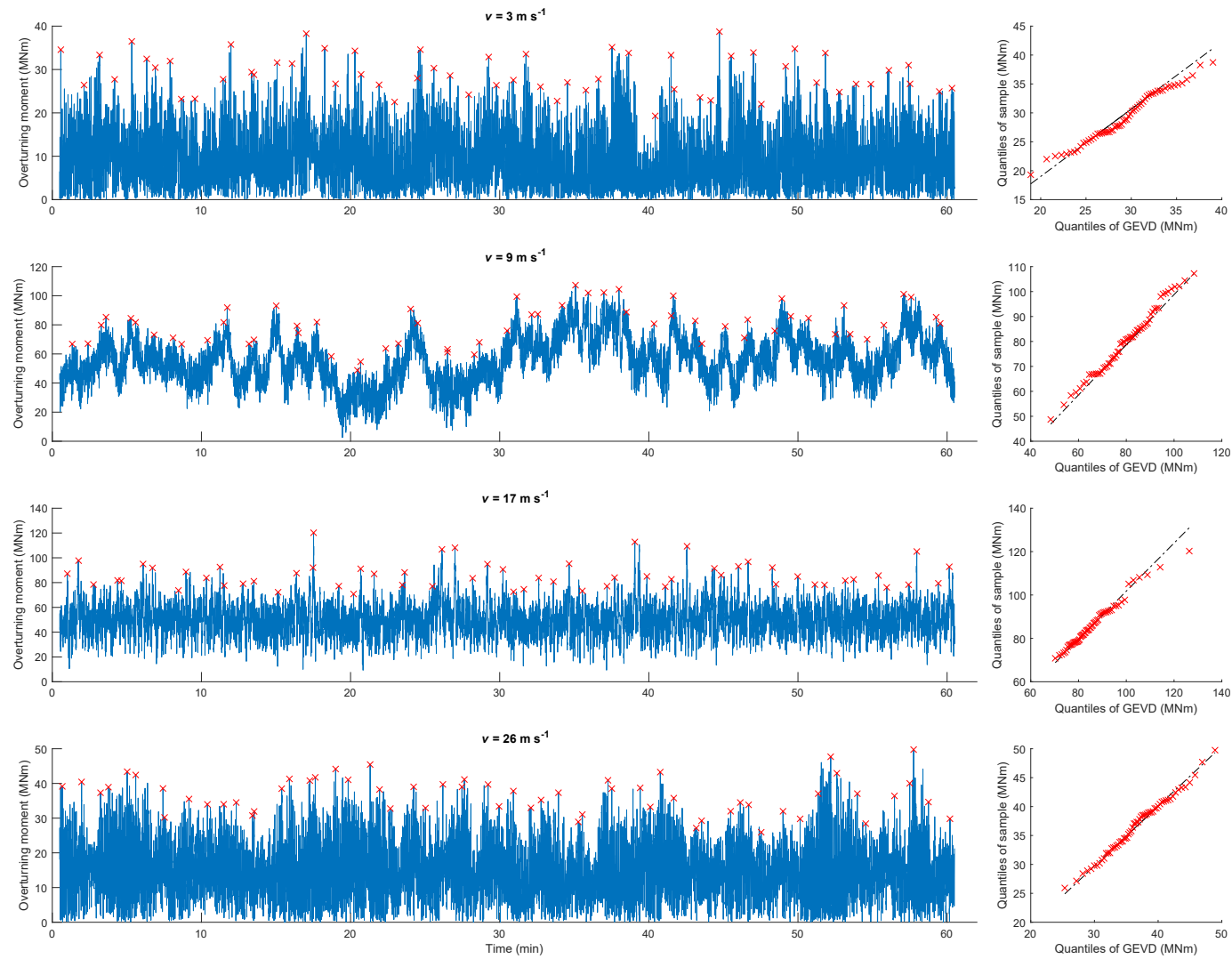


Figure 7.7: Time series of hourly simulations at wind speeds of $3, 9, 17$ and 26 m s^{-1} (from top to bottom) at a sea state of $h_s = 1 \text{ m}$ and $t_p = 6.51 \text{ s}$. Red crosses represent the maxima of 1-minute blocks. In the right panels quantile-quantile plots of the generalized extreme value distributions (GEVDs) that were fitted to the block maxima are shown.

In addition to the 30 m response emulator, we built an emulator for the bending moment at 10 m water depth. At 10 m water depth, the wind's relative contribution is higher and the wave's relative contribution lower than at 30 m water depth. Thus, annual maxima of the 10 m moment can occur at different environmental conditions than annual maxima of the 30 m moment. The response emulator for the 10 m moment was defined based upon the 30 m emulator, assuming that wind and wave can be approximated as point forces at known heights (further details are given in Section A.3). The median responses of both emulators are visualized in Figure 7.11.

7.3.3 ISOLATING THE EFFECT OF APPROXIMATIONS IN CONTOUR METHODS

To isolate the effects of each approximation introduced in the environmental contour method, four quantities were derived from the 1000-year time series, corresponding to the 50-year responses estimated under various assumptions. For each 1-hour time step of the 1000-year series, both a stochastic and deterministic response was generated. The deterministic responses were calculated by always using the median short-term response instead of a random quantile. The 50-year responses for the stochastic and deterministic time series were then calculated either from the annual maxima, or from all hourly values, under the assumption of independence. In both cases, the empirical distribution derived from either the annual maxima or hourly values is used to calculate return values. The various return value estimates are denoted:

- x_{s50} : calculated from annual maxima of the time series of stochastic responses
- x_{d50} : calculated from annual maxima of the time series of deterministic responses
- \tilde{x}_{s50} : calculated from all hourly-maximum stochastic responses, under the assumption of independence
- \tilde{x}_{d50} : calculated from all hourly values of deterministic responses, under the assumption of independence

Under the assumption that the artificial time series and the response emulator represent reality, the estimator x_{s50} will be unbiased. It will have some degree of sampling uncertainty though as both, blocks of the artificial time series and hourly maximum responses given an environmental condition are sampled from distributions. For simplicity, we call x_{s50} the “true response”.

By comparing x_{s50} and \tilde{x}_{s50} (or x_{d50} and \tilde{x}_{d50}), we can assess the impact of neglecting serial correlation in the metocean conditions. By comparing x_{s50} and x_{d50} (or \tilde{x}_{s50} and \tilde{x}_{d50}), we can assess the impact of assuming a deterministic response. The impact of assuming a linearized failure surface and reducing the design problem to a 2D contour is assessed by comparing various contour-based response estimators: Two based on 2D IFORM contours [263], two based on 2D highest density contours [100] and one based on a 3D highest density contour. We denote these estimators as x_{c50} . The 2D contours were calculated from wind speed - wave height joint distributions and a fixed relationship for the peak period (or, equivalently, wave steepness) given a wind speed and wave height is assumed. For the 2D contours, the peak period associated with each design condition was calculated based on the observations with the highest 1% of significant wave height values for a given wind speed interval (Figure 7.12). Two different methods were used to establish a relation between steepness and wind speed for large values of significant wave height. In one case, the median steepness for the high H_s records was calculated as a function of wind speed. The empirical median values, s_{median} , were then approximated using the function

$$s_{median} = 0.012 + \frac{0.0021}{1 + \exp[-0.3(v - 10)]}, \quad (7.4)$$

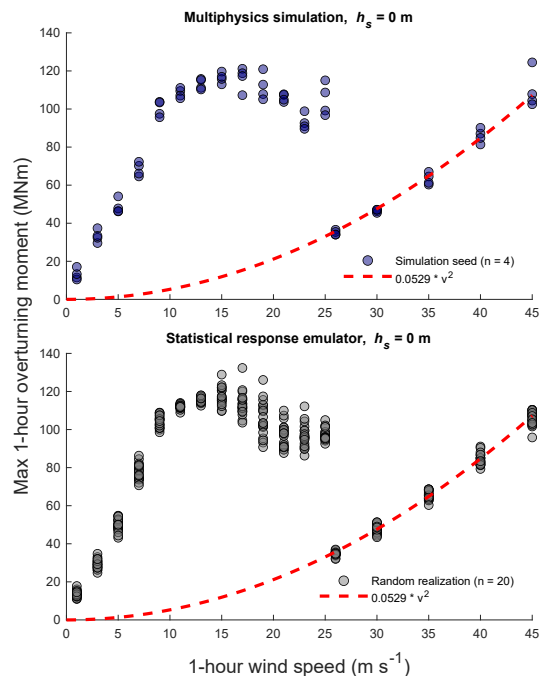


Figure 7.8: Responses at different wind speeds during calm sea ($h_s = 0 \text{ m}$). Maxima from multiphyics simulations (top) and the response emulator (bottom) showed good qualitative agreement. The mud-line overturning moment peaked during power production, but this peak would be exceeded at much higher wind speed during parked mode (ca. $45 - 50 \text{ m s}^{-1}$). In parked mode the wind turbine did not vary its pitch angle anymore such that the overturning moment increases – like the drag force – with the square of the wind speed.

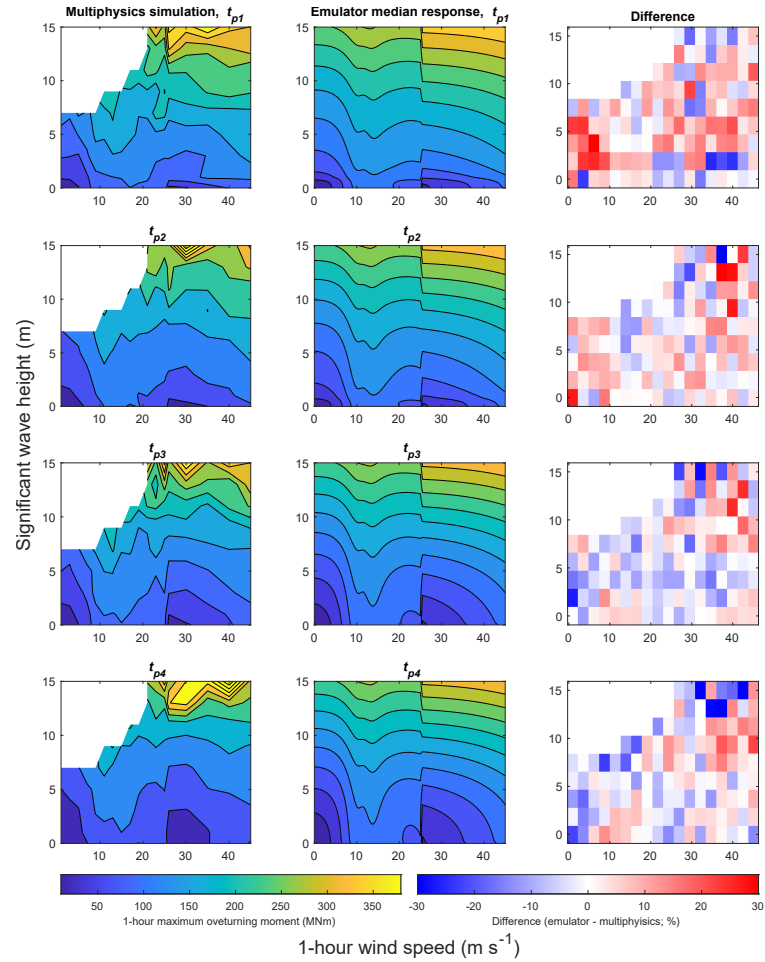


Figure 7.9: Response across the wind speed - wave height variable space. Difference between the response from the multiphysics simulation and the emulator's median response predictions were below 20% for most environmental conditions.

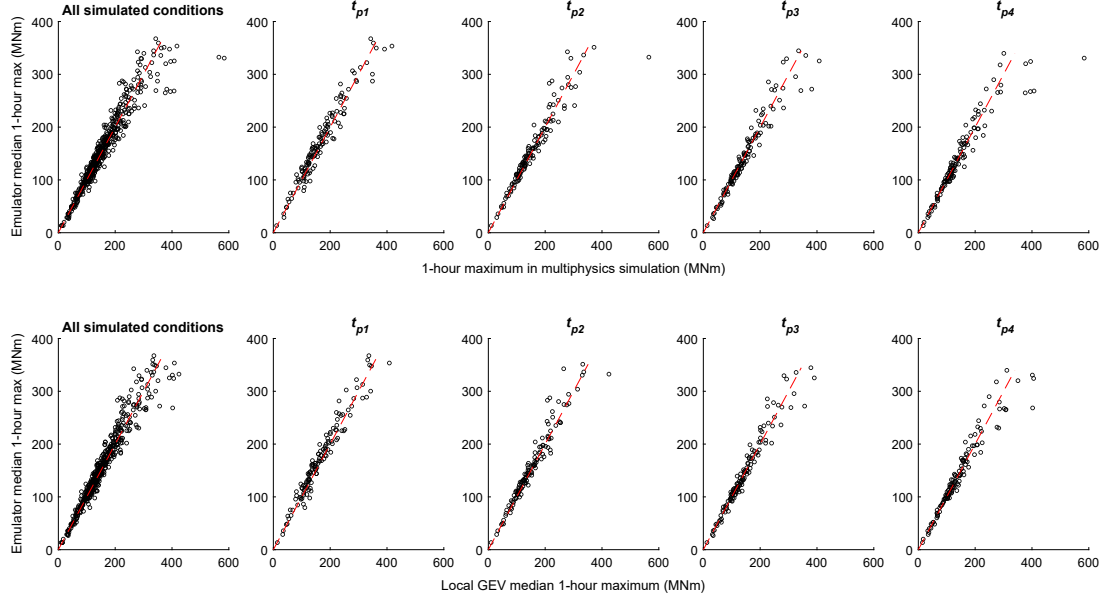


Figure 7.10: Comparison between multiphysics simulations and the response emulator. Top: Median 1-hour maximum from emulator versus realized maximum in the multiphysics simulation. Bottom: Median 1-hour maximum from emulator versus median 1-hour maximum from the locally fitted generalized extreme value (GEV) distribution. Dashed lines represent perfect agreement between emulator and simulation.

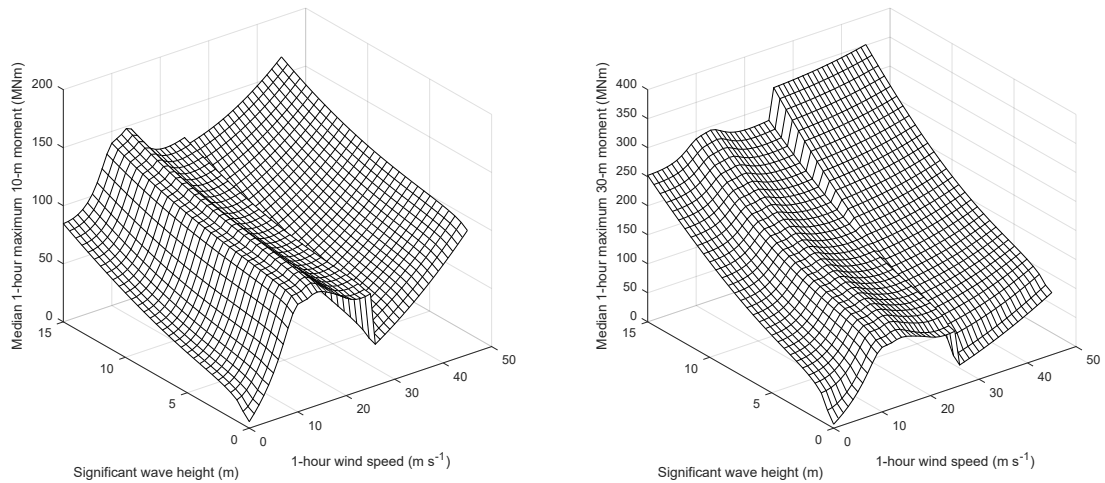


Figure 7.11: Median response of the two statistical response emulators at $t_p = t_{p2} = \sqrt{2\pi h_s/g \cdot 0.04}$ where $g = 9.81 \text{ m s}^{-2}$. At the cut-out wind speed of 25 m s^{-1} the responses have a discontinuity. There, the 10 m moment generally drops while the 30 m moment drops at low wave heights, but jumps at high wave heights.

where steepness is calculated based on peak spectral period, t_p , and v is in m s^{-1} . In the other case, based on a visual inspection of the data, the maximum steepness at a given wind speed and large H_s was approximated as

$$s_{max} = \begin{cases} 0.021 + 0.0017v & \text{if } v \leq 19 \text{ m s}^{-1} \\ 0.054, & \text{otherwise.} \end{cases} \quad (7.5)$$

Since the turbine's eigenperiod is around 3 s, for a given value of significant wave height and wind speed, sea states with higher steepness led to larger loads. The contour estimates using s_{max} , will therefore be more conservative than those using s_{median} . However, since the highest values of steepness at this location tend to occur for lower values of H_s at a given wind speed (see Figure 7.4), assuming that the highest loads occur along the environmental contour may not be conservative, since a lower value of H_s with a higher value of steepness may lead to larger loads in this case. This effect cannot be represented using the 2D contours, but can be accounted for using a 3D contour. For the 3D highest density contour, a deterministic relationship for $T_p|V, H_s$ is not required, as the relation between the three variables is already specified by the contour.

The underlying joint distribution to calculate the contours was the empirical distribution, derived from an artificial time series with a length of ca. 2.5 million years, generated using the same method used to generate the 1000-year times series. For all five contours, the estimate for the 50-year extreme moment was taken as the point along the contour that caused the highest response (using the response emulator).

7.4 RESULTS AND DISCUSSION

Figure 7.13 shows response time series for the 10 m and 30 m moment. In the top two panels the response is assumed to be deterministic (this is achieved by evaluating the response emulator at the 0.5 quantile at every time step) while in the bottom two panels the response is stochastic. In all cases the response time series has a roughly linear relationship with the wind speed time series if the wind speed is below ca. 15 m s^{-1} . As expected, the moment at 30 m water depth is higher than the moment at 10 m water depth.

While short periods of the four response time series showed similarities (Figure 7.13), the annual maxima of the complete 1000-year time series have different characteristics (Figure 7.14): Annual maxima of the 30 m moment are higher than annual maxima of the 10 m moment and have a greater variability. The 10 m moment annual maxima vary between ca. 110 and 130 MNm (deterministic) and ca. 130 and 180 MNm (stochastic), the 30 m moment annual maxima vary between 150 and 300 MNm (deterministic) and 180 and 420 MNm (stochastic). This difference can be explained by the type of wind speed - wave height environmental conditions that cause the annual maxima. Figure 7.15 shows the combinations of wind speed and significant wave height leading to the annual maximum bending moment at 10 m and 30 m, with the color denoting the corresponding size of the annual maximum value. The 10 m moment extremes are mostly caused by environmental conditions of medium wind speeds ($13 - 20 \text{ m s}^{-1}$) during power production, but the largest values of the annual maximum 30 m moment are mostly caused by high wind speed - high wave height events when the turbine is shut down. The 50-year responses for the four considered cases are listed in Table 7.4, as 114 MNm (10 m, deterministic), 252 MNm (30 m, deterministic), 158 MNm (10 m, stochastic) and 305 MNm (30 m, stochastic).

The different response characteristics also influence the accuracy of contour-based estimates. Lines of constant response of the 30 m moment show that there is only one region of high response

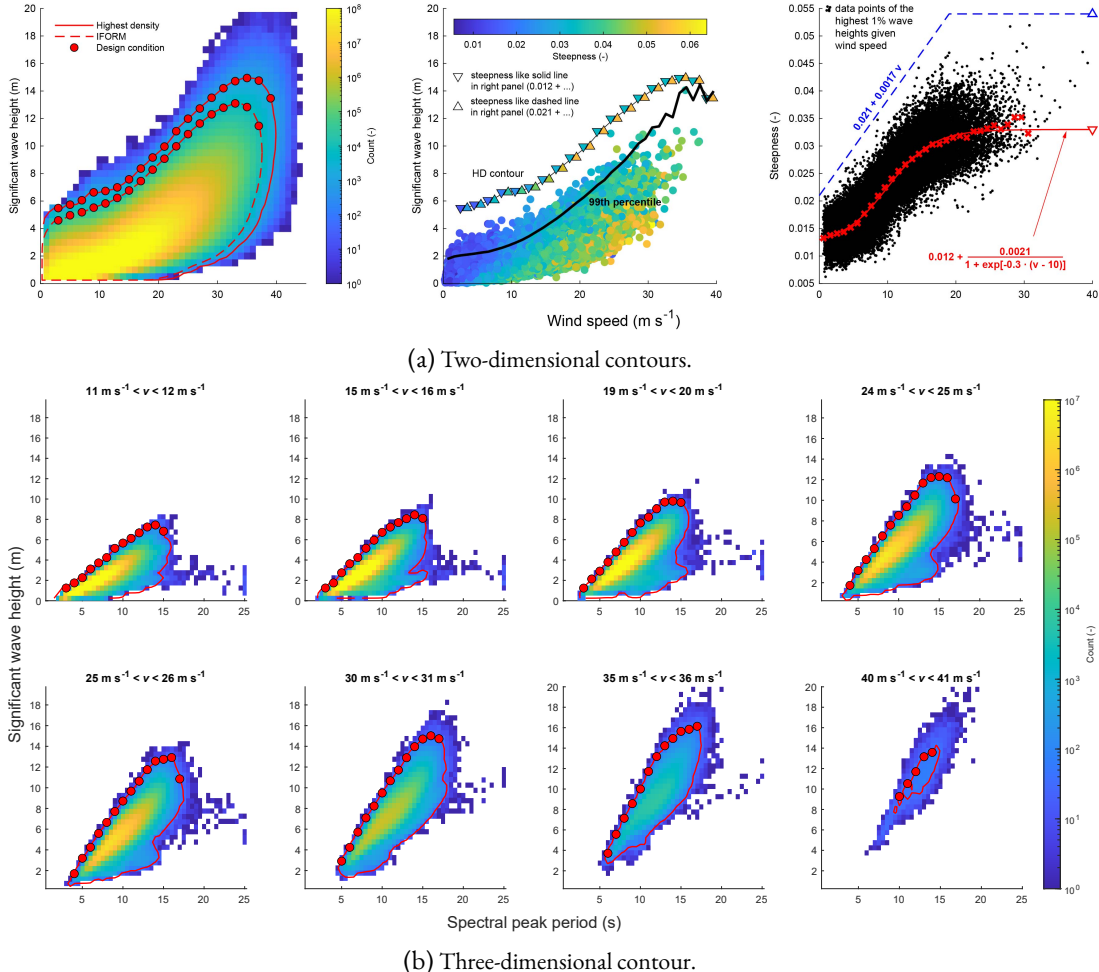


Figure 7.12: 50-year environmental contours. The contours are based on the empirical distribution of an artificial time series with a length of ca. 2.5 million years. Design conditions are plotted as circles. (a) Two-dimensional IFORM and highest density contours. Two types of deterministic relationships for steepness conditional on wind speed were considered such that four different 2D contours were constructed. In the first type steepness was modeled as the median steepness of the highest 1% wave heights and in the second type it was modeled as the maximum steepness of the highest 1% of wave heights (right panel). (b) Slices of the three-dimensional highest density contour. A threshold of 40 data points per cell defines the constant density contour.

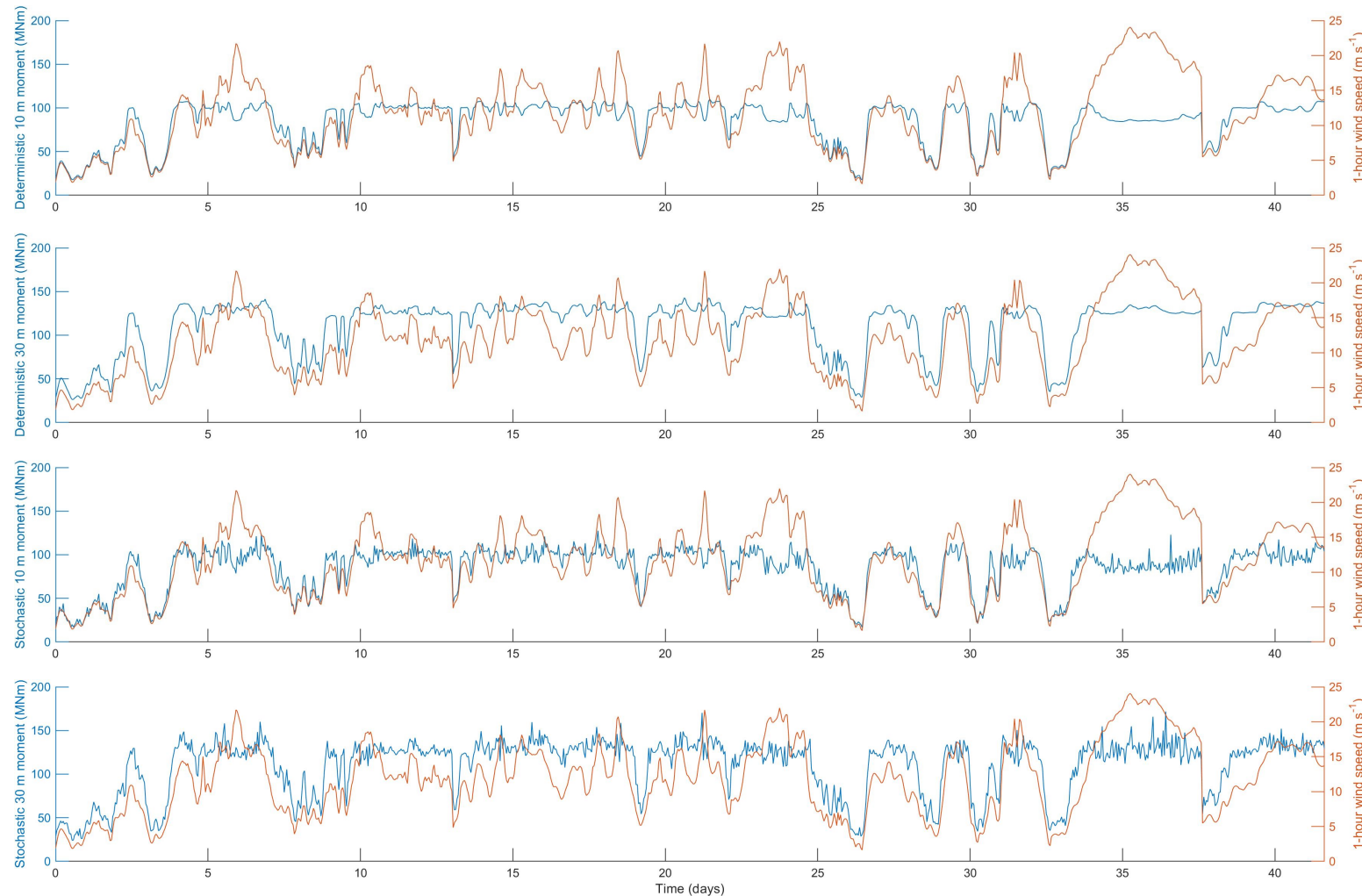


Figure 7.13: Snippets of the hourly response time series simulated with the statistical response emulator for the moment at 10 m water depth and at 30 m water depth. Top two panels: Deterministic response (the emulator was evaluated at the 0.5 quantile). Bottom two panels: Stochastic response (the emulator was evaluated at random quantiles).

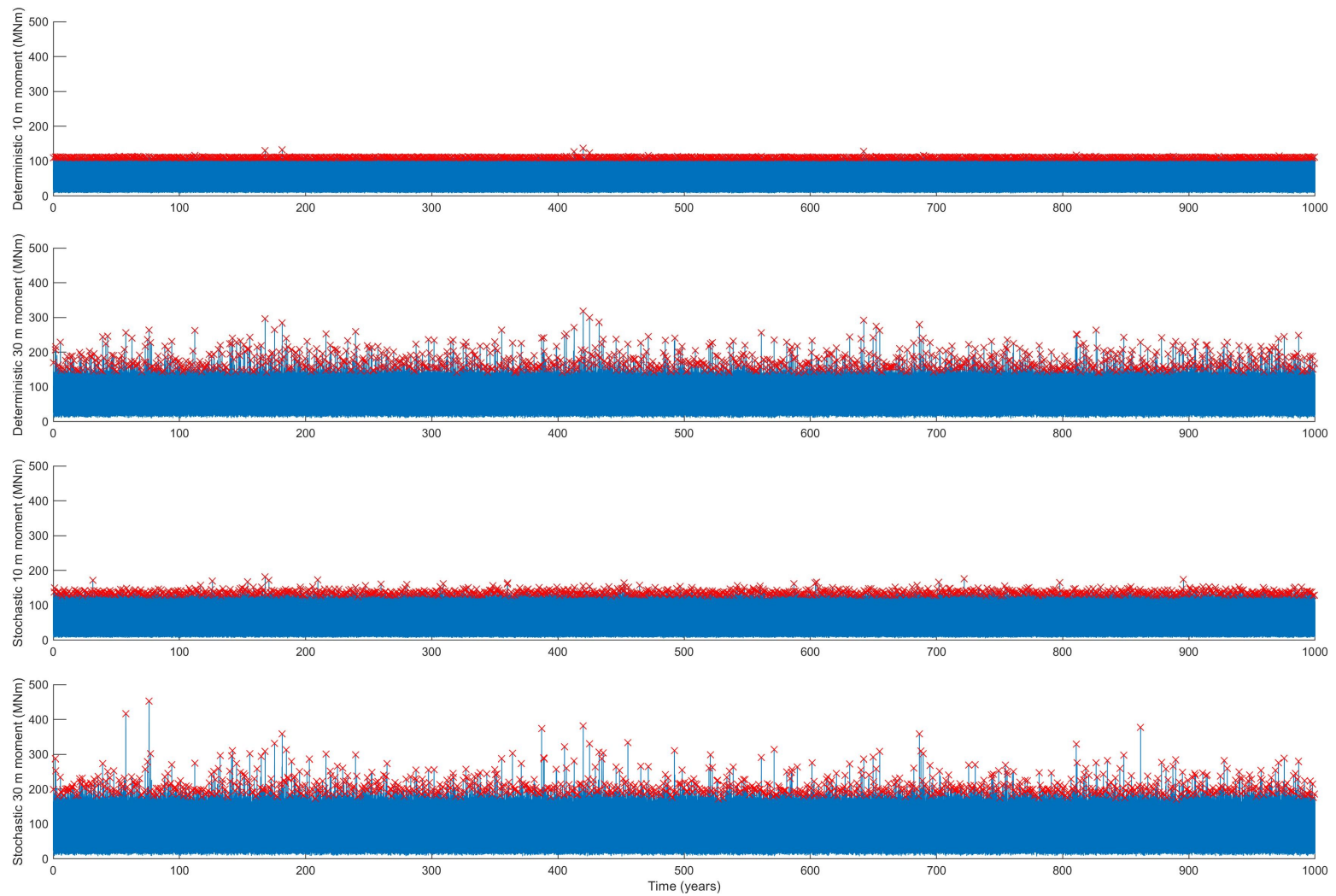


Figure 7.14: Full 1000-year response time series (moment at 10 m water depth and at 30 m water depth). Top two panels: Deterministic response (the emulator was evaluated at the 0.5 quantile). Bottom two panels: Stochastic response (the emulator was evaluated at random quantiles). Red crosses represent annual maxima.

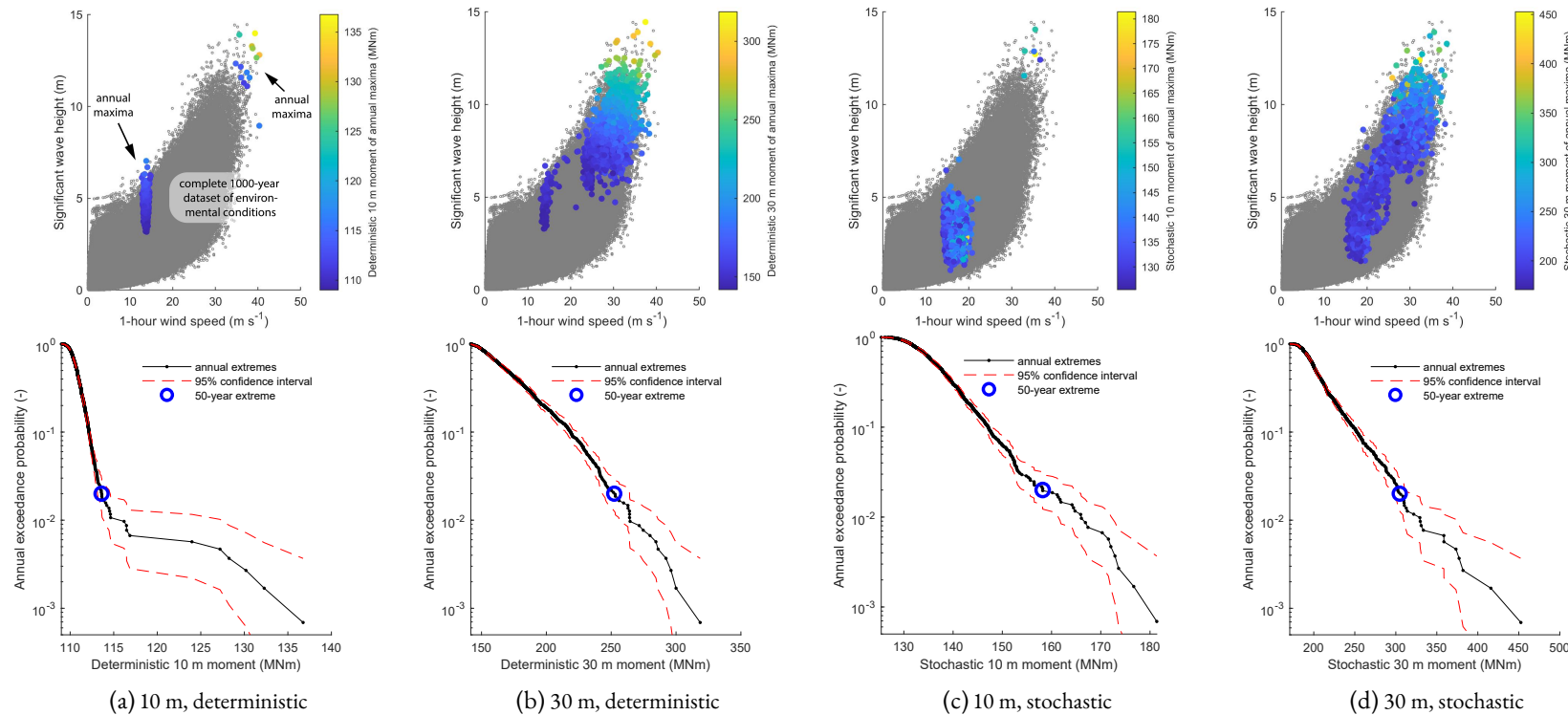


Figure 7.15: Top row: Combinations of wind speed and significant wave height where the annual maximum bending moments occurred in the 1000-year time series. Color of points indicates corresponding annual maximum load. Bottom row: Exceedance probability of annual maximum moment.

Method	b_{50} (MNm)	b_{50}^* (-)	r_{50} (MNm)	r_{50}^* (-)
Annual maxima of 1000-year time series with a stochastic short-term response (“true”), x_{s50}	158	1.000	305	1.000
Annual maxima of 1000-year time series with a deterministic short-term response, x_{d50}	114	0.721	252	0.827
Continuous 1000-year response time series with a stochastic short term response, \tilde{x}_{s50}	158	1.000	312	1.025
Continuous 1000-year response time series with a deterministic short-term response, \tilde{x}_{d50}	119	0.752	276	0.905
2D IFORM contour with median steepness	114	0.722	281	0.921
2D IFORM contour with high steepness	119	0.750	292	0.957
2D HD contour with median steepness	133	0.843	329	1.080
2D HD contour with high steepness	137	0.867	339	1.111
3D HD contour	141	0.889	358	1.174

Table 7.4: Comparison of estimates for the 50-year extreme moment at 10 and 30 m water depth (b_{50} and r_{50} , respectively). The contour-based estimates were calculated by evaluating the short-term response at the 0.5 quantile. b_{50}^* and r_{50}^* are the estimated 50-year moments normalized by the true 50-year moments at 10 and 30 m water depth, respectively.

along the IFORM contour (Figure 7.16). For the 10 m response, however, there are two regions of high response along the contour and response lines at the level of the contour-based estimate are strongly non-convex. This suggests that contour-based estimates will be less conservative for the 10 m moment than they are for the 30 m moment. In particular, for IFORM contours, the assumption of a linearized failure surface is justified for the 30 m moment but is violated for the 10 m moment.

Figure 7.17 shows the contours and the response values at their design conditions. When the short-term response was evaluated at the 0.5 quantile – as prescribed in the wind turbine design standard IEC 61400-3-1 [129] – all contour-based estimates of the 50-year 10 m moment, b_{50} , were lower than the true b_{50} value. For the 30 m moment, the two IFORM-based estimates were lower than the true r_{50} value while the highest density-based estimates were higher than the true value. While not prescribed in IEC’s standard [129], for other marine structures, it is common practice to account for the response’ short-term variability by evaluating the contour’s design at a response quantile higher than 0.5. Which quantile needs to be chosen to account for short-term variability depends upon response characteristics of the application of interest. For example, Baarholm et al. [8] found that for the natural gas platform “troll A” the required quantile varied for the considered response variables, but was about 0.8.

Here, we found that for the 50-year 10 m moment, b_{50} , IFORM contours needed to be evaluated at the 0.99 quantile, 2D highest density contours at the 0.9 quantile and 3D highest density contours at the 0.8 quantile (Figure 7.18). Note that this compensation did not only account for the effect of the response’s short-term variability, but also balanced the effects of serial correlation and of contour construction: Contours were derived from the joint distribution of all 1-hour environmental conditions. Some of the environmental conditions that occurred at the tails of the joint distribution, however, were serially correlated, causing the contour to artificially inflate. Derbanne and Hauteclercque [44] explain this effect and show de-clustering can be used to eliminate this effect. Contour construction is another source of bias: While IFORM contours use a non-conservative definition of exceedance for offshore wind turbines (due to the linearization of the failure surface), highest density contours use an overly conservative definition of exceedance (some of the data points that are

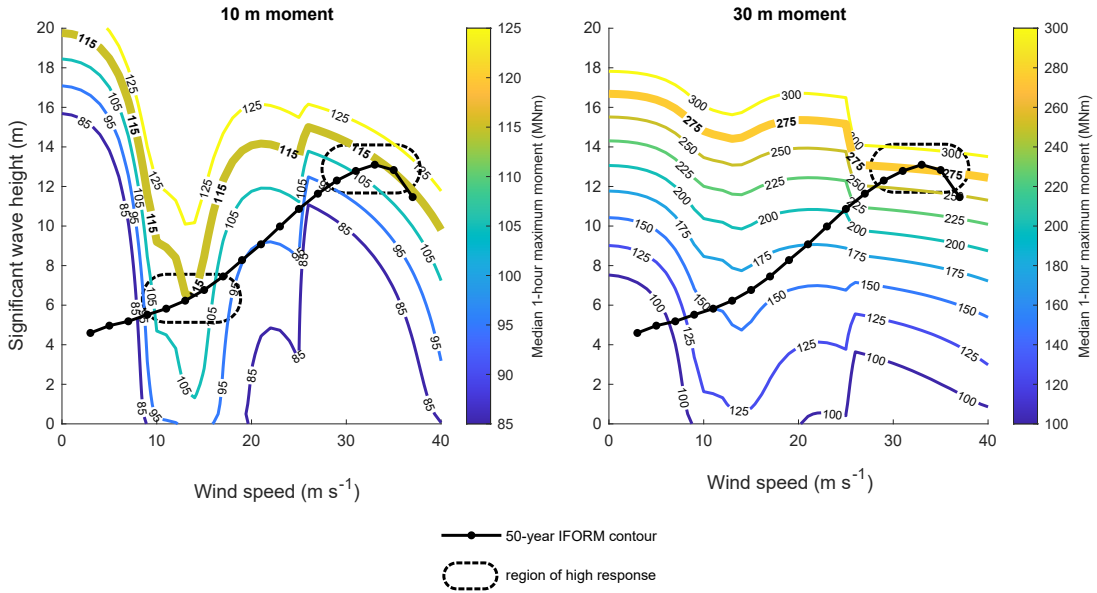


Figure 7.16: Lines of constant response and IFORM contour. The extreme response of the 30 m water depth moment is dominated by high wind speed - high wave height events while the extreme response of the 10 m water depth moment is influenced by both, mid wind speed and high wind speed events. The IFORM contour's assumption of a single linearized failure surface roughly holds at 30 m water depth, but is violated at 10 m water depth because the failure surface has two “regions of high response” along the environmental contour. Spectral peak period was calculated according to Expression 7.4.

counted as exceedance do not lead to failure-relevant loads). The effect of the type of contour on the conservatism is discussed in [96, 158].

The effect of the contour type (IFORM, highest density, steepness assumption) can be better analyzed if short-term variability is “turned off.” Thus, we can compare contour-based estimates with FLTA based estimates where the short-term response is deterministic. As contours are derived from the serially correlated hourly data, an appropriate comparison is the 50-year quantile from the continuous 1000-year deterministic response time series. This quantile is also affected by serial correlation, but not by the response’s short-term variability. For the 10 m moment, this estimate is 119 MNm. When the median steepness value is used, the IFORM-based estimate is 114 MNm and the HD-based estimate is 133 MNm (Table 7.4). Thus, as expected, IFORM’s definition of exceedance is non-conservative while HD’s definition of exceedance is overly conservative. This comparison also suggests that using the median steepness of the highest 1% of waves at a given wind speed is conservative enough because when the maximum steepness is used the IFORM-based estimate is 119 MNm, which is the same as the estimate from the 1000-year time series. We know, however, that by IFORM’s contour construction definition, we should get a response less than 119 MNm. Thus, in the maximum steepness case IFORM’s non-conservative exceedance definition is balanced by the overly conservative assumption of a too high steepness value and consequently a too low spectral peak period value.

The different types of biases are visualized in Figure 7.19. They comprise bias due to contour construction, due to serial correlation and due to short-term variability. The analysis shows that bias due to contour construction can lead to an under- or overestimation of the response. The bias

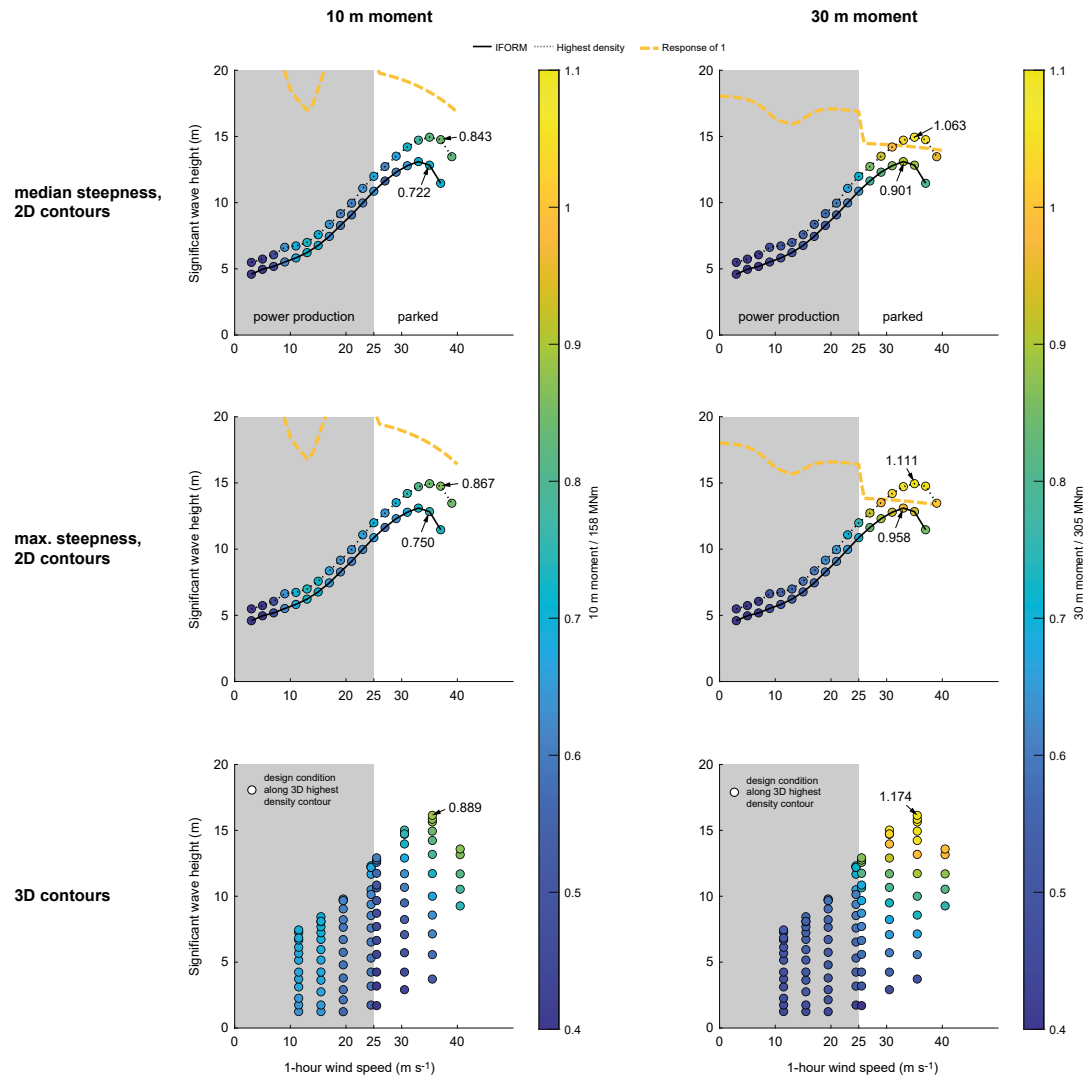


Figure 7.17: Response at the contours' design conditions normalized by the true 50-year response. Design conditions were evaluated at the 0.5 quantile.

due to serial correlation always leads to an overestimation and the bias due to neglecting short-term variability always leads to an underestimation. Consequently, overall bias can be positive or negative.

The biggest source of bias in the estimate of b_{50} is due to the response's short-term variability. Because contour design conditions are evaluated at a single short-term response quantile, they have a negative bias due to ignoring short-term variability. In principle, total bias – the sum of contour construction, serial correlation and short-term variability bias – can be compensated by evaluating the contour's design condition at a higher quantile of the short-term response. However, there is no theoretical support for compensating bias due to contour construction and due to serial correlation by evaluating the short-term response at a higher quantile. If the bias effect is taken into account, it would be more logical to compensate the biases of contour construction and serial correlation by inflating or deflating the contour. An IFORM contour is too small if the failure surface is non-convex (as is the case here) and a contour based on serially correlated environmental data is too large.

The results of this study are sensitive to the response and to the environment. While we aimed to build a high-quality response emulator and a high-quality statistical model to produce artificial time series, two aspects might deviate from reality: The response emulator's GEV distribution's shape parameter is positive at medium wind speeds of about 18 m s^{-1} , which means that the distribution does not have an upper bound. In reality, there is an upper bound. Thus, the estimated distribution has some bias in the tail. By performing multiphysics simulations longer than 1 hour and possibly using the maxima from blocks longer than 1 minute one could estimate the tail better. Another possible bias is our model for the distribution of significant wave height. Given that the considered site has a water depth of 30 m, the model might overestimate the occurrence of very high wave heights. Both aspects are important because for some response variables the extremes occur at the mid-wind speed region and for other variables they occur at the high wind speed - high wave height region. If the response at mid wind speeds is different or the environment at high wind speeds, the differences between the true 50-year response and the contour-based estimate could change.

Similarly, that means that the results are sensitive if a different response variable is analyzed that we did not consider here or if a different offshore site is analyzed. Some results however, likely hold for other response variables and other offshore sites:

1. Due to a wind turbine's controller there will always be response variables where the contour has two regions of high response in the wind speed - significant wave height variable space, which implies a non-convex failure surface. Therefore, an IFORM contour is a non-conservative way to construct a contour. To avoid this source of non-conservatism, an ISORM or highest density contour can be constructed instead. However, if spectral peak period is varied deterministically with H_s and V , this relationship can offset the non-conservatism of the IFORM contour.
2. Serial correlation leads to an overestimation of the contour-based estimate. In this study the effect was up to 8%.
3. The response short-term variability leads to an underestimation of the contour-based estimate. In this study the effect was between 17 an 28%.
4. If there is a clear understanding, which spectral peak periods cause an unfavorable response, a 2D wind speed - wave height contour can be used instead of a 3D contour, together with a typical unfavorable T_p value. Although such probabilistic-deterministic variable combinations are theoretically fuzzy, they greatly reduce the number of design conditions along the "contour" that need to be evaluated. If there is no clear understanding about which T_p values are unfavorable, a 3D "contour" should be constructed.

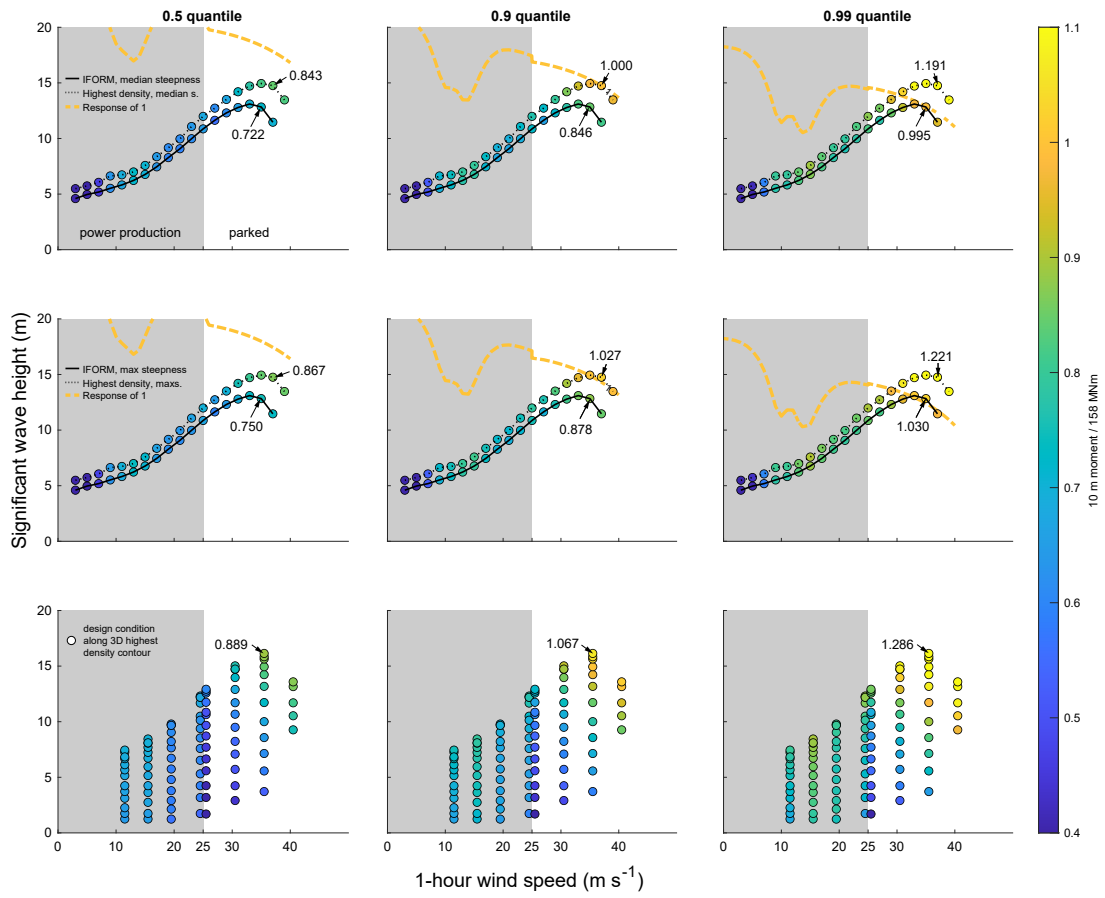


Figure 7.18: 10 m moment at the contours' design conditions normalized by the true 50-year response. The design conditions are evaluated at various quantiles of the short-term response. In the journal publication that this section is based on [94], panels of the 0.8 quantile are shown too.

Future research on the long-term response of offshore wind turbines could explore other response variables and other sites. It would be interesting to explore the upper bound of bias for contour-based estimates. Additionally, future research could explore how more environmental variables could be considered during the estimation of the long-term response. Implicitly, we assumed in this study that only wind speed, significant wave height, and spectral peak period change over time. This means that we assumed that wind and wave always come from the same direction and that sea level, current, turbulence structure, spectrum type and many other variables are constant. At the moment, it is unclear how big the influence of this assumption is. Other variables could be incorporated into either FLTA or contour-based estimates. However, estimating joint distributions and conducting enough response simulations, becomes problematic as the number of variables increases.

7.5 CONCLUSIONS

In this work, we analyzed how well the long-term extreme response of an offshore wind turbine can be estimated based on environmental contours. The question was motivated by the fact that authoritative design standards recommend the use of environmental contours for wind turbine design, however, it was unclear how these contour-based estimates compare to the true long-term response. Offshore wind turbine design is particularly concerned with the 50-year extreme response. As es-

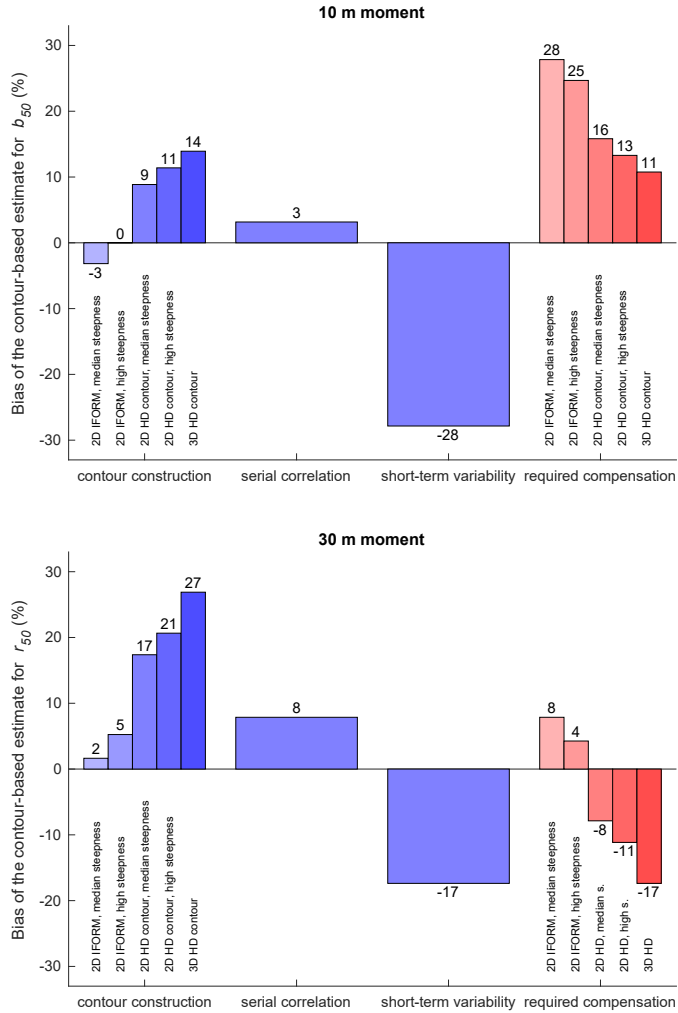


Figure 7.19: Sources of bias for the contour-based estimates. Contour construction bias can be negative or positive, however, serial correlation bias is always positive and short-term variability bias is always negative. The contour's design conditions were evaluated at the 0.5 quantile of the short-term response. Contour construction bias: $x_{c50} - \tilde{x}_{d50}$, serial correlation bias: $\tilde{x}_{d50} - x_{d50}$, short-term variability bias: $x_{d50} - x_{s50}$, overall required compensation: $x_{s50} - x_{c50}$. Definitions for these variables are given in Section 7.3.3.

7 Case study: Structural design of an offshore wind turbine

timating the true 50-year extreme response with high accuracy requires the characterization of the response over at least one order of magnitude longer time periods than the return period of interest, we used a statistical response emulator for the short-term response and a statistical model to generate environmental data of arbitrary lengths.

A high-accuracy estimate of the response was obtained by simulating the short-term response of continuous 1000-year artificial time series using a response emulator. The emulator was previously created based on multiphysics simulations that were performed across the complete wind-wave variable space. We considered five different environmental contours, including the approach that is currently recommended in the design standard IEC 61400-3-1 [129]. We found that – as already suggested by other authors – the recommended IFORM contour approach can underestimate the response to some degree because it assumes a convex failure surface. However, this effect was only apparent in some response variables such as the 10 m moment, but it did not play a role in others such as the 30 m moment. In addition, the effect was relatively small in the affected response variables. Other sources of bias of the contour-based estimates were serial correlation and short-term variability. For the 10 m moment short-term variability was by far the strongest source of bias. The broader literature on marine structures proposed to compensate for this effect by evaluating the contour's design condition at a higher quantile of the short-term response. Currently, this is not mentioned in the wind turbine design standard [129], which recommends using the average of the maxima of several stochastic realizations. For a symmetric distribution this is equivalent with evaluating the distribution of the maxima of the short-term response at the 0.5 quantile, in other words, taking the median maximum. Here, we found that this could dramatically underestimate the true 50-year response. For the 50-year extreme of the moment at 10 m water depth the design conditions needed to be evaluated at the 0.99 quantile to compensate the bias, otherwise the true response was underestimated by 25–28% (depending upon which relationship for $T_p|V, H_s$ was considered). Alternatively, if a highest density contour were used instead of an IFORM contour, its design conditions needed to be evaluated at the 0.9 quantile to compensate for the bias.

The differences between contour-based estimates and the true 50-year return values, however, were very sensitive to the type of response (moment at 30 m water depth or moment at 10 m water depth) and are likely also very sensitive to the offshore site: The turbine's controller succeeds in pitching the blades to reduce loads as wind speeds increase, however, as a side-effect long-term extremes might occur during power production or during parked condition – depending upon the response variable and the site's environmental conditions. This makes estimating the extreme response based on an environmental contour particularly challenging as the response's short-term variability at these two states can be very different. Thus, the bias in a contour-based estimate due to short-term variability can vary depending on the response variable and offshore site characteristics. The full long-term analysis used in this work can be used to calculate an unbiased estimator of the long-term extreme response and to identify the different sources of bias associated with a contour-based estimate.

DATA AVAILABILITY

The artificial time series and the results of the multiphysics simulation are available as a Zenodo repository at <https://doi.org/10.5281/zenodo.5013306>. The scripts used in the analysis of this study are available as a GitHub repository at <https://github.com/ahaselsteiner/2021-extreme-response>.

8 CONCLUSIONS AND OUTLOOK

8.1 MAIN FINDINGS

This thesis addressed the design process of offshore structures, with a focus on offshore wind turbines. Three problematic steps in the current design process were identified and new methods were proposed to address these problems. The three steps were:

- Modeling the long-term probability distribution of significant wave height F_{H_s} ;
- Modeling the wind and wave joint distribution F_{V,H_s,T_p} ; and
- Defining joint N -year environmental extremes that lead to an N -year structural response.

To address the first step, it was shown that the long-term distribution of significant wave height can be modeled with an exponentiated Weibull distribution and that it performs better than the state-of-the-art model, the translated Weibull distribution. The translated Weibull distribution lacks the ability to describe both, the body and the tail of the distribution accurately. When plotted on Weibull paper, empirical data describe a bending curve indicating that a 2-parameter Weibull distribution or a translated Weibull distribution, with their single shape parameter cannot describe the observations accurately. The exponentiated Weibull distribution has a second shape parameter that gives the model the required flexibility to describe the shape of the empirical distribution. When plotted on Weibull paper, the second shape parameter controls the curvature of the line.

Based on six datasets, it was shown that the exponentiated Weibull distribution can describe empirical wave height data better than the translated Weibull distribution when the same parameter estimation technique is used. When one is interested in very high quantiles of significant wave height as in this work, one can use weights in the parameter estimation procedure. A weighted least squares fitting method that prioritizes observations of high wave height was proposed. This method allowed predicting the height of the highest 0.1% wave height values with a mean absolute error of less than 0.5 m (0.37 ± 0.08 m; mean and standard deviation over six datasets).

For the second step, new models for the wind and wave joint distribution were proposed and assessed. As the exponentiated Weibull distribution was found to be advantageous to model the marginal distribution of significant wave height, it was also used in a two-dimensional joint model of wind speed and significant wave height and in a two-dimensional joint model of significant wave height and zero-up-crossing period. Further, a novel idea to model the dependence structure of these environmental variables was explored: Instead of considering only dependence functions based on goodness-of-fit, dependence functions that can be interpreted physically were proposed. The dependence structure of wind speed and significant wave height was modeled such that the median significant wave height conditional on wind speed increases with $\tilde{h}_s = c_6 + c_7 v^{c_8}$ where c_6 , c_7 , and c_8 are parameters that are estimated based on empirical data. The advantage of this model structure is that one can interpret c_6 as the part of significant wave height that is not generated by wind at the same place and the same time and the second term that contains c_7 and c_8 as the part that is generated by local winds. Then, the parameter c_8 describes the type of wind sea. Oceanographers have developed various theories for wind seas that imply different values of c_8 . Thus, the model's estimated

8 Conclusions and outlook

parameter values can be compared with expectations based on oceanographic reasoning. If the parameter values pass such a validity check, trust might be higher if they are used for extrapolation. Compared to the wind speed - significant wave height joint model that is currently recommended in engineering guidelines, this novel model seemed to describe the dependence structure better.

The third issue that was addressed in this thesis was how N -year environmental extremes could be defined that should lead to an N -year structural response. It was shown that the method that is currently mostly used to define such joint extremes, the inverse first-order reliability method (IFORM), is non-conservative if the structural response has certain characteristics: If the structural response function is non-monotonic and the contour that describes joint extremes has multiple regions of high response, N -year environmental extremes lead to an extreme response with a return period of less than N years. It was proposed that, alternatively, N -year environmental extremes can be defined as the boundary of a highest density region that is exceeded on average once every N years anywhere. When the response of an offshore structure is evaluated at the environmental conditions along such an N -year highest density contour the highest structural response will always have a return period of at least N years (for a deterministic response function). Thus, this definition for joint environmental extremes will lead to conservative design loads, irrespective of the topological characteristics of the response function.

Finally, a case study on the extreme response of an offshore wind turbine was conducted. This case study served to test the appropriateness of the overall design methodology for offshore structures that was described in this thesis. Furthermore, it explored the sources of bias in various environmental contour methods. Based on 516 hourly multiphysics simulations, a statistical response emulator was developed that described how the offshore wind turbine behaved at any given wind speed, significant wave height, spectral peak period variable value. It was found that – as expected – the state-of-the-art IFORM environmental contour method led to non-conservative results. However, most of the underestimation was due to the response' short-term variability. The bias due to the way the joint environmental extremes were defined had a much smaller influence. The results suggest that the design practice described in IEC's current offshore wind standard [129] should be adapted: A higher quantile than the median of the short-term response should be used as the design value.

To support researchers and practitioners who design or analyze offshore structures, the methods and models that were developed in this thesis were integrated into a methodology for the design process of offshore structures. Furthermore, they were implemented in an open-source software package. This software was written in Python and can be used as an importable package. As of autumn 2021 seventeen external persons openly interacted with the software package (they asked questions via emails, via the GitHub repository or “starred” the repository, which is a way to recommend the software). These persons included persons working at universities, shipbuilding companies and wind turbine manufacturing companies. The software package is written in such a way that it can be easily extended with other models to describe offshore environmental conditions and other methods to construct environmental contours. The author of this thesis intends to keep maintaining the software.

8.2 OPEN QUESTIONS AND FUTURE RESEARCH

The new insights presented in this thesis on modeling the offshore environment and on estimating a structure's extreme response also shed light on important research questions that are still open.

8.2.1 MODELING THE ENVIRONMENT

It was found that the exponentiated Weibull distribution can describe the empirical distribution of significant wave height well. This study was statistically descriptive but did not aim to understand the physical mechanisms why significant wave height data roughly follows an exponentiated Weibull distribution. Aiming to bring together physical models of ocean waves and the statistical description of significant wave height's long-term distribution would be an interesting topic for future research. The long-term distribution of wind speed is often described with a 2-parameter Weibull distribution, an exponentiated Weibull distribution with a shape parameter $\delta = 1$, such that similar theories might apply to wind speed and wave height.

New models for the joint description of wind speed, significant wave height, and wave period were proposed. One aspect not addressed in this thesis is the modeling of the region of very low spectral peak periods for a given significant wave height. Due to wave breaking, there is a limit on how low zero-up-crossing period or spectral peak period can become for a given H_s value. This wave breaking limit is not well captured in current joint distribution models. New joint models of significant wave height and wave period that better respect this wave breaking limit could be developed in future research.

In this thesis, both the marginal distribution of H_s and the joint distribution of wave height and wind speed were modeled as global models where hourly observations were assumed to be independent and identically distributed. Obviously, this is a strong simplification that causes some bias. If a distribution function based on serially correlated data is used to estimate a return value, it will overestimate the true return value [159]. This type of bias affects marginal return values such as the 50-year extreme significant wave height but also joint extremes such as the 50-year wind speed - wave height contour. Future research could further analyze this type of bias and explore how it could be compensated, for example, by making use of the sub-asymptotic extremal index or by estimating correction factors.

Formulating these open issues as research questions, we can ask:

- Which physics explains why the long-term distribution of significant wave height roughly follows an exponentiated Weibull distribution?
- How can joint models of significant wave height and wave period better respect the wave breaking limit?
- How large is the bias of assuming that hourly observations are independent and how could it be compensated?

8.2.2 ESTIMATING THE EXTREME RESPONSE

This thesis explored how the extreme response of a structure can be estimated with the environmental contour method. It showed under which conditions the traditional inverse first-order reliability method yields non-conservative results and proposed an alternative for these cases: the highest density contour method. It also showed that the construction of the contour is only one source of bias and that serial correlation between the environmental conditions and variability in the structure's short-term response are other important sources of bias. One type of assumption, however, was not explored. Here, joint models of only three environmental variables were considered: wind speed, significant wave height and wave period. The variation over time of these environmental variables were considered to affect the structural response the most. Of course, also changing values of wind and wave direction, turbulence intensity, ocean current, sea level, and other variables affect the response.

8 Conclusions and outlook

Future research could explore how strong each of these variables influence the structural response and how much bias one introduces if one assumes that these variables are constant.

Another topic for futures research is how to handle the effects of a changing climate on estimates of a structure's extreme response. Climate models can be used to predict how environmental conditions might change in the future. For the environmental contour method, however, it represents a challenge of how to integrate such projections into the method. Contours are constructed based on joint distribution models, which implicitly assume a stationary climate. Consequently, for contour methods, a joint distribution model that represents a type of average of future environmental conditions over the structure's expected lifetime would need to be used.

Formulated as research questions, we can ask:

- How much bias does assuming that various environmental variables are constant over time introduce in estimates of the extreme response of a structure?
- How can knowledge about a changing climate be incorporated into the environmental contour method?

Studying the current design process of offshore wind turbines also raised some questions that are not about improving methods, but related to the consequences when we design wind turbines following current guidelines and standards. Turbines are designed to withstand 50-year extreme events, but allow failure for rarer storm events. This design philosophy made the author question:

- What are the consequences if a 100-year storm event occurs?
- How many wind turbines will be destroyed and how severely will overall energy supply be affected if such a storm event occurs?

8.2.3 USING DESIGN CONTOURS IN OTHER FIELDS

The environmental contour method is a structural design method for dealing with multiple environmental conditions that change over time. It describes these changing environmental conditions as random variables. Then joint environmental extremes with a given return period can be found and a structure to withstand these environmental conditions can be designed. In frameworks of a general product development process such as Pahl and Beitz's methodology [203], these extreme environmental conditions represent design requirements. Obviously, in a design process, not only extreme environmental conditions, but various types of requirements must be fulfilled. Given that the environmental contour method is in principle mathematically abstract and not inherently connected to wave heights or wind speeds, it might be a useful method for other fields of design.

Ergonomics is a field that also deals with requirements that are derived from random variables. As an example, consider the design process of a car's seat. It is a typical requirement that the seat must be ergonomic for both extraordinarily short and extraordinarily tall persons. In ergonomics – similar to structural design – often the joint distribution of variables must be considered as the dependence structure between variables allows designers to differentiate whether some variable combinations are important or irrelevant. For example, the designer of a car seat might consider two variables, a person's total height and a person's hip height. The seat should then fit a person with a very high total height and hip height but also a person with a very low total height and hip height. However, it is questionable whether the seat should also be designed for someone with a very high total height and very low hip height, as the existence of such a person is extremely unlikely. Considering the joint distribution of these variables and deriving a contour can support designers of the car seat with

8.2 Open questions and future research

reasonable design requirements. Thus, the framework of the environmental contour method could be generalized to non-environmental variables. In a conference paper [101], we proposed such a generalization and showed how contours can be used to design a power tool such as a hand-held drill that can be held comfortably by at least 90% of the population.

Future work could explore this direction further and compare methods, which help designers deal with extreme requirements in various fields of design. Potentially, a framework that connects the field of general engineering design based on Pahl and Beitz's design methodology [203] and the field of statistics of extremes [39] could be developed – with the entity of a requirement serving as the connection point between the two fields.

A APPENDIX

A.1 DEFINITIONS FOR BIVARIATE EXCEEDANCE

This section provides mathematical definitions for the concepts described in the section on multivariate extremes (Section 2.2.2). Serinaldi [227] defined the probabilities p_{AND} and p_{OR} . In this thesis, we refer to these as “AND exceedance probability” and “OR exceedance probability” and see them as categories of more specific exceedance probabilities. In the following, 14 probabilities of exceedance that belong to four categories will be defined: “AND exceedance probability,” “OR exceedance probability,” “angular exceedance probability,” and “isodensity exceedance probability” (Figure A.1).

AND exceedance probabilities can be differentiated by the direction of exceedance. These probabilities are based on regions where both variables exceed a threshold:

$$p_{\text{AND} >>} := \Pr(X_1 > x_1 \cap X_2 > x_2), \quad (\text{A.1})$$

$$p_{\text{AND} ><} := \Pr(X_1 > x_1 \cap X_2 < x_2), \quad (\text{A.2})$$

$$p_{\text{AND} <>} := \Pr(X_1 < x_1 \cap X_2 > x_2), \quad (\text{A.3})$$

$$p_{\text{AND} <<} := \Pr(X_1 < x_1 \cap X_2 < x_2). \quad (\text{A.4})$$

All points within the variable space that have a particular AND exceedance probability define an AND exceedance boundary (Figure A.1).

A similar differentiation is possible for OR exceedance probabilities, which are based on regions where either X_1 or X_2 exceeds a threshold:

$$p_{\text{OR} >>} := \Pr(X_1 > x_1 \cup X_2 > x_2), \quad (\text{A.5})$$

$$p_{\text{OR} ><} := \Pr(X_1 > x_1 \cup X_2 < x_2), \quad (\text{A.6})$$

$$p_{\text{OR} <>} := \Pr(X_1 < x_1 \cup X_2 > x_2), \quad (\text{A.7})$$

$$p_{\text{OR} <<} := \Pr(X_1 < x_1 \cup X_2 < x_2). \quad (\text{A.8})$$

An OR exceedance boundary is the set of all points within the variable space that has a particular OR exceedance probability (Figure A.1).

“Angular exceedance probabilities” p_{ANG} are based on exceedance regions that use a straight line with angle θ to the abscissa as their boundary (Figure A.1). Marginal exceedance probabilities are special cases of these probabilities: at angles of 0, 90, 180, and 270 degrees the angular exceedance becomes pure marginal exceedance of X_1 or X_2 . If angular exceedance probability is defined in the original variable space it is expressed as

$$p_{\text{ANG},0} := \Pr[X_1 \cos(\theta) + X_2 \sin(\theta) > c_{\text{ANG}}], \quad (\text{A.9})$$

A Appendix

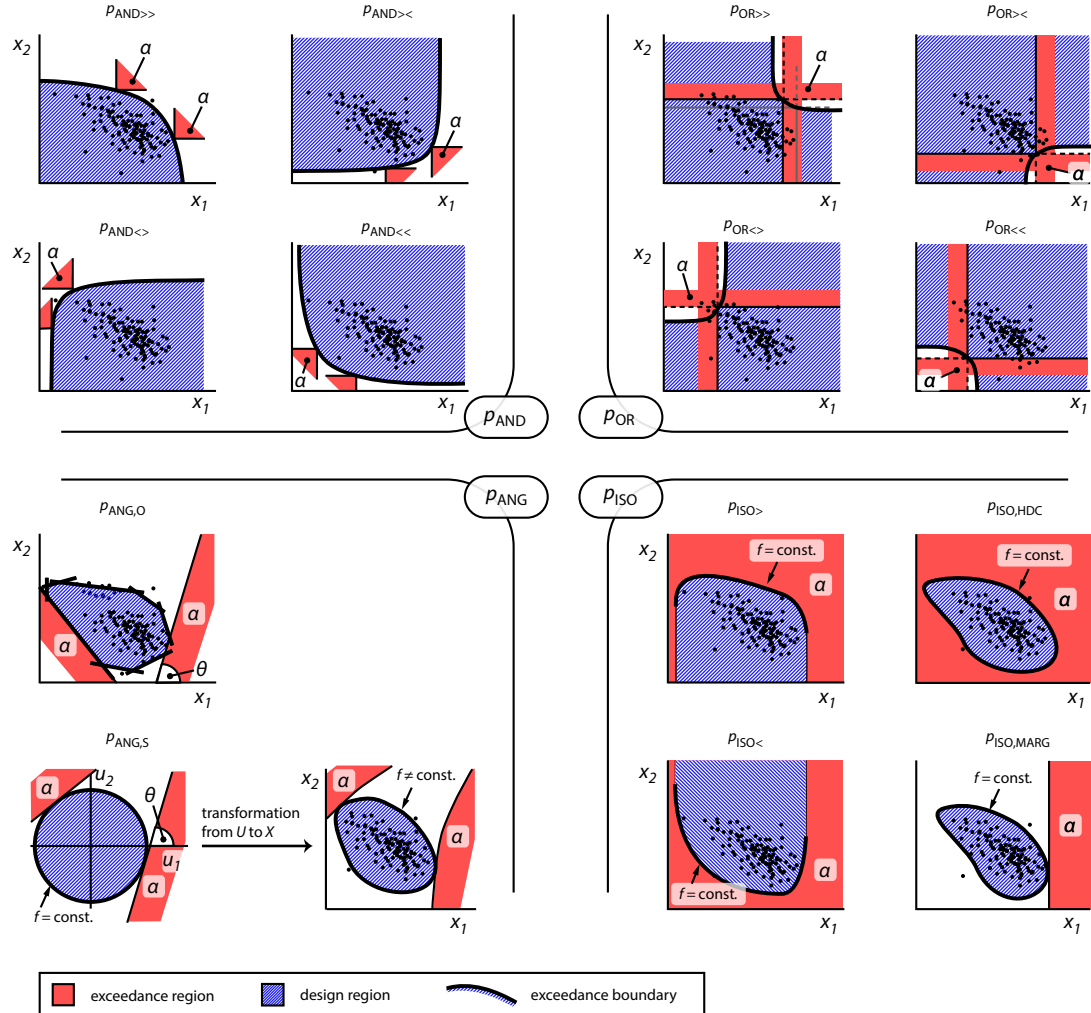


Figure A.1: Selection of possible definitions for bivariate exceedance that belong to the groups of “AND exceedance,” “OR exceedance,” “angular exceedance,” and “isodensity exceedance.” Each type of exceedance probability contains probability content $\alpha \in [0, 1]$, which in offshore structural design is usually determined based on a prescribed target reliability (see Section 2.3). Some types of exceedance have many exceedance regions (AND, OR, ANG; only some sample exceedance regions are plotted in these cases), while others have a single exceedance region (ISO). For simplicity, the outer regions that are far away from the exceedance boundaries of some exceedance regions are not shown here (for example, AND exceedance regions extend beyond the regions shown in red).

A.1 Definitions for bivariate exceedance

where $c_{\text{ANG}} \in \mathbb{R}$ is a constant that is determined when values for $p_{\text{ANG},0}$ and θ are given ($p_{\text{ANG},0} = \alpha$ with $\alpha \in [0, 1]$; $\theta \in [0, 360 \text{ deg}]$). Huseby et al. [124] used $p_{\text{ANG},0}$ in an environmental contour method.

Sometimes, however, it can be advantageous to define angular exceedance in the standard normal space (see, for example, [263]). Then, the definition of this exceedance region involves the transformation of the original random variables into random variables that are standard normal distributed:

$$p_{\text{ANG,S}} := \Pr(\Phi^{-1}[F_{X_1}(X_1)] \cos(\theta) + \Phi^{-1}[F_{X_2|X_1}(X_2)] \sin(\theta) > c_{\text{ANG}}), \quad (\text{A.10})$$

where Φ^{-1} denotes the inverse standard normal distribution function and F_{X_1} and $F_{X_2|X_1}$ denote the distribution functions of the original random variables X_1 and X_2 , respectively. Standard normal distributed variables are typically denoted as U [27, 215, 263] such that the equation can be written as

$$p_{\text{ANG,S}} = \Pr[U_1 \cos(\theta) + U_2 \sin(\theta) > c_{\text{ANG}}]. \quad (\text{A.11})$$

In standard normal space, c_{ANG} is constant over θ and often radius β , in structural design called “reliability index,” is used. The probability that the exceedance boundary is exceeded anywhere can therefore be expressed using the reliability index. This total exceedance probability is obviously greater than the probability that exceedance occurs at a single angle:

$$\Pr(\sqrt{U_1^2 + U_2^2} > \beta) > p_{\text{ANG,S}}. \quad (\text{A.12})$$

The last category is “isodensity exceedance” and comprises definitions that make use of a curve of constant probability density (Figure A.1). One definition for isodensity exceedance is defining the exceedance region by exceeding the boundary of a so-called highest density region [100, 126]. Then any point \mathbf{x} whose density value is less than a density threshold f_m contributes to the probability of exceedance $p_{\text{ISO,HDC}}$:

$$\begin{aligned} E &:= \{\mathbf{x} \in \mathbb{R}^2 : f(\mathbf{x}) < f_m\}, \\ p_{\text{ISO,HDC}} &:= \Pr(\mathbf{X} \in E). \end{aligned} \quad (\text{A.13})$$

This kind of isodensity exceedance is used in the highest density contour method presented in this thesis and in stand-alone publications [100, 101].

If isodensity is desired, but only high values of one variable are of interest, for example, high values of X_2 , a subset of all points that fulfill $f(\mathbf{x}) = f_m$ can be used as the exceedance boundary. Let $H_u(x_1)$ denote a function that, for a given x_1 value, returns the maximum x_2 value of all points that have probability density f_m and $-\infty$ if no x_2 value fulfills the condition:

$$H_u(x_1) = \begin{cases} \max\{x_2 \in \mathbb{R} : f(x_1, x_2) = f_m\}, & \text{if } \{x_2 \in \mathbb{R} : f(x_1, x_2) = f_m\} \neq \emptyset \\ -\infty, & \text{otherwise.} \end{cases} \quad (\text{A.14})$$

Based on H_u we can define the exceedance region $E_>$ and the probability of exceedance $p_{\text{ISO}>}$:

$$E_> := \{\mathbf{x} \in \mathbb{R}^2 : x_2 > H_u(x_1)\}, \quad (\text{A.15})$$

$$p_{\text{ISO}>} := \Pr(\mathbf{X} \in E_>). \quad (\text{A.16})$$

A Appendix

Exceedance probability	Design region's probability p_{DR}
$p_{AND^*} = \alpha$	$\Rightarrow p_{DR} < 1 - \alpha$
$p_{OR^*} = \alpha$	$\Rightarrow p_{DR} > 1 - \alpha$
$p_{ANG^\dagger} = \alpha$	$\Rightarrow p_{DR} < 1 - 2\alpha$
$p_{ISO>} = \alpha$	$\Rightarrow p_{DR} = 1 - \alpha$
$p_{ISO<} = \alpha$	$\Rightarrow p_{DR} = 1 - \alpha$
$p_{ISO,HDC} = \alpha$	$\Rightarrow p_{DR} = 1 - \alpha$
$p_{ISO,MARG} = \alpha$	$\Rightarrow p_{DR} < 1 - \alpha$

Table A.1: Relationship between the probability of exceedance and the design region's probability for alternative definitions of exceedance. * = True for any direction of exceedance (indices $>>$, $><$, $<>$ and $<<$).
 \dagger = True for $p_{ANG,O}$ and $p_{ANG,S}$.

Although not entirely the same, a similar exceedance probability was used by Haver [109, 110] in an environmental contour method.

Similarly, if low values are of interest, the exceedance probability $p_{ISO<}$ can be used. We define it based on the function $H_l(x_1)$ that returns the lowest x_2 value that fulfills $f(x_1, x_2) = f_m$ and ∞ if no x_2 value fulfills the condition:

$$H_l(x_1) = \begin{cases} \min\{x_2 \in \mathbb{R} : f(x_1, x_2) = f_m\}, & \text{if } \{x_2 \in \mathbb{R} : f(x_1, x_2) = f_m\} \neq \emptyset \\ \infty, & \text{otherwise.} \end{cases} \quad (\text{A.17})$$

Then

$$E_< := \{\mathbf{x} \in \mathbb{R}^2 : x_2 < H_l(x_1)\}, \quad (\text{A.18})$$

$$p_{ISO<} := \Pr(\mathbf{X} \in E_<). \quad (\text{A.19})$$

Yet another option for “isodensity exceedance” that has been proposed [197] is to use marginal exceedance of the first variable. Based on the N -year marginal return value $x_{1,[N]}$ (see Expression 2.11) the conditional mean value of X_2 given $x_{1,[N]}$ is chosen [197]. Then, all values within the variable space with the same probability density as $f[(x_{1,[N]}, \text{mean}(X_2|x_{1,[N]}))]$ are considered to have the exceedance probability that is associated to the marginal return value $x_{1,[N]}$:

$$p_{ISO,MARG} := \Pr(X_1 > x_{1,[N]}, X_2 > -\infty) = \Pr(X_1 > x_{1,[N]}) = 1 - F_{X_1}(x_{1,[N]}), \quad (\text{A.20})$$

where F_{X_1} is the marginal distribution function of random variable X_1 .

Given that, in principle, there are infinite possibilities how bivariate exceedance probability can be defined, these 14 definitions are only a subset of the possibilities. Other definitions that have been used can be found, for example, in references [27, 109, 110].

A.2 LONG-TERM DISTRIBUTION OF THE SIGNIFICANT WAVE HEIGHT

ESTIMATORS BASED ON WEIGHTED LEAST SQUARES

The estimation method of the three parameters of the exponentiated Weibull distribution, α , β and δ is based on the “Weibull paper linearization” that is commonly used for the 2-parameter Weibull distribution (see, for example, Scholz [224]). In the following, this method will be described in detail.

A.2 Long-term distribution of the significant wave height

The inverse cumulative distribution function of the exponentiated Weibull distribution reads

$$x = \alpha[-\log_e(1 - p^{1/\delta})]^{1/\beta}. \quad (\text{A.21})$$

Taking the logarithm with base 10 gives

$$\log_{10}(x) = \log_{10}(\alpha) + \frac{1}{\beta} \log_{10}[-\log_e(1 - p^{1/\delta})], \quad (\text{A.22})$$

which shows a linear relationship between $\log_{10}(x)$ and $\log_{10}[-\log_e(1 - p^{1/\delta})]$.

Thus, when writing $\log_{10}(x) = x^*$, $\log_{10}(\alpha) = a$, $\frac{1}{\beta} = b$ and $\log_{10}[-\log_e(1 - p^{1/\delta})] = p^*$ we get the simple expression

$$x^* = a + bp^*. \quad (\text{A.23})$$

This linear relationship allows the use of standard linear regression techniques to estimate the parameters a and b and, with these parameters, the distribution's parameters α and β .

Here, we have chosen to minimize the weighted squared deviations between the observed and the predicted values. Let the function Q express the sum of the weighted squared errors:

$$Q(a, b; \delta) = \sum_{i=1}^n w_i(x_i^* - \hat{x}_i^*)^2 = \sum_{i=1}^n w_i[(x_i^* - (a + bp_i^*))]^2, \quad (\text{A.24})$$

where p_i^* is the normalized p_i value,

$$p_i^* = \log_{10}[-\log_e(1 - p_i^{1/\delta})]. \quad (\text{A.25})$$

We can find the weighted least squares (WLS) estimators \hat{a} and \hat{b} by differentiating $Q(a, b)$ and finding its root:

$$\frac{\partial Q(a, b)}{\partial a} = -2 \sum_{i=1}^n w_i[x_i^* - (a + bp_i^*)] = 0, \quad (\text{A.26})$$

$$\frac{\partial Q(a, b)}{\partial b} = -2 \sum_{i=1}^n w_i p_i^*[x_i^* - (a + bp_i^*)] = 0. \quad (\text{A.27})$$

Solving for a in Equation A.26 leads to

$$\hat{a} = \bar{x}^* - \hat{b}\bar{p}^*, \quad (\text{A.28})$$

where $\bar{x}^* = \sum_{i=1}^n w_i x_i^*$ and $\bar{p}^* = \sum_{i=1}^n w_i p_i^*$. Similarly, by solving for b in Equation A.27 and by using Equation A.28, we can derive an expression for \hat{b} :

$$\hat{b} = \frac{\sum_{i=1}^n (w_i p_i^* x_i^*) - \bar{x}^* \bar{p}^*}{\sum_{i=1}^n (w_i p_i^{*2}) - \bar{p}^{*2}} \quad (\text{A.29})$$

With \hat{a} and \hat{b} we can calculate $\hat{\alpha}$ and $\hat{\beta}$:

$$\hat{\alpha} = 10^{\hat{a}}, \quad (\text{A.30})$$

$$\hat{\beta} = 1/\hat{b}. \quad (\text{A.31})$$

A Appendix

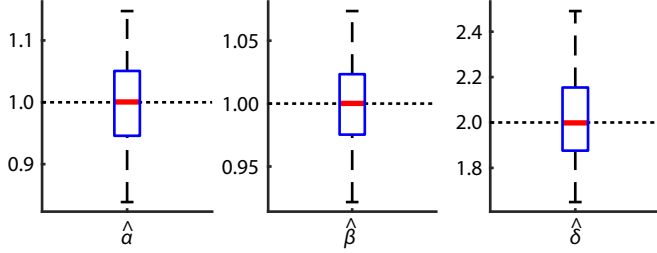


Figure A.2: Box plots of the estimated parameters of an exponentiated Weibull distribution. The true distribution has the parameters $\alpha = 1$, $\beta = 1$ and $\delta = 2$. The thick line represents the median and the box the 25th and 75th percentile. 100 samples, each with 100,000 data points were used for the estimation.

Thus, for any given δ value we can explicitly compute the WLS-estimators $\hat{\alpha}$ and $\hat{\beta}$.

We are, however, still missing an expression for the estimator $\hat{\delta}$. To derive this expression, let us define a function that returns the weighted squared error of an exponentiated Weibull distribution with a given parameter δ as

$$Q_\delta(\delta) = Q(\hat{\alpha}, \hat{\beta}; \delta). \quad (\text{A.32})$$

The WLS-estimator $\hat{\delta}$ is the δ value that minimizes this function:

$$\hat{\delta} = \underset{\delta}{\operatorname{argmin}}[Q_\delta(\delta)]. \quad (\text{A.33})$$

We did not try to find an analytical solution to Equation A.33. Instead, we used Matlab's function `fminsearch.m` to compute the minimum.

To evaluate whether the implemented weighted least squares estimation method works correctly, we estimated the parameters based on samples that were drawn from a known distribution. We drew 100 samples, each with 100,000 data points, from an exponentiated Weibull distribution with parameters $\alpha = 1$, $\beta = 1$ and $\delta = 2$. The estimated parameters were $\hat{\alpha} = 0.996 \pm 0.067$, $\hat{\beta} = 0.998 \pm 0.033$, and $\hat{\delta} = 2.023 \pm 0.183$ ($N = 100$; Figure A.2) where the values after the \pm -sign represent standard deviations.

COMPARISON WITH GAMMA AND BETA DISTRIBUTIONS

Two additional 3-parameter distributions were tested: The generalized gamma distribution that was proposed by Ochi [198],

$$f(x) = \frac{c}{\Gamma(m)} \lambda^{cm} x^{cm-1} \exp[-(\lambda x)^c], \quad (\text{A.34})$$

and a 3-parameter beta distribution of the second kind that was proposed by Ferreira and Guedes Soares [63],

$$f(x) = \frac{\alpha}{B(k, n - k + 1)} \frac{(\alpha x)^{n-k}}{(1 + \alpha x)^{n+1}}. \quad (\text{A.35})$$

These distributions were fitted to the six datasets using maximum likelihood estimation and overall mean absolute error was calculated. The errors were 0.0317 ± 0.0203 m and 0.0294 ± 0.0177 m ($N = 6$) for the gamma distribution and the beta distribution, respectively (Table A.2).

Distribution	Dataset						Mean \pm standard dev.
	A	B	C	D	E	F	
Translated Weibull	0.0941	0.0532	0.0492	0.0662	0.0604	0.0964	0.0699 \pm 0.0205
Exponentiated Weibull	0.0105	0.0219	0.0252	0.0241	0.0174	0.0561	0.0259\pm0.0158
Generalized gamma	0.0644	0.0339	0.0150	0.0205	0.0115	0.0447	0.0317 \pm 0.0203
3-parameter beta	0.0112	0.0256	0.0273	0.0308	0.0190	0.0626	0.0294 \pm 0.0177

Table A.2: Overall mean absolute error of the four tested 3-parameter distributions. All distributions were fitted using maximum likelihood estimation. Bold letters indicate the lowest error for the particular dataset.

A.3 CASE STUDY

The coordinates of the four 2D contours are listed in Table A.3.

Two response emulators were used in the study presented in Chapter 7. Both are conditional generalized extreme value (GEV) distributions. The location parameter μ , its scale parameter σ , and its shape parameter ξ were modeled as functions of wind speed, wave height and wave period.

The response emulator for the 1-min maxima of the overturning moment at 30 m water depth, R , reads:

$$F_{1min}(r|v, h_s, t_p) = F_{1min}[r; \mu(v, h_s, t_p), \sigma(v, h_s, t_p), \xi(v, h_s)], \quad (\text{A.36})$$

where

$$\begin{aligned} \mu(v, h_s, t_p) &= \sqrt{\mu_{wind}^2 + \mu_{wave}^2} \\ \mu_{wind} &= \begin{cases} a_1 v + a_2/[1 + a_3(v - a_4)^2] - a_2/[1 + a_3(0 - a_4)^2] & \text{if } v \leq 25 \text{ m s}^{-1} \\ a_5 v^2, & \text{otherwise} \end{cases} \\ \mu_{wave} &= \begin{cases} \mu_{wave,pp} & \text{if } v \leq 25 \text{ m s}^{-1} \\ a_6 \mu_{wave,pp}, & \text{otherwise} \end{cases} \\ \mu_{wave,pp} &= a_7 h_s \{1 + a_8 \exp[a_9 |t_p - a_{10}|]\} \end{aligned} \quad (\text{A.37})$$

with $a_1 = 3.26 \times 10^6$, $a_2 = 7.10 \times 10^7$, $a_3 = 0.0408$, $a_4 = 11.6$, $a_5 = 3.9 \times 10^4$, $a_6 = 1.3$, $a_7 = 7.41 \times 10^6$, $a_8 = 3.53$, $a_9 = -0.328$, $a_{10} = 3$,

$$\begin{aligned} \sigma(v, h_s, t_p) &= \sqrt{\sigma_{wave}^2 + \sigma_{wind}^2} \\ \sigma_{wind} &= \begin{cases} b_1 v + b_2/[1 + b_3(v - b_4)^2] + b_5/[1 + b_6(v - b_7)^2] & \text{if } v \leq 25 \text{ m s}^{-1} \\ b_8 v^2, & \text{otherwise} \end{cases} \\ \sigma_{wave} &= \begin{cases} \sigma_{wave,pp} & \text{if } v \leq 25 \text{ m s}^{-1} \\ b_9 \sigma_{wave,pp}, & \text{otherwise} \end{cases} \\ \sigma_{wave,pp} &= b_{10} h_s^{1.5} \{1 + b_{11} \exp[b_{12} |t_p - b_{13}|]\} \end{aligned} \quad (\text{A.38})$$

A Appendix

IFORM $V (\text{m s}^{-1})$	$H_s (\text{m})$	$T_p^{\text{median}} (\text{s})$	$T_p^{\text{min}} (\text{s})$	Highest density			
				$V (\text{m s}^{-1})$	$H_s (\text{m})$	$T_p^{\text{median}} (\text{s})$	$T_p^{\text{min}} (\text{s})$
3	4.60	14.35	10.60	3	5.49	15.68	11.58
5	4.96	14.17	10.35	5	5.74	15.23	11.13
7	5.18	13.56	10.01	7	6.06	14.65	10.82
9	5.52	12.99	9.82	9	6.63	14.24	10.77
11	5.82	12.45	9.64	11	6.73	13.38	10.37
13	6.23	12.17	9.57	13	6.99	12.9	10.14
15	6.77	12.19	9.60	15	7.58	12.9	10.16
17	7.45	12.47	9.72	17	8.36	13.21	10.3
19	8.28	12.94	9.91	19	9.16	13.61	10.43
21	9.08	13.43	10.38	21	9.96	14.06	10.87
23	9.98	14.01	10.88	23	11.08	14.76	11.46
25	10.86	14.57	11.35	25	11.99	15.31	11.92
27	11.64	15.06	11.75	27	12.73	15.75	12.29
29	12.30	15.47	12.08	29	13.51	16.21	12.66
31	12.79	15.76	12.31	31	14.20	16.61	12.98
33	13.10	15.95	12.47	33	14.72	16.91	13.21
35	12.83	15.78	12.34	35	14.94	17.03	13.31
37	11.46	14.92	11.66	37	14.75	16.92	13.23
				39	13.47	16.17	12.64

Table A.3: Design conditions derived from the four two-dimensional wind speed - wave height 50-year environmental contours. T_p^{median} represents the spectral peak period that was calculated based on the median steepness at the highest 1% of waves at a given wind speed bin and T_p^{min} represents the value based on the maximum steepness (and therefore minimum period).

with $b_1 = 1.16 \times 10^5$, $b_2 = 2.45 \times 10^7$, $b_3 = 0.064$, $b_4 = 11.6$, $b_5 = -1.79 \times 10^7$, $b_6 = 0.2$, $b_7 = 11.6$, $b_8 = 4700$, $b_9 = 1.3$, $b_{10} = 5.04 \times 10^5$, $b_{11} = 11.9$, $b_{12} = -0.613$, $b_{13} = 3$, and

$$\xi(v, h_s) = \xi_{wind} + h_s^{1/3} \frac{(c_1 - \xi_{wind})}{c_2}$$

$$\xi_{wind} = \begin{cases} c_3 + c_4/[1 + c_5(v - c_6)^2] + c_7/[1 + c_8(v - c_9)^2], & \text{if } v \leq 25 \text{ m s}^{-1} \\ c_{10}, & \text{otherwise} \end{cases} \quad (\text{A.39})$$

with $c_1 = -0.01$, $c_2 = 15^{1/3}$, $c_3 = -0.1$, $c_4 = -0.5$, $c_5 = 0.15$, $c_6 = 12.5$, $c_7 = 0.23$, $c_8 = 0.05$, $c_9 = 18.5$, $c_{10} = -0.2$.

Consequently, the model has 33 parameters ($a_1, \dots, a_{10}, b_1, \dots, b_{13}, c_1, \dots, c_{10}$). Figure A.3 shows how the GEV distribution's parameters change over wind speed at calm sea ($H_s = 0$ m). Figure A.4 visualizes the parameter values across the complete variable space of wind speed, wave height and wave period.

The response emulator for the bending moment at 10 m water depth was built based on the assumption that the wave and wind loads can be approximated as point forces acting on the mean water surface level and the hub height, respectively (Figure A.5). Then, a moment balance based on the turbine's geometry suggests that at 10 m water depth, the wave forces contribute with a lever of 10 m and wind forces with a lever of 100 m, while they contribute with levers of 30 m and 120 m for the mudline overturning moment. Thus, if the individual contributions from wave and wind on the mudline overturning moment are known, they can be converted to the respective contributions for the 10 m bending moment. Based on that idea we defined the 10 m response emulator as:

$$F_{1min}(b|v, h_s, t_p) = F_{1min}[b; \mu_b(v, h_s, t_p), \sigma_b(v, h_s, t_p), \xi(v, h_s)], \quad (\text{A.40})$$

where

$$\mu_b = \sqrt{5/6\mu_{wind}^2 + 1/3\mu_{wave}^2} \quad (\text{A.41})$$

and

$$\sigma_b = \sqrt{5/6\sigma_{wind}^2 + 1/3\sigma_{wave}^2}. \quad (\text{A.42})$$

The terms μ_{wind} , μ_{wave} , σ_{wind} , σ_{wave} , and ξ are the same as in the 30 m emulator.

The response emulators of the 1-hour maxima are calculated as

$$F_{1h}(r|v, h_s, t_p) = [F_{1min}(r|v, h_s, t_p)]^{60}, \quad (\text{A.43})$$

$$F_{1h}(b|v, h_s, t_p) = [F_{1min}(b|v, h_s, t_p)]^{60}. \quad (\text{A.44})$$

Implementations of these two response emulators in Matlab are publicly available:

- <https://github.com/ahaselsteiner/2021-extreme-response/blob/master/02-scripts/ResponseEmulator.m>
- <https://github.com/ahaselsteiner/2021-extreme-response/blob/master/02-scripts/ResponseEmulator10mWaterDepth.m>

A Appendix

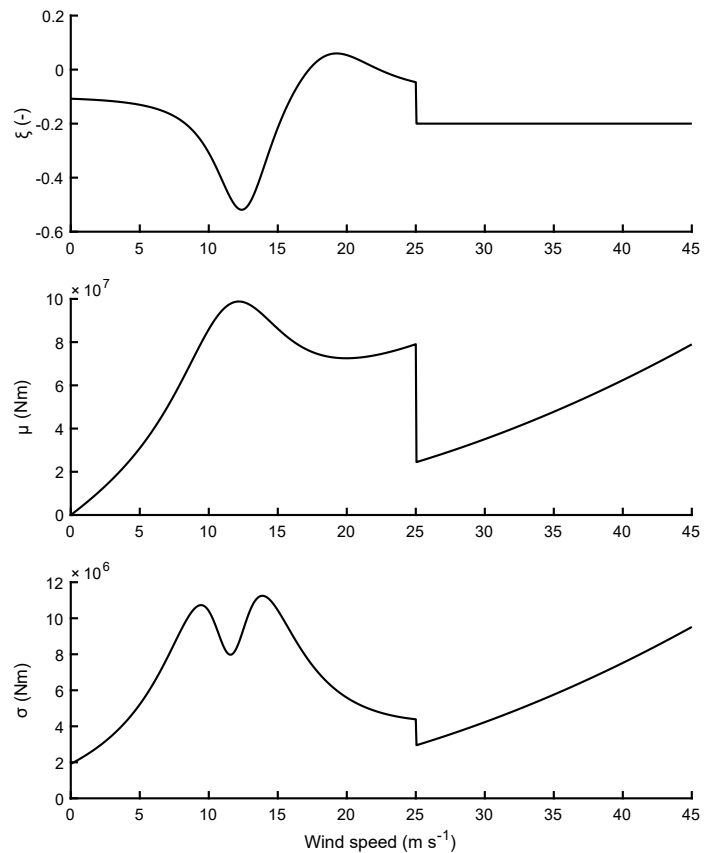


Figure A.3: Emulator's model for the generalized extreme value distribution's parameter values at calm sea (significant wave height of 0 m).

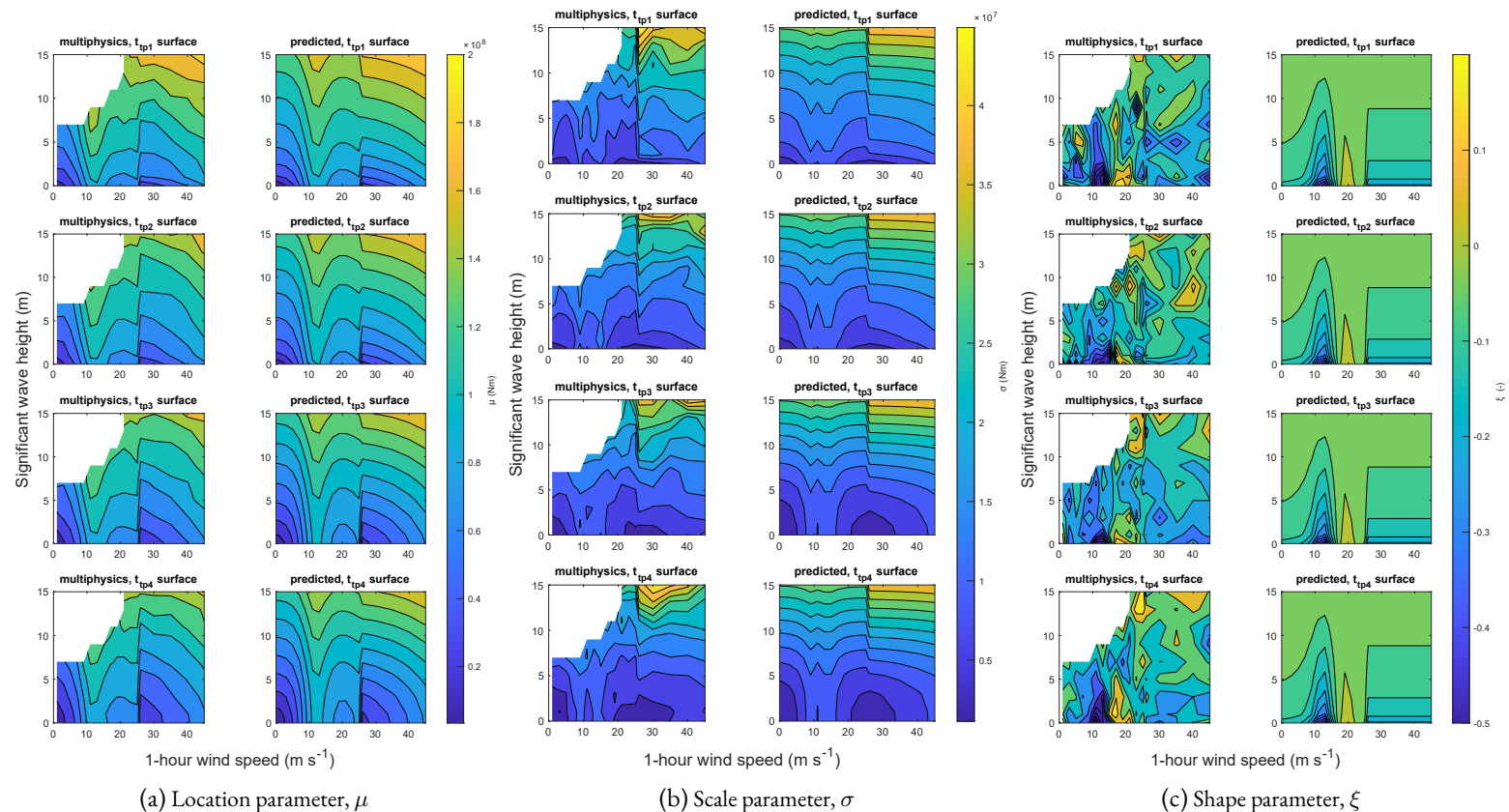


Figure A.4: Parameters of the generalized extreme value distribution across the considered variable space. In 516 1-hour simulations μ , σ , and ξ were estimated (“multiphysics” values). These 516 values were used to fit a model that predicts (μ, σ, ξ) over the complete variable space (“predicted” values).

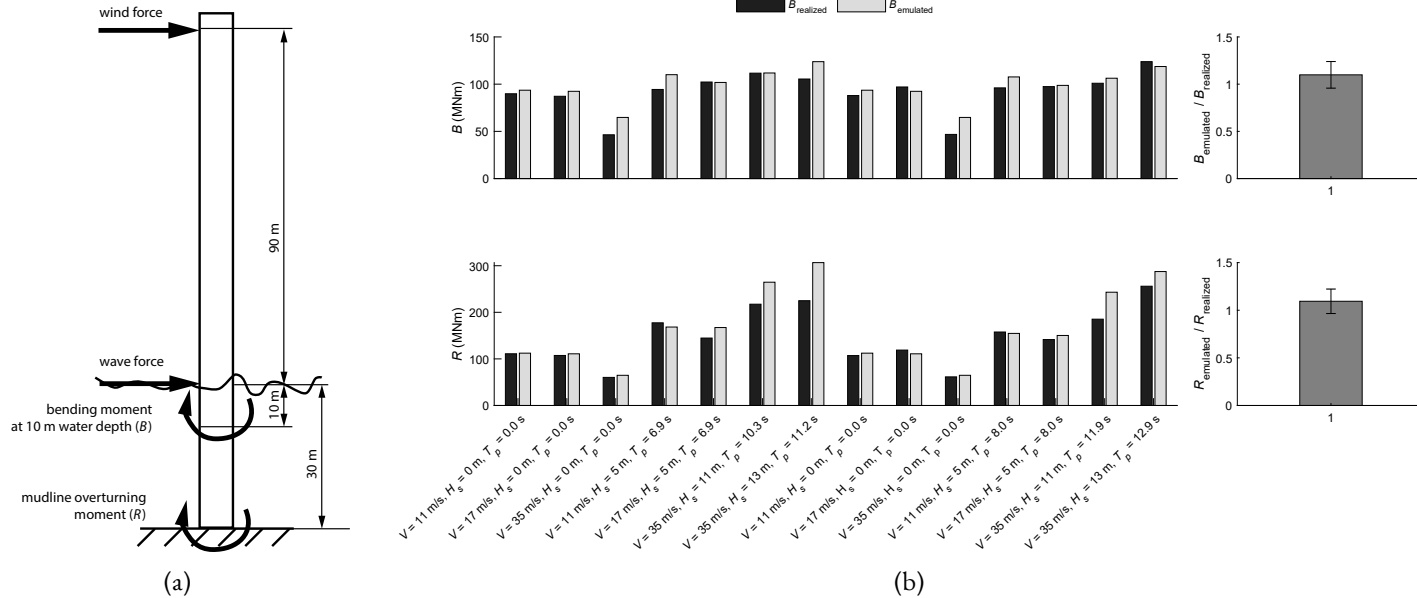


Figure A.5: (a) The response emulator for the 10 m moment is based on the emulator for the 30 m moment. By assuming that wind and wave forces can be approximated as a point forces the moment at 10 m can be calculated based on a moment balance. (b) The differences between the emulated 10 m moment and the 10 m moment in multiphysics simulations are similar to the differences between the emulated 30 m moment and the 30 m moment in multiphysics simulations.

BIBLIOGRAPHY

1. P. Agarwal and L. Manuel. "Simulation of offshore wind turbine response for long-term extreme load prediction". *Engineering Structures* 31:10, 2009, pp. 2236–2246. DOI: [10.1016/j.engstruct.2009.04.002](https://doi.org/10.1016/j.engstruct.2009.04.002).
2. A. Ahlström. "Aeroelastic simulation of wind turbine dynamics". Doctoral thesis. Royal Institute of Technology, 2005.
3. A Albers, N. Bursac, and E. Wintergerst. "Produktgenerationsentwicklung – Bedeutung und Herausforderungen aus einer entwicklungsmethodischen Perspektive". In: *Stuttgarter Symposium für Produktentwicklung 2015*. 2015.
4. A. Albers, M. Behrendt, S. Klingler, N. Reiß, and N. Bursac. "Agile product engineering through continuous validation in PGE-Product Generation Engineering". *Design Science* 3, 2017, pp. 1–19. DOI: [10.1017/dsj.2017.5](https://doi.org/10.1017/dsj.2017.5).
5. L. Almefelt, F. Berglund, P. Nilsson, and J. Malmqvist. "Requirements management in practice: Findings from an empirical study in the automotive industry". *Research in Engineering Design* 17, 2006, pp. 113–134. DOI: [10.1007/s00163-006-0023-5](https://doi.org/10.1007/s00163-006-0023-5).
6. C. Armstrong, C. Chin, I. Penesis, and Y. Drobyshevski. "Sensitivity of vessel responses to environmental contours of extreme sea states". In: *Proc. 34th International Conference on Ocean, Offshore and Arctic Engineering (OMAE 2015)*. American Society of Mechanical Engineers (ASME), 2015. DOI: [10.1115/OMAE2015-41680](https://doi.org/10.1115/OMAE2015-41680).
7. G. S. Baarholm, S. Haver, and C. M. Larsen. "Wave sector dependent contour lines". *Proc. 26th International Conference on Ocean, Offshore and Arctic Engineering (OMAE 2007)*, 2007, pp. 277–285. DOI: [10.1115/OMAE2007-29417](https://doi.org/10.1115/OMAE2007-29417).
8. G. S. Baarholm, S. Haver, and O. D. Økland. "Combining contours of significant wave height and peak period with platform response distributions for predicting design response". *Marine Structures* 23:2, 2010, pp. 147–163. DOI: [10.1016/j.marstruc.2010.03.001](https://doi.org/10.1016/j.marstruc.2010.03.001).
9. E. Bachynski, M. Thys, and V. Delhaye. "Dynamic response of a monopile wind turbine in waves: Experimental uncertainty analysis for validation of numerical tools". *Applied Ocean Research* 89, 2019, pp. 96–114. DOI: [10.1016/j.apor.2019.05.002](https://doi.org/10.1016/j.apor.2019.05.002).
10. E. E. Bachynski and M. Collu. "Offshore support structure design". In: *Renewable Energy from the Oceans: From wave, tidal and gradient systems to offshore wind and solar*. 2019, pp. 271–319. DOI: [10.1049/pbp0129e_ch7](https://doi.org/10.1049/pbp0129e_ch7).
11. Y. Bao, Z. Song, and F. Qiao. "FIO-ESM version 2.0: Model description and evaluation". *Journal of Geophysical Research: Oceans* 125:6, 2020, pp. 1–21. DOI: [10.1029/2019JC016036](https://doi.org/10.1029/2019JC016036).
12. R. E. Barlow and F. Proschan. *Statistical theory of reliability and life testing*. Holt, Rinehart and Winston, New York, NY, USA, 1975. ISBN: 0-03-085853-4.
13. J. A. Battjes. "Long-term wave height distributions at seven stations around the British Isles". *Deutsche Hydrographische Zeitschrift* 25:4, 1972, pp. 179–189. DOI: [10.1007/BF02312702](https://doi.org/10.1007/BF02312702).

Bibliography

14. J. Battjes. *Long-term wave height distribution at seven stations around the British islands*. Technical report. National Institute of Oceanography, 1970.
15. J. Beirlant, Y. Goegebeur, J. Segers, and J. Teugels. *Statistics of extremes: Theory and applications*. 2004. ISBN: 0471976474.
16. E. M. Bitner-Gregersen. “Comparison of wind and wave climate in open sea and coastal waters”. *Ocean Engineering* 170, 2018, pp. 199–208. DOI: [10.1016/j.oceaneng.2018.10.016](https://doi.org/10.1016/j.oceaneng.2018.10.016).
17. E. M. Bitner-Gregersen. “Joint met-ocean description for design and operations of marine structures”. *Applied Ocean Research* 51, 2015, pp. 279–292. DOI: [10.1016/j.apor.2015.01.007](https://doi.org/10.1016/j.apor.2015.01.007).
18. E. M. Bitner-Gregersen and S. Haver. “Joint environmental model for reliability calculations”. In: *Proc. 1st International Offshore and Polar Engineering Conference (ISOPE 1991)*. Edinburgh, United Kingdom, 1991, pp. 246–253.
19. L. T. M. Blessing and A. Chakrabarti. *DRM, a Design Research Methodology*. Springer, London, Great Britain, 2009. DOI: [10.1007/978-1-84882-587-1](https://doi.org/10.1007/978-1-84882-587-1).
20. L. van den Bos, W. Bierbooms, A. Alexandre, B. Sanderse, and G. van Bussel. “Fatigue design load calculations of the offshore NREL 5 MW benchmark turbine using quadrature rule techniques”. *Wind Energy* 23, 2020, pp. 1181–1195. DOI: [10.1002/we.2470](https://doi.org/10.1002/we.2470).
21. C. Bouth, S. Schafhirt, L. Ziegler, and M. Muskulus. “Lifetime extension for large offshore wind farms: Is it enough to reassess fatigue for selected design positions?” *Energy Procedia* 137, 2017, pp. 523–530. DOI: [10.1016/j.egypro.2017.10.381](https://doi.org/10.1016/j.egypro.2017.10.381).
22. J. Bowers, I. Morton, and G. Mould. “Extreme value analysis of the structural response of a single point moored vessel”. *Underwater Technology* 22:3, 1997, pp. 87–93. DOI: [10.3723/175605497783258986](https://doi.org/10.3723/175605497783258986).
23. G. E. P. Box and G. C. Tiao. “Bayesian inference in statistical analysis”. In: Wiley, 1992, pp. 76–148. DOI: [10.1002/9781118033197.ch2](https://doi.org/10.1002/9781118033197.ch2).
24. A. Brown, W. Gorter, P. Tromans, P. Jonathan, and P. Verlaan. “Design approach for turret moored vessels in highly variable squall conditions”. In: *Proc. 36th International Conference on Ocean, Offshore and Arctic Engineering (OMAE 2017)*. American Society of Civil Engineers, 2017. DOI: [10.1115/OMAE2017-61005](https://doi.org/10.1115/OMAE2017-61005).
25. D. J. T. Carter and P. G. Challenor. “Estimating return values of wave height.” *Quarterly Journal of the Royal Meteorological Society*, 1981, pp. 259–266.
26. E. Castillo, A. S. Hadi, N. Balakrishnan, and J. M. Sarabia. *Extreme value and related models with applications in engineering and science*. Wiley, Hoboken, NJ, USA, 2004. ISBN: 047167172X.
27. W. Chai and B. J. Leira. “Environmental contours based on inverse SORM”. *Marine Structures* 60, 2018, pp. 34–51. DOI: [10.1016/j.marstruc.2018.03.007](https://doi.org/10.1016/j.marstruc.2018.03.007).
28. A. Chakrabarti and L. T. M. Blessing. *An anthology of theories and models of design*. Springer, Heidelberg, Germany, 2014. DOI: [10.1007/978-1-4471-6338-1](https://doi.org/10.1007/978-1-4471-6338-1).
29. W. Chen, J. K. Allen, K.-L. Tsui, and F. Mistree. “A procedure for robust design: Minimizing variations caused by noise factors and control factors”. *Journal of Mechanical Design* 118, 1996, pp. 478–485. DOI: [10.1115/1.2826915](https://doi.org/10.1115/1.2826915).

30. X. Chen, Z. Jiang, Q. Li, Y. Li, and N. Ren. “Extended environmental contour methods for long-term extreme response analysis of offshore wind turbines”. *Journal of Offshore Mechanics and Arctic Engineering* 142:5, 2020. DOI: [10.1115/1.4046772](https://doi.org/10.1115/1.4046772).
31. Z. Y. Chen, S. Yao, and J. Q. Lin. “Formalisation of product requirements: from natural language descriptions to formal specifications”. *International Journal of Manufacturing Research* 2:3, 2007, pp. 362–387.
32. Z. Y. Chen and Y. Zeng. “Classification of product requirements based on product environment”. *Concurrent Engineering* 14:3, 2006, pp. 219–230. DOI: [10.1177/1063293X06068389](https://doi.org/10.1177/1063293X06068389).
33. P. W. Cheng. “A reliability based design methodology for extreme responses of offshore wind turbines”. Doctoral thesis. Technische Universiteit Delft, 2002.
34. Z. Cheng, E. Svangstø, T. Moan, and Z. Gao. “Long-term joint distribution of environmental conditions in a Norwegian fjord for design of floating bridges”. *Ocean Engineering* 191, 2019, p. 106472. DOI: [10.1016/j.oceaneng.2019.106472](https://doi.org/10.1016/j.oceaneng.2019.106472).
35. G. Clarindo, A. P. Teixeira, and C. Guedes Soares. “Environmental wave contours by inverse FORM and Monte Carlo Simulation with variance reduction techniques”. *Ocean Engineering* 228, 2021, p. 108916. DOI: [10.1016/j.oceaneng.2021.108916](https://doi.org/10.1016/j.oceaneng.2021.108916).
36. J. O. Clark. “System of systems engineering and family of systems engineering from a standards perspective”. In: *IEEE SysCon 2009 - 3rd Annual IEEE International Systems Conference*. IEEE, Vancouver, Canada, 2009. DOI: [10.1109/SYSCON.2009.4724201](https://doi.org/10.1109/SYSCON.2009.4724201).
37. R. G. Coe, C. Michelen, A. Eckert-Gallup, and C. Sallaberry. “Full long-term design response analysis of a wave energy converter”. *Renewable Energy* 116, 2018, pp. 356–366. DOI: [10.1016/j.renene.2017.09.056](https://doi.org/10.1016/j.renene.2017.09.056).
38. R. G. Coe, C. Michelen, A. Eckert-Gallup, Y.-H. Yu, and J. van Rij. “WDRT: A toolbox for design-response analysis of wave energy converters”. In: *Proc. 4th Marine Energy Technology Symposium*. Washington, DC, USA, 2016.
39. S. Coles. *An introduction to statistical modeling of extreme values*. Springer, Heidelberg, Germany, 2001. DOI: [10.1007/978-1-4471-3675-0](https://doi.org/10.1007/978-1-4471-3675-0).
40. L. Cozzi, B. Wanner, C. Donovan, A. Toril, and W. Yu. *Offshore Wind Outlook 2019*. Technical report. International Energy Agency, 2019.
41. R. Damiani, J. Jonkman, and G. Hayman. *SubDyn User's Guide and Theory Manual*. Technical report. National Renewable Energy Laboratory, 2015.
42. D. P. Dee et al. “The ERA-Interim reanalysis: Configuration and performance of the data assimilation system”. *Quarterly Journal of the Royal Meteorological Society* 137:656, 2011, pp. 553–597. DOI: [10.1002/qj.828](https://doi.org/10.1002/qj.828).
43. Y. Y. Deng, M. Haigh, W. Pouwels, L. Ramaekers, R. Brandsma, S. Schimschar, J. Grözinger, and D. de Jager. “Quantifying a realistic, worldwide wind and solar electricity supply”. *Global Environmental Change* 31, 2015, pp. 239–252. DOI: [10.1016/j.gloenvcha.2015.01.005](https://doi.org/10.1016/j.gloenvcha.2015.01.005).
44. Q. Derbanne and G. de Hauteclercque. “A new approach for environmental contour and multivariate de-clustering”. In: *Proc. 38th International Conference on Ocean, Offshore and Arctic Engineering (OMAE 2019)*. American Society of Mechanical Engineers (ASME), 2019.

Bibliography

45. Q. Derbanne, G. de Hauteclocque, and M. Dumont. “How to account for short-term and long-term variability in the prediction of the 100 years response?” In: *Proc. 36th International Conference on Ocean, Offshore and Arctic Engineering (OMAE 2017)*. American Society of Mechanical Engineers (ASME), 2017. DOI: [10.1115/omae2017-61701](https://doi.org/10.1115/omae2017-61701).
46. N. Dimitrov. “Inverse directional simulation: an environmental contour method providing an exact return period”. *Journal of Physics: Conference Series*, 2020. DOI: [10.1088/1742-6596/1618/6/062048](https://doi.org/10.1088/1742-6596/1618/6/062048).
47. DNV GL. *Recommended practice DNVGL-RP-C205: Environmental conditions and environmental loads*. Technical report. 2017.
48. B. Dose, H. Rahimi, I. Herráez, B. Stoevesandt, and J. Peinke. “Fluid-structure coupled computations of the NREL 5 MW wind turbine by means of CFD”. *Renewable Energy* 129, 2018, pp. 591–605. DOI: [10.1016/j.renene.2018.05.064](https://doi.org/10.1016/j.renene.2018.05.064).
49. B. Dose, H. Rahimi, B. Stoevesandt, and J. Peinke. “Fluid-structure coupled investigations of the NREL 5 MW wind turbine for two downwind configurations”. *Renewable Energy* 146, 2020, pp. 1113–1123. DOI: [10.1016/j.renene.2019.06.110](https://doi.org/10.1016/j.renene.2019.06.110).
50. E. F. Eastoe and J. A. Tawn. “Modelling the distribution of the cluster maxima of exceedances of subasymptotic thresholds”. *Biometrika* 99:1, 2012, pp. 43–55. DOI: [10.1093/biomet/asr078](https://doi.org/10.1093/biomet/asr078).
51. A. Eckert, N. Martin, R. G. Coe, B. Seng, Z. Stuart, and Z. Morrell. “Development of a comparison framework for evaluating environmental contours of extreme sea states”. *Journal of Marine Science and Engineering* 9, 2021. DOI: [10.3390/jmse9010016](https://doi.org/10.3390/jmse9010016).
52. A. Eckert-Gallup and N. Martin. “Kernel density estimation (KDE) with adaptive bandwidth selection for environmental contours of extreme sea states”. In: *OCEANS 2016 MTS/IEEE Monterey*. Institute of Electrical and Electronics Engineers (IEEE). 2016. DOI: [10.1109/OCEANS.2016.7761150](https://doi.org/10.1109/OCEANS.2016.7761150).
53. A. C. Eckert-Gallup, C. J. Sallaberry, A. R. Dallman, and V. S. Neary. “Application of principal component analysis (PCA) and improved joint probability distributions to the inverse first-order reliability method (I-FORM) for predicting extreme sea states”. *Ocean Engineering* 112, 2016, pp. 307–319. DOI: [10.1016/j.oceaneng.2015.12.018](https://doi.org/10.1016/j.oceaneng.2015.12.018).
54. B. Efron and R. J. Tibshirani. *An introduction to the bootstrap*. Chapman & Hall, 1993.
55. J. H. J. Einmahl, L. D. Haan, and A. Krajina. “Estimating extreme bivariate quantile regions”. *Extremes* 16, 2013, pp. 121–145. DOI: [10.1007/s10687-012-0156-z](https://doi.org/10.1007/s10687-012-0156-z).
56. M. D. Esteban, J. J. Diez, J. S. López, and V. Negro. “Why offshore wind energy?” *Renewable Energy* 36, 2011, pp. 444–450. DOI: [10.1016/j.renene.2010.07.009](https://doi.org/10.1016/j.renene.2010.07.009).
57. F. W. Scholz. “Maximum likelihood estimation”. In: *Encyclopedia of statistical sciences*. Ed. by S. Kotz, C. Read, N. Balakrishnan, B. Vidakovic, and N. Johnson. 2006. DOI: [10.1002/0471667196.ess1571.pub2](https://doi.org/10.1002/0471667196.ess1571.pub2).
58. T. Fazeres-Ferradosa, F. Taveira-Pinto, E. Vanem, M. T. Reis, and L. das Neves. “Asymmetric copula-based distribution models for met-ocean data in offshore wind engineering applications”. *Wind Engineering* 42, 2018, pp. 304–334. DOI: [10.1177/0309524X18777323](https://doi.org/10.1177/0309524X18777323).
59. G. Feld, P. Jonathan, and D. Randell. “On the estimation and application of directional design criteria”. In: *Proc. 38th International Conference on Ocean, Offshore and Arctic Engineering (OMAE 2019)*. 2019. DOI: [10.1115/OMAE2019-96586](https://doi.org/10.1115/OMAE2019-96586).

60. J. Fernandes, E. Henriques, A. Silva, and M. A. Moss. "Requirements change in complex technical systems: an empirical study of root causes". *Research in Engineering Design* 26, 2015, pp. 37–55. DOI: [10.1007/s00163-014-0183-7](https://doi.org/10.1007/s00163-014-0183-7).
61. J. A. Ferreira and C. Guedes Soares. "An application of the peaks over threshold method to predict extremes of significant wave height". *Journal of Offshore Mechanics and Arctic Engineering* 120:3, 1998, pp. 165–176. DOI: [10.1115/1.2829537](https://doi.org/10.1115/1.2829537).
62. J. A. Ferreira and C. Guedes Soares. "Modelling bivariate distributions of significant wave height and mean wave period". *Applied Ocean Research* 24:1, 2002, pp. 31–45. DOI: [10.1016/S0141-1187\(02\)00006-8](https://doi.org/10.1016/S0141-1187(02)00006-8).
63. J. A. Ferreira and C. Guedes Soares. "Modelling the long-term distribution of significant wave height with the Beta and Gamma models". *Ocean Engineering* 26:8, 1999, pp. 713–725. DOI: [10.1016/S0029-8018\(98\)00022-5](https://doi.org/10.1016/S0029-8018(98)00022-5).
64. C. A. Ferro and J. Segers. "Inference for clusters of extreme values". *Journal of the Royal Statistical Society. Series B: Statistical Methodology* 65, 2003, pp. 545–556. DOI: [10.1111/1467-9868.00401](https://doi.org/10.1111/1467-9868.00401).
65. G. Fischer. "Installation and operation of the research platform FINO 1 in the North Sea". In: *Offshore Wind Energy: Research on Environmental Impacts*. Springer, Berlin, Germany, 2006, pp. 237–253. ISBN: 3540346767. DOI: [10.1007/978-3-540-34677-7_15](https://doi.org/10.1007/978-3-540-34677-7_15).
66. T. Fischer, W. de Vries, and B. Schmidt. *Upwind Design Basis - IJmuiden Shallow Water Site*. Technical report. 2010. URL: <http://resolver.tudelft.nl/uuid:a176334d-6391-4821-8c5f-9c91b6b32a27>.
67. J. Fogle, P. Agarwal, and L. Manuel. "Towards an improved understanding of statistical extrapolation for wind turbine extreme loads". *Wind Energy* 11:6, 2008, pp. 613–635. DOI: [10.1002/we.303](https://doi.org/10.1002/we.303).
68. E. Fontaine, P. Orsero, A. Ledoux, R. Nerzic, M. Prevosto, and V. Quiniou. "Reliability analysis and response based design of a moored FPSO in West Africa". *Structural Safety* 41, 2013, pp. 82–96. DOI: [10.1016/j.strusafe.2012.08.002](https://doi.org/10.1016/j.strusafe.2012.08.002).
69. G. Z. Forristall. "How should we combine long and short term wave height distributions?" In: *Proc. 27th International Conference on Offshore Mechanics and Arctic Engineering (OMAE 2008)*. American Society of Mechanical Engineers (ASME), 2008.
70. G. Z. Forristall. "On the use of directional wave criteria". *Journal of Waterway, Port, Coastal and Ocean Engineering* 130:5, 2004, pp. 272–275. DOI: [10.1061/\(ASCE\)0733-950X\(2004\)130:5\(272\)](https://doi.org/10.1061/(ASCE)0733-950X(2004)130:5(272)).
71. General Electric. *Haliade-X offshore wind turbine*. 2021. URL: <https://www.ge.com/renewableenergy/wind-energy/offshore-wind/haliade-x-offshore-turbine> (visited on 10/06/2021).
72. J. S. Gero. "Design prototypes : A knowledge representation schema for design". *AI Magazine* 11:4, 1990. DOI: [10.1609/aimag.v11i4.854](https://doi.org/10.1609/aimag.v11i4.854).
73. J. S. Gero and U. Kannengiesser. "The situated function-behaviour-structure framework". *Design Studies* 25, 2004, pp. 373–391. DOI: [10.1016/j.destud.2003.10.010](https://doi.org/10.1016/j.destud.2003.10.010).
74. F. I. G. Giske, B. J. Leira, and O. Øiseth. "Long-term extreme response analysis of marine structures using inverse SORM". *Journal of Offshore Mechanics and Arctic Engineering* 140:5, 2018. DOI: [10.1115/1.4039718](https://doi.org/10.1115/1.4039718).

Bibliography

75. F. I. G. Giske, K. A. Kvåle, B. J. Leira, and O. Øiseth. "Long-term extreme response analysis of a long-span pontoon bridge". *Marine Structures* 58, 2018, pp. 154–171. DOI: [10.1016/j.marstruc.2017.11.010](https://doi.org/10.1016/j.marstruc.2017.11.010).
76. F. I. G. Giske, B. J. Leira, and O. Øiseth. "Full long-term extreme response analysis of marine structures using inverse FORM". *Probabilistic Engineering Mechanics* 50, 2017, pp. 1–8. DOI: [10.1016/j.probengmech.2017.10.007](https://doi.org/10.1016/j.probengmech.2017.10.007).
77. T. Gourlay, A. von Graefe, V. Shigunov, and E. Lataire. "Comparison of Aqwa, GL Rankine, Moses, Octopus, PDSTRIP and WAMIT with model test results for cargo ship wave-induced motions in shallow water". In: *Proc. 34th International Conference on Ocean, Offshore and Arctic Engineering (OMAE 2015)*. American Society of Mechanical Engineers (ASME), 2015. DOI: [10.1115/OMAE2015-41691](https://doi.org/10.1115/OMAE2015-41691).
78. O. Gramstad, C. Agrell, E. Bitner-Gregersen, B. Guo, E. Ruth, and E. Vanem. "Sequential sampling method using Gaussian process regression for estimating extreme structural response". *Marine Structures* 72, 2020, p. 102780. DOI: [10.1016/j.marstruc.2020.102780](https://doi.org/10.1016/j.marstruc.2020.102780).
79. O. Gramstad, E. Vanem, and E. M. Bitner-Gregersen. "Uncertainty of environmental contours due to sampling variability". In: *Proc. 37th International Conference on Ocean, Offshore and Arctic Engineering (OMAE 2018)*. American Society of Mechanical Engineers (ASME), Madrid, Spain, 2018. DOI: [10.1115/OMAE2018-77810](https://doi.org/10.1115/OMAE2018-77810).
80. N. Groll and R. Weisse. "A multi-decadal wind-wave hindcast for the North Sea 1949 - 2014: coastDat2". *Earth System Science Data* 9, 2017, pp. 955–968. DOI: [10.5194/essd-9-955-2017](https://doi.org/10.5194/essd-9-955-2017).
81. N. Groll and R. Weisse. *coastDat-2 North Sea wave hindcast for the period 1949-2014 performed with the wave model WAM*. 2016. DOI: [10.1594/WDCC/coastDat-2_WAM-North_Sea](https://doi.org/10.1594/WDCC/coastDat-2_WAM-North_Sea).
82. C. Guedes Soares. "Long term distribution of non-linear wave induced vertical bending moments". *Marine Structures* 6, 1993, pp. 475–483. DOI: [10.1016/0951-8339\(93\)90033-Y](https://doi.org/10.1016/0951-8339(93)90033-Y).
83. C. Guedes Soares and A. C. Henriques. "Statistical uncertainty in long-term distributions of significant wave height". *Journal of Offshore Mechanics and Arctic Engineering* 118, 1996, pp. 284–291. DOI: [10.1115/1.2833917](https://doi.org/10.1115/1.2833917).
84. J. Häfele, C. Hübner, C. G. Gebhardt, and R. Rolfes. "An improved two-step soil-structure interaction modeling method for dynamical analyses of offshore wind turbines". *Applied Ocean Research* 55, 2016, pp. 141–150. DOI: [10.1016/j.apor.2015.12.001](https://doi.org/10.1016/j.apor.2015.12.001).
85. Z. S. Haghayeghi and M. J. Ketabdar. "A long-term joint probability model for metocean circular and linear characteristics". *Applied Ocean Research* 75, 2018, pp. 143–152. DOI: [10.1016/j.apor.2018.03.009](https://doi.org/10.1016/j.apor.2018.03.009).
86. Z. S. Haghayeghi and M. J. Ketabdar. "Development of environmental contours for circular and linear metocean variables". *International Journal of Renewable Energy Research* 7:2, 2017, pp. 682–693.
87. M. Hallin, D. Paindaveine, and M. Šiman. "Multivariate quantiles and multiple-output regression quantiles: From L1 optimization to halfspace depth". *Annals of Statistics* 38:2, 2010, pp. 635–669. DOI: [10.1214/09-AOS723](https://doi.org/10.1214/09-AOS723).
88. Á. Hannesdóttir, M. Kelly, and N. Dimitrov. "Extreme wind fluctuations: Joint statistics, extreme turbulence, and impact on wind turbine loads", 2019, pp. 325–342. DOI: [10.5194/wes-4-325-2019](https://doi.org/10.5194/wes-4-325-2019).

89. H. F. Hansen, D. Randell, A. R. Zeeberg, and P. Jonathan. “Directional–seasonal extreme value analysis of North Sea storm conditions”. *Ocean Engineering* 195, 2020. DOI: [10.1016/j.oceaneng.2019.106665](https://doi.org/10.1016/j.oceaneng.2019.106665).
90. A. F. Haselsteiner. *compute-hdc: Highest density contour method in Matlab (version 1.1.1)*. 2019. URL: <https://github.com/ahaselsteiner/compute-hdc/releases/tag/1.1.1>.
91. A. F. Haselsteiner, R. G. Coe, and L. Manuel. “A second benchmarking exercise on estimating extreme environmental conditions”. *Ocean Engineering*, 2021. DOI: [10.1016/j.oceaneng.2021.109111](https://doi.org/10.1016/j.oceaneng.2021.109111).
92. A. F. Haselsteiner, R. G. Coe, L. Manuel, W. Chai, B. Leira, G. Clarindo, C. Guedes Soares, N. Dimitrov, A. Sander, J.-H. Ohlendorf, K.-D. Thoben, G. de Hauteclercque, E. Mackay, P. Jonathan, C. Qiao, A. Myers, A. Rode, A. Hildebrandt, B. Schmidt, and E. Vanem. “A benchmarking exercise for environmental contours”. *Ocean Engineering* 236, 2021. DOI: [10.1016/j.oceaneng.2021.109504](https://doi.org/10.1016/j.oceaneng.2021.109504).
93. A. F. Haselsteiner, R. G. Coe, L. Manuel, P. T. T. Nguyen, N. Martin, and A. Eckert-Gallup. “A benchmarking exercise on estimating extreme environmental conditions: Methodology & baseline results”. In: *Proc. 38th International Conference on Ocean, Offshore and Arctic Engineering (OMAE 2019)*. American Society of Mechanical Engineers (ASME), 2019. DOI: [10.1115/OMAE2019-96523](https://doi.org/10.1115/OMAE2019-96523).
94. A. F. Haselsteiner, M. Frieling, E. Mackay, A. Sander, and K.-D. Thoben. “Long-term response of an offshore turbine: How accurate are contour-based estimates?” *Renewable Energy* 181, 2021, pp. 945–965. DOI: [10.1016/j.renene.2021.09.077](https://doi.org/10.1016/j.renene.2021.09.077).
95. A. F. Haselsteiner, J. Lehmkuhl, T. Pape, K.-L. Windmeier, and K.-D. Thoben. “ViroCon: A software to compute multivariate extremes using the environmental contour method”. *SoftwareX* 9, 2019, pp. 95–101. DOI: [10.1016/j.softx.2019.01.003](https://doi.org/10.1016/j.softx.2019.01.003).
96. A. F. Haselsteiner, E. Mackay, and K.-D. Thoben. “Reducing conservatism in highest density environmental contours”. *Applied Ocean Research* 117, 2021, p. 102936. DOI: [10.1016/j.apor.2021.102936](https://doi.org/10.1016/j.apor.2021.102936).
97. A. F. Haselsteiner, J.-H. Ohlendorf, S. Oelker, L. Ströer, K.-D. Thoben, K. Wiedemann, E. De Ridder, and S. Lehmann. “Lifting wind turbine components from a floating vessel: A review on current solutions and open problems”. In: *Proc. 37th International Conference on Ocean, Offshore and Arctic Engineering (OMAE 2018)*. American Society of Mechanical Engineers (ASME), 2018. DOI: [10.1115/OMAE2018-78659](https://doi.org/10.1115/OMAE2018-78659).
98. A. F. Haselsteiner, J.-H. Ohlendorf, S. Oelker, L. Ströer, K.-D. Thoben, K. Wiedemann, E. De Ridder, and S. Lehmann. “Lifting wind turbine components from a floating vessel: A review on current solutions and open problems”. *Journal of Offshore Mechanics and Arctic Engineering* 141:5, 2019, p. 050801. DOI: [10.1115/1.4042385](https://doi.org/10.1115/1.4042385).
99. A. F. Haselsteiner, J.-H. Ohlendorf, and K.-D. Thoben. “Environmental contours based on kernel density estimation”. In: *Proc. 13th German Wind Energy Conference (DEWEK 2017)*. Bremen, Germany, 2017. URL: <https://arxiv.org/ftp/arxiv/papers/1710/1710.07156.pdf>.
100. A. F. Haselsteiner, J.-H. Ohlendorf, W. Wosniok, and K.-D. Thoben. “Deriving environmental contours from highest density regions”. *Coastal Engineering* 123, 2017, pp. 42–51. DOI: [10.1016/j.coastaleng.2017.03.002](https://doi.org/10.1016/j.coastaleng.2017.03.002).

Bibliography

101. A. F. Haselsteiner, R. Reisenhofer, J.-H. Ohlendorf, and K.-D. Thoben. “Design for extremes: A contour method for defining requirements based on multivariate extremes”. In: *Proc. 22nd International Conference on Engineering Design (ICED19)*. 2019, pp. 1433–1442. DOI: [10.1017/dsi.2019.149](https://doi.org/10.1017/dsi.2019.149).
102. A. F. Haselsteiner, A. Sander, J.-H. Ohlendorf, and K.-D. Thoben. “Global hierarchical models for wind and wave contours: Physical interpretations of the dependence functions”. In: *Proc. 39th International Conference on Ocean, Offshore and Arctic Engineering (OMAE 2020)*. American Society of Mechanical Engineers (ASME), 2020. DOI: [10.1115/OMAE2020-18668](https://doi.org/10.1115/OMAE2020-18668).
103. A. F. Haselsteiner and K.-D. Thoben. “Predicting wave heights for marine design by prioritizing extreme events in a global model”. *Renewable Energy* 156, 2020, pp. 1146–1157. DOI: [10.1016/j.renene.2020.04.112](https://doi.org/10.1016/j.renene.2020.04.112).
104. K. Hasselmann, T. Barnett, E. Bouws, H. Carlson, D. Cartwright, K. Enke, J. Ewing, H. Gienapp, D. Hasselmann, P. Kruseman, A. Meerburg, P. Müller, D. Olbers, K. Richter, W. Sell, and H. Walden. “Measurements of wind-wave growth and swell decay during the Joint North Sea Wave Project (JONSWAP)”. *Ergänzungsheft zur Deutschen Hydrographischen Zeitschrift* 8:12, 1973, pp. 8–95.
105. A. Hatchuel and B. Weil. “A new approach of innovative design: An introduction to C-K theory”. In: *Proc. International Conference on Engineering Design (ICED 03)*. Stockholm, Sweden, 2003.
106. A. Hatchuel and B. Weil. “C-K design theory: an advanced formulation”. *Research in Engineering Design* 19, 2009, pp. 181–192. DOI: [10.1007/s00163-008-0043-4](https://doi.org/10.1007/s00163-008-0043-4).
107. G. de Hauteclercque, E. Mackay, and E. Vanem. “Quantitative assessment of environmental contour approaches (preprint from March 2021)”, 2021. DOI: [10.13140/RG.2.2.10068.12161](https://doi.org/10.13140/RG.2.2.10068.12161).
108. S. Haver and S. Winterstein. “Environmental contour lines: A method for estimating long term extremes by a short term analysis”. *Transactions of the Society of Naval Architects and Marine Engineers* 116, 2009, pp. 116–127.
109. S. Haver. “On the joint distribution of heights and periods of sea waves”. *Ocean Engineering* 14:5, 1987, pp. 359–376. DOI: [10.1016/0029-8018\(87\)90050-3](https://doi.org/10.1016/0029-8018(87)90050-3).
110. S. Haver. “Wave climate off northern Norway”. *Applied Ocean Research* 7:2, 1985, pp. 85–92. DOI: [10.1016/0141-1187\(85\)90038-0](https://doi.org/10.1016/0141-1187(85)90038-0).
111. J. E. Heffernan and J. A. Tawn. “A conditional approach for multivariate extreme values”. *Journal of the Royal Statistical Society. Series B (Statistical Methodology)* 66:3, 2004, pp. 497–546. DOI: [10.1111/j.1467-9868.2004.02050.x](https://doi.org/10.1111/j.1467-9868.2004.02050.x).
112. M. A. Hemer, Y. Fan, N. Mori, A. Semedo, and X. L. Wang. “Projected changes in wave climate from a multi-model ensemble”. *Nature Climate Change* 3:5, 2013, pp. 471–476. DOI: [10.1038/nclimate1791](https://doi.org/10.1038/nclimate1791).
113. E. Heredia-Zavoni and R. Montes-Iturriaga. “Modeling directional environmental contours using three dimensional vine copulas”. *Ocean Engineering* 187, 2019. DOI: [10.1016/j.oceaneng.2019.06.007](https://doi.org/10.1016/j.oceaneng.2019.06.007).
114. B. J. Hightower, R. Ingersoll, D. D. Chin, C. Lawhon, A. F. Haselsteiner, and D. Lentink. “Design and analysis of aerodynamic force platforms for free flight studies”. *Bioinspiration & Biomimetics* 12:6, 2017, p. 064001. DOI: [10.1088/1748-3190/aa7eb2](https://doi.org/10.1088/1748-3190/aa7eb2).

115. L. H. Holthuijsen. *Waves in oceanic and coastal waters*. Cambridge University Press, Cambridge, United Kingdom, 2007. ISBN: 978-0-511-27021-5.
116. J. T. Horn, E. Bitner-Gregersen, J. R. Krokstad, B. J. Leira, and J. Amdahl. “A new combination of conditional environmental distributions”. *Applied Ocean Research* 73, 2018, pp. 17–26. DOI: [10.1016/j.apor.2018.01.010](https://doi.org/10.1016/j.apor.2018.01.010).
117. J.-T. Horn and S. R. Winterstein. “Extreme response estimation of offshore wind turbines with an extended contour-line method”. *Journal of Physics: Conference Series* 1104, 2018. DOI: [10.1088/1742-6596/1104/1/012031](https://doi.org/10.1088/1742-6596/1104/1/012031).
118. J.-T. H. Horn, J. R. Krokstad, and J. Amdahl. “Joint probability distribution of environmental conditions for design of offshore wind turbines”. In: *Proc. 36th International Conference on Ocean, Offshore and Arctic Engineering (OMAE 2017)*. American Society of Mechanical Engineers (ASME), Trondheim, Norway, 2017. DOI: [10.1115/OMAE2017-61451](https://doi.org/10.1115/OMAE2017-61451).
119. W. Huang and S. Dong. “Joint distribution of significant wave height and zero-up-crossing wave period using mixture copula method”. *Ocean Engineering* 219, 2021, p. 108305. DOI: [10.1016/j.oceaneng.2020.108305](https://doi.org/10.1016/j.oceaneng.2020.108305).
120. V. Hubka and W. E. Eder. *Theory of technical systems*. 2nd ed. Springer, Berlin, Germany, 1988. ISBN: 9783642521232.
121. A. B. Huseby, E. Vanem, and K. Eskeland. “Evaluating properties of environmental contours”. In: *Safety and Reliability, Theory and Applications*. CRC Press, 2017. ISBN: 978-1138629370.
122. A. B. Huseby, E. Vanem, and B. Natvig. “A new Monte Carlo method for environmental contour estimation”. In: *European Safety and Reliability Conference (ESREL)*. European Safety and Reliability Association (ESRA). 2014, pp. 2091–2098.
123. A. B. Huseby. *Riscue (version 2.7)*. 2018. URL: <http://riscue.org/>.
124. A. B. Huseby, E. Vanem, and B. Natvig. “A new approach to environmental contours for ocean engineering applications based on direct Monte Carlo simulations”. *Ocean Engineering* 60, 2013, pp. 124–135. DOI: [10.1016/j.oceaneng.2012.12.034](https://doi.org/10.1016/j.oceaneng.2012.12.034).
125. A. B. Huseby, E. Vanem, and B. Natvig. “Alternative environmental contours for structural reliability analysis”. *Structural Safety* 54, 2015, pp. 32–45. DOI: [10.1016/j.strusafe.2014.12.003](https://doi.org/10.1016/j.strusafe.2014.12.003).
126. R. J. Hyndman. “Computing and graphing highest density regions”. *The American Statistician* 50:2, 1996, pp. 120–126. DOI: [10.2307/2684423](https://doi.org/10.2307/2684423).
127. A. Incevik, J. Bowers, G. Mould, and O. Yilamz. “Response-based extreme value analysis of moored offshore structures due to wave, wind and current”. *Journal of Marine Science and Technology* 3, 1998, pp. 145–150. DOI: [10.1007/BF02492921](https://doi.org/10.1007/BF02492921).
128. International Electrotechnical Commission. *Wind energy generation systems - Part 1: Design requirements*. Technical report IEC 61400-1:2019-02. 2019.
129. International Electrotechnical Commission. *Wind energy generation systems - Part 3-1: Design requirements for fixed offshore wind turbines*. Technical report IEC 61400-3-1. 2019.
130. International Electrotechnical Commission. *Wind energy generation systems - Part 3-2: Design requirements for floating offshore wind turbines*. Technical report IEC TS 61400-3-2. 2019.

Bibliography

131. International Energy Agency. *Offshore Wind*. 2021. DOI: <https://www.iea.org/reports/offshore-wind>.
132. N. H. Jasper. "Statistical distribution patterns of ocean waves and of wave-induced ship stresses and motions, with engineering applications". *The Society of Naval Architects and Marine Engineers Transactions* 64, 1956.
133. P. Jonathan and K. Ewans. "Statistical modelling of extreme ocean environments for marine design: A review". *Ocean Engineering* 62, 2013, pp. 91–109. DOI: [10.1016/j.oceaneng.2013.01.004](https://doi.org/10.1016/j.oceaneng.2013.01.004).
134. P. Jonathan, K. Ewans, and J. Flynn. "On the estimation of ocean engineering design contours". *Journal of Offshore Mechanics and Arctic Engineering* 136:4, 2014, p. 041101. DOI: [10.1115/1.4027645](https://doi.org/10.1115/1.4027645).
135. P. Jonathan, J. Flynn, and K. Ewans. "Joint modelling of wave spectral parameters for extreme sea states". *Ocean Engineering* 37, 2010, pp. 1070–1080.
136. M. Jones, D. Randell, K. Ewans, and P. Jonathan. "Statistics of extreme ocean environments: Non-stationary inference for directionality and other covariate effects". *Ocean Engineering* 119, 2016, pp. 30–46. DOI: [10.1016/j.oceaneng.2016.04.010](https://doi.org/10.1016/j.oceaneng.2016.04.010).
137. J. Jonkman, S. Butterfield, W. Musial, and G. Scott. *Definition of a 5-MW reference wind turbine for offshore system development*. Technical report. 2009. DOI: [10.2172/947422](https://doi.org/10.2172/947422).
138. J. Jonkman and W. Musial. *Offshore code comparison collaboration (OC3) for IEA Task 23 offshore wind technology and deployment*. Technical report. 2010. URL: <https://www.nrel.gov/docs/fy11osti/48191.pdf>.
139. J. Jonkman et al. "Offshore code comparison collaboration continuation (OC4), Phase I - Results of coupled simulations of an offshore wind turbine with jacket support structure (Preprint)". In: *Proc. International Society of Offshore and Polar Engineers conference*. Rhodes, Greece, 2012.
140. C. Jung and D. Schindler. "Wind speed distribution selection – A review of recent development and progress". *Renewable and Sustainable Energy Reviews* 114, 2019, p. 109290. DOI: [10.1016/j.rser.2019.109290](https://doi.org/10.1016/j.rser.2019.109290).
141. D. Karmakar, H. Bagbancı, and C. Guedes Soares. "Long-term extreme load prediction of spar and semisubmersible floating wind turbines using the environmental contour method". *Journal of Offshore Mechanics and Arctic Engineering* 138:2, 2016, p. 021601. DOI: [10.1115/1.4032099](https://doi.org/10.1115/1.4032099).
142. A. G. Koohi Kheili, Y. Drobyshevski, M. Kimiae, and M. Efthymiou. "Iterative methodology for response based analysis of an FPSO mooring system". *Marine Structures* 78, 2021, p. 102973. DOI: [10.1016/j.marstruc.2021.102973](https://doi.org/10.1016/j.marstruc.2021.102973).
143. D. Krause, G. Beckmann, S. Eilmus, N. Gebhardt, H. Jonas, and R. Rettberg. "Integrated development of modular product families: A methods toolkit". In: *Advances in Product Family and Product Platform Design: Methods and Applications*. Ed. by T. W. Simpson, J. R. Jiao, Z. Siddique, and K. Hölttä-Otto. Springer, 2013. Chap. 10. DOI: [10.1007/978-1-4614-7937-6](https://doi.org/10.1007/978-1-4614-7937-6).
144. T. D. Kreidler. "The offshore petroleum industry: The formative years, 1945-1962". PhD thesis. Texas Tech University, 1997.
145. H. E. Krogstad. "Height and period distributions of extreme waves". *Applied Ocean Research* 7:3, 1985, pp. 158–165. DOI: [10.1016/0141-1187\(85\)90008-2](https://doi.org/10.1016/0141-1187(85)90008-2).

146. M. Kühn. "Dynamics and design optimisation of offshore wind energy conversion systems". Doctoral thesis. Technische Universiteit Delft, 2001. ISBN: 9076468079.
147. M. R. Leadbetter. "Extremes and local dependence in stationary sequences". *Zeitschrift für Wahrscheinlichkeitstheorie und Verwandte Gebiete* 65, 1983, pp. 291–306. DOI: 10.1007/BF00532484.
148. B. J. Leira. "A comparison of stochastic process models for definition of design contours". *Structural Safety* 30, 2008, pp. 493–505. DOI: 10.1016/j.strusafe.2007.09.006.
149. M. Lewis. *GE's huge Haliade-X 14 MW offshore wind turbine is now operational*. 2021. URL: <https://electrek.co/2021/10/05/ge-huge-haliade-x-14-mw-offshore-wind-turbine-is-now-operational/> (visited on 10/06/2021).
150. L. Li, Z. M. Yuan, Y. Gao, X. Zhang, and T. Tezdogan. "Investigation on long-term extreme response of an integrated offshore renewable energy device with a modified environmental contour method". *Renewable Energy* 132, 2019, pp. 33–42. DOI: 10.1016/j.renene.2018.07.138.
151. L. Li, Z. Gao, and T. Moan. "Joint environmental data at five European offshore sites for design of combined wind and wave energy devices". *Journal of Offshore Mechanics and Arctic Engineering* 137, 2015, p. 031901. DOI: 10.1115/1.4029842.
152. Q. Li, Z. Gao, and T. Moan. "Modified environmental contour method for predicting long-term extreme responses of bottom-fixed offshore wind turbines". *Marine Structures* 48, 2016, pp. 15–32. DOI: 10.1016/j.marstruc.2016.03.003.
153. Q. Li, Z. Gao, and T. Moan. "Modified environmental contour method to determine the long-term extreme responses of a semi-submersible wind turbine". *Ocean Engineering* 142, 2017, pp. 563–576. DOI: 10.1016/j.oceaneng.2017.07.038.
154. Y. Lin, S. Dong, and S. Tao. "Modelling long-term joint distribution of significant wave height and mean zero-crossing wave period using a copula mixture". *Ocean Engineering* 197, 2020, p. 106856. DOI: 10.1016/j.oceaneng.2019.106856.
155. J. Liu, E. Thomas, A. Goyal, and L. Manuel. "Design loads for a large wind turbine supported by a semi-submersible floating platform". *Renewable Energy* 138, 2019, pp. 923–936. DOI: 10.1016/j.renene.2019.02.011.
156. C. Lucas and C. Guedes Soares. "Bivariate distributions of significant wave height and mean wave period of combined sea states". *Ocean Engineering* 106, 2015, pp. 341–353. DOI: 10.1016/j.oceaneng.2015.07.010.
157. E. Mackay, R. G. Coe, A. F. Haselsteiner, and L. Manuel. "A second benchmarking exercise on estimating extreme environmental conditions". In: *Proc. 40th International Conference on Ocean, Offshore and Arctic Engineering (OMAE2021)*. American Society of Mechanical Engineerings (ASME), 2021, OMAE2021-64874. DOI: 10.1115/OMAE2021-64874.
158. E. Mackay and A. F. Haselsteiner. "Marginal and total exceedance probabilities of environmental contours". *Marine Structures* 75, 2021. DOI: 10.1016/j.marstruc.2020.102863.
159. E. Mackay, G. de Hauteclercque, E. Vanem, and P. Jonathan. "The effect of serial correlation in environmental conditions on estimates of extreme events (preprint from March 2021)", 2021. DOI: 10.13140/RG.2.2.14004.78723.

Bibliography

160. E. Mackay and L. Johanning. "A generalised equivalent storm model for long-term statistics of ocean waves". *Coastal Engineering* 140, 2018, pp. 411–428. DOI: [10.1016/j.coastaleng.2018.06.001](https://doi.org/10.1016/j.coastaleng.2018.06.001).
161. E. Mackay and L. Johanning. "Long-term distributions of individual wave and crest heights". *Ocean Engineering* 165, 2018, pp. 164–183. DOI: [10.1016/j.oceaneng.2018.07.047](https://doi.org/10.1016/j.oceaneng.2018.07.047).
162. E. Mackay and P. Jonathan. "Sampling properties and empirical estimates of extreme events". *Ocean Engineering* 239, 2021, p. 109791. DOI: [10.1016/j.oceaneng.2021.109791](https://doi.org/10.1016/j.oceaneng.2021.109791).
163. E. B. Mackay and P. Jonathan. "Estimation of environmental contours using a block resampling method". In: *Proc. 39th International Conference on Ocean, Offshore and Arctic Engineering (OMAE 2020)*. American Society of Mechanical Engineers (ASME), 2020. DOI: [10.1115/OMAE2020-18308](https://doi.org/10.1115/OMAE2020-18308).
164. E. B. L. Mackay and L. Johanning. "A simple and robust method for calculating return periods of ocean waves". In: *Proc. 37th International Conference on Ocean, Offshore and Arctic Engineering (OMAE 2018)*. American Society of Mechanical Engineers (ASME), 2018. DOI: [10.1115/OMAE2018-78729](https://doi.org/10.1115/OMAE2018-78729).
165. H. O. Madsen, S. Krenk, and N. C. Lind. *Methods of structural safety*. Dover Publications, Mineola, NY, USA, 2006.
166. L. Manuel, P. T. T. Nguyen, J. Canning, R. G. Coe, A. C. Eckert-Gallup, and N. Martin. "Alternative approaches to develop environmental contours from metocean data". *Journal of Ocean Engineering and Marine Energy* 4:4, 2018, pp. 293–310. DOI: [10.1007/s40722-018-0123-0](https://doi.org/10.1007/s40722-018-0123-0).
167. P. Marshall, M. Rezvan, and A. Gunatunga. "Response based criteria for west of Shetlands". *Journal of Offshore Technology* 3:2, 1995, pp. 42–45.
168. J. Mathisen and E. Bitner-Gregersen. "Joint distributions for significant wave height and wave zero-up-crossing period". *Applied Ocean Research* 12, 1990, pp. 93–103. DOI: [10.1016/S0141-1187\(05\)80033-1](https://doi.org/10.1016/S0141-1187(05)80033-1).
169. S. Mazaheri and M. J. Downie. "Response-based method for determining the extreme behaviour of floating offshore platforms". *Ocean Engineering* 32, 2005, pp. 363–393. DOI: [10.1016/j.oceaneng.2004.08.004](https://doi.org/10.1016/j.oceaneng.2004.08.004).
170. F. Mazas. "Extreme events: A framework for assessing natural hazards". *Natural Hazards*, 2019. DOI: [10.1007/s11069-019-03581-9](https://doi.org/10.1007/s11069-019-03581-9).
171. A. McKay, A. de Pennington, and J. Baxter. "Requirements management: A representation scheme for product specifications". *Computer-Aided Design* 33, 2001, pp. 511–520. DOI: [10.1016/S0010-4485\(01\)00050-1](https://doi.org/10.1016/S0010-4485(01)00050-1).
172. M. Menéndez, F.J. Méndez, C. Izaguirre, A. Luceño, and I.J. Losada. "The influence of seasonality on estimating return values of significant wave height". *Coastal Engineering* 56, 2009, pp. 211–219. DOI: [10.1016/j.coastaleng.2008.07.004](https://doi.org/10.1016/j.coastaleng.2008.07.004).
173. G. M. Mocko and S. J. Fenves. *NISTIR 6996: A Survey of Design – Analysis Integration Issues*. Technical report. National Institute of Standards and Technology (NIST).
174. N. R. Moloney, D. Faranda, and Y. Sato. "An overview of the extremal index". *Chaos* 29, 2019. DOI: [10.1063/1.5079656](https://doi.org/10.1063/1.5079656).

175. R. Montes-Iturriaga and E. Heredia-Zavoni. "Assessment of uncertainty in environmental contours due to parametric uncertainty in models of the dependence structure between metocean variables". *Applied Ocean Research* 64, 2017. DOI: 10.1016/j.apor.2017.02.006.
176. R. Montes-Iturriaga and E. Heredia-Zavoni. "Environmental contours using copulas". *Applied Ocean Research* 52, 2015. DOI: 10.1016/j.apor.2015.05.007.
177. R. Montes-Iturriaga and E. Heredia-Zavoni. "Multivariate environmental contours using C-vine copulas". *Ocean Engineering* 118, 2016, pp. 68–82. DOI: 10.1016/j.oceaneng.2016.03.011.
178. A. Morató, S. Sriramula, N. Krishnan, and J. Nichols. "Ultimate loads and response analysis of a monopile supported offshore wind turbine using fully coupled simulation". *Renewable Energy* 101, 2017, pp. 126–143. DOI: 10.1016/j.renene.2016.08.056.
179. P.J. Moriarty and A. Hansen. *AeroDyn Theory Manual*. Technical report. National Renewable Energy Laboratory, 2005.
180. P.J. Moriarty, W.E. Holley, and S. Butterfield. *Extrapolation of extreme and fatigue loads using probabilistic methods*. Technical report. National Renewable Energy Laboratory (NREL), 2004. URL: <http://www.nrel.gov/docs/fy05osti/34421.pdf>.
181. J. Morim et al. "Robustness and uncertainties in global multivariate wind-wave climate projections". *Nature Climate Change* 9:9, 2019, pp. 711–718. DOI: 10.1038/s41558-019-0542-5.
182. G.S. Mudholkar and D.K. Srivastava. "Exponentiated Weibull family for analyzing bathtub failure-rate data". *IEEE Transactions on Reliability* 42:2, 1993, pp. 299–302. DOI: 10.1109/24.229504.
183. L.R. Muir and A.H. El-Shaarawi. "On the calculation of extreme wave heights: A review". *Ocean Engineering* 13:1, 1986, pp. 93–118. DOI: 10.1016/0029-8018(86)90006-5.
184. M.J. Muliawan, Z. Gao, and T. Moan. "Application of the contour line method for estimating extreme responses in the mooring lines of a two-body floating wave energy converter". *Journal of Offshore Mechanics and Arctic Engineering* 135, 2013, p. 031301. DOI: 10.1115/1.4024267.
185. A. Myers, S. Arwade, V. Valamanesh, S. Hallowell, and W. Carswell. "Strength, stiffness, resonance and the design of offshore wind turbine monopiles". *Engineering Structures* 100, 2015, pp. 332–341. DOI: 10.1016/j.engstruct.2015.06.021.
186. S. Nadarajah, G.M. Cordeiro, and E.M. Ortega. "The exponentiated Weibull distribution: A survey". *Statistical Papers* 54:3, 2013, pp. 839–877. DOI: 10.1007/s00362-012-0466-x.
187. A. Naess and O. Gaidai. "Estimation of extreme values from sampled time series". *Structural Safety* 31:4, 2009, pp. 325–334. DOI: 10.1016/j.strusafe.2008.06.021.
188. A. Naess and O. Gaidai. "Monte Carlo methods for estimating the extreme response of dynamical systems". *Journal of Engineering Mechanics* 134:8, 2008, pp. 628–636. DOI: 10.1061/(asce)0733-9399(2008)134:8(628).
189. A. Naess. "Technical note: On the long-term statistics of extremes". *Applied Ocean Research* 6:4, 1984, pp. 227–228. DOI: 10.1016/0141-1187(84)90061-0.
190. A. Naess and T. Moan. "Random environmental process". In: *Stochastic dynamics of marine structures*. Cambridge University Press, Cambridge, United Kingdom, 2013, pp. 191–208. DOI: 10.1017/CBO9781139021364.

Bibliography

191. A. Naess and T. Moan. *Stochastic dynamics of marine structures*. Cambridge University Press, Cambridge, United Kingdom, 2013. DOI: [10.1017/CBO9781139021364](https://doi.org/10.1017/CBO9781139021364).
192. National Data Buoy Center. *Handbook of automated data quality control checks and procedures*. Technical report. 2009, pp. 1–78.
193. National Renewable Energy Laboratory. *OpenFAST Documentation: Release 1.0*. Technical report. 2010. URL: https://readthedocs.org/projects/openfast-wave-stretching/downloads/pdf/f-wave{_}stretching/.
194. V. S. Neary, S. Ahn, B. E. Seng, M. N. Allahdadi, T. Wang, Z. Yang, and R. He. “Characterization of extreme wave conditions for wave energy converter design and project risk assessment”. *Journal of Marine Science and Engineering* 8, 2020. DOI: [10.3390/jmse8040289](https://doi.org/10.3390/jmse8040289).
195. N. Nordenström. “A method to predict long-term distributions of waves and wave-induced motions and loads on ships and other floating structures”. Doctoral thesis. Chalmers University, 1973.
196. N. Nordenström. *Methods for predicting long term distributions of wave loads and probability of failure for ships*. Technical report. DNV report no. 69-21-S. Det Norske Veritas, 1969.
197. NORSO. *NORSOK standard N-003: Actions and action effects*. Technical report. 2007.
198. M. K. Ochi. “New approach for estimating the severest sea state”. In: *23rd International Conference on Coastal Engineering*. American Society of Civil Engineers, Venice, Italy, 1992, pp. 512–525. DOI: [10.1061/9780872629332.038](https://doi.org/10.1061/9780872629332.038).
199. M. K. Ochi and J. E. Wahlen. “Prediction of severest significant wave height”. *Coastal Engineering* Chapter 36, 1980, pp. 587–599.
200. M. Ochi. *Ocean waves: The stochastic approach*. Cambridge University Press, Cambridge, United Kingdom, 1998. ISBN: 978052101767-1.
201. S. Oelker, M. Lewandowski, A. A. Alla, J.-H. Ohlendorf, and A. F. Haselsteiner. “Logistikzenarien für die Errichtung von Offshore-Windparks: Herausforderungen der Wirtschaftlichkeitsbetrachtung neuer Logistikkonzepte”. *Industrie 4.0 Management* 33, 2017, pp. 24–28.
202. A. P. Orimolade, S. Haver, and O. T. Gudmestad. “Estimation of extreme significant wave heights and the associated uncertainties: A case study using NORAS10 hindcast data for the Barents Sea”. *Marine Structures* 49, 2016, pp. 1–17. DOI: [10.1016/j.marstruc.2016.05.004](https://doi.org/10.1016/j.marstruc.2016.05.004).
203. G. Pahl and W. Beitz. *Engineering design: a systematic approach*. Springer, London, United Kingdom, 1996. ISBN: 3-540-19917-9.
204. B. Paltridge. “Thesis and dissertation writing: An examination of published advice and actual practice”. *English for Specific Purposes* 21:2, 2002, pp. 125–143. DOI: [10.1016/S0889-4906\(00\)00025-9](https://doi.org/10.1016/S0889-4906(00)00025-9).
205. W. J. Pierson and L. Moskowitz. “A proposed spectral form for fully developed wind seas based on the similarity theory of S. A. Kitaigorodskii”. *Journal of Geophysical Research* 69:24, 1964, pp. 5181–5190. DOI: [10.1029/JZ069i024p05181](https://doi.org/10.1029/JZ069i024p05181).
206. C. Qiao and A. Myers. “A new IFORM-Rosenblatt framework for calculation of environmental contours”. *Ocean Engineering* 238, 2021, p. 109622. DOI: [10.1016/j.oceaneng.2021.109622](https://doi.org/10.1016/j.oceaneng.2021.109622).

207. P. Ragan and L. Manuel. "Statistical extrapolation methods for estimating wind turbine extreme loads". *Journal of Solar Energy Engineering* 130:3, 2008, p. 031011. DOI: 10.1115/1.2931501.
208. G. K. V. Ramachandran, L. Vita, A. Krieger, and K. Mueller. "Design basis for the feasibility evaluation of four different floater designs". *Energy Procedia* 137, 2017, pp. 186–195. DOI: 10.1016/j.egypro.2017.10.345.
209. D. Randell, G. Feld, K. Ewans, and P. Jonathan. "Distributions of return values for ocean wave characteristics in the South China Sea using directional-seasonal extreme value analysis". *Environmetrics* 26:6, 2015, pp. 442–450. DOI: 10.1002/env.2350.
210. E. A. Rendon and L. Manuel. "Long-term loads for a monopile-supported offshore wind turbine". *Wind Energy* 17, 2014, pp. 209–223. DOI: 10.1002/we.1569.
211. S. Rezaei, A. K. Marvasty, S. Nadarajah, and M. Alizadeh. "A new exponentiated class of distributions: Properties and applications". *Communications in Statistics - Theory and Methods* 46:12, 2017, pp. 6054–6073. DOI: 10.1080/03610926.2015.1116579.
212. A. N. Robertson and J. M. Jonkman. "Loads analysis of several offshore floating wind turbine concepts". In: *Proc. 21st International Offshore and Polar Engineering Conference (ISOPE 2011)*. 2011.
213. A. N. Robertson et al. "OC5 project phase II: Validation of global loads of the DeepCwind floating semisubmersible wind turbine". *Energy Procedia* 137, 2017, pp. 38–57. DOI: 10.1016/j.egypro.2017.10.333.
214. P. E. Rook. "Controlling software projects". *Software Engineering Journal*, 1986, pp. 7–16. DOI: 10.1049/sej.1986.0003.
215. M. Rosenblatt. "Remarks on a multivariate transformation". *The Annals of Mathematical Statistics* 23:3, 1952, pp. 470–472.
216. E. Ross, O. C. Astrup, E. Bitner-Gregersen, N. Bunn, G. Feld, B. Gouldby, A. Huseby, Y. Liu, D. Randell, E. Vanem, and P. Jonathan. "On environmental contours for marine and coastal design". *Ocean Engineering*, 2019. DOI: 10.1016/j.oceaneng.2019.106194.
217. L. V. Sagrilo, A. Naess, and A. S. Doria. "On the long-term response of marine structures". *Applied Ocean Research* 33, 2011, pp. 208–214. DOI: 10.1016/j.apor.2011.02.005.
218. A. Sander, A. F. Haselsteiner, K. Barat, M. Janssen, S. Oelker, J.-H. Ohlendorf, and K.-D. Thoben. "Relative motion during single blade installation: Measurements from the North Sea". In: *Proc. 39th International Conference on Ocean, Offshore and Arctic Engineering (OMAE 2020)*. American Society of Mechanical Engineers (ASME), 2020. DOI: 10.1115/OMAE2020-18935.
219. K. Saranyasoontorn and L. Manuel. "Efficient models for wind turbine extreme loads using inverse reliability". *Journal of Wind Engineering and Industrial Aerodynamics* 92, 2004, pp. 789–804.
220. K. Saranyasoontorn and L. Manuel. "On assessing the accuracy of offshore wind turbine reliability-based design loads from the environmental contour method". *International Journal of Offshore and Polar Engineering* 15:2, 2006, pp. 132–140. ISSN: 1053-5381.
221. K. Saranyasoontorn and L. Manuel. "Design loads for wind turbines using the environmental contour method". *Journal of Solar Energy Engineering* 128:4, 2006, pp. 554–561. DOI: 10.1115/1.2346700.

Bibliography

222. C. Scarrott and A. MacDonald. "A review of extreme value threshold estimation and uncertainty quantification". *REVSTAT – Statistical Journal* 10:1, 2012, pp. 33–60.
223. B. Schmidt. "Kombinierte extreme Einwirkungen für Offshore-Windenergieanlagen". Doctoral thesis. Leibniz Universität Hannover, 2017.
224. F. Scholz. *Weibull probability paper*. 2008. URL: <http://faculty.washington.edu/fscholz/DATAFILES498B2008/WeibullPaper.pdf> (visited on 08/20/2019).
225. M. Seidel, S. Voormeeren, and J. B. van der Steen. "State-of-the-art design processes for offshore wind turbine support structures: Practical approaches and pitfalls during different stages in the design process". *Stahlbau* 85:9, 2016, pp. 583–590. ISSN: 14371049. DOI: [10.1002/stab.201610404](https://doi.org/10.1002/stab.201610404).
226. R. Sell and M. Tamre. "Integration of V-model and SysML for advanced mechatronics system design". In: *Proc. Research and Education on Mechatronics Conference REM05*. 2005, pp. 276–280.
227. F. Serinaldi. "Dismissing return periods!" *Stochastic Environmental Research and Risk Assessment* 29:4, 2015, pp. 1179–1189. DOI: [10.1007/s00477-014-0916-1](https://doi.org/10.1007/s00477-014-0916-1).
228. F. Silva-González, E. Heredia-Zavoni, and R. Montes-Iturriaga. "Development of environmental contours using Nataf distribution model". *Ocean Engineering* 58, 2013, pp. 27–34. DOI: [10.1016/j.oceaneng.2012.08.008](https://doi.org/10.1016/j.oceaneng.2012.08.008).
229. F. Silva-González, A. Vázquez-Hernández, L. Sagrilo, and R. Cuamatzi. "The effect of some uncertainties associated to the environmental contour lines definition on the extreme response of an FPSO under hurricane conditions". *Applied Ocean Research* 53, 2015, pp. 190–199. DOI: [10.1016/j.apor.2015.09.005](https://doi.org/10.1016/j.apor.2015.09.005).
230. H. A. Simon. *The Sciences of the Artificial*. 3rd ed. MIT Press, Cambridge, Massachusetts, USA, 1996. ISBN: 9780262193740.
231. Z. Song, Y. Bao, D. Zhang, Q. Shu, Y. Song, and F. Qiao. "Centuries of monthly and 3-hourly global ocean wave data for past, present, and future climate research". *Scientific Data* 7:1, 2020, pp. 1–11. DOI: [10.1038/s41597-020-0566-8](https://doi.org/10.1038/s41597-020-0566-8).
232. R. G. Standing, R. Eichaker, H. D. Lawes, B. Campbell, and R. B. Corr. "Benefits of applying response-based design methods to deepwater FPSOs". *Proceedings of the Annual Offshore Technology Conference*, 2002. DOI: [10.4043/14232-ms](https://doi.org/10.4043/14232-ms).
233. N. P. Suh. "Axiomatic design theory for systems". *Research in Engineering Design* 10, 1998, pp. 189–209.
234. N. P. Suh. *Axiomatic design: Advances and applications*. Oxford University Press, New York, NY, USA, 2001. ISBN: 0195134664.
235. R. Teixeira, M. Nogal, and A. O'Connor. "On the suitability of the generalized Pareto to model extreme waves". *Journal of Hydraulic Research* 56:6, 2018, pp. 755–770. DOI: [10.1080/00221686.2017.1402829](https://doi.org/10.1080/00221686.2017.1402829).
236. E. Thomas, J. Liu, A. Goyal, and L. Manuel. "Long-term loads on a large offshore wind turbine supported by a semi-submersible platform". In: *Proc. 34th Wind Energy Symposium*. San Diego, California, USA, 2016. DOI: [10.2514/6.2016-1995](https://doi.org/10.2514/6.2016-1995).
237. P. Thompson, Y. Cai, D. Reeve, and J. Stander. "Automated threshold selection methods for extreme wave analysis". *Coastal Engineering* 56:10, 2009, pp. 1013–1021. DOI: [10.1016/j.coastaleng.2009.06.003](https://doi.org/10.1016/j.coastaleng.2009.06.003).

238. P. S. Tromans and L. Vanderschuren. "Response based design conditions in the North Sea: Application of a new method". In: *Proceedings of the Annual Offshore Technology Conference*. 1995, pp. 387–397. DOI: [10.4043/7683-ms](https://doi.org/10.4043/7683-ms).
239. M. J. Tucker. "An improved 'Battjes' method for predicting the probability of extreme waves". *Applied Ocean Research* 11:4, 1989, pp. 212–218. DOI: [10.1016/0141-1187\(89\)90020-5](https://doi.org/10.1016/0141-1187(89)90020-5).
240. M. J. Tucker and E. G. Pitt. *Waves in ocean engineering*. Elsevier, Amsterdam, Netherlands, 2001. ISBN: 9780080435664.
241. L. Tvedt. "Proban - Probabilistic analysis". *Structural Safety* 28, 2006, pp. 150–163. DOI: [10.1016/j.strusafe.2005.03.003](https://doi.org/10.1016/j.strusafe.2005.03.003).
242. U.S. Energy Information Administration. *Electricity data*. URL: <https://www.eia.gov/international/data/world/electricity/> (visited on 09/30/2021).
243. V. Valamanesh, A. T. Myers, and S. R. Arwade. "Multivariate analysis of extreme metocean conditions for offshore wind turbines". *Structural Safety* 55, 2015, pp. 60–69.
244. E. Vanem. "Copula-based bivariate modelling of significant wave height and wave period and the effects of climate change on the joint distribution". In: *Proc. 35th International Conference on Ocean, Offshore and Arctic Engineering (OMAE 2016)*. American Society of Mechanical Engineers (ASME), 2016. DOI: [10.1115/OMAE2016-54314](https://doi.org/10.1115/OMAE2016-54314).
245. E. Vanem. "3-dimensional environmental contours based on a direct sampling method for structural reliability analysis of ships and offshore structures". *Ships and Offshore Structures* 14:1, 2019. DOI: [10.1080/17445302.2018.1478377](https://doi.org/10.1080/17445302.2018.1478377).
246. E. Vanem. "A comparison study on the estimation of extreme structural response from different environmental contour methods". *Marine Structures* 56, 2017, pp. 137–162. DOI: [10.1016/j.marstruc.2017.07.002](https://doi.org/10.1016/j.marstruc.2017.07.002).
247. E. Vanem. "A simple approach to account for seasonality in the description of extreme ocean environments". *Marine Systems & Ocean Technology* 13:2-4, 2018, pp. 63–73. DOI: [10.1007/s40868-018-0046-6](https://doi.org/10.1007/s40868-018-0046-6).
248. E. Vanem. "Joint statistical models for significant wave height and wave period in a changing climate". *Marine Structures* 49, 2016, pp. 180–205. DOI: [10.1016/j.marstruc.2016.06.001](https://doi.org/10.1016/j.marstruc.2016.06.001).
249. E. Vanem. "Uncertainties in extreme value modelling of wave data in a climate change perspective". *Journal of Ocean Engineering and Marine Energy* 1:4, 2015, pp. 339–359. DOI: [10.1007/s40722-015-0025-3](https://doi.org/10.1007/s40722-015-0025-3).
250. E. Vanem and E. M. Bitner-Gregersen. "Alternative environmental contours for marine structural design - A comparison study". *Journal of Offshore Mechanics and Arctic Engineering* 137, 2015, p. 51601. DOI: [10.1115/1.4031063](https://doi.org/10.1115/1.4031063).
251. E. Vanem and E. M. Bitner-Gregersen. "Stochastic modelling of long-term trends in the wave climate and its potential impact on ship structural loads". *Applied Ocean Research* 37, 2012, pp. 235–248. DOI: [10.1016/j.apor.2012.05.006](https://doi.org/10.1016/j.apor.2012.05.006).
252. E. Vanem, O. Gramstad, and E. M. Bitner-Gregersen. "A simulation study on the uncertainty of environmental contours due to sampling variability for different estimation methods". *Applied Ocean Research* 91, 2019, pp. 1–15. DOI: [10.1016/j.apor.2019.101870](https://doi.org/10.1016/j.apor.2019.101870).

Bibliography

253. E. Vanem, B. Guo, E. Ross, and P. Jonathan. "Comparing different contour methods with response-based methods for extreme ship response analysis". *Marine Structures* 69, 2020. DOI: [10.1016/j.marstruc.2019.102680](https://doi.org/10.1016/j.marstruc.2019.102680).
254. E. Vanem, A. Hafver, and G. Nalvarte. "Environmental contours for circular-linear variables based on the direct sampling method". *Wind Energy* October, 2019, pp. 1–12. DOI: [10.1002/we.2442](https://doi.org/10.1002/we.2442).
255. E. Vanem and A. B. Huseby. "Environmental contours based on a direct sampling approach and the IFORM approach: Contribution to a benchmark study". In: *Proc. 39th International Conference on Ocean, Offshore and Arctic Engineering (OMAE 2020)*. American Society of Mechanical Engineers (ASME), 2020. DOI: [10.1115/OMAE2020-18041](https://doi.org/10.1115/OMAE2020-18041).
256. J. Velarde, E. Vanem, C. Kramhøft, and J. D. Sørensen. "Probabilistic analysis of offshore wind turbines under extreme resonant response: Application of environmental contour method". *Applied Ocean Research* 93, 2019, p. 101947. DOI: [10.1016/j.apor.2019.101947](https://doi.org/10.1016/j.apor.2019.101947).
257. P. M. Videiro and T. Moan. "Efficient evaluation of long-term distributions". In: *Proc. 18. International Conference On Offshore Mechanics and Artic Engineering (OMAE99)*. 1999.
258. P. M. Videiro, J. S. Monsalve Giraldo, F. J. Mendes de Sousa, C. M. Peri Machado dos Santos, and L. V. S. Sagrilo. "Long-term analysis using a scatter diagram key region to evaluate the extreme response of steel risers". *Marine Structures* 64, 2019, pp. 322–340. DOI: [10.1016/j.marstruc.2018.11.011](https://doi.org/10.1016/j.marstruc.2018.11.011).
259. W. Visser. "Design: One, but in different forms". *Design Studies* 30, 2009, pp. 187–223. DOI: [10.1016/j.destud.2008.11.004](https://doi.org/10.1016/j.destud.2008.11.004).
260. F. Vorpahl, H. Schwarze, T. Fischer, M. Seidel, and J. Jonkman. "Offshore wind turbine environment, loads, simulation, and design". *WIREs Energy Environ* 2, 2013, pp. 548–570. DOI: [10.1002/wene.52](https://doi.org/10.1002/wene.52).
261. S. Wang, X. Wang, and W. L. Woo. "A comparison of response-based analysis and environmental contour methods for FPSO green water assessment". In: *Proc. 37th International Conference on Ocean, Offshore and Arctic Engineering (OMAE 2018)*. American Society of Mechanical Engineers (ASME), 2018. DOI: [10.1115/OMAE2018-77841](https://doi.org/10.1115/OMAE2018-77841).
262. A. Weissman, S. K. Gupta, X. Fiorentini, R. Sudarsan, and R. D. Sriram. *NISTIR 7626: Formal representation of product design specifications for validating product design*. Technical report. National Institute of Standards and Technology, 2009, pp. 1411–1422. DOI: [10.1115/detc2009-87307](https://doi.org/10.1115/detc2009-87307).
263. S. R. Winterstein, T. C. Ude, C. A. Cornell, P. Bjerager, and S. Haver. "Environmental parameters for extreme response: Inverse FORM with omission factors". In: *Proc. 6th International Conference on Structural Safety and Reliability (ICOSSAR 93)*. Innsbruck, Austria, 1993.
264. S. R. Winterstein. "Nonlinear vibration models for extremes and fatigue". *Journal of Engineering Mechanics* 114:10, 1988, pp. 1772–1790. DOI: [10.1061/\(ASCE\)0733-9399\(1988\)114:10\(1772\)](https://doi.org/10.1061/(ASCE)0733-9399(1988)114:10(1772)).
265. S. R. Winterstein, A. K. Jha, and S. Kumar. "Reliability of floating structures: Extreme response and load factor design". *Journal of Waterway, Port, Coastal and Ocean Engineering* 125:4, 1999, pp. 163–169. DOI: [10.1061/\(ASCE\)0733-950X\(1999\)125:4\(163\)](https://doi.org/10.1061/(ASCE)0733-950X(1999)125:4(163)).

Bibliography

266. R. Wiser, J. Rand, J. Seel, P. Beiter, E. Baker, E. Lantz, and P. Gilman. “Expert elicitation survey predicts 37% to 49% declines in wind energy costs by 2050”. *Nature Energy* 6:5, 2021, pp. 555–565. DOI: [10.1038/s41560-021-00810-z](https://doi.org/10.1038/s41560-021-00810-z).
267. L. Wrang, E. Katsidoniaki, E. Nilsson, A. Rutgersson, J. Rydén, and M. Göteman. “Comparative analysis of environmental contour approaches to estimating extreme waves for offshore installations for the baltic sea and the north sea”. *Journal of Marine Science and Engineering* 9, 2021. DOI: [10.3390/jmse9010096](https://doi.org/10.3390/jmse9010096).
268. D. E. Wright. “A note on the construction of highest posterior density intervals”. *Applied Statistics* 35:1, 1986, pp. 49–53.
269. D. C. Wynn and P.J. Clarkson. “Process models in design and development”. *Research in Engineering Design* 29, 2018, pp. 161–202. DOI: [10.1007/s00163-017-0262-7](https://doi.org/10.1007/s00163-017-0262-7).
270. Y. Xu, O. Øiseth, T. Moan, and A. Naess. “Prediction of long-term extreme load effects due to wave and wind actions for cable-supported bridges with floating pylons”. *Engineering Structures* 172, 2018, pp. 321–333. ISSN: 0141-0296. DOI: [10.1016/j.engstruct.2018.06.023](https://doi.org/10.1016/j.engstruct.2018.06.023).
271. K. Yang. *Design for six sigma: Roadmap to product development*. 2nd ed. McGraw-Hill, New York, NY, USA, 2003. ISBN: 0-07-143599-9.
272. I. R. Young, S. Zieger, and A. V. Babanin. “Global trends in wind speed and wave height”. *Science* 332, 2011, pp. 451–455. DOI: [10.1126/science.1197219](https://doi.org/10.1126/science.1197219).
273. A. Zanon, M. De Gennaro, and H. Kühnelt. “Wind energy harnessing of the NREL 5 MW reference wind turbine in icing conditions under different operational strategies”. *Renewable Energy* 115, 2018, pp. 760–772. DOI: [10.1016/j.renene.2017.08.076](https://doi.org/10.1016/j.renene.2017.08.076).
274. P. Zhang and S. Huang. “Review of aeroelasticity for wind turbine: Current status, research focus and future perspectives”. *Frontiers in Energy* 5:4, 2011, pp. 419–434. DOI: [10.1007/s11708-011-0166-6](https://doi.org/10.1007/s11708-011-0166-6).
275. Y. Zhang, C. W. Kim, M. Beer, H. Dai, and C. Guedes Soares. “Modeling multivariate ocean data using asymmetric copulas”. *Coastal Engineering* 135, 2018, pp. 91–111. DOI: [10.1016/j.coastaleng.2018.01.008](https://doi.org/10.1016/j.coastaleng.2018.01.008).
276. M. Zimmermann and J. E. von Hoessle. “Computing solution spaces for robust design”. *International Journal for Numerical Methods in Engineering* 94, 2013, pp. 290–307. DOI: [10.1002/nme](https://doi.org/10.1002/nme).

DECLARATIONS

PUBLISHED PAPERS

Parts of this thesis have been published in the following journal and conference papers:

- **Paper 1:** A. F. Haselsteiner, J.-H. Ohlendorf, W. Wosniok, and K.-D. Thoben. “Deriving environmental contours from highest density regions”. *Coastal Engineering* 123, 2017, pp. 42–51. DOI: [10.1016/j.coastaleng.2017.03.002](https://doi.org/10.1016/j.coastaleng.2017.03.002)
- **Paper 2:** A. F. Haselsteiner, J. Lehmkuhl, T. Pape, K.-L. Windmeier, and K.-D. Thoben. “ViroCon: A software to compute multivariate extremes using the environmental contour method”. *SoftwareX* 9, 2019, pp. 95–101. DOI: [10.1016/j.softx.2019.01.003](https://doi.org/10.1016/j.softx.2019.01.003)
- **Paper 3:** A. F. Haselsteiner and K.-D. Thoben. “Predicting wave heights for marine design by prioritizing extreme events in a global model”. *Renewable Energy* 156, 2020, pp. 1146–1157. DOI: [10.1016/j.renene.2020.04.112](https://doi.org/10.1016/j.renene.2020.04.112)
- **Paper 4:** A. F. Haselsteiner, A. Sander, J.-H. Ohlendorf, and K.-D. Thoben. “Global hierarchical models for wind and wave contours: Physical interpretations of the dependence functions”. In: *Proc. 39th International Conference on Ocean, Offshore and Arctic Engineering (OMAE 2020)*. American Society of Mechanical Engineers (ASME), 2020. DOI: [10.1115/OMAE2020-18668](https://doi.org/10.1115/OMAE2020-18668)
- **Paper 5:** E. Mackay and A. F. Haselsteiner. “Marginal and total exceedance probabilities of environmental contours”. *Marine Structures* 75, 2021. DOI: [10.1016/j.marstruc.2020.102863](https://doi.org/10.1016/j.marstruc.2020.102863)
- **Paper 6:** A. F. Haselsteiner, M. Frieling, E. Mackay, A. Sander, and K.-D. Thoben. “Long-term response of an offshore turbine: How accurate are contour-based estimates?” *Renewable Energy* 181, 2021, pp. 945–965. DOI: [10.1016/j.renene.2021.09.077](https://doi.org/10.1016/j.renene.2021.09.077)
- **Paper 7:** A. F. Haselsteiner, E. Mackay, and K.-D. Thoben. “Reducing conservatism in highest density environmental contours”. *Applied Ocean Research* 117, 2021, p. 102936. DOI: [10.1016/j.apor.2021.102936](https://doi.org/10.1016/j.apor.2021.102936)

During the time that the author worked towards his doctoral degree he also published papers that were related to the thesis but did not become part of it:

- A. F. Haselsteiner, J.-H. Ohlendorf, and K.-D. Thoben. “Environmental contours based on kernel density estimation”. In: *Proc. 13th German Wind Energy Conference (DEWEK 2017)*. Bremen, Germany, 2017. URL: <https://arxiv.org/ftp/arxiv/papers/1710/1710.07156.pdf>
- A. F. Haselsteiner, R. G. Coe, L. Manuel, P. T. T. Nguyen, N. Martin, and A. Eckert-Gallup. “A benchmarking exercise on estimating extreme environmental conditions: Methodology

Declarations

& baseline results". In: *Proc. 38th International Conference on Ocean, Offshore and Arctic Engineering (OMAE 2019)*. American Society of Mechanical Engineers (ASME), 2019. DOI: [10.1115/OMAE2019-96523](https://doi.org/10.1115/OMAE2019-96523)

- A. F. Haselsteiner, R. Reisenhofer, J.-H. Ohlendorf, and K.-D. Thoben. "Design for extremes: A contour method for defining requirements based on multivariate extremes". In: *Proc. 22nd International Conference on Engineering Design (ICED19)*. 2019, pp. 1433–1442. DOI: [10.1017/dsi.2019.149](https://doi.org/10.1017/dsi.2019.149)
- A. F. Haselsteiner, R. G. Coe, L. Manuel, W. Chai, B. Leira, G. Clarindo, C. Guedes Soares, N. Dimitrov, A. Sander, J.-H. Ohlendorf, K.-D. Thoben, G. de Hauteclercque, E. Mackay, P. Jonathan, C. Qiao, A. Myers, A. Rode, A. Hildebrandt, B. Schmidt, and E. Vanem. "A benchmarking exercise for environmental contours". *Ocean Engineering* 236, 2021. DOI: [10.1016/j.oceaneng.2021.109504](https://doi.org/10.1016/j.oceaneng.2021.109504)
- A. F. Haselsteiner, R. G. Coe, and L. Manuel. "A second benchmarking exercise on estimating extreme environmental conditions". *Ocean Engineering*, 2021. DOI: [10.1016/j.oceaneng.2021.109111](https://doi.org/10.1016/j.oceaneng.2021.109111)
- E. Mackay, R. G. Coe, A. F. Haselsteiner, and L. Manuel. "A second benchmarking exercise on estimating extreme environmental conditions". In: *Proc. 40th International Conference on Ocean, Offshore and Arctic Engineering (OMAE2021)*. American Society of Mechanical Engineers (ASME), 2021, OMAE2021-64874. DOI: [10.1115/OMAE2021-64874](https://doi.org/10.1115/OMAE2021-64874)

He also pursued other research projects that resulted in publications during the time he worked towards his doctoral degree:

- S. Oelker, M. Lewandowski, A. A. Alla, J.-H. Ohlendorf, and A. F. Haselsteiner. "Logistikzenarien für die Errichtung von Offshore-Windparks: Herausforderungen der Wirtschaftlichkeitsbetrachtung neuer Logistikkonzepte". *Industrie 4.0 Management* 33, 2017, pp. 24–28
- B.J. Hightower, R. Ingersoll, D. D. Chin, C. Lawhon, A. F. Haselsteiner, and D. Lentink. "Design and analysis of aerodynamic force platforms for free flight studies". *Bioinspiration & Biomimetics* 12:6, 2017, p. 064001. DOI: [10.1088/1748-3190/aa7eb2](https://doi.org/10.1088/1748-3190/aa7eb2)
- A. F. Haselsteiner, J.-H. Ohlendorf, S. Oelker, L. Ströer, K.-D. Thoben, K. Wiedemann, E. De Ridder, and S. Lehmann. "Lifting wind turbine components from a floating vessel: A review on current solutions and open problems". In: *Proc. 37th International Conference on Ocean, Offshore and Arctic Engineering (OMAE 2018)*. American Society of Mechanical Engineers (ASME), 2018. DOI: [10.1115/OMAE2018-78659](https://doi.org/10.1115/OMAE2018-78659)
- A. F. Haselsteiner, J.-H. Ohlendorf, S. Oelker, L. Ströer, K.-D. Thoben, K. Wiedemann, E. De Ridder, and S. Lehmann. "Lifting wind turbine components from a floating vessel: A review on current solutions and open problems". *Journal of Offshore Mechanics and Arctic Engineering* 141:5, 2019, p. 050801. DOI: [10.1115/1.4042385](https://doi.org/10.1115/1.4042385)
- A. Sander, A. F. Haselsteiner, K. Barat, M. Janssen, S. Oelker, J.-H. Ohlendorf, and K.-D. Thoben. "Relative motion during single blade installation: Measurements from the North Sea". In: *Proc. 39th International Conference on Ocean, Offshore and Arctic Engineering (OMAE 2020)*. American Society of Mechanical Engineers (ASME), 2020. DOI: [10.1115/OMAE2020-18935](https://doi.org/10.1115/OMAE2020-18935)

AUTHORSHIP STATEMENTS AND COLLABORATIONS

As made clear by referencing publications in preambles of some chapters, this thesis also contains contributions by other researchers. While this thesis was written solely by Andreas Haselsteiner, individual studies presented in the thesis were previously published together with co-authors. The author of this thesis paid attention to ensure that the reader of the thesis understands which original papers are presented in which chapters. In addition, he paid attention to only present results and writing where he had the major contribution in the original study.

Science has moved towards paying more attention, which parts of publications have been contributed by which authors. Some journals either require or encourage authors to submit “contribution statements” with the manuscript to briefly describe who contributed what. In three of the publications that were also presented in this thesis, such statements were jointly formulated (Table D.1).

In the remaining papers (see section “Published papers”), no such contribution statements were formulated. However, six of the seven publications that became part of this thesis were studies in which the author of this thesis made the main contribution and created the original draft of the manuscript. In these studies, he was listed as the first author. The study on marginal and total exceedance probabilities of environmental contours [158] was conducted by Ed Mackay and the author of this thesis. In this publication, Ed Mackay led the writing of the overall manuscript while the author of this thesis led the section on examples. This thesis only presents one of these examples. The software virocon that was presented in Section 6.2 was written by multiple developers. The repository’s git version control system provides a full track record, which makes transparent who developed what.

The author of this thesis acknowledges and thanks all co-authors of the publications that contributed to this thesis, namely Wei Chai, Guilherme Clarindo, Ryan Coe, Nikolay Dimitrov, Aubrey Eckert-Gallup, Ásta Hannesdóttir, Gillaume de Hauteclercque, Arndt Hildebrandt, Arne Bang Huseby, Jan-Hendrik Ohlendorf, Jannik Lehmkuhl, Bernt Leira, Philip Jonathan, Lance Manuel, Ed Mackay, Nevin Martin, Andrew Myers, Phong Nguyen, Tobias Pape, Chai Qiao, Rafael Reisenhofer, Anna Rode, Aljoscha Sander, Boso Schmidt, Carlos Guedes Soares, Klaus-Dieter Thoben, Erik Vanem, Kai-Lukas Windmeier, and Werner Wosniok.

Declarations

Publication	Published contribution statement
A. F. Haselsteiner and K.-D. Thoben. "Predicting wave heights for marine design by prioritizing extreme events in a global model". <i>Renewable Energy</i> 156, 2020, pp. 1146–1157. DOI: 10.1016/j.renene.2020.04.112	"Andreas F. Haselsteiner: Conceptualization, Methodology, Software, Validation, Formal analysis, Writing - original draft, Writing - review & editing, Visualization. Klaus-Dieter Thoben: Supervision, Funding acquisition."
A. F. Haselsteiner, M. Frieling, E. Mackay, A. Sander, and K.-D. Thoben. "Long-term response of an offshore turbine: How accurate are contour-based estimates?" <i>Renewable Energy</i> 181, 2021, pp. 945–965. DOI: 10.1016/j.renene.2021.09.077	"AFH and EM conceptualized this study. MF performed the multiphysics simulations, with support from AS and AFH. EM developed the environmental model and generated the artificial time series. AFH developed the response emulator. AFH lead the analysis and writing of the paper. AFH, EM, AS and MF edited and revised the original draft. KDT provided supervision."
A. F. Haselsteiner, E. Mackay, and K.-D. Thoben. "Reducing conservatism in highest density environmental contours". <i>Applied Ocean Research</i> 117, 2021, p. 102936. DOI: 10.1016/j.apor.2021.102936	"Andreas F. Haselsteiner: Conceptualization, Methodology, Software, Formal analysis, Writing - Original Draft, Writing - Review & Editing, Visualization. Ed Mackay: Conceptualization, Methodology, Writing - Review & Editing. Klaus-Dieter Thoben: Supervision."

Table D.1: Published contribution statements of publications that presented results of this thesis.

WÜRDIGUNG STUDENTISCHER ARBEITEN

ACKNOWLEDGING STUDENTS WHO CONTRIBUTED TO THIS THESIS. The legal framework that handles the process to obtain the Dr.-Ing. degree at University of Bremen, the *Promotionsordnung (Dr.-Ing.) der Universität Bremen für den Fachbereich 4 (Produktionstechnik) vom 20.08.2020*, asks to acknowledge the work of students who contributed to this thesis. The author of this thesis is very thankful to the students who contributed to this work.

In der vorliegenden Arbeit sind Ergebnisse enthalten, die im Rahmen der Betreuung folgender studentischer Arbeit entstanden sind:

Studierende	Name der Arbeit	Abgabejahr
Niklas Bergmann, Christian Castens, Jannik Lehmkuhl, Tjark Meyer, Kai-Lukas Windmeier	Entwicklung einer Web-App zur Berechnung von Extrem-Umweltbedingungen für die mechanische Auslegung	2017
Lars Bekow, Adrian Drewinski, Jana Thielbar	Erweiterung der Open-Source-Software ViroCon: Datensatz-Integration und Monte-Carlo-Methode	2020

Declarations

Cover page's artwork

The cover image was created by utilizing an artificial intelligence algorithm that applied the style of Roy Lichtenstein's painting "Drowning Girl" to a photograph of the "Alpha Ventus Offshore Wind Park". Afterwards the image was processed using Adobe Illustrator by the author of this thesis. The algorithm was applied using the website <https://creator.nightcafe.studio>. The used photograph of the wind park was obtained from Wikimedia Commons under a Creative Commons license (CC BY-SA 3.0): https://en.wikipedia.org/wiki/File:Alpha_Ventus_Windmills.JPG

Doctoral thesis
University of Bremen